

Rotation-Vibration Spectra of Linear Acetylene for Characterising Astrophysical Atmospheres

Katy L. Chubb

A dissertation submitted in partial fulfillment
of the requirements for the degree of
Doctor of Philosophy
of
University College London.

Department of Physics and Astronomy
University College London

September 24, 2018

I, Katy L. Chubb, confirm that the work presented in this thesis is my own. Where information has been derived from other sources, I confirm that this has been indicated in the work.

Abstract

This thesis presents research carried out as part of the ExoMol project, towards calculating theoretical spectra for the main isotopologue of acetylene, $^{12}\text{C}_2\text{H}_2$, for use in characterising hot exoplanet or cool stellar atmospheres. A large component of this work was in the development of numerical methods for treating linear polyatomic molecules such that these calculations could be carried out in an efficient and feasible way; ro-vibrational calculations of linear molecules are very non-trivial and require a unique treatment in order to avoid singularities in the Hamiltonian. A novel approach was employed in variational nuclear motion programme TROVE, which involves the use of a finite \mathcal{D}_{nh} symmetry group and classification of ro-vibrational states using the vibrational angular momentum operator, \hat{L}_z . This has been used in nuclear-motion calculations to compute an *ab initio* linelist of $^{12}\text{C}_2\text{H}_2$ covering 13.9 million transitions between 2.7 million states, up to a rotational excitation of $J = 58$.

In order to facilitate an accurate calculated spectra, available experimental data of $^{12}\text{C}_2\text{H}_2$ were collated and analysed to obtain an accurate set of 11,213 empirical energy levels using the MARVEL procedure. As demonstrated, these can be used to produce a high-accuracy potential energy surface and subsequent semi-empirical model for the ro-vibrational energies and intensities of acetylene, which can be computed up to high ro-vibrational excitations. Calculations using this semi-empirical model are in progress for an accurate high-temperature linelist, expected to be valid up to 1000–1200 K. This will be published in due course and will be appropriate for characterising exoplanet and cool stellar atmospheres; these ongoing calculations are discussed.

Impact Statement

The work outlined in this thesis forms a solid base for any future research related to ro-vibrational energy and intensity calculations of linear molecules, for acetylene in particular. The methods which have been implemented in the nuclear-motion routine used by the ExoMol group, TROVE, are general and can be applied to other general nuclear-motion routines. These updates have been used to calculate an *ab initio* linelist for acetylene and can also be used to compute the molecular spectra for other linear molecules, such as cyanoacetylene, C₃HN, for example (which is potentially important in exoplanet atmospheres and in investigating that of Titan), or propynylidyne, C₃H. New *ab initio* potential energy and dipole moment surfaces are also presented, which can be used by the spectroscopic community.

An acetylene linelist will be beneficial to astronomers, in the fields of both low-resolution and high-resolution astronomical spectroscopy, in the search for acetylene in astrophysical environments; in particular the atmospheres of hot exoplanets or cool stars.

The MARVEL analysis of ¹²C₂H₂ which was undertaken as part of this thesis was performed in collaboration with secondary-school students between 16–18 years of age as part of a scheme called ORBYTS (Original Research by Young Twinkle Students). The general method of conducting a MARVEL analysis of a particular molecule has been subsequently used in other ORBYTS collaborations with secondary-school students. It is hoped that including students in real peer-reviewed research from an early age will encourage them to explore STEM-related subjects and engage them in modern scientific methods.

Publications

Publications Relevant to this Thesis

K. L. Chubb, M. Joseph, J. Franklin, N. Choudhury, T. Furtenbacher, A. G. Császár, G. Gaspard, P. Oguoko, A. Kelly, S. N. Yurchenko, J. Tennyson, and C. Sousa-Silva, MARVEL analysis of the measured high-resolution spectra of C₂H₂, *JQSRT*, 204, 42-55, 2018 (10.1016/j.jqsrt.2017.08.018)

K. L. Chubb, A. Yachmenev, J. Tennyson, and S. N. Yurchenko, Treating linear molecule HCCH in calculations of rotation-vibration spectra, *J. Chem. Phys.*, 149(1), 014101, 2018 (10.1063/1.5031844)

K. L. Chubb, P. Jensen, and S. N. Yurchenko, Symmetry adaptation of the rotation-vibration theory for linear molecules, *Symmetry*, 10(5), 137, 2018 (10.3390/sym10050137)

K. L. Chubb, J. Tennyson, and S. N. Yurchenko, ExoMol Molecular linelists – XXXIV. The spectrum of Acetylene, *MNRAS*, (In prep.), 2018

Other Publications

K. L. Chubb, O. V. Naumenko, S. Keely, S. Bartolotto, S. MacDonald, M. Mukhtar, A. Grachov, J. White, E. Coleman, Anwen Liu, A. Z. Fazliev, E. R. Polovtseva, V. M. Horneman, A. Campargue, T. Furtenbacher, A. G. Császár, S. N. Yurchenko, and J. Tennyson, MARVEL analysis of the measured high-resolution rovibrational spectra of H₂S, *JQSRT.*, 218, 178–186, 2018 (10.1016/j.jqsrt.2018.07.012)

A. Owens, E. J. Zak, **K. L. Chubb**, S. N. Yurchenko, J. Tennyson, and A. Yachmenev, Simulating electric-field interactions with polar molecules using spectroscopic databases, *Sci. Rep.*, 45068, 7, 2017 (10.1038/srep45068)

J. J. Spake, D. K. Sing, T. M. Evans, A. Oklopčić, V. Bourrier, L. Kreidberg, B. V. Rackham, and J. Irwin, D. Ehrenreich, A. Wyttenbach, H. R. Wakeford, Y. Zhou, **K. L. Chubb**, N. Nikolov, J. M. Goyal, G. W. Henry, M. H. Williamson, S. Blumenthal, D. R. Anderson, C. Hellier, D. Charbonneau, S. Udry, and N. Madhusudhan, Helium in the eroding atmosphere of an exoplanet, *Nature*, 557, 68–70, 2018 (10.1038/s41586-018-0067-5)

J. Tennyson, S. N. Yurchenko, A. F. Al-Refai, E. J. Barton, **K. L. Chubb**, P. A. Coles, S. Diamantopoulou, M. N. Gorman, C. Hill, A. Z. Lam, L. Lodi, L. K. McKemmish, Y. Na, A. Owens, O. L. Polyansky, T. Rivlin, C. Sousa-Silva, D. S. Underwood, A. Yachmenev, and E. Zak, The ExoMol database: molecular line lists for exoplanet and other hot atmospheres, *J. Mol. Spectrosc.*, 327, 73–94, 2016 (10.1016/j.jms.2016.05.002)

L. K. McKemmish, **K. L. Chubb**, T. Rivlin, J. S. Baker, M. Gorman, A. Heward, W. Dunn, and M. Tessenyi, Bringing pupils into the ORBYTS of research, *Astronomy & Geophysics.*, 58(5), 5.11, 2017 (10.1093/astro-geo/atx169)

C. Sousa-Silva, L. K. McKemmish, **K. L. Chubb**, J. Baker, E. J. Barton, M. N. Gorman, T. Rivlin, J. Tennyson, Original Research By Young Twinkle Students (ORBYTS): When can students start performing original research?, *Phys. Educ.*, 53, 015020, 2018 (10.1088/1361-6552/aa8f2a)

K. L. Chubb, R. Hood, T. Wilson, J. Holdship, and S. Hutton, Discovering new variable stars at Key Stage 3, *Phys. Educ.*, 52(3), 035011, 2017 (10.1088/1361-6552/aa649f)

Acknowledgements

I am immensely grateful to Sergey Yurchenko and Jonathan Tennyson, who have been my mentors over the course of my PhD. I cannot imagine a more enjoyable and productive group to be a part of than ExoMol, with always entertaining and informative weekly group meetings, or a more supportive and enthusiastic supervisor than Sergey.

I am honoured to have met so many wonderful and interesting people over the last few years. A special mention goes to Andy Maxwell; I cannot express how grateful I am to have met him. Along with everyone in the ExoMol group, in particular my office mates Maire Gorman, Lorenzo Lodi, Andrey Yachmenev, Alec Owens, Phil Coles, Barry Mant and Victoria Clark, I would like to thank Harry Banks, Jacob Lang, Richard Juggins, Rosie Hood, Jon Holdship, Will Jennings, Tom Galley, Ahmed Al-Refaie, Duncan Little, Tom Meltzer, and many others, for making being at UCL so enjoyable. There have been some strange conversations and awful puns, but it has been a lot of fun.

I would like to sincerely thank all my co-authors, who are mentioned in the details of the publications related to this thesis. I am grateful to the ORBYTS team for their support, especially Clara Sousa-Silva and Laura McKemmish.

This work was supported by the ERC under Advanced Investigator Project 267219 and by STFC Projects No. ST/M001334/1 and ST/J002925. I acknowledge the use of the UCL Legion High Performance Computing Facility (Legion@UCL), and associated support services, along with the DiRAC@Darwin HPC cluster, the UK HPC facility for particle physics, astrophysics and cosmology, supported by STFC and BIS, and the DiRAC DIaL cluster at the University of Leicester.

For my Grandma, Eileen, who would've been a great scientist if society had let her.

For my Grandad, Tom, who was.

For my Parents, who taught me the joys of maths, science and nature from an early age.

And for my Brother, Chris, who may now call me "Doctor Chubb".

Contents

1	Introduction	25
2	Background	29
2.1	Motivation	29
2.2	Spectroscopy	31
2.3	Ro-vibrational Spectroscopy	34
2.3.1	The Ro-vibrational Schrödinger Equation	35
2.3.2	Ro-vibrational Spectra	36
2.4	Exoplanet Detection and Characterisation	39
2.4.1	Exoplanet Detection	40
2.4.2	Exoplanet Characterisation	41
2.4.3	High-Resolution Doppler Spectroscopy	43
2.5	Radiative Transfer	44
2.5.1	Retrieval Codes	46
2.6	Spectral Databases	46
2.6.1	The ExoMol Database	47
2.6.2	Line Broadening Parameters	48
3	Acetylene Theory	50
3.1	Quantum Number Labelling	50
3.2	Symmetry Labelling	53
3.3	<i>e/f</i> Labelling in Linear Molecules	55
3.4	<i>Ortho/Para</i> Labelling	56

3.5	Selection Rules	58
3.6	Polyad Number	58
3.7	Partition Function	59
4	The Symmetry of Linear Molecules for Ro-vibrational Applications	61
4.1	Background: $\mathcal{D}_{\infty h}$ Symmetry Groups	62
4.2	The Correlation of \mathcal{D}_{nh} and $\mathcal{D}_{\infty h}$ Symmetry Groups	69
4.3	Generating Operations of \mathcal{D}_{nh} Groups	73
4.4	Transformation Matrices of \mathcal{D}_{nh} Groups	75
4.5	Chapter Summary	79
5	MARVEL Analysis of the Ro-vibrational Energy Levels of $^{12}\text{C}_2\text{H}_2$	82
5.1	MARVEL Theory	83
5.1.1	Quantum Number Labelling	85
5.2	Experimental Sources	86
5.2.1	Comments on the Experimental Sources in Table 5.2	91
5.2.2	General Comments	94
5.2.3	Other Comments	95
5.3	Results	96
5.4	Comparison to Other Derived Energy Levels	104
5.5	Comments and Updates Subsequent to the MARVEL Analysis	110
5.6	The MARVEL Analysis of H_2^{32}S	111
5.7	Chapter Summary	112
5.8	Supplementary Data	113
6	The Singularity Issue for Linear Molecules	116
6.1	Nuclear-Motion Routine TROVE	118
6.2	Ro-vibrational Calculations in TROVE	119
6.3	Construction of the Kinetic Energy Operator in TROVE	120
6.4	Chapter Summary	125

7	Approaches to Dealing with Linear Molecules	127
7.1	The $(3N - 5)$ -approach to Dealing with Linear Molecules	127
7.1.1	The Coordinate System and KEO	128
7.1.2	Symmetrisation using the TROVE $(3N - 5)$ -approach .	131
7.1.3	Numerical Example of Basis Set Symmetrisation	140
7.1.4	Even vs. Odd \mathcal{D}_{nh} Symmetries	143
7.2	The $(3N - 6)$ -approach to Dealing with Linear Molecules	145
7.3	Chapter Summary	148
8	Variational Calculations of Acetylene	151
8.1	<i>Ab Initio</i> Calculations (MOLPRO)	151
8.2	Potential Energy Surfaces	151
8.2.1	Linearised $(3N - 5)$ Potential Energy Surface	152
8.2.2	Non-Linearised $(3N - 5)$ Potential Energy Surface	155
8.2.3	$(3N - 6)$ Potential Energy Surface	156
8.3	Dipole Moment Surfaces: $(3N - 5)$ Linearised Coordinates . . .	158
8.4	<i>Ab initio</i> Line List	160
8.4.1	Variational Calculations	160
8.4.2	Comparison to Other Data	162
8.4.3	Discussion of Results	163
8.5	Chapter Summary	166
9	The aCeTY linelist	168
9.1	Variational Calculations	169
9.1.1	Temperature Dependence	170
9.2	Empirical Refinement of the PES	171
9.2.1	Empirical Refinement Theory	171
9.2.2	Empirical Refinement Example	173
9.3	Band Centre Replacement	176
9.4	Intensities	177
9.5	Chapter Summary	178

<i>Contents</i>	12
10 Conclusions and Future Work	179
Bibliography	183

List of Figures

2.1	An illustration of vibrational (ν) and rotational (J) energy level structure, with labelled examples of P ($\Delta J = -1$), Q ($\Delta J = 0$) and R ($\Delta J = +1$) branch transitions, all within the ground electronic state.	31
2.2	An illustration of the approximate wavelength regions of the electromagnetic (EM) spectrum. Low energy rotational transitions are typically found in the microwave region, medium energy ro-vibrational transitions in the infrared (IR) and higher energy electronic transitions in the visible and ultraviolet (UV) regions.	33
2.3	The transit method makes detections of exoplanets by observing a relative dip in the brightness of the host star as the planet passes in front, as illustrated here. Image credit: NASA Ames. .	39
2.4	Observed spectra from HD189733b (a “hot Jupiter”) collected from the Hubble space telescope at a variety of wavelengths (black triangles), and corresponding models with just water (blue) and a combination of water and methane (orange). This figure is taken from Ref. [119].	42
3.1	Different conformations of acetylene and vinylidene. a) acetylene in its linear equilibrium configuration, b) acetylene in its trans configuration, c) acetylene in its cis configuration, and d) after isomerisation to vinylidene.	51

- 3.2 An illustration of the vibrational modes of acetylene. ν_1 is a symmetric C-H stretch, ν_2 is a symmetric C-C stretch, ν_3 is an antisymmetric C-H stretch, ν_4 and ν_5 are doubly degenerate bending modes, which are symmetric (trans) and antisymmetric (cis), respectively. There are therefore 5 vibrational modes leading to 7 vibrational degrees of freedom in total. 52
- 4.1 A graphical abstract to represent the substitution of n (right) for ∞ (left) in the $\mathcal{D}_{\infty h}$ point group 69
- 5.1 MARVEL energy levels (cm^{-1}) as a function of rotational quantum number, J , for all the vibrational energy bands in the *ortho* component of the principal spectroscopic network analysed in this paper. 98
- 5.2 MARVEL energy levels (cm^{-1}) as a function of rotational quantum number, J , for all the vibrational energy bands in the *para* component of the principal spectroscopic network analysed in this paper. 99
- 5.3 A representation of the *Ortho* component of the principal spectroscopic network of $^{12}\text{C}_2\text{H}_2$ produced using MARVEL input data. 100
- 5.4 A representation of the *Para* component of the principal spectroscopic network of $^{12}\text{C}_2\text{H}_2$ produced using MARVEL input data. 101
- 5.5 Alternative *ortho* (left) and *para* (right) components of the spectroscopic network of $^{12}\text{C}_2\text{H}_2$ produced using MARVEL input data. 102
- 5.6 Differences between the energy term values given in 17LyCa [45] and this work as a function of rotational angular momentum quantum number, J 107

- 5.7 Deviations of energy levels in cm^{-1} between this work and 16AmFaHe [46] as a function of rotational angular momentum quantum number, J . Different colours represent different designations of e/f and u/g 109
- 5.8 Deviations of energy levels in cm^{-1} between this work and 16AmFaHe [46] as a function of the number of transitions that link to the energy level in the present dataset. 110
- 5.9 Representations of the *ortho* (left) and *para* (right) components of the experimental spectroscopic network of H_2^{32}S produced using MARVEL input data. 112
- 6.1 The Euler angles describing the orientation of the molecular (x,y,z) axis (red) from the laboratory (X,Y,Z) axis (black). Here, θ is the angle between the Z and z axes, ϕ is the angle from X to the projection of z on the $X-Y$ plane, and χ is the angle between from ON (purple) to the y -axis (where O is the origin of both axes and ON defines the node line, which is the intersection of the $X-Y$ and the $x-y$ planes. ON is also perpendicular to both the z and Z axes. χ is therefore the azimuthal angle about the z -axis). 121
- 6.2 The geometry of HCCH as described using $3N-6$ internal curvilinear coordinates ξ ($R, r_1, r_2, \theta_1, \theta_2$ and τ) 121
- 7.1 HCCH as described using the $3N-5$ coordinates employed in TROVE (see text). \vec{R} is the vector (of length R) pointing from the first to the second carbon atom, C_1 to C_2 , while \vec{r}_i are the two CH_i bond vectors (of lengths r_i). The $\Delta x_1, \Delta x_2, \Delta y_1$ and Δy_2 notation of this diagram and Eq. (7.3) is to reflect the Cartesian projections of the CH_i bond vectors. 129

- 7.2 The block diagonal structure of a Hamiltonian matrix in the \mathcal{D}_{nh} irreducible representation. The empty (white) cells indicate blocks of vanishing matrix elements. It should be noted that, although \mathbf{B} -symmetries will be present for even values of n , they are not physical and do not appear as a block of matrix elements to be diagonalised. 133
- 7.3 Comparison of the exact bending wave function given by Eq. (7.28) with $k, t = 0$ (black line in both panels), with least squares fits of standard Legendre polynomial series truncated at; $n_{\max} = 2$ (blue), 6 (red), and 10 (orange), for $L_n(\alpha)$ (panel a) and $L_n(\cos \alpha)$ (panel b). The fit was done on an equidistant grid of α_1 values from $\alpha_1 = 0$ to 1 degree. Figure reprinted with permission from Ref. [24]. 149
- 8.1 A comparison of the residuals of the $(3N - 5)$ linearised coordinate PES fit with the $(3N - 5)$ non-linearised coordinate PES fit using the same grid of *ab initio* points 156
- 8.2 A comparison of the residuals of the $(3N - 5)$ linearised coordinate PES fit of Section 8.2.1 with the $(3N - 6)$ coordinate PES fit, both expanded up to 8^{th} order and using the same equilibrium values and the same grid of *ab initio* points 158
- 8.3 Residuals of the dipole moment surface fit up to $14,000 \text{ cm}^{-1}$ (for the x , y and z -components of the dipole) using the set of $(3N - 5)$ linearised coordinates of Figure 7.1. 160
- 8.4 Comparison of TROVE room-temperature *ab initio* spectrum (with linearised coordinates, up to 8^{th} order expansion) with ASD-1000 [44], up to $10,000 \text{ cm}^{-1}$ (TROVE calculations up to $J=58$; transitions to higher J were not within the specified energy window of below $10,000 \text{ cm}^{-1}$). 163

- 8.5 Comparison of the TROVE room-temperature *ab initio* spectrum (using linearised coordinates, up to 8th order expansion) with the ¹²C₂H₂ data from HITRAN-2016 [88], up to 10,000 cm⁻¹ (TROVE calculations up to $J = 58$; transitions to higher J were not within the specified energy window of below 10,000 cm⁻¹). 164
- 8.6 Comparison of the region around the ν_3 band from the TROVE room-temperature *ab initio* spectrum (using linearised coordinates, up to 8th order expansion) with the same band using ¹²C₂H₂ data from HITRAN-2016 [88]. 165
- 8.7 Comparison of the ν_5 band from the TROVE room-temperature *ab initio* spectrum (using linearised coordinates, up to 8th order expansion) with the same band using ¹²C₂H₂ data from HITRAN-2016 [88]. 165
- 9.1 An illustration of how the spectra of acetylene varies with temperature, using the *ab initio* linelist of Chapter 8, with low-resolution (1 cm⁻¹) cross-sections computed using ExoCross [168] at a variety of temperatures between 296–1000 K. . 174
- 9.2 An illustration of how different potential energy surfaces, with the same dipole moment surface, can have an effect on the intensities, in this case the $(\nu_4 + \nu_5)^0$ band (see Table 8.2). PES-1 and PES-2 were fit to the same $3N - 5$ function and *ab initio* points as described in Section 8.2.1, but with different weighting parameters. A small basis set is used for testing purposes ($P_{\max}=8$ for the primitive basis set and reduced to 6 after contraction, according to Eq. (8.13)) due to the computational cost of high-basis-set calculations. 178

List of Tables

3.1	Quantum numbers used to classify the energy states of acetylene, $^{12}\text{C}_2\text{H}_2$	53
3.2	Symmetry labels for the ro-vibrational states of a linear molecule such as $^{12}\text{C}_2\text{H}_2$. The <i>e/f</i> labels are defined in Section 3.3 (see also Ref. [190]) and <i>ortho/para</i> define the nuclear-spin state [56, 191] (see Section 3.4).	54
3.3	Parity of states in $^{12}\text{C}_2\text{H}_2$ based on the symmetry labels used in this work.	55
3.4	Allowed combinations of symmetry labels for ro-vibrational states (including spin) of $^{12}\text{C}_2\text{H}_2$, where <i>s</i> = symmetric, <i>a</i> = antisymmetric, ‘Total’ is how the ro-vibronic wavefunction, including the nuclear spin, acts under permutation symmetry. . .	57
3.5	Values of the total internal partition function Q and for the vibrational partition function Q_V at 296 K for acetylene from various sources.	60

- 4.1 Character table for the MS group $\mathcal{D}_{\infty h}(\text{M})$. Γ_1 – Γ_6 are several alternative notations for the irreducible representations of $\mathcal{D}_{\infty h}(\text{M})$. Γ_1 and Γ_6 are the most commonly used notations for $^{12}\text{C}_2\text{H}_2$ (and have been adopted throughout this thesis). Γ_3 is customarily used for $\mathbf{C}_{2v}(\text{M})$ and Γ_5 is for $\mathbf{C}_{2h}(\text{M})$ (Table A-8 of Ref. [189]). g and u stand for the German gerade (even) and ungerade (odd), related to the permutation-inversion operation $(p)^*$. $+$ or $-$ parity are determined by the spatial inversion operator E^* 65
- 4.2 Common character table for the point group $\mathcal{D}_{\infty h}$ and the Extended Molecular Symmetry (EMS) group $\mathcal{D}_{\infty h}(\text{EM})$, with the elements of each group defined in the text. 67
- 4.3 The irreducible representation Γ of $\mathcal{D}_{\infty h}(\text{EM})$ spanned by the rotational wavefunction $|J, k\rangle$ of a linear molecule in the absence of external electric and magnetic fields. The irrep depends on k , the z -axis projection in units of \hbar , of the rotational angular momentum. 68
- 4.4 Symmetry operations of the \mathcal{D}_{nh} groups, for even and odd n . σ_h , σ_v and σ_d represent reflections in planes perpendicular to the molecular axis, containing the molecular axis, and bisecting the angle between a pair of C_2 axes, respectively. An improper rotation S_n^r is a rotation by $r(\frac{2\pi}{n})$ ($r = 1 \dots n - 2$) followed by a reflection in the plane perpendicular to the molecular axis and containing the nuclear center-of-mass. C_n^r represents rotations by $r(\frac{2\pi}{n})$, where $r = 1 \dots n - 1$. See Ref. [189] for further details on these symmetry operations. 71
- 4.5 Character table for the \mathcal{D}_{nh} group, for odd n ($n \geq 5$)^a 72

- 4.6 Character table for the \mathcal{D}_{nh} group, for even n ($n \geq 4$). The C_2 operation is included explicitly for even n here, though it can be contained within the definition for C_n^r (when $r = \frac{n}{2}$); see the footnote of Table 4.5. 73
- 4.7 The correspondence between the g/u (gerade/ungerade) notation of the irreps of \mathcal{D}_{nh} (even n) and the $'/'$ notation of the irreps of \mathcal{D}_{nh} (odd n), based on K (the absolute value of the projection, in units of \hbar , onto the molecule-fixed z -axis of the rotational angular momentum). 74
- 4.8 Generating operations for the \mathcal{D}_{nh} groups (n even and n odd). 75
- 4.9 Irreducible representations for the D_{nh} groups and their characters under the generating operations R_+ , R'_+ and R_- 76
- 4.10 Transformation matrices, for the \mathcal{D}_{nh} (n -even and n -odd) groups generated by the rotational basis functions $|J, 0, +\rangle = |J, 0\rangle$ for $K = 0$ and $(|J, K, +\rangle, |J, K, -\rangle)$ for $K > 0$, with $\varepsilon = 2\pi/n$ 78
- 4.11 Irreducible representation transformation matrices of the \mathcal{D}_{nh} group for n even, generated by the rotational basis functions $(|J, K, +\rangle, |J, K, -\rangle)$ for $K > 0$ [189]. $\varepsilon = \frac{2\pi}{n}$, r is an integer used to identify the group operations, and $1 \leq K \leq \frac{n}{2} - 1$ 80
- 4.12 Irreducible representation transformation matrices of the \mathcal{D}_{nh} group for n odd, generated by the rotational basis functions $(|J, K, +\rangle, |J, K, -\rangle)$ for $K > 0$ [189]. E'_K and E''_K functions have even and odd K , respectively (Table 4.7), and so the present table has been simplified accordingly. $\varepsilon = \frac{2\pi}{n}$, r is an integer used to identify the group operations, and $1 \leq K \leq \frac{n-1}{2}$ 81
- 5.1 Extract from the MARVEL input file for the *ortho* transitions. The full file is supplied as part of the supplementary information of the associated publication [56]. All transition energy term values and uncertainties (unc) are in units of cm^{-1} 87

5.2	Data sources used in this study with wavelength range, numbers of transitions and approximate temperature of the experiment. A/V stands for the number of transitions analysed/verified. 'RT' stands for room temperature. See section 5.2.1 for the notes.	88
5.2	Data sources used in this study with wavelength range, numbers of transitions and approximate temperature of the experiment. A/V stands for the number of transitions analysed/verified. 'RT' stands for room temperature. See section 5.2.1 for the notes.	89
5.2	Data sources used in this study with wavelength range, numbers of transitions and approximate temperature of the experiment. A/V stands for the number of transitions analysed/verified. 'RT' stands for room temperature. See section 5.2.1 for the notes.	90
5.3	Data sources considered but not used in this work.	90
5.4	Changes in labelling between 15LyVaCa [184], 17LyCa_FTS15 [45] and this work, in the form $(v_1v_2v_3v_4^lv_5^l)^K$. See comment (31) in the text.	93
5.5	Extract from the MARVEL output file for the <i>ortho</i> transitions. The full file is supplied as part of the supplementary information to the associated publication [56]. All energy term values and uncertainties are in units of cm^{-1}	97
5.6	Vibrational energy levels (cm^{-1}) from the MARVEL analysis of $^{12}\text{C}_2\text{H}_2$	102
5.7	Comparison of pure rotational levels from the present MARVEL analysis of $^{12}\text{C}_2\text{H}_2$ with those of 16AmFaHe [46] and 17LyPe [44].	105
5.8	Supplied supplementary data files.	113
5.9	Definition of columns in files 1 and 2.	114


5.10	Definition of columns in files 3 and 4.	115
7.1	Quantum numbers used to classify the energy states of $^{12}\text{C}_2\text{H}_2$ in TROVE. See Table 3.1 for description of the experimental quantum numbers.	135
7.2	Symmetries of the symmetrised rotational basis set used by TROVE, Eqs. (7.17),7.18 for different combinations of J , K and τ (where τ ($= 0,1$) and $K = k $); each 2D representation E_{Kg} state has an a and b component, represented by the different values of τ . See Table 4.7 for an explanation of the differing notation of Γ_{rot} for even and odd values of n	138
7.3	Transformation matrices based on those of Table 4.11 for the \mathcal{D}_{nh} (n even) group (relating to the symmetry operations of Table 4.4), where n is even, for transforming the set of 7 vibrational coordinates ($\xi = \{R, r_1, r_2, \Delta x_1, \Delta y_1, \Delta x_2, \Delta y_2\}$, as illustrated in Figure 7.1) used in the calculations of Chapter 8. m is an integer for the bounds given for each operation, used to form ϵ_m , where $\epsilon = \frac{2\pi}{n}$ in all cases. The transformation is given in terms of two-component vectors $\vec{\rho}_1 = (\Delta x_1, \Delta y_1)^T$ and $\vec{\rho}_2 = (\Delta x_2, \Delta y_2)^T$, which transform as E_{1u} with the corresponding transformation matrices $\mathbf{M}_R^{E_{1u}}$ (with R denoting the general group operation) from Table 4.11.	140
7.4	An example of some rotational, vibrational and ro-vibrational assignments (see Section 3.1 for the meaning of these assignments) with associated symmetries (Γ_r , Γ_v and Γ_{r-v} , respectively) from ro-vibrational calculations using TROVE of $^{12}\text{C}_2\text{H}_2$ using different (even/odd) values of n for \mathcal{D}_{nh} . In each case $L_{\max} = 4$. The energies are identical for symmetries of higher n than those shown here, but converge towards the experimental values as the polyad number (Eq. 8.13) is increased; a low value is used here for demonstration purposes.	144

- 8.1 Comparison of the *ab initio* (before refinement) fundamental and some combination vibrational band centers of this work against the calculated energy term values \tilde{E}^{calc} (cm^{-1}) presented in Urru *et al.* [43] and experimental energy term values \tilde{E}^{obs} (cm^{-1}) from Refs. [302], [56] and [43]. The obs.-calc. value given is the difference between \tilde{E}^{obs} and \tilde{E}^{calc} (cm^{-1}) (this work). 166
- 8.2 Comparison of vibrational band intensities (S_{calc}) between this work (tw) and Ref. [366], along with S_{obs} , also from Ref. [366]. Intensities were converted from $\text{cm}^{-2}\text{atm}^{-1}$ to $\text{cm}/\text{molecule}$ using the conversion of $1 \text{ cm}^{-2}\text{atm}^{-1}$ at $296 \text{ K} = 4.033 \times 10^{-20} \text{ cm}/\text{molecule}$ [367]. The observed values of the $(2\nu_4 + \nu_5)^1 I$ and $(2\nu_4 + \nu_5)^1 II$ bands are cited in Ref. [366] as from private communication with G. Di Lonardo. $\frac{O-C}{O}$ gives the relative obs.-calc. ($S_{\text{obs}}-S_{\text{calc}}/S_{\text{obs}}$) percentage difference between this work and the observed values presented in Ref. [366]. The band centers ($\tilde{\nu}$) are in cm^{-1} 167
- 9.1 The completeness of the *ab initio* linelist of Chapter 8 at a variety of temperatures for a maximum lower energy level value of $4,000 \text{ cm}^{-1}$, measured using the calculated partition function (PF). 171
- 9.2 The completeness of the *ab initio* linelist of Chapter 8 at a variety of temperatures for a maximum lower energy level value of $6,000 \text{ cm}^{-1}$ 172
- 9.3 The completeness of the *ab initio* linelist of Chapter 8 at a variety of temperatures for a maximum lower energy level value of $8,000 \text{ cm}^{-1}$ 173

9.4	Vibrational energy levels (cm^{-1}) from the MARVEL analysis in comparison with those calculated by TROVE, before and after the refinement procedure. NT stands for NumTrans, the number of transitions linking each state in the MARVEL procedure.	175
-----	--	-----

Chapter 1

Introduction

Exoplanet (Noun) • *A planet which exists outside of our solar system.* 

Though the existence of exoplanets has been theorised for much longer, the first officially confirmed detection was around a pulsar in 1992 [1] and the first orbiting a sun-like star in 1995 [2]. The latter planet, 51 Pegasi b, is termed a “hot Jupiter” due to its large size and close-in orbit, and was the first insight into how different other solar systems could be to our own. Since then the number of exoplanet detections has come hurtling in, with almost 4000 confirmed detections as of June 2018 [3]. It has been predicted that there is, on average, at least one planet around every star in the Milky Way [4]. With these new discoveries inevitably comes the desire for a new branch of astrophysics; the atmospheric characterisation of exoplanets.

At the temperatures of many exoplanets and cool stars (up to around 3000 – 4000 K [5, 6]), molecules are often expected in abundance [7]. An essential component in the analysis of such astrophysical atmospheres is therefore accurate and comprehensive spectroscopic data for all molecules of astrophysical importance, for a variety of pressures and temperatures. While a large amount of highly accurate data have been determined experimentally for a number of such molecules, they have largely been measured at room-temperature and are thus not well suited to the modelling of high-temperature environments; theoretical data are required for this purpose. The ExoMol project [8, 9] was set up for this reason, to produce a database of computed line lists appropri-

ate for modelling exoplanet, brown dwarf or cool stellar atmospheres. As a result, high quality variational spectra which are appropriate up to high temperatures have been calculated for a host of molecules as part of the ExoMol project, including CH₄ [10, 11, 12], HCN/HNC [13], PH₃ [14], H₂O₂ [15], SO₂ [16], H₂S [17], SO₃ [18], VO [19], CO₂ [20], SiH₄ [21], H₂O [22], C₂H₄ [23], and, due to the work outlined in this thesis, C₂H₂ [24]. The spectral analysis of the latter molecule, acetylene, is desirable for a number of astrophysical applications, including the retrieval of exoplanet atmospheres [25, 26, 27], investigations into cool carbon-rich stars [28, 29, 30], and potentially for the study of brown dwarf atmospheres [31]. Acetylene, also known by its chemical formula C₂H₂ or HCCH, is a four-atomic (tetratomic) molecule which is linear in its equilibrium configuration. The rotation-vibration spectrum of a polyatomic molecule of this size, at the temperatures of exoplanets and cool stars, typically spans the infra-red region of the electromagnetic spectrum. In this region, only transitions between rotation-vibration (ro-vibrational) levels are important; electronic transitions are of too high energy to be of interest. Such ro-vibrational calculations essentially require a solution to the nuclear-motion Schrödinger equation, with some approximations required to enable feasible computational treatment. The challenge with acetylene comes with its linear geometry at equilibrium structure; linear molecules require special consideration for calculations of ro-vibrational energies [24, 32], as will be explored in this thesis. The special treatment of linear molecules in theoretical calculations has previously been adequately addressed for calculations involving linear triatomic molecules [33, 34, 20, 35, 36, 37], but not for linear molecules with four or more atoms.

There have been a number of previous attempts to perform *ab initio* variational calculations on the ground electronic state of C₂H₂ [38, 39, 40, 41, 42, 43], but these are apparently currently too computationally demanding to make them viable for calculations up to the highly rotationally excited states that have been calculated in this work, and only data for low ro-vibrational ex-

citations are presented in the literature. Effective Hamiltonian and similar approaches have been implemented to obtain spectra up to a relatively high excitation [44, 45, 46, 47]. However, while such approaches are stereotypically very good in areas of the spectrum with much experimental data, they would not be expected to extrapolate so accurately up to higher energies and thus do not offer the coverage that variational calculations do. Comprehensive, accurate opacities and cross sections for C_2H_2 , valid up to high temperatures, are therefore still needed for many areas of astrophysics. In this thesis a variational approach is presented, based on a mixture of *ab initio* and empirical models, which can be used in high ro-vibrational energy calculations to produce accurate high-temperature opacities and cross sections for C_2H_2 .

A review of the software used to model molecules as part of the ExoMol project is given in Ref. [48]: DUO [49] computes vibronic spectra for diatomics, DVR3D [34] computes rotation-vibration spectra for triatomics, and TROVE [50, 51] computes rotation-vibration spectra for general polyatomic systems. All three programs are publicly available from <https://github.com/ExoMol>. A large part of the work presented in this thesis is in developing numerical methods for treating small-to-medium linear polyatomic molecules, with particular focus on $^{12}\text{C}_2\text{H}_2$, and implementing them into variational nuclear motion programme TROVE (Theoretical ROVibrational Energies) [50, 51], which computes the ro-vibrational energy levels and the probabilities of transitions between them. As will be shown (see Chapters 4 and 7), this implementation involves the introduction of a finite \mathcal{D}_{nh} symmetry group (instead of the infinite-order $\mathcal{D}_{\infty h}$ group) and classification of ro-vibrational states using the vibrational angular momentum operator, \hat{L}_z , with the value of vibrational angular momentum, l , giving an indication of the value of n in \mathcal{D}_{nh} which should be used.

Highly accurate experimentally determined data provide an essential component in the calculation of a high-quality linelist, for both effective Hamiltonian and the majority of variational approaches. Fortunately for $^{12}\text{C}_2\text{H}_2$, a

wealth of experimental ro-vibrational spectral data has been recorded over the decades [45, 46, 52, 53, 54]. In the current work, all such experimental data that could be gathered from the literature was collated and analysed for the main isotopologue of acetylene, $^{12}\text{C}_2\text{H}_2$, to provide a set of empirically derived energy levels (Chapter 5), which are used in calculations of a high-accuracy linelist for $^{12}\text{C}_2\text{H}_2$.

This thesis is structured as follows. Chapter 2 gives some background and theory, with specifics for acetylene given in Chapter 3. The symmetry group used to classify the ro-vibrational states in a linear centrosymmetric molecule such as acetylene is introduced in Chapter 4, with general transformation matrices presented for the \mathcal{D}_{nh} group (Chubb *et al.* [55]). The collation and analysis of experimental transition data for acetylene is outlined in Chapter 5 (Chubb *et al.* [56]), which has led to a set of experimentally determined energy levels to be used in the process of calculating a high-accuracy linelist. The singularity issue for linear molecules is described in Chapter 6, with two alternative approaches to dealing with it ($3N - 5$ and $3N - 6$) introduced in Chapter 6 and investigated in detail in Chapter 7. The ($3N - 5$) approach, which was fully implemented into TROVE over the course of this research, makes use of the \mathcal{D}_{nh} symmetry group, and is utilised in order to calculate the *ab initio* linelist, which is presented in Chapter 8, along with *ab initio* potential energy and dipole moment surfaces. Chapters 6, 7 and 8 all relate to the published work of Chubb *et al.* [24]. Chapter 9 outlines current work on the aCeTY linelist, which will be highly accurate and, as demonstrated, should be appropriate up to around 1000–1200 K. This will be published in due course. Conclusions and future work are given in Chapter 10.

Chapter 2

Background

2.1 Motivation

Acetylene, HCCH, is a linear tetratomic unsaturated hydrocarbon whose spectra is important in a large range of environments. On Earth, these range from the hot, monitoring of oxy-acetylene flames which are widely used for welding and related activities [57, 58], to the temperate, monitoring of acetylene in breath, giving insights into the nature of exhaled smoke [59], vehicle exhausts [58], and other air-born pollutants [60]. Acetylene is also important in the production of synthetic diamonds using carbon-rich plasma [61]. Further out in our solar system, acetylene is found in the atmospheres of cold gas giants Saturn [62, 63], Uranus [64] and Jupiter [65, 66], the hydrothermal plumes of Enceladus [67], and in the remarkably early-earth-like atmosphere of Titan [68, 69], where there has even been some speculation as to acetylene's role in potential non-earth-like life [70, 71, 69, 72, 73, 74] and reactions involving molecules of pre-biotic interest [68, 71, 69]. It has been detected on comets such as Hyakotake [75], Halley, and 67P/Churyumov-Gerasimenko [76]. Even further into the galactic neighbourhood, acetylene appears in star forming regions [77], is speculated to be an important constituent of clouds in the upper atmospheres of brown dwarfs and exoplanets [78, 25, 31, 79, 80, 81], and is thought to play an important role in dust formation [82] and AGB star evolution and atmospheric composition [47, 83, 28, 84, 85, 86], providing a major source of

opacity in cool carbon stars [87, 84]. The first analysis of the atmosphere of a “super-Earth” exoplanet, 55 Cancri e [27], speculates that acetylene could be present in its atmosphere; however the spectral data available at the time did not allow for an accurate verification of its presence in such a high temperature environment. A similar conclusion was found for “hot Jupiter” extrasolar planet HD 189733b [26] and for carbon-rich stars in the LMC [28, 29, 30].

Alternative spectral data was used in the cases listed here; low-temperature data from HITRAN [88] in the case of Refs. [28, 26] and opacity sampling from Ref. [89] in the case of Refs. [29, 30]. The difference between using HITRAN and theoretical ExoMol spectra has been highlighted in works such as [90], which demonstrates a significant (and observable with instruments such as the James Webb Space Telescope (JWST), see Section 2.4.2) difference between the use of the two spectral data sources for phosphine. HITRAN is a database of largely experimental data obtained at room-temperature; obtaining such data at high temperature is a challenge [91], causing HITRAN to be reliable at room-temperature but incomplete at higher temperatures, with very many of the weak lines which can become important missing. This makes it ineffective for modelling the spectra of cool stars or hot exoplanets. Similarly, the opacity sampling data of Jørgensen [89] used by Refs. [29, 30] is not suitable for requirements of high resolution spectra and some differences have been noted between predicted and modelled spectra, especially for the bands around $3.1 \mu\text{m}$ and $14 \mu\text{m}$ [92]. Various other extensive spectral databases besides ExoMol and HITRAN include HITEMP [93], CDMS [94], GEISA [95], TheoReTS [96], SPECTRA [97], MeCaSDA and ECaSDa [98]. Accurate high-temperature variationally computed spectra have been produced for molecules such as CH_4 [99, 100, 101, 102, 103], PH_3 [104], NH_3 [105, 106] and C_2H_4 [107], but for C_2H_2 there is either not an extensive coverage of data that is appropriate for modelling up to high temperatures [96, 94, 93, 88] or the spectra were calculated based on the theory of effective Hamiltonians [46, 44], which tend to extrapolate poorly for high rotationally or vibrationally excited

states for which no experimental data is available. Spectral data for acetylene, valid up to high temperatures, is therefore still desirable for many areas of astrophysics.

2.2 Spectroscopy

Every molecule or atom has a unique set of quantised energy levels, the energies of which are dictated by the laws of quantum mechanics. For an atom these are related to the internal energy of the component electrons only (electronic energy levels), but for a molecule the energy can also be due to vibrational and rotational motions, with the relative sizes of these types of energy levels given by:

$$E_{\text{electronic}} > E_{\text{vibrational}} > E_{\text{rotational}}. \quad (2.1)$$

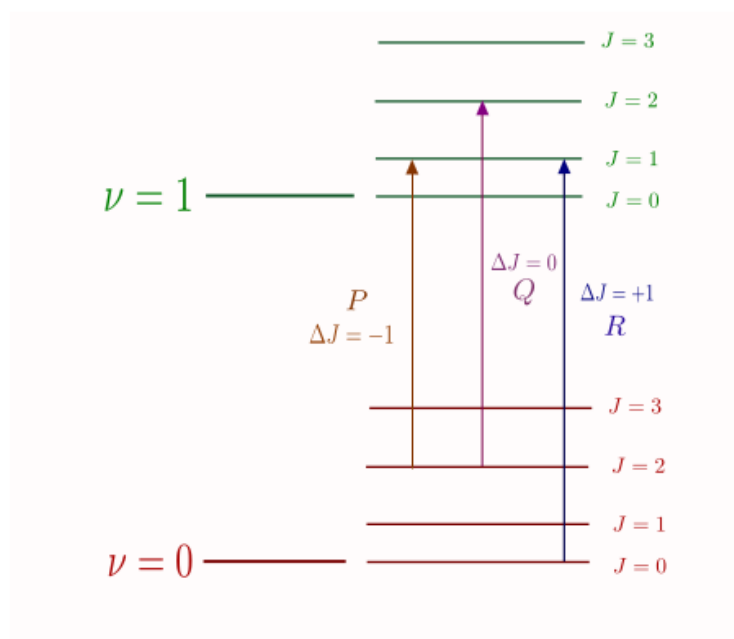


Figure 2.1: An illustration of vibrational (ν) and rotational (J) energy level structure, with labelled examples of P ($\Delta J = -1$), Q ($\Delta J = 0$) and R ($\Delta J = +1$) branch transitions, all within the ground electronic state.

As illustrated in Figure 2.1, the vibrational levels are sub-levels of the electronic states, and the rotational levels are further sub-levels of the vibrational states. The ground state is the lowest energy state, where all quantum numbers

(rotational, vibrational and electronic) are zero. The ground ro-vibronic (rotational, vibrational and electronic) state retains some energy as a result of the Heisenberg uncertainty principle, known as the zero point energy (ZPE). The energies of higher quantised levels are typically given relative to the ground ro-vibronic state, along with the relative integer quantum number labels given assignments upwards from 0. It is the differences in energy between these levels which is important; if some incident electromagnetic light on a molecular species¹ includes a photon of an energy² exactly equal to the difference between two energy levels, then this photon of energy will be absorbed by the molecule, and it will jump from the initial lower energy level to the upper energy level (assuming a transition between the two particular states is allowed by the rules of quantum mechanics). Similarly, a photon of energy can be emitted in order for a jump downwards in energy levels to be made. Transitions, due to either absorption or emission of photons, cannot, however, occur between all energy states in a molecule. The probability of a transition between two states is determined by quantum mechanical selection rules (see Section 3.5), with some transitions strongly allowed and some weakly allowed or forbidden. These transitions, a difference between two energy level states, are typically either given in units relating to wavelengths λ (microns, μm) or transition frequency $\tilde{\nu}$ (wavenumbers, cm^{-1}), with $\tilde{\nu}(\text{cm}^{-1}) = \frac{10,000}{\lambda(\mu\text{m})}$. Energy, E , frequency, ν , and wavelength, λ , are all related by Planck's constant, h , and the speed of light, c , via

$$E = h\nu = \frac{hc}{\lambda}, \quad (2.2)$$

where $h = 6.626068 \times 10^{-34} \text{J}\cdot\text{s}$. \tilde{E} , in units of cm^{-1} , is often known as the energy term value.

For a molecule, the type of motion which is induced due to the absorption of a photon of energy can either be purely rotational in nature (which

¹The same applies to atomic species, but the focus of this thesis is on molecules, so references to atoms will be dropped from now on.

²The terms 'energy' and 'frequency' are often used interchangeably, as demonstrated by Equation (2.2).

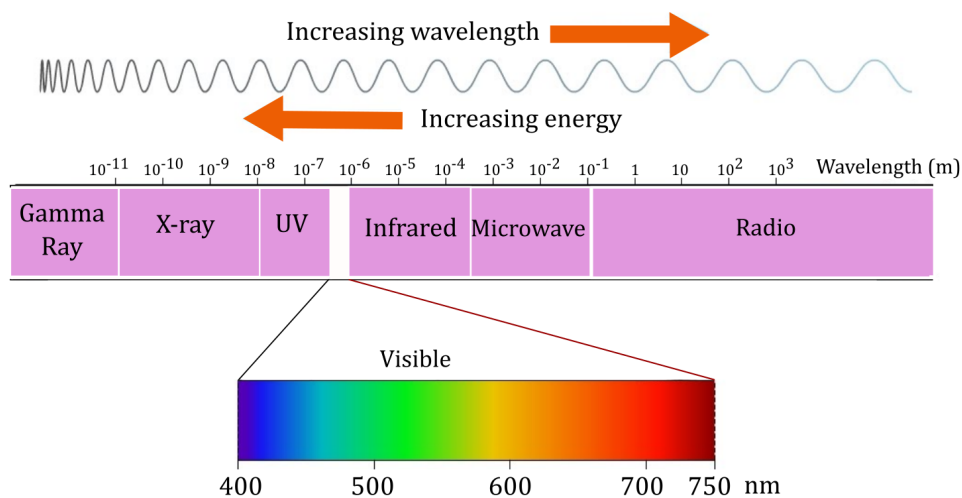


Figure 2.2: An illustration of the approximate wavelength regions of the electromagnetic (EM) spectrum. Low energy rotational transitions are typically found in the microwave region, medium energy ro-vibrational transitions in the infrared (IR) and higher energy electronic transitions in the visible and ultraviolet (UV) regions.

is related to radiation being absorbed in the microwave region of the electromagnetic (EM) spectrum, as shown in Figure 2.2), a combination of rotational and vibrational, known as “ro-vibrational” (typically the infra-red (IR) region of the EM spectrum), or a combination of rotational, vibrational and electronic, known as “ro-vibronic” (typically the UV/visible region). For polyatomic molecules (those composed of more than two atoms) such as acetylene, the region of importance for astrophysical environments such as warm exoplanets and cool stars is the IR, where ro-vibrational transitions dominate (see Section 2.3).

The unique set of energy levels, E , (as illustrated in Figure 2.1, but with E in Eq. (2.3) representing all types of energy level, not just electronic) are

essentially found by solving the Schrödinger equation

$$\hat{H}\Psi = E\Psi \quad (2.3)$$

where \hat{H} is the Hamiltonian operator and Ψ the wavefunction related to the species in question. This eigenvalue equation is commonly constructed in matrix form in order to be solved numerically using a variational approach. The ro-vibrational version of Equation (2.3) will be explored in Section 2.3.

2.3 Ro-vibrational Spectroscopy

As mentioned in the previous section, the region of importance for astrophysical environments such as molecule-dominated exoplanets and cool stars [6] is the infra-red, where ro-vibrational transitions dominate for polyatomic molecules such as acetylene. For these polyatomic molecules, transitions between any electronic energy levels occur at an energy much larger than expected in such environments and so will be ignored for the purpose of this thesis; focus will be on the transitions which occur between rotation-vibration levels in the ground electronic state of Figure 2.1 only. The transitions between different electronic states are usually important for smaller, diatomic (two-atom) molecules. In order for a molecule to exhibit pure rotational transitions, it should have a permanent dipole (at least this is the case in the rigid-rotor approximation, when centrifugal distortion is ignored), which is not the case for a linear symmetric molecule such as acetylene; the charge is distributed evenly relative to the centre of mass when the molecule is in its equilibrium configuration, at the ground ro-vibronic state. In practise, rotational motion will break the symmetry of a linear molecule due to centrifugal distortion, leading to a relatively weak rotational spectrum, which can in theory be observed. A molecule with an asymmetric charge distribution and therefore a permanent dipole such as H_2^{32}S or HCN will exhibit a dipole-allowed rotational spectra [108] (see Section 5.6), which can be observed in the microwave region of the EM spectrum. These lower energy transitions will typically be observed in cooler astrophysical environments, such as the interstellar medium (ISM) [6].

2.3.1 The Ro-vibrational Schrödinger Equation

The unique set of ro-vibrational energy levels for a particular polyatomic molecule are found by solving the ro-vibrational Schrödinger equation:

$$\hat{H}_{rv}\Psi_{rv} = E_{rv}\Psi_{rv}, \quad (2.4)$$

the general form of which is given in Eq. (2.3). An exact solution to Eq. (2.4) is numerically unfeasible, so approximations have to be used. The most significant of these is the Born-Oppenheimer (B-O) approximation, where the motions of the electrons are treated separately to those of the nuclei, an approximation usually considered valid due to the relatively much larger mass of the latter in comparison to the former. The use of the B-O approximation enables the concept of a potential energy surface (PES), via solution of an electronic Schrödinger equation. In Eq. (2.4), the Hamiltonian \hat{H}_{rv} is formed from the kinetic energy operator (KEO), \hat{T} , and potential energy function, V :

$$\hat{H}_{rv} = \hat{T} + V. \quad (2.5)$$

The electronic Schrödinger equation is solved at each position of the nuclear coordinates, from which arises the term “clamped nucleus” Hamiltonian (see, for example, Ref. [109]):

$$[\hat{T}_e + \hat{V}_e]\Psi_e = E_e\Psi_e, \quad (2.6)$$

which will enable a solution to the nuclear Schrödinger equation of Eq. (2.4) in the following way. \hat{T}_e and \hat{V}_e represent the kinetic energy operator of the electrons and the Coulomb potential energy operator, respectively. In atomic units, these are expressed as:

$$\hat{T}_e = -\frac{1}{2} \sum_{j=1}^{n_e} \nabla^2(\bar{R}_{ej}), \quad (2.7)$$

and

$$\hat{V}_e = - \sum_{i=1}^n \sum_{j=1}^{n_e} \frac{Z_i}{|\bar{R}_{ej} - \bar{R}_{ni}^{(k)}|} + \sum_{i<j}^{n_e} \frac{1}{|\bar{R}_{ej} - \bar{R}_{ei}|}. \quad (2.8)$$

Here, the subscripts e and n denote the electrons and nuclei, respectively. n_e and n give the number of electrons and nuclei, respectively, Z gives their charges, ∇ is the Laplacian, $\bar{\mathbf{R}}_e$ and $\bar{\mathbf{R}}_n$ refer to the whole set of electron and nuclear vector positions, respectively, and the (k) superscript of $\bar{\mathbf{R}}_{ni}^{(k)}$ refers to a particular set of nuclear coordinates at which Eq. (2.8) is evaluated.

For each (k) configuration of the nuclei, there is a corresponding potential energy of the electrons, given by a sum of the energy eigenvalue, E_e , from the solution of the electronic Schrödinger equation (Eq. (2.6)) and the nuclear repulsion potential energy:

$$E^{(E)}(\bar{\mathbf{R}}_n^{(k)}) = E_e^{(E)}(\bar{\mathbf{R}}_n^{(k)}) + \sum_{i < j}^n \frac{Z_i Z_j}{|\bar{\mathbf{R}}_{nj}^{(k)} - \bar{\mathbf{R}}_{ni}^{(k)}|}. \quad (2.9)$$

The potential energy surface $E^{(E)}(\bar{\mathbf{R}}_n)$ of the electrons is thus built as a function of the internal molecular coordinates, by evaluating Eq. (2.9) at a large number of nuclear geometries (k) . The nuclear Schrödinger equation, Eq. (2.4), can then be solved to find the ro-vibrational energy eigenvalues, with the potential energy surface V in Equation (2.5) given by the electronic potential energy surface $E^{(E)}(\bar{\mathbf{R}}_n)$. Electronic structure packages such as MOLPRO [110] are available to solve the electronic structure calculations of Eq. (2.9), while nuclear motion programmes such as TROVE (Theoretical ROVibrational Energies) [50, 51] have been written to compute the ro-vibrational energy levels of Eq. (2.4). The exact form of the kinetic energy operator (KEO) as implemented in TROVE is given in Section 6.3, with modifications for linear molecules outlined in Section 7.1.

2.3.2 Ro-vibrational Spectra

A linelist (ro-vibrational or otherwise) is comprised of the set of energy levels found by solving Eq. (2.4) which are unique to a particular molecule, along with the probability of the transitions between them. The probability of a transition is often given in the form of an Einstein-coefficient; A_{ji} is defined as the Einstein-A coefficient for spontaneous emission (the number of transitions per second from state j to state i), and is used for measuring the likelihood of a

particular transition (the transition strength). A_{ji} is related to the Einstein-B coefficient, B_{ij} , for absorption:

$$B_{ij} = \frac{c^3}{8\pi h \tilde{\nu}_{ji}^3} \frac{g_j}{g_i} A_{ji}, \quad (2.10)$$

with $\tilde{\nu}_{ji}$ the transition frequency between the two states, c the speed of light, h the Planck constant, and g_i and g_j the nuclear spin quantum numbers for the two states (see Section 3.4).

The Einstein-A coefficient, A_{ji} , for a particular transition from state i to state j is calculated by:

$$A_{ji} = \frac{8\pi^4 \tilde{\nu}_{ij}^3}{3h} (2J_j + 1) S(j \leftarrow i), \quad (2.11)$$

where J_j is the rotational quantum number associated with the upper energy level (for absorption) and $S(j \leftarrow i)$ is the transition strength:

$$S(j \leftarrow i) = \sum_{A=X,Y,Z} |\langle \Psi_j | \mu_A | \Psi_i \rangle|^2. \quad (2.12)$$

Here, μ_A is the dipole moment vector (usually given in units of Debye), in a space-fixed (laboratory-fixed) axis system XYZ , with μ_A the component of the dipole moment along the axis $A = X, Y, Z$. The dipole moment is related to a transition between states i and j , where Ψ_i to Ψ_j are the complete internal wavefunctions, and it essentially describes the charge distribution in a molecule. The transition strength will be zero for a transition over which the dipole doesn't change, which is why the fundamental C-C and symmetric C-H stretches are not featured in the IR spectrum for acetylene.

The Einstein-A coefficients are temperature independent, but can be used to calculate the temperature-dependent absolute intensity of a transition between an initial state i and final state j :

$$I(j \leftarrow i) = \frac{A_{ij}}{8\pi c} g_{ns} (2J_j + 1) \frac{\exp(-c_2 \frac{\tilde{E}_i}{T})}{Q(T) \tilde{\nu}_{ij}^2} \left[1 - \exp\left(\frac{-c_2 \tilde{\nu}_{ij}}{T}\right) \right], \quad (2.13)$$

where g_{ns} the nuclear statistical weight (also known as the nuclear degeneracy, as it gives the number of states with the same energy but different quantum

numbers; see Section 3.4 for more details), J_j is the rotational quantum number of the final state, \tilde{E}_i the energy term value (typically in units of cm^{-1}) of the initial state, $Q(T)$ the temperature dependent partition function, $\tilde{\nu}_{ij}$ the transition frequency between the two states and $c_2 = \frac{hc}{k}$ is the second radiation constant, with k the Boltzmann constant.

Absorption cross-sections, σ_{ν} , require the evaluation of the intensity of a transition (Eq. (2.13)) along with a corresponding line profile, due to the atmospheric processes which lead to a broadening of the spectral lines; in reality there is no idealised stick spectrum (which is essentially a plot of transition frequencies and line intensities, with no line profiles). More details on broadening processes and line profiles can be found in Section 2.6.2. The absorption cross-sections are typically evaluated across a series of frequency bins in a given frequency range, which will determine the spectral resolution. Ideally the resolution should match that of the instrument which was used to measure the observational data to be analysed using atmospheric retrieval codes (these are designed to solve the radiative transfer equation; see Section 2.5). If a frequency range from $\tilde{\nu}_{min}$ to $\tilde{\nu}_{max}$ is used with N grid points, then

$$\Delta\tilde{\nu} = \frac{\tilde{\nu}_{max} - \tilde{\nu}_{min}}{N} \quad (2.14)$$

will represent the resolution of the spectrum.

In order to be useful in atmospheric models, the number density of a particular molecular state needs to be taken into account along with the absorption cross-section; when multiplied together they give the absorption coefficient α_{ν} . The initial distribution of energy states is determined by the Boltzmann distribution, which describes the number density n_i of a molecular state i as a fraction of the total number density of the species, n :

$$\frac{n_i}{n} = \frac{g_i e^{-E_i/kT}}{\sum_m g_m e^{-E_m/kT}} = \frac{g_i e^{-E_i/kT}}{Q}, \quad (2.15)$$

where Q is the total internal partition function, E_i is the energy of each i molecular state (relative to the ground ro-vibronic state), k is Boltzmann's

constant, T is the temperature, g_i is the degeneracy of a particular state (see Section 3.4), and m is the sum over all molecular states.

2.4 Exoplanet Detection and Characterisation

A popular mode of detection and characterisation of exoplanets, restricted to planets which happen to pass in front of their host star from the point of view of an observer on (or very close to) Earth, is the transit method, as illustrated in Figure 2.3.

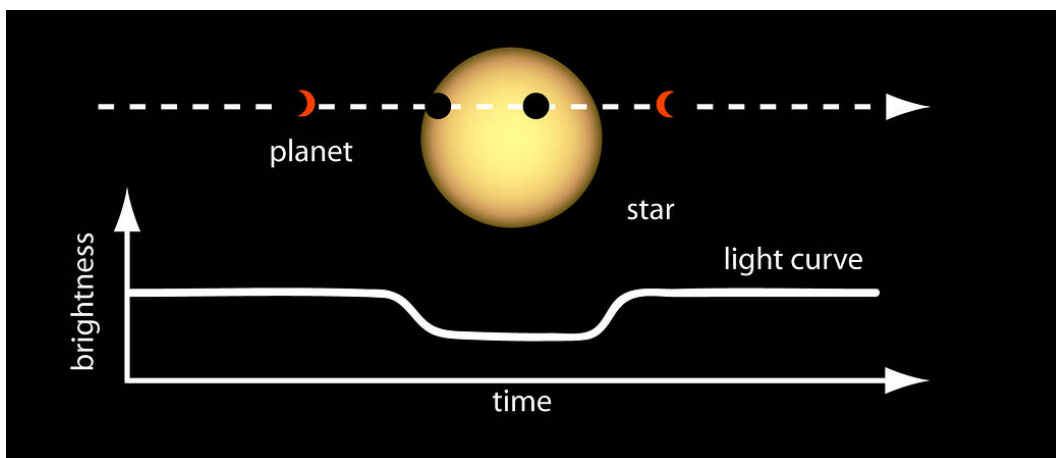


Figure 2.3: The transit method makes detections of exoplanets by observing a relative dip in the brightness of the host star as the planet passes in front, as illustrated here. Image credit: NASA Ames.

While a detection results from a periodic dip in the intensity of the stellar light, due to the planet blocking a proportion of the stellar surface, there is more to be discovered if the transiting planet has an atmosphere. In this case the light during the primary transit (when the planet passes in front of the star) and the secondary transit (as it passes behind) can be compared at a variety of wavelengths and analysed in order to deduce the absorption and emission processes at work, respectively. With no external influences the light emitted from a star can be modelled as a black-body spectrum which only depends on the emitter's temperature [6]. In the case of this light passing through an atmosphere, there will be subtleties in the spectra as a result of molecules or

atoms absorbing characteristic frequencies of light from the stellar blackbody spectrum. It is important, however, to note that the stars themselves have an atmosphere with their own absorption features which will need to be taken into account during any analysis. For very hot stars, only atoms would be able to exist in such high-temperature conditions, but for cooler stars and exoplanets (up to around 3000–6000 K [5, 6]), molecules are often expected in abundance [7].

Direct imaging is one alternative method of detection and characterisation, however it is currently limited to big (more massive than Jupiter), bright, young (heated predominantly from their interior) planets which are located far from their host star [111, 79]. High-resolution Doppler spectroscopy is a complementary method of molecular atmospheric detection, as briefly outlined in Section 2.4.3.

2.4.1 Exoplanet Detection

As aforementioned, there have been almost 4000 confirmed exoplanet detections as of July 2018 [3], with predictions placing on average at least one planet around every star in the Milky Way [4]. According to the NASA exoplanet archive [3], the vast majority of exoplanet detections to date, approximately 80%, have been via the transit method. Almost all other detections have been via the radial velocity method, with only around 1% as a result of direct imaging and other methods such as micro-lensing.

Notable exoplanetary detections, with more than one earth-sized planet in a system within the so-called “habitable zone” (the region in which life, as we know it, could potentially exist [112]), include Kepler-62 [113] and TRAPPIST-1 [114]. A review of the instrumentation used for the detection and characterisation of exoplanets can be found in Ref. [115], though it should be noted that this is now a few years out of date. Of the planets which were detected using the transit method, around 80% were as a result of the NASA Kepler mission [116] and 10% the follow-up K2 mission, making them the major source of exoplanet detections to date.

2.4.2 Exoplanet Characterisation

The atmospheric characterisation of exoplanets is a big motivation for the work outlined in this thesis, with a number of molecular detections made to date [117, 118, 119, 120, 121, 122, 27, 123, 124, 125, 126, 127, 128, 129]. As previously mentioned, the transit method is one of the principle techniques which is currently used for both detection of exoplanets and the characterisation of their atmospheres.

The dip in light intensity which is observed via the transit method (Figure 2.3), due to the relative ratio of the size of the star to the size of the planet, will vary dependent on the wavelength region which is being observed. Plotting the relative decrease in brightness at a variety of different wavelengths will give a measure of the amount of incident radiation absorbed at that particular wavelength and therefore an absorption spectra can be inferred. Figure 2.4 gives an observed spectra from a planet, HD189733b (a “hot Jupiter”), orbiting a binary star system which is 63 light years away [119]. The black triangles give the observational data, collected from the Hubble space telescope at a variety of wavelengths. The blue spectra is based on a model which includes the spectral data of water (based on theoretical calculations by the ExoMol group [130]), and the orange is methane [131] and water combined together [132, 119]. It can clearly be seen that the model which includes both water and methane fits the observed data much better than the pure water model. These models are found as a result of solving the radiative transfer processes in the exoplanetary atmosphere, as outlined in Section 2.5.

The first potential detection of a molecule on an exoplanet was water vapour in 2007 [120], made by the Spitzer Infrared Spectrograph (IRS). The detection was based on only three observational data points, with relatively large error bars. The quality of observational data has improved since then, as illustrated by Figure 2.4, and is expected to greatly improve in the future with instruments such as the James Webb Space Telescope (JWST) [133, 134] and ARIEL (Atmospheric Remote-sensing Exoplanet Large-survey) [135, 136, 137]

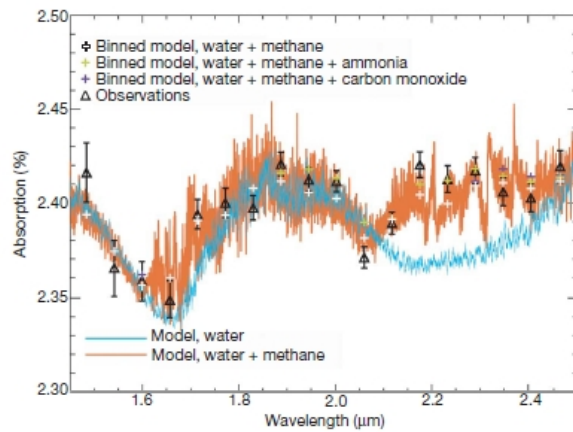


Figure 2.4: Observed spectra from HD189733b (a “hot Jupiter”) collected from the Hubble space telescope at a variety of wavelengths (black triangles), and corresponding models with just water (blue) and a combination of water and methane (orange). This figure is taken from Ref. [119].

due to launch in the coming years. ARIEL [135, 136, 137] was recently selected as a mission for ESA and is due for launch in 2028 with the aim to conduct a population characterisation study on around 1000 targets. The launch date for the next big exoplanetary characterisation mission, JWST [133, 134], has now been pushed back to at least 2020.

Another upcoming mission is Twinkle [138, 139, 140], a UK-led exoplanetary atmosphere mission which is set to launch into earth-orbit by 2022 and will be the first mission designed to be purely dedicated to the characterisation of exoplanetary atmospheres. The satellite will target a list of previously discovered exoplanets which are known to transit in front of their host star, in order to search for molecular features in their atmospheres. As part of the Twinkle Space Mission’s educational programme, EduTwinkle, students between the ages of 15 and 18 have been performing original research associated with the exploration of space since January 2016. This programme is called ORBYTS (Original Research by Young Twinkle Students) [141, 142]; the work of Chapter 5 is based on the published work of Refs.[56] and [143], respectively, which were undertaken as ORBYTS collaborations.

2.4.3 High-Resolution Doppler Spectroscopy

As well as the (currently) relatively low-resolution detections of molecules in transiting exoplanet atmospheres, a complementary method of astrophysical detection, where molecular lines in a planetary spectrum are shifted in wavelength due to the radial velocity of the planet, is high-resolution Doppler spectroscopy. Detections are made via typically ground-based spectrographs which can operate at a much higher resolution than those in space [144, 26]; it was using one of these instruments that enabled acetylene to be first detected in an astronomical environment in 1989 [145], from a high-resolution ($R=15,000$, where $R=\frac{\lambda}{\Delta\lambda}$ is the resolving power and $\Delta\lambda$ is the smallest distinguishable wavelength at a wavelength of λ) ground-based telescope, the Infrared Telescope Facility (IRTF) [146]. The orbital velocities of the target planets, typically “hot Jupiters”, are generally much higher than the stellar orbital velocities, enabling the identification of those molecular lines of the planetary atmosphere which will be shifted more in comparison to those of the star (and also when compared to the Earth’s telluric spectrum, which is not shifted) [79].

CRIRES (CRyogenic high-resolution InfraRed Echelle Spectrograph) is another high-resolution instrument (upto $R \sim 100,000$) which has enabled the first ground-based detections of carbon monoxide and water in the atmospheres of hot giant exoplanets [147, 148, 149]. It has been noted that CRIRES would be sensitive to detection of acetylene in hot Jupiter atmospheres, in particular in the $3.1 \mu\text{m}$ region [148, 26]. However, it has also been noted that the spectroscopic data for $^{12}\text{C}_2\text{H}_2$ is incomplete in HITRAN, in particular the weak lines which become important at higher temperatures [26], and there appears to be a general demand for such data [150, 92] (see Section 2.1).

It is therefore important and of use to the high-resolution exoplanet and astrophysical community to not only provide a complete linelist, but to ensure experimental data is utilised to make the data as accurate as possible. In Chapter 5, the collation and analysis of a large amount of experimentally determined ro-vibrational transition data for acetylene was undertaken with

this aim in mind. The data can be used to refine a theoretically calculated potential energy surface or to replace calculated energy levels (which will typically be less accurate than experimental data), in order to ensure maximum accuracy of a theoretical linelist.

2.5 Radiative Transfer

Radiative transfer describes the process of radiation being altered as it passes through a volume of gas. Only a basic summary of radiative transfer will be outlined here; a full account can be found elsewhere (e.g. Ref. [111]).

Ideally all absorption, emission and scattering processes should be taken into account when modelling the radiation which emerges from the top of an exoplanetary atmosphere. Molecules dominate at the temperatures and pressures of a typical exoplanetary atmosphere and so the principle contribution to changes in radiation will be due to molecular processes. The radiative transfer equation (assuming an atmosphere that does not change with time), describing the change in intensity I of some EM radiation, over a distance s of gas is given by:

$$\frac{\partial I(x, \hat{n}, \nu)}{\partial s} = -\kappa(x, \nu)I(x, \hat{n}, \nu) + \varepsilon(x, \hat{n}, \nu), \quad (2.16)$$

where the first term, $-\kappa(x, \nu)I(x, \hat{n}, \nu)$, describes the losses in intensity, and the second, $\varepsilon(x, \hat{n}, \nu)$, the gains in intensity. Here, κ is the extinction coefficient and ε the emission coefficient. The intensity, I , is defined as the amount of energy passing through a surface area dA , with differential solid angle $d\omega$ centred about \hat{n} , per frequency interval $d\nu$ and unit time dt :

$$dE(\nu, t) = I(x, \hat{n}, \nu, t) \hat{n} \cdot \hat{\kappa} d\omega dA d\nu dt. \quad (2.17)$$

Here, $\hat{\kappa}$ is a vector normal to the surface dA . Note that the time dependence of the intensity is often omitted in the solutions of radiative transfer [111]. The terms in Equations (2.16) and (2.17) are functions of the location x in the planetary atmosphere (which is often used interchangeably with the pressure P and temperature T [111]), the vector \hat{n} about which the solid angle $d\omega$ is oriented, and the frequency ν .

The opacity of an atmosphere describes how hard it is for radiation to pass through it, and is dependant on the number density of each type of molecule, the spread of energy levels, and their individual absorbing, emitting and scattering properties. The spread of energy levels for each molecule is temperature-dependent, given by the Boltzmann distribution of Eq. (2.15).

The opacity is typically represented by the extinction coefficient κ (with units of m^{-1}), which includes all processes that remove energy from a beam of radiation, and is therefore composed of the absorption coefficient $\alpha_{\nu}(T, P, \nu)$ and the scattering coefficient $\sigma_s(T, P, \nu)$ (which will not be explored in this thesis; a detailed account can be found elsewhere, e.g. Refs. [111, 6]). Integrating the extinction coefficient over the path z of the radiation being observed gives the optical depth, τ :

$$\tau = \int \kappa dz. \quad (2.18)$$

The total absorption coefficient $\alpha_{\nu}(T, P, \nu)$ is the sum of absorption coefficients of all molecular species present in an atmosphere, each of which is composed of the molecular number density n_{ji} for each energy state i of a molecule multiplied by the corresponding absorption cross-section σ . The means to calculate the absorption coefficients and cross-sections for molecules of astrophysical interest are provided by databases such as ExoMol (see Section 2.6.1).

The concept of local thermal equilibrium (LTE) is often employed for radiative transfer calculations, which is a valid assumption in regions of the atmosphere where changes in temperature and pressure are small when compared to the photon mean free path (which is the reciprocal of the extinction coefficient κ). This is thought to be the case in planetary atmospheres which have a high density of particles and which therefore have enough collisional processes that matter and radiation will be in thermal equilibrium. It should be noted, however, that an atmosphere will depart from LTE at its boundary, and other low pressure environments, where radiative processes dominate over collisional ones. The use of LTE makes finding a solution to the radiative transfer equation, Eq. (2.16), much easier as it enables to use of a Boltzmann

distribution (see Section 2.2, Equation (2.15)) to describe the molecular energy level population as a function of temperature only.

2.5.1 Retrieval Codes

There are several exoplanet retrieval codes in use by the exoplanetary characterisation community, with the aim to solve the radiative transfer equation, giving the propagation of radiation through a medium, many of which use ExoMol data (where available) as input into the spectral models.

Three alternative retrieval codes were recently compared by Baudino *et al.* [90]; ATMO [151, 152, 153], petitCODE [154, 155] and Exo-REM [156]. It has been previously mentioned that there was found to be a significant difference between using HITRAN and ExoMol data for phosphine. Various other parameters which could affect the modelling of the same planet using different codes were also investigated, including differences in chemical processes and in the atomic or molecular line shape used. The models have subsequently been updated based on this investigation, where problem parameters were identified [90]. Other successful retrieval models which have led to detections of atmospheric species on exoplanets include τ -rex [157, 158], which has been used in combination with RobERt [159], an algorithm based on deep-belief neural networks trained to identify likely molecular signatures to include in the full radiative transfer model, to model a large number of hot exoplanetary atmospheres [27, 160, 161], and CHIMERA [162] which has detected water in WASP-12b [128] and WASP-43b [163], and NEMESIS [164]. These retrieval codes often also provide the capability for forward modelling, where a spectrum is produced based on given input criteria.

2.6 Spectral Databases

Extensive molecular spectroscopic databases include ExoMol [8, 9], HITRAN [165], HITEMP [93], CDMS [94], GEISA [95], TheoReTS [96], SPECTRA [97], PNNL [166], MeCaSDa and ECaSDa [98]. The work undertaken in this thesis was done as a part of the ExoMol project.

2.6.1 The ExoMol Database

The ExoMol project [8, 9, 167] was set up to provide a database of *ab initio* line lists appropriate for modelling exoplanet, brown dwarf or cool stellar atmospheres. The data which is provided by the ExoMol database (a full account of which can be found in Ref. [9]) for each molecule of astrophysical interest is comprised of:

- a “.states” file, giving the molecule’s unique set of energy levels, along with a full set of quantum numbers (the ro-vibrational quantum numbers for C₂H₂ are given in Section 3.1)
- a “.trans” file, giving the transition probabilities between allowed energy states, in the form of Einstein-A coefficients
- (for some molecules) a “.broad” file, describing the broadening parameters (typically for self, air, hydrogen or helium broadening) for the transitions, as a function of rotational quantum number J
- a “.pf” file, giving the temperature dependent partition function (see Section 3.7)

The Einstein-A coefficients, A_{ji} , given in Eq. (2.10) (in units of s^{-1}), which are included in the ExoMol database represent the likelihood of a transition between two particular states and are temperature and pressure independent. These need to be converted into a suitable format, which is dependent on temperature and pressure, for use in any code related to the process of radiative transfer, as introduced in Section 2.5. ExoCross is a general program for generating spectra from molecular line lists [168], and accepts several formats including those of ExoMol and HITRAN. It produces cross-sections to a resolution that is determined by Eq. (2.14), and can also produce thermodynamic quantities such as temperature dependent partition functions (see Section 3.7).

2.6.2 Line Broadening Parameters

An observed spectrum will not simply be a pure stick spectrum (a list of line positions and line intensities); there will be some broadening of the spectral lines associated with various atmospheric processes. The main types of line broadening in an exoplanetary atmosphere are Doppler and pressure broadening. There is also some natural broadening of a line due to the Heisenberg uncertainty principle and the associated uncertainty in the determination of energy, however it is usually negligible in exoplanetary atmospheres in comparison to the other types of broadening and so is often ignored. Doppler broadening arises due to the thermal velocities of atmospheric molecules, and is thus dependent on temperature, giving a Gaussian line profile. Pressure (or collisional) broadening, which, as the name suggests, is pressure-dependent, leads to a Lorentzian profile. A convolution of Gaussian and Lorentz profiles gives a so-called Voigt profile; the efficient and accurate computation of a Voigt profile has been the subject of a number of publications, for example Refs. [168, 169, 170, 171, 172, 173, 174]. The exact form of the line profile is also dependent on the broadener; the atomic or molecular species which is colliding with the molecule in question. Typically, self, air, hydrogen and helium are important broadeners for atmospheric characterisation [175]. Where available, broadening parameters are provided as part of the ExoMol database, as specified in Ref. [175] (as of 2017), but there is demand for such parameters to be made available for a wider range of molecules and broadeners [170]. A more comprehensive account of line broadening is not necessary for the purpose of this thesis, and can be found elsewhere, see e.g. Ref. [111, 168].

Broadening coefficients for C_2H_2 are included in the HITRAN-2016 database [176], taken from Ref. [177] for self and air broadening, and Ref. [178] for H, He and CO_2 broadening. Other broadening coefficients for C_2H_2 can be found in Ref. [179] for O_2 broadening, Refs. [180, 181, 177, 182, 183, 184, 185, 186] for self-broadening, and Ref. [187] for N_2 broadening. The temperature dependence of N_2 broadening coefficients for acetylene can also be found in

Ref. [188]. It should be noted that the other referenced broadening coefficients here would have largely been obtained at room-temperature.

Chapter 3

Acetylene Theory

Acetylene, also known by its chemical formula C_2H_2 or $HCCH$, is a tetratomic (four-atomic) molecule which is linear in its equilibrium configuration. The two carbon atoms are joined by a triple bond (due to two π bonds and one σ bond), with single bonds joining the hydrogens either side. At high energies, acetylene undergoes an isomerization to vinylidene, as illustrated in Figure 3.1, expected to occur at around $15,000\text{ cm}^{-1}$ above the acetylene ground state [40]. The vibrational modes of acetylene are illustrated in Figure 3.2. This thesis is only concerned with the main isotopologue of acetylene, $^{12}C_2H_2$.

3.1 Quantum Number Labelling

The 11 quantum numbers that are typically used for labelling the upper and lower states of $^{12}C_2H_2$, and will be used throughout much of this thesis, are detailed in Table 3.1.

Each vibrational mode quantum number is given in normal mode notation; ν_1 represents the symmetric C-H stretch ν_1 , ν_2 the symmetric C-C stretch ν_2 , ν_3 the antisymmetric C-H stretch ν_3 , and ν_4 and ν_5 the doubly degenerate bending modes, ν_4 (symmetric) and ν_5 (antisymmetric), respectively. l_4 and l_5 are the vibrational angular momentum quantum numbers associated with ν_4 and ν_5 , respectively, with $|l| = \nu, \nu - 2 \dots 1$ for odd ν , $|l| = \nu, \nu - 2 \dots 0$ for even ν . J is the quantum number associated with rotational angular momentum, \mathbf{J} . $K = |k|$ is the rotational quantum number, with k corresponding to the

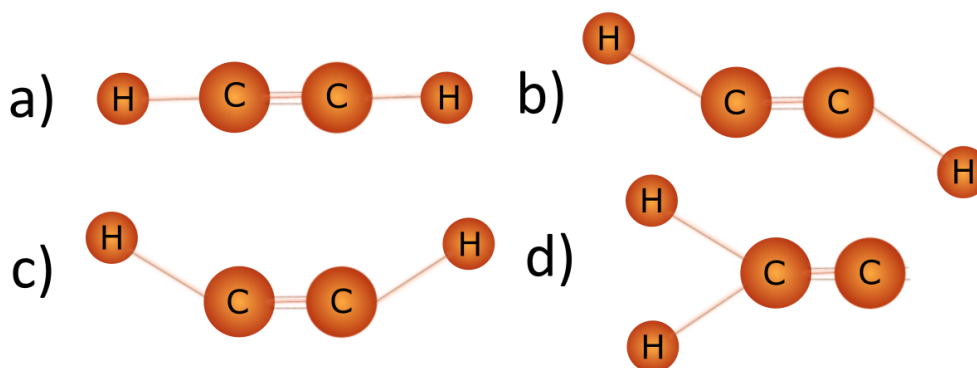


Figure 3.1: Different conformations of acetylene and vinylidene. a) acetylene in its linear equilibrium configuration, b) acetylene in its trans configuration, c) acetylene in its cis configuration, and d) after isomerisation to vinylidene.

projection of the rotational angular momentum, \mathbf{J} , on the molecular z -axis (in units of \hbar). For a linear molecule such as acetylene, K is also equal to the total vibrational angular momentum quantum number, $L \equiv |l| = |\ell_4 + \ell_5|$ (see Section 7.1), and therefore K is sometimes also referred to as the total vibrational angular momentum. The phase convention of Ref. [54] is followed in the assignment of quantum numbers carried out in Chapter 5; $K \equiv |k| = |\ell_4 + \ell_5|$ with $\ell_4 \geq 0$ if $k = 0$. The e or f labelling is also used, along with the nuclear spin state (*ortho* or *para*); see Sections 3.3 and 3.4, respectively.

Throughout this thesis the notations $(v_1 v_2 v_3 v_4^{\ell_4} v_5^{\ell_5})^K$ will be used to describe vibrational states and $(v_1 v_2 v_3 v_4^{\ell_4} v_5^{\ell_5})^K, J, e/f, ortho/para$ to describe ro-vibrational states. The e and f labelling combined with J and nuclear spin state (*ortho* or *para*) gives the rigorous designation of each state. Other quantum number labels are approximate but, besides representing the underlying physics, are necessary to uniquely distinguish each state. The convention for labelling a transition between two states is to give the upper state notation on the left, followed by a dash, and the lower state notation on the right. It is also conventional to label upper state quantum numbers as, for example, J' and lower state quantum numbers as J'' . The notation P(16) will typically mean

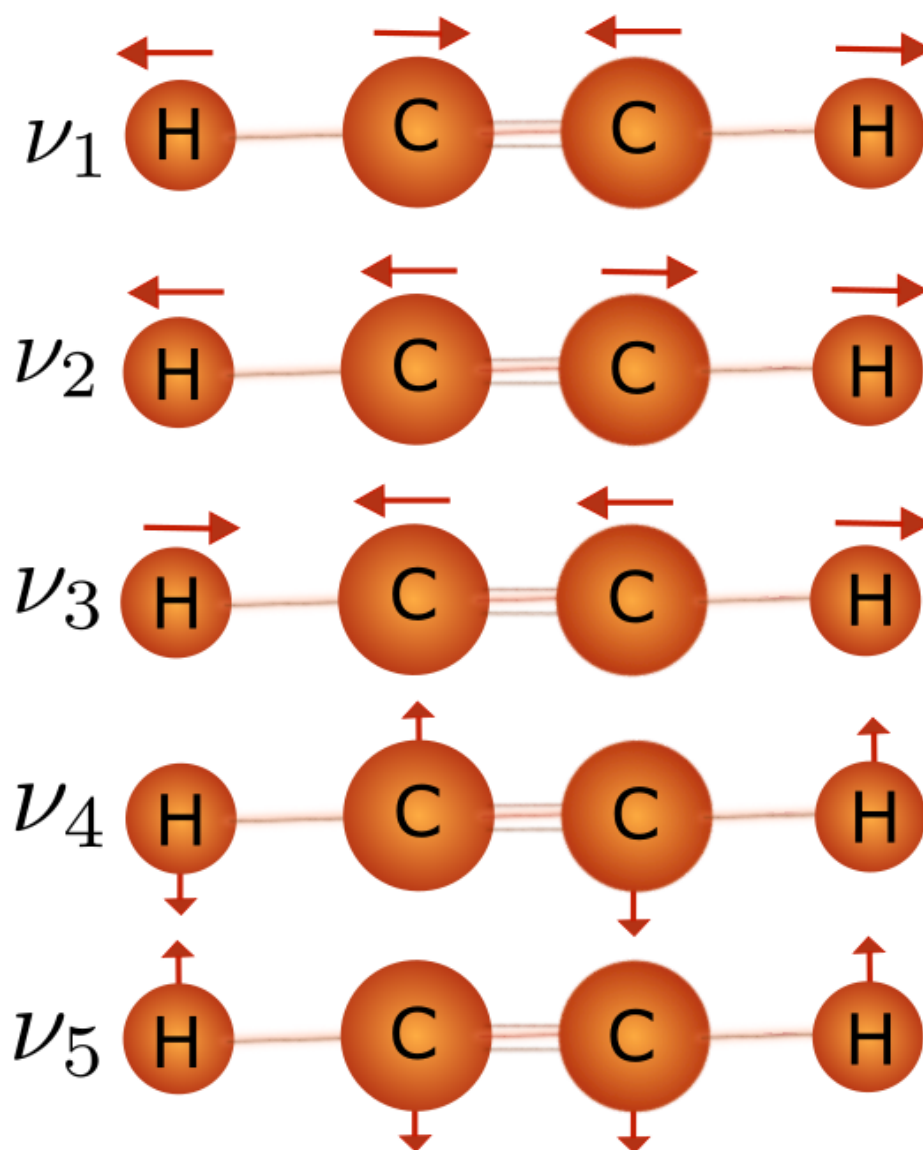


Figure 3.2: An illustration of the vibrational modes of acetylene. ν_1 is a symmetric C-H stretch, ν_2 is a symmetric C-C stretch, ν_3 is an antisymmetric C-H stretch, ν_4 and ν_5 are doubly degenerate bending modes, which are symmetric (trans) and antisymmetric (cis), respectively. There are therefore 5 vibrational modes leading to 7 vibrational degrees of freedom in total.

Table 3.1: Quantum numbers used to classify the energy states of acetylene, $^{12}\text{C}_2\text{H}_2$.

Label	Description
ν_1	CH symmetric stretch (σ_g^+)
ν_2	CC symmetric stretch (σ_g^+)
ν_3	CH antisymmetric stretch (σ_u^+)
ν_4	Symmetric (trans) bend (π_g)
ℓ_4	Vibrational angular momentum associated with ν_4
ν_5	Antisymmetric (cis) bend (π_u)
ℓ_5	Vibrational angular momentum associated with ν_5
$L = l $	Total vibrational angular momentum, $ \ell_4 + \ell_5 $
$K = k $	Rotational quantum number; z-projection of the rotational quantum number, J
J	Quantum number associated with rotational angular momentum, \mathbf{J} .
e/f	Symmetry relative to the Wang transformation (rotational state parity, see Section 3.3)
<i>ortho/para</i>	Nuclear spin state, see Section 3.4

$J'' = 16$ and therefore $J' = J'' - 1 = 15$ (where, a rotational P-branch transition is defined as $\Delta J = J' - J'' = -1$, a Q-branch transition as $\Delta J = J' - J'' = 0$ and an R-branch transition as $\Delta J = J' - J'' = +1$).

3.2 Symmetry Labelling

The symmetry of a linear molecule such as HCCH will be explored in more detail in Chapter 4, but will be touched upon here. For a linear molecule such as $^{12}\text{C}_2\text{H}_2$ both the rotational Ψ_r and vibrational Ψ_v contributions to the ro-vibrational wavefunction, Ψ_{rv} , should transform according to the point group for centrosymmetric linear molecules, $D_{\infty h}$. The $D_{\infty h}$ point group spans an infinite number of irreducible representations; $\Sigma_{g/u}^{+/-}$ ($K = 0$), $\Pi_{g/u}^{+/-}$ ($K = 1$), $\Delta_{g/u}^{+/-}$ ($K = 2$) etc. However, after combining the rotational and vibrational parts to make the ro-vibrational state, Ψ_{rv} , only the $K = 0$ states (i.e. Σ_g^+ , Σ_g^- , Σ_u^+ , Σ_u^-) can lead to a total nuclear-rotation-vibrational state which obeys the proper nuclear statistics, as described in Section 3.4. These are the irreducible elements of the $D_{2h}(\text{M})$ group [189], which according to the labelling scheme of this thesis correspond to the four pairs: *e ortho*, *e para*, *f ortho* and *f para*.

The correspondence depends on whether J is even or odd, as given in Table 3.2.

Table 3.2: Symmetry labels for the ro-vibrational states of a linear molecule such as $^{12}\text{C}_2\text{H}_2$. The e/f labels are defined in Section 3.3 (see also Ref. [190]) and *ortho/para* define the nuclear-spin state [56, 191] (see Section 3.4).

		e/f <i>ortho/para</i>			
J odd:	Σ_g^+ A_{1g}	$+s$	f	<i>para</i>	
	Σ_u^- A_{1u}	$-s$	e	<i>para</i>	
	Σ_g^- A_{2g}	$-a$	e	<i>ortho</i>	
	Σ_u^+ A_{2u}	$+a$	f	<i>ortho</i>	
J even:	Σ_g^+ A_{1g}	$+s$	e	<i>para</i>	
	Σ_u^- A_{1u}	$-s$	f	<i>para</i>	
	Σ_g^- A_{2g}	$-a$	f	<i>ortho</i>	
	Σ_u^+ A_{2u}	$+a$	e	<i>ortho</i>	

For example, the vibrational state ν_5 (Π_u) can be combined with the $J = 1, K = 1$ (Π_g) rotational state to produce three ro-vibrational combinations of Σ_u^+ , Σ_u^- and Δ_u ($D_{\infty h}$ point group). However only the Σ_u^- , Σ_u^+ states are allowed by nuclear statistics. Here ν_5 , Π_u , K , Π_g are not rigorous quantum numbers, while $J = 1$, e/f and *ortho/para* are. Thus these two ro-vibrational states are assigned $(0000^0 1^1)^1, J=1, e, \textit{para}$ and $(0000^0 1^1)^1, J=1, f, \textit{ortho}$, respectively. It should be also noted that generally neither K nor ν_1, \dots, ν_5 are good quantum numbers¹. However the quantity $(-1)^{\nu_3+\nu_5}$ is a good quantum number as it defines the conserved u/g symmetry as follows: a state is ungerade if $(-1)^{\nu_3+\nu_5} = -1$ and gerade if $(-1)^{\nu_3+\nu_5} = +1$. The $+/-$ labelling is derived from e/f and J , as given in Table 3.3. Whether a state has $+$ or $-$ parity is determined by the spatial inversion operator E^* , which is part of the

¹A good quantum number is one which uniquely describes a state which is not mixed by a state with a different value of that same quantum number. More formally, a good quantum number is one whose operator commutes with the Hamiltonian.

$\mathcal{D}_{\infty h}(M)$ molecular symmetry (MS) group (see Section 4.1). States of a linear molecule are often also classified based on the inversion operation, with states which are left unchanged called ‘gerade’ and labelled with a subscript g , and those whose phase changes to opposite are called ‘ungerade’ and labelled u , as in Table 3.2.

Table 3.3: Parity of states in $^{12}\text{C}_2\text{H}_2$ based on the symmetry labels used in this work.

e/f	J	Parity
e	Odd	–
e	Even	+
f	Odd	+
f	Even	–

3.3 *e/f* Labelling in Linear Molecules

An interaction known as ℓ -doubling occurs in linear molecules, which splits the rotational, J , levels in certain vibrational states. The symmetry describing these states is based on the total vibrational angular momentum quantum number, K , as outlined in Section 3.2. There are, for example, two distinct states in the $2\nu_4$ band; one with $K = 0$ (Σ_g^+ , $(0002^0 0^0)^0$) and the other $K = 2$ (Δ_g , $(0002^2 0^0)^2$). In this case, an interaction between the states leads to a splitting of the ro-vibrational levels in the $K = 2$ (Δ_g) sublevel, called ℓ -doubling; the split states are labelled as e and f . The e -level corresponding to the $K = 2$ (Δ_g) state, Δ_e , and the level corresponding to the $K = 0$ (Σ_g^+) state, Σ_e , repel each other, while Δ_f is unaffected. This effect is approximately $J(J+1)$ dependent and so becomes increasingly important at higher rotational excitations [109]. If a ro-vibrational state has no rotational splitting (as is the case if both $\ell_4=0$ and $\ell_5 = 0$, but not if $\ell_4 = 1$ and $\ell_5 = -1$), the state is always labelled e and there is no corresponding f state.

Levels with parity $+(-1)^J$ are called e levels and those with parity $-(-1)^J$

are called *f* levels. In other words, *e* and *f* levels transform in the same way as the rotational levels of $^1\Sigma^+$ and $^1\Sigma^-$ states, respectively [190]. The *e/f* labelling for linear molecules was originally introduced by Brown *et al.* [190] in order to eliminate issues relating to Pliva's *c/d* labelling [192] and the *s/a* labelling of Winnemisser and Winnemisser [193]. More information on the *e/f* rotational splitting can be found in Herman *et al.* [109].

3.4 *Ortho/Para Labelling*

Herman and Lievin [191] give an excellent description of the *ortho* and *para* states of acetylene, which is summarised here. The hydrogen atoms in the main isotopologue of acetylene are spin- $\frac{1}{2}$ particles and therefore, as Fermions, obey Fermi-Dirac rules [189, 56, 191]. The ^{12}C carbon atoms of $^{12}\text{C}_2\text{H}_2$, the only isotopologue considered in this thesis, are spin-0 and so do not need to be considered here.

The complete internal wavefunction of $^{12}\text{C}_2\text{H}_2$ is given by $\Phi_{\text{int}} = \Phi_{\text{elec}} \Phi_{\text{rv}} \Phi_{\text{ns}}$, where Φ_{elec} is the electronic wavefunction, Φ_{rv} is the rotation-vibration wavefunction, and Φ_{ns} is the nuclear-spin wavefunction.

The symmetry operation (*p*) (which is part of the $\mathcal{D}_{\infty\text{h}}(\text{M})$ molecular symmetry (MS) group (see Section 4.1)) describes a permutation of identical particles; when applied to $^{12}\text{C}_2\text{H}_2$ it implies permutation of the two hydrogen atoms. The total wavefunction must either be symmetric or antisymmetric upon such a transformation. In the case of fermions, as for $^{12}\text{C}_2\text{H}_2$, it must be antisymmetric. The permutation symmetry of the ground electronic state is totally symmetric upon interchange of identical atoms and so the electronic part of the wavefunction can be ignored for this situation.

Two nuclear wavefunctions of hydrogen exist; $\Psi_{1/2}$ and $\Psi_{-1/2}$ (where \pm gives the projection m_I of the nuclear spin $I = \frac{1}{2}$). There are four ways of combining the two wavefunctions which represent the spin of the two H atoms in $^{12}\text{C}_2\text{H}_2$:

$$\Psi_{1/2}^{(1)} \Psi_{1/2}^{(2)}, \quad (3.1)$$

Table 3.4: Allowed combinations of symmetry labels for ro-vibrational states (including spin) of $^{12}\text{C}_2\text{H}_2$, where s = symmetric, a = antisymmetric, ‘Total’ is how the ro-vibronic wavefunction, including the nuclear spin, acts under permutation symmetry.

u/g	$+/-$	Ro-vib.	Nuclear spin	Total
u	$+$	a	<i>Ortho</i>	a
u	$-$	s	<i>Para</i>	a
g	$+$	s	<i>Para</i>	a
g	$-$	a	<i>Ortho</i>	a

$$\Psi_{1/2}^{(1)}\Psi_{-1/2}^{(2)} + \Psi_{-1/2}^{(1)}\Psi_{1/2}^{(2)}, \quad (3.2)$$

$$\Psi_{1/2}^{(1)}\Psi_{-1/2}^{(2)} - \Psi_{-1/2}^{(1)}\Psi_{1/2}^{(2)}, \quad (3.3)$$

$$\Psi_{-1/2}^{(1)}\Psi_{-1/2}^{(2)}, \quad (3.4)$$

three of which are symmetric (ortho) and one which is symmetric (para) upon permutation of the H nuclei.

If the ro-vibrational part of the wavefunction is antisymmetric under permutation symmetry (resulting from a combination of g and $-$ or u and $+$; see Section 3.2), i.e. $(p)\Psi_{\text{rv}} = (-1)\Psi_{\text{rv}}$, then the nuclear spin state must be *ortho* and if the ro-vibrational part of the wavefunction is symmetric ($g, +$ or $u, -$), i.e. $(p)\Psi_{\text{rv}} = (+1)\Psi_{\text{rv}}$, then the nuclear spin state must be *para* (see Table 3.4). This ensures that the total wavefunction $\Phi_{\text{int}} = \Phi_{\text{elec}}\Phi_{\text{rv}}\Phi_{\text{ns}}$ is always anti-symmetric (as Φ_{elec} is totally symmetric for $^{12}\text{C}_2\text{H}_2$).

The g_{ns} factors, also known as the nuclear-spin quantum numbers, enter the intensity formula of rovibrational transitions (see Eq. 2.13; g_{ns} is 1 for A_{1g} and A_{1u} (para) states and 3 for A_{2g} and A_{2u} (ortho) states in $^{12}\text{C}_2\text{H}_2$; as there is no mixing between ortho and para states g_{ns} is the same for the upper and the

lower state); thus, *ortho* transitions generally have three times the intensity of *para* transitions. This is sometimes referred to as intensity alternation. It is assumed that *ortho* and *para* states do not interconvert; such transitions are very weakly allowed [194] but have yet to be observed for $^{12}\text{C}_2\text{H}_2$.

3.5 Selection Rules

The rigorous selection rules governing rotation-vibration transitions for a symmetric linear molecule (molecular group $D_{\infty h}(M)$) are given by

$$\Delta J = \pm 1 \quad \text{with} \quad e \leftrightarrow e \quad \text{or} \quad f \leftrightarrow f, \quad (3.5)$$

$$\Delta J = \pm 0 \quad \text{with} \quad e \leftrightarrow f \quad (3.6)$$

$$J' + J'' \neq 0 \quad (3.7)$$

$$u \leftrightarrow g \quad (3.8)$$

The first two equations here correspond to the standard selection rule $+ \leftrightarrow -$ for the dipole transitions in terms of the parities. A Q-branch ($\Delta J = 0$) is only possible if there is a change in vibrational angular momentum during a transition. This does not occur for Σ ($K = 0$) states, in which case only P and R branches are possible ($\Delta J = -1$ and $\Delta J = +1$, respectively).

3.6 Polyad Number

The polyad number of a molecule is typically used to group vibrational states ($\nu_1, \nu_2, \nu_3, \nu_4, \nu_5$, as defined in Section 3.1), with states in the same polyad having approximately equal energies.

For acetylene the polyad number, P , is typically given [53] by:

$$P = 3\nu_1 + 5(\nu_2 + \nu_3) + \nu_4 + \nu_5 \leq P_{\max}. \quad (3.9)$$

The maximum value, P_{\max} , is used as a means to restrict the basis set employed in variational calculations (see Section 8.4).

3.7 Partition Function

As introduced in Section 2.3.2, the number density of a particular molecular state as a fraction of the total number density of the molecular species is given by the Boltzmann law in Eq. (2.15). The total internal partition function, Q , is a sum over all molecular states, weighting each by their probability of occupation at a given temperature, and therefore offers an indication of the completeness of a calculated linelist at a particular temperature:

$$Q = \sum_{i=1}^N g_{ns}^{(i)} (2J+1) e^{-\frac{c_2 \tilde{E}_i}{T}}. \quad (3.10)$$

Here, $c_2 = \frac{hc}{k}$ is the second radiative constant, \tilde{E}_i is the energy term value of each i molecular state (relative to the ground ro-vibronic state), T is the temperature, $g_{ns}^{(i)}$ is the nuclear statistical weight of each i molecular state, and the sum is over all molecular states.

The total internal partition function, Q , is a product of the rotation-vibration (Q_{RV}) and electronic components (Q_E), however $Q_E=1$ in the ground electronic state, so only the ro-vibrational components need to be taken into account in the current work. An approximation is sometimes used whereby the vibrational part of the internal partition function, Q_V , is estimated (which assumes separation of the vibrational and rotational degrees of freedom) in order to compute vibrational transition moment values. Different values of Q and Q_V are given by different sources in Table 3.5. It should be noted that the physics or atmospheric convention is for the ratio of the nuclear degeneracy spin factors to be taken as 1:3 (*para:ortho*). This is the convention that is typically employed in spectroscopy and is used throughout this thesis and in Table 3.5. The astronomer convention uses $\frac{1}{4} : \frac{3}{4}$ (*para:ortho*), which leads to a factor of 4 difference in the partition function values (see, for example, Ref. [195]).

Table 3.5: Values of the total internal partition function Q and for the vibrational partition function Q_V at 296 K for acetylene from various sources.

Year	Reference	Q	Q_V
2017	[196]	414.03	
2011	[195]	412.3	
2000	[197]	412.525	
2000	[198]	417.5	1.1774
1990	[199]	405.867	

Chapter 4

The Symmetry of Linear Molecules for Ro-vibrational Applications

The use of molecular symmetry has applications in a range of fields, including molecular spectroscopy and the construction of molecular wavefunctions, ligand-field theory, material science, and electronic structure calculations [200, 201, 202, 203, 189]. The use of a symmetry-adapted basis set has been shown to make calculations of ro-vibrational energies far more efficient by reducing the size of the Hamiltonian matrix to be diagonalized [200], which is important in ensuring that such calculations are computationally viable. Intensity calculations are dependent on the symmetry of the ro-vibrational states, mainly due to the selection rules imposed by the nuclear spin statistics associated with different irreducible representations [200] (see Section 3.4), and so a full understanding of a molecule's symmetry group and how to utilise its properties in numerical calculations is vital in the production of a high-temperature linelist.

In this chapter a numerical application of linear-molecule symmetry properties, described by the $\mathcal{D}_{\infty h}$ point group, is formulated in terms of lower-order \mathcal{D}_{nh} symmetry groups with finite n . Character tables and irreducible representation transformation matrices are presented for \mathcal{D}_{nh} groups with arbitrary

n -values. The even- n \mathcal{D}_{nh} group is subsequently used in the construction of symmetry-adapted ro-vibrational basis functions for solving the Schrödinger equations of acetylene in Section 7.1.2 (and can be used for general linear molecules of $\mathcal{D}_{\infty h}$ point group symmetry).

Previous to Chubb *et al.* [55], the work of which is presented in this chapter, it appears that no transformation matrices for $\mathcal{D}_{\infty h}$ had been reported in the literature, although the corresponding character tables have been published many times (see, for example Ref. [204]). Hegelund *et al.* [205] have, however, described the transformation properties of the customary rigid-rotor/harmonic-oscillator basis functions (see, for example, Refs. [189, 206, 207]) for \mathcal{D}_{nh} point groups with arbitrary $n \geq 3$ (see also Section 12.4 of Ref. [189]), which can be used in the formulation of transformation matrices.

This chapter is structured as follows. Section 4.1 gives an overview of the rotational and vibrational symmetry classifications and groups for a centrosymmetric linear molecule, Section 4.2 introduces the \mathcal{D}_{nh} symmetry groups and their correlation with $\mathcal{D}_{\infty h}$, Section 4.3 introduces the concept of generating operations, and Section 4.4 presents the corresponding irreducible-representation transformation matrices.

4.1 Background: $\mathcal{D}_{\infty h}$ Symmetry Groups

For a centrosymmetric molecule such as acetylene, HCCH, the geometrical symmetry of its equilibrium configuration is described by the $\mathcal{D}_{\infty h}$ point group, which contains the following group elements:

$$\mathcal{D}_{\infty h} = \{E, C_{\infty}^{\epsilon}, \sigma_v^{(\epsilon/2)}, i, S_{\infty}^{\pi+\epsilon}, C_2^{(\epsilon/2)}\}. \quad (4.1)$$

Here, E is the identity operation¹, C_{∞}^{ϵ} is a (right-handed) rotation of the molecule by ϵ about the molecular z -axis (the axis along which all atoms are aligned when a molecule is in its linear geometry), $\sigma_v^{(\epsilon/2)}$ is a reflection in a

¹The effect of the identity operation is to “do nothing” and it is thus included as an operation in all molecular symmetry groups.

plane containing the molecular axis, i is the point group inversion operation², $S_{\infty}^{\pi+\varepsilon}$ is an improper rotation by $\pi + \varepsilon$ about the molecular axis (with $S_{\infty}^{\pi+\varepsilon} = C_{\infty}^{\varepsilon} \sigma_h$, where σ_h is a reflection in the xy plane), and $C_2^{(\varepsilon/2)}$ is a rotation by π about an axis perpendicular to the molecular axis [189]. As the angle ε can take on any value from $0 \cdots 2\pi$, it is evident that this group is of infinite order.

In contrast to the physical shape of a molecule on which the point group is based, the molecular symmetry (MS) group is defined as one whose elements do not change the energy of the molecule; more formally, whose elements commute with the Hamiltonian of the molecule. It is derived from the full complete nuclear permutation inversion (CNPI) group, which for $^{12}\text{C}_2\text{H}_2$ is:

$$\{E, (12), (34), (12)(34), E^*, (12)^*, (34)^*, (12)(34)^*\}, \quad (4.2)$$

with 1 and 2 representing the hydrogen protons and 3 and 4 the carbon nuclei and (ij) indicating a permutation of identical particles i and j ($i, j = 1$ and 2 or 3 and 4 in this case). To form the MS group from Equation 4.2 all unfeasible elements need to be removed (based on the principle of feasibility, first introduced by Longuet-Higgins [208, 189]). For a centrosymmetric linear molecule, such as acetylene, the unfeasible elements are (12) , (34) , $(12)^*$, and $(34)^*$. In a more compact form, the permutation operator, (p) , represents the simultaneous interchange of all pairs of identical nuclei about the molecular midpoint [189]. E is the identity operation, E^* is the spatial inversion operation, which inverts the positions of all particles (nuclei and electrons) through the molecular centre of mass, and $(p)^* = (p)E^* = E^*(p)$ is the permutation-inversion operation [189].

The molecular vibrational states (assuming a totally symmetric singlet electronic state) of a centrosymmetric linear molecule span the representations of the $\mathcal{D}_{\infty h}$ point group of infinite order (Equation (4.1)), but the symmetry properties of the combined rotation-vibration states must satisfy the nuclear-statistics requirements and transform according to the irreducible representa-

²This operation is only present for centrosymmetric molecules. It is formally defined as a rotation by π about the molecular z -axis, combined with a reflection in the xy plane.

tions (irreps) of the finite-order molecular symmetry (MS) group, which is, based on the above, defined as:

$$\mathcal{D}_{\infty h}(M) = \{E, (\rho), E^*, (\rho)^*\}. \quad (4.3)$$

The point group and molecular symmetry group for a linear molecule are evidently not isomorphic to one another; one is of finite order and the other infinite. This makes them unique amongst other types of molecule; the geometric symmetry at equilibrium structure of a rigid³ nonlinear molecule can be described by a point group which is isomorphic to its molecular symmetry group. Incidentally, the molecular symmetry group of a rigid linear centrosymmetric molecule, $\mathcal{D}_{\infty h}(M)$, is isomorphic to the MS group of a rigid nonlinear centrosymmetric molecule, $C_{2v}(M)$ (this is the MS group of, for example, H₂O). This can be verified using Longuet-Higgins' principle of feasibility [208], and holds for all chain molecules, irrespective of whether they have a linear or bent equilibrium structure. The irreducible representations (irreps) of MS group $\mathcal{D}_{\infty h}(M)$ are given in Table 4.1, with several alternative notations for the irreducible representations given.

³In this context, a rigid molecule is defined as one whose vibration can be described as oscillations around a single potential energy minimum, as is the case for acetylene.

Table 4.1: Character table for the MS group $\mathcal{D}_{\infty h}(\text{M})$. Γ_1 – Γ_6 are several alternative notations for the irreducible representations of $\mathcal{D}_{\infty h}(\text{M})$. Γ_1 and Γ_6 are the most commonly used notations for $^{12}\text{C}_2\text{H}_2$ (and have been adopted throughout this thesis). Γ_3 is customarily used for $\mathbf{C}_{2v}(\text{M})$ and Γ_5 is for $\mathbf{C}_{2h}(\text{M})$ (Table A-8 of Ref. [189]). g and u stand for the German gerade (even) and ungerade (odd), related to the permutation-inversion operation $(p)^*$. $+$ or $-$ parity are determined by the spatial inversion operator E^* .

Γ_1	Γ_2	Γ_3	Γ_4	Γ_5	Γ_6	E	(p)	E^*	$(p)^*$
Σ_g^+	$+s$	A_1	A^+	A_g	A_{1g}	1	1	1	1
Σ_u^+	$+a$	B_2	B^+	B_u	A_{2u}	1	-1	1	-1
Σ_g^-	$-a$	B_1	B^-	B_g	A_{2g}	1	-1	-1	1
Σ_u^-	$-s$	A_2	A^-	A_u	A_{1u}	1	1	-1	-1

For a rigid linear molecule, the infinite-order point group obviously provides a much more detailed symmetry description than the finite MS group. Although the MS group provides the symmetry operations relevant for describing the ‘fully coupled’ ro-vibrational wavefunctions of a molecule, the point group symmetry gives rise to useful information, in particular for the separate vibrational, and rotational basis functions used to express the fully coupled wavefunctions, and so it is often advantageous to employ the latter.

As seen in Section 3.4, the complete internal wavefunction of $^{12}\text{C}_2\text{H}_2$, Φ_{int} , is subject to Fermi-Dirac statistics [189, 56, 191]. It was shown that nuclear spin statistics require Φ_{int} to change sign under the operation (p) in the $\mathcal{D}_{\infty h}(\text{M})$ group elements of Eq. (4.3) in the case of $^{12}\text{C}_2\text{H}_2$. The nuclear-spin wavefunction Φ_{ns} does not depend on the spatial coordinates of the nuclei and so it is invariant under the ‘geometrical’ symmetry operations of the point group $\mathcal{D}_{\infty h}$. It is also invariant under MS group operation E^* , but it may have its sign changed by (p) . Thus, it can have Σ_g^+ or Σ_u^+ symmetry in $\mathcal{D}_{\infty h}(\text{M})$ (Table 4.1).

Bunker and Papoušek [209] introduced the so-called Extended Molecular Symmetry (EMS) Group which, for a centrosymmetric linear molecule, is isomorphic to the $\mathcal{D}_{\infty h}$ point group. The operations in $\mathcal{D}_{\infty h}(\text{EM})$ can be written as:

$$E(=E_0), E_{\varepsilon}, (p)_{\varepsilon}, E_{\varepsilon}^*, (p)_{\varepsilon}^* \quad (4.4)$$

where the angle ε satisfies $0 \leq \varepsilon < 2\pi$. The effect of the elements of the EMS group is much the same as those of the MS group, with the main difference being that the EMS group operations also mimic a rotation by ε about the molecular z -axis.

The irreducible representations of $\mathcal{D}_{\infty h}$ and $\mathcal{D}_{\infty h}(\text{EM})$ are listed in Table 4.2. It should be noted here that the point group inversion operation, i , should be distinguished from the spatial inversion operation, E^* , which inverts the positions of all particles (nuclei and electrons) through the molecular centre of mass and is a part of the $\mathcal{D}_{\infty h}(\text{M})$ MS group. i is only present for centrosymmetric molecules, and gives the u/g label on vibronic states, while E^* gives the $+/-$ parity label. Four of the irreps are one-dimensional: Σ_g^+ , Σ_g^- , Σ_u^+ , and Σ_u^- and an infinite number are two-dimensional: $\Pi_{g/u}$, $\Delta_{g/u}$, $\Phi_{g/u}$, $\Gamma_{g/u}$, $H_{g/u}$, $I_{g/u}$, \dots . In the alternative and more compact notation, the 2D irreps are given by E_{ng} and E_{nu} , where $n = 1, 2, \dots, \infty$. The rotational basis functions $\Phi_{J,k}^{\text{rot}} = |J, k\rangle$ span the irreducible representations of $\mathcal{D}_{\infty h}(\text{EM})$ as given in Table 4.3.

Table 4.2: Common character table for the point group $\mathcal{D}_{\infty h}$ and the Extended Molecular Symmetry (EMS) group $\mathcal{D}_{\infty h}(\text{EM})$, with the elements of each group defined in the text.

$D_{\infty h}(\text{EM})$:	E_0	E_{ε}	\dots	∞E_{ε}^*	$(12)_{\pi}^*$	$(12)_{\pi+\varepsilon}^*$	\dots	$\infty(12)_{\varepsilon}$
$D_{\infty h}$:	E	$2C_{\infty}^{\varepsilon}$	\dots	$\infty C_{\infty}^{(\varepsilon/2)}$	i	$2S_{\infty}^{\pi+\varepsilon}$	\dots	$\infty C_2^{(\varepsilon/2)}$
Σ_g^+, A_{1g} :	1	1	\dots	1	1	1	\dots	1
Σ_u^+, A_{2u} :	1	1	\dots	1	-1	-1	\dots	-1
Σ_g^-, A_{2g} :	1	1	\dots	-1	1	1	\dots	-1
Σ_u^-, A_{1u} :	1	1	\dots	-1	-1	-1	\dots	1
Π_g, E_{1g} :	2	$2\cos\varepsilon$	\dots	0	2	$2\cos\varepsilon$	\dots	0
Π_u, E_{1u} :	2	$2\cos\varepsilon$	\dots	0	-2	$-2\cos\varepsilon$	\dots	0
Δ_g, E_{2g} :	2	$2\cos 2\varepsilon$	\dots	0	2	$2\cos 2\varepsilon$	\dots	0
Δ_u, E_{2u} :	2	$2\cos 2\varepsilon$	\dots	0	-2	$-2\cos 2\varepsilon$	\dots	0
Φ_g, E_{3g} :	2	$2\cos 3\varepsilon$	\dots	0	2	$2\cos 3\varepsilon$	\dots	0
Φ_u, E_{3u} :	2	$2\cos 3\varepsilon$	\dots	0	-2	$-2\cos 3\varepsilon$	\dots	0
Γ_g, E_{4g} :	2	$2\cos 4\varepsilon$	\dots	0	2	$2\cos 4\varepsilon$	\dots	0
Γ_u, E_{4u} :	2	$2\cos 4\varepsilon$	\dots	0	-2	$-2\cos 4\varepsilon$	\dots	0
H_g, E_{5g} :	2	$2\cos 5\varepsilon$	\dots	0	2	$2\cos 5\varepsilon$	\dots	0
H_u, E_{5u} :	2	$2\cos 5\varepsilon$	\dots	0	-2	$-2\cos 5\varepsilon$	\dots	0
\vdots	\vdots	\vdots	\dots	\vdots	\vdots	\vdots	\dots	\vdots

Table 4.3: The irreducible representation Γ of $\mathcal{D}_{\infty h}(\text{EM})$ spanned by the rotational wavefunction $|J, k\rangle$ of a linear molecule in the absence of external electric and magnetic fields. The irrep depends on k , the z -axis projection in units of \hbar , of the rotational angular momentum.

k	Γ
0	Σ_g^+ (J even)
	Σ_g^- (J odd)
± 1	Π_g
± 2	Δ_g
± 3	Φ_g
\vdots	\vdots

For a linear centrosymmetric molecule, both the rotational and vibrational basis functions can be classified according to the irreps of the infinite-order $\mathcal{D}_{\infty h}(\text{EM})$. This group is defined such that the effect of the operations on the vibrational coordinates are identical to those of the point group $\mathcal{D}_{\infty h}$. It follows from the discussion given above, however, that only the operations in the MS group $\mathcal{D}_{\infty h}(\text{M})$ (corresponding to $\varepsilon = 0$ for the operations in $\mathcal{D}_{\infty h}(\text{EM})$) are relevant for determining the requirements of Fermi-Dirac and Bose-Einstein statistics. The complete ro-vibrational Hamiltonian does not commute with $\mathcal{D}_{\infty h}(\text{EM})$ operations with $\varepsilon > 0$ [189], and therefore any ro-vibrational basis function $\Phi_{J,k,v,l}$ must be invariant to them. It is seen from Table 4.2 that consequently, $\Phi_{J,k,v,l}$ can only span one of the four irreducible representations Σ_g^+ , Σ_g^- , Σ_u^+ , and Σ_u^- of the EMS group $\mathcal{D}_{\infty h}(\text{EM})$. These four irreps, Σ_g^+ , Σ_g^- , Σ_u^+ , and Σ_u^- , are also denoted e ortho, e para, f ortho and f para, in the labelling scheme of Chapter 5. The correspondence depends on whether J is even or odd and is given in Table 3.2.

The rotational and vibrational wavefunctions $\Phi_{J,k}^{\text{rot}}$ and $\Phi_{v,\ell}^{\text{vib}}$, respectively, are symmetry classified in $\mathcal{D}_{\infty h}(\text{EM})$ and there are no restrictions as to their

possible symmetries. However, the fact that the product function $\Phi_{J,k,v,l}$ must transform according to a 1D irrep introduces restrictions on the possible combinations of $\Phi_{J,k}^{\text{rot}}$ and $\Phi_{v,\ell}^{\text{vib}}$; these restrictions limit the physically useful combinations to those with $k = \ell$. For example, the vibrational state ν_5 (with vibrational basis functions $\Phi_{\nu_5=1,\ell=\pm 1}^{\text{vib}}$ of Π_u symmetry in $\mathcal{D}_{\infty h}(\text{EM})$) of $^{12}\text{C}_2\text{H}_2$ can be combined with the $\Phi_{J,k}^{\text{rot}}$ rotational wavefunctions having $(J,k) = (1,\pm 1)$ (and Π_g symmetry) to produce three ro-vibrational combinations with symmetries Σ_u^+ , Σ_u^- and Π_u in $\mathcal{D}_{\infty h}(\text{EM})$. However only the Σ_u^+ and Σ_u^- states obey nuclear spin statistics and the Π_u state must be discarded.

4.2 The Correlation of \mathcal{D}_{nh} and $\mathcal{D}_{\infty h}$ Symmetry Groups

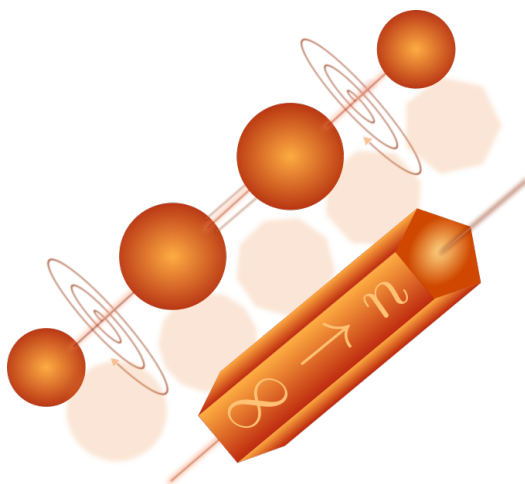


Figure 4.1: A graphical abstract to represent the substitution of n (right) for ∞ (left) in the $\mathcal{D}_{\infty h}$ point group

As illustrated in Figure 4.1, $\mathcal{D}_{\infty h}$ is the geometrical symmetry group of a smooth object, such a cylinder or centrosymmetric linear molecule, which can be rotated about its principal axis an infinite number of times without changing the apparent geometrical shape. The faces on either of its end are also equivalent. Similarly, \mathcal{D}_{nh} is the geometrical symmetry group of a regular polygon with n vertices (i.e., a regular n -gon), whose upper and lower surfaces

are equivalent, so it can be rotated n times around its principal axis with no observable change. $\mathcal{D}_{\infty h}$ can thus be thought of as the limiting case of a progression of \mathcal{D}_{nh} groups: $\mathcal{D}_{\infty h} = \lim_{n \rightarrow \infty} \mathcal{D}_{nh}$. As previously mentioned above, a large component of the work presented in this thesis is to implement an appropriate symmetry for the ro-vibrational basis functions employed in TROVE calculations. However, owing to the infinitely many operations and irreps of the $\mathcal{D}_{\infty h}$ point group, its use is impracticable. Consequently, $\mathcal{D}_{\infty h}$ is approximated by \mathcal{D}_{nh} with a suitably large arbitrary value of n . In order to do this, and to find a suitable value for n , the correlation between \mathcal{D}_{nh} and $\mathcal{D}_{\infty h}$ must first be considered.

The symmetry operations of \mathcal{D}_{nh} are listed in Table 4.4, with different operations for n even and n odd. The difference in group structure and the labelling of the irreps are caused by the fact that for n even, the point group inversion i (as should be distinguished from the spatial inversion operation E^* of the MS group) is present in \mathcal{D}_{nh} , whereas for n odd it is not. Since $i \in \mathcal{D}_{\infty h}$, in some sense an even- n \mathcal{D}_{nh} is more similar to $\mathcal{D}_{\infty h}$ than an odd- n \mathcal{D}_{nh} . It could be argued that only even- n \mathcal{D}_{nh} groups should be considered in the limit of $n \rightarrow \infty$; this is the approach that has been taken in this work (see Section 7.1.2).

Table 4.4: Symmetry operations of the \mathcal{D}_{nh} groups, for even and odd n . σ_h , σ_v and σ_d represent reflections in planes perpendicular to the molecular axis, containing the molecular axis, and bisecting the angle between a pair of C_2 axes, respectively. An improper rotation S_n^r is a rotation by $r(\frac{2\pi}{n})$ ($r = 1 \dots n - 2$) followed by a reflection in the plane perpendicular to the molecular axis and containing the nuclear center-of-mass. C_n^r represents rotations by $r(\frac{2\pi}{n})$, where $r = 1 \dots n - 1$. See Ref. [189] for further details on these symmetry operations.

Symmetry operation	Number of operations	Description
Even n :		
E	1	Identity
C_n^r	$n - 1$	Rotations about the n -fold molecular axis
C_2'/C_2''	n	n rotations by π about axes perpendicular to the molecular axis
i	1	Point group inversion
S_n^r	$n - 2$	Improper rotation (see caption)
σ_h	1	Horizontal reflection (see caption)
σ_v	$n/2$	Vertical reflection (see caption)
σ_d	$n/2$	Diagonal reflection (see caption)
Total:	$4n$	
Odd n :		
E	1	Identity
C_n^r	$n - 1$	Rotations about the n -fold molecular axis
C_2'	n	n rotations by π about axes perpendicular to the molecular axis
S_n^r	$n - 1$	Improper rotation (see caption)
σ_h	1	Horizontal reflection (see caption)
σ_v	n	Vertical reflection (see caption)
Total:	$4n$	

The character table for general \mathcal{D}_{nh} of odd n (where $n \geq 5$; \mathcal{D}_{3h} is a special case) is given in Table 4.5, and for even n (where $n \geq 4$; \mathcal{D}_{2h} is a special case)

in Table 4.6. Table 4.5 shows that an even- n \mathcal{D}_{nh} group has four 1D irreps called A_{1g} , A_{2g} , A_{1u} , and A_{2u} and $(n-2)$ 2D irreps, of which half are called E_{rg} and the other half E_{ru} ($r = 1, 2, \dots, n/2 - 1$). All of these irreps correlate with irreps of $\mathcal{D}_{\infty h}$ denoted by the same names as in Table 4.2. In addition, the even- n \mathcal{D}_{nh} group has another four 1D irreps called B_{1g} , B_{1u} , B_{2g} , B_{2u} . These B -type irreps have no counterparts in $\mathcal{D}_{\infty h}$ and so basis functions of these symmetries are unphysical in the context of approximating $\mathcal{D}_{\infty h}$ by \mathcal{D}_{nh} , and should be discarded. It was noted above that the point group inversion operation i is contained in $\mathcal{D}_{\infty h}$ and in even- n \mathcal{D}_{nh} , but not in odd- n \mathcal{D}_{nh} (the character under i gives the u/g label for ro-vibrational states). Table 4.7 gives the correspondence between the labelling of irreps of odd- n \mathcal{D}_{nh} , even- n \mathcal{D}_{nh} and $\mathcal{D}_{\infty h}$.

Table 4.5: Character table for the \mathcal{D}_{nh} group, for odd n ($n \geq 5$)^a

Irrep	k	E	$2C_n^r$ ($r = 1 \dots \frac{n-1}{2}$)	C_2'	σ_h	σ_v	$2S_n^r$ ($r = 1 \dots \frac{n-1}{2}$)
A_1'		+1	+1	+1	+1	+1	+1
A_2'		+1	+1	-1	+1	-1	+1
E_k'	1 2 ⋮ $\frac{n-1}{2}$	+2	$2 \cos(\frac{2\pi kr}{n})$	0	+2	0	$2 \cos(\frac{2\pi kr}{n})$
A_1''		+1	+1	+1	-1	-1	-1
A_2''		+1	+1	-1	-1	+1	-1
E_k''	1 2 ⋮ $\frac{n-1}{2}$	+2	$2 \cos(\frac{2\pi kr}{n})$	0	-2	0	$-2 \cos(\frac{2\pi kr}{n})$

^a For each value of r in $2C_n^r$ and $2S_n^r$ there exists two operations with the same rotation angle and character; one clockwise and one anticlockwise. This is purely convention and an alternative would be to use the operations C_n^r and S_n^r , with $r = 1 \dots n-1$, all clockwise.

Table 4.6: Character table for the \mathcal{D}_{nh} group, for even n ($n \geq 4$). The C_2 operation is included explicitly for even n here, though it can be contained within the definition for C_n^r (when $r = \frac{n}{2}$); see the footnote of Table 4.5.

Irrep	k	E	$2C_n^r$ ($r = 1 \dots \frac{n-2}{2}$)	C_2	C_2'	C_2''	i	σ_h	σ_v	σ_d	$2S_n^r$ ($r = 1 \dots \frac{n-2}{2}$)
A_{1g}		+1	+1	+1	+1	+1	+1	+1	+1	+1	+1
A_{2g}		+1	+1	+1	-1	-1	+1	+1	-1	-1	+1
B_{1g}		+1	$-i$	$-\frac{n}{2}$	+1	-1	+1	$-\frac{n}{2}$	$-\frac{n}{2}$	$+\frac{n}{2}$	$-\frac{in}{2}$
B_{2g}		+1	$-i$	$-\frac{n}{2}$	-1	+1	+1	$-\frac{n}{2}$	$+\frac{n}{2}$	$-\frac{n}{2}$	$-\frac{in}{2}$
E_{kg}	1 2 ⋮ $\frac{n}{2}-1$	+2	$2\cos(\frac{2\pi kr}{n})$	$2(-1)^k$	0	0	+2	$2(-1)^k$	0	0	$2\cos(\frac{2\pi kr}{n})$
A_{1u}		+1	+1	+1	+1	+1	-1	-1	-1	-1	-1
A_{2u}		+1	+1	+1	-1	-1	-1	-1	+1	+1	-1
B_{1u}		+1	$-i$	$-\frac{n}{2}$	+1	-1	-1	$+\frac{n}{2}$	$+\frac{n}{2}$	$-\frac{n}{2}$	$+\frac{in}{2}$
B_{2u}		+1	$-i$	$-\frac{n}{2}$	-1	+1	-1	$+\frac{n}{2}$	$-\frac{n}{2}$	$+\frac{n}{2}$	$+\frac{in}{2}$
E_{ku}	1 2 ⋮ $\frac{n}{2}-1$	+2	$2\cos(\frac{2\pi kr}{n})$	$2(-1)^k$	0	0	-2	$2(-1)^{k+1}$	0	0	$-2\cos(\frac{2\pi kr}{n})$

The general formulation of the irreducible representations of \mathcal{D}_{nh} for arbitrary n is outlined in Section 4.3 below.

4.3 Generating Operations of \mathcal{D}_{nh} Groups

All point groups can be defined in terms of generating operations, from which all operations in the group can be expressed as products of. An example in terms of C_{3v} point group operations can be found in Ref. [55]. Hegelund *et al.* [205] give the generating operations for general molecular point groups, including \mathcal{D}_{nh} (for both n even and n odd), which are also given in Table 4.8. Here, σ_h is a reflection in a horizontal plane (perpendicular to the n -fold axis),

Table 4.7: The correspondence between the g/u (gerade/ungerade) notation of the irreps of \mathcal{D}_{nh} (even n) and the $'/'$ notation of the irreps of \mathcal{D}_{nh} (odd n), based on K (the absolute value of the projection, in units of \hbar , onto the molecule-fixed z -axis of the rotational angular momentum).

K	Γ (even n)	Γ (odd n)	$\mathcal{D}_{\infty h}$ (EM)
0	A_{1g}	A_1'	Σ_g^+
	A_{1u}	A_1''	Σ_u^+
	A_{2g}	A_2'	Σ_g^-
	A_{2u}	A_2''	Σ_u^-
> 0 , even	E_{kg}	E_k'	$\Delta_g, \Gamma_g, I_g \dots$
	E_{ku}	E_k''	$\Delta_u, \Gamma_u, I_u \dots$
> 0 , odd	E_{kg}	E_k''	$\Pi_g, \Phi_g, H_g \dots$
	E_{ku}	E_k'	$\Pi_u, \Phi_u, H_u \dots$

i is the point group inversion, C_n is a rotation by $\frac{2\pi}{n}$ about the molecular z -axis, and $C_2^{(x)}$ is a rotation by π about the molecule-fixed x axis.

Table 4.8: Generating operations for the \mathcal{D}_{nh} groups (n even and n odd).

Point group	R_+	R'_+	R_-
\mathcal{D}_{nh}, n odd	C_n	σ_h	$C_2^{(x)}$
\mathcal{D}_{nh}, n even	C_n	i	$C_2^{(x)}$

All operations in a \mathcal{D}_{nh} group can be obtained as products involving three generating operations which are conventionally given the notation of R_+ , R'_+ , and R_- (the $+$ and $-$ notation here are in reference to whether the signs of L and K are kept the same ($+$) or change ($-$) under the action of the generating operations on general ro-vibrational functions, $\Psi_{rv}^{(V,L,J,K,m)}$).

In the process of expressing the elements of \mathcal{D}_{nh} in terms of the generating operations of Table 4.8, the following relations can be used:

$$\sigma^{(xz)} = C_2^{(x)} \sigma_h \quad (n \text{ odd}), \text{ and} \quad (4.5)$$

$$\sigma^{(xz)} = C_2^{(x)} C_n^{n/2} i \quad (n \text{ even}), \quad (4.6)$$

with $C_n^{n/2}$ denoting a rotation by π about the z axis.

When the transformation properties of an object under R_+ , R'_+ , and R_- are known, the transformation properties under all other operations in a \mathcal{D}_{nh} point group can be unambiguously constructed. The characters under the generating operations R_+ , R'_+ , and R_- for irreps of the \mathcal{D}_{nh} groups (odd and even n) are given in Table 4.9.

4.4 Transformation Matrices of \mathcal{D}_{nh} Groups

In practical applications of representation theory, such as the symmetry adaptation and description of ro-vibrational basis functions which are required for the work of this thesis, it is not sufficient to have the irreducible-representation characters of Table 4.9 only. The groups of matrices that constitute irreducible

Table 4.9: Irreducible representations for the D_{nh} groups and their characters under the generating operations R_+ , R'_+ and R_- .

D_{nh}	E	R_+	R'_+	R_-
(n even)		($= C_n$)	($= i$)	($= C_2^{(x)}$)
A_{1g}	1	1	1	1
A_{2g}	1	1	1	-1
B_{1g}	1	-1	1	1
B_{2g}	1	-1	1	-1
E_{rg}^a	2	$2 \cos \frac{2\pi r}{n}$	2	0
A_{1u}	1	1	-1	1
A_{2u}	1	1	-1	-1
B_{1u}	1	-1	-1	1
B_{2u}	1	-1	-1	-1
E_{ru}^a	2	$2 \cos \frac{2\pi r}{n}$	-2	0
D_{nh}	E	R_+	R'_+	R_-
(n odd)		($= C_n$)	($= \sigma_h$)	($= C_2^{(x)}$)
A'_1	1	1	1	1
A'_2	1	1	1	-1
$E'_r{}^b$	2	$2 \cos \frac{2\pi r}{n}$	2	0
A''_1	1	1	-1	1
A''_2	1	1	-1	-1
$E''_r{}^b$	2	$2 \cos \frac{2\pi r}{n}$	-2	0

^a $r = 1, 2, \dots, \frac{n}{2} - 1$. ^b $r = 1, 2, \dots, \frac{n-1}{2}$.

representations of the \mathcal{D}_{nh} group with an arbitrary finite n -value are also required; as mentioned previously, these will differ for n even and n odd. For the 1D irreps (of type A and B , in the notation of Tables 4.2 and 4.9) the 1×1 transformation matrices simply equal the character in Table 4.9 and, in general, the characters of Tables 4.6 (n even) and 4.5 (n odd). For the 2D irreps (of type E , in the notation of Table 4.2) 2×2 matrices whose traces are the characters in Tables 4.9, 4.6 and 4.5, are required. Once a set of irreducible-representation transformation matrices are known for a particular symmetry group, symmetrised basis functions (with transformation properties defined by the irreducible-representation matrices) can be determined.

The transformation matrices for the generating operations for the \mathcal{D}_{nh} (n -even and n -odd) groups are given in Table 4.10. If all operations of the \mathcal{D}_{nh} group are formulated in terms of these generating operations then the analogous matrix products of the transformation matrices of Table 4.10 can be made in order to give the corresponding transformation matrices for all operations of the \mathcal{D}_{nh} group. It is seen that the rotational basis functions $|J, 0\rangle$ and $(|J, K, +\rangle, |J, K, -\rangle)$ generate g-type symmetries of \mathbf{D}_{nh} only for n even. This is because, as explained in Section 4.5 of Ref. [189], the point group inversion i and its MS-group counterpart \hat{O}_i do not change the Euler angles, i.e., the rotational coordinates. Consequently, the rotational functions are invariant to these operations. The transformation matrices for u -type irreps have also been added to Table 4.11, which can be thought of as generated by functions $(|J, K, \pm\rangle |v_u = 1\rangle)$, where $|v_u = 1\rangle$ is the vibrational wavefunction for the fundamental level of a (probably hypothetical) vibrational mode v_u of A_{1u} symmetry.

The representation matrices are given in Table 4.11 for n even and in Table 4.12 for n odd. These matrices can be used to symmetrise the basis sets of centrosymmetric linear molecules in general nuclear-motion routines. This has been fully implemented into TROVE (see Section 7.1.2), and used in the ro-vibrational energy and intensity calculations of Chapter 8.

Table 4.10: Transformation matrices, for the \mathcal{D}_{nh} (n -even and n -odd) groups generated by the rotational basis functions $|J, 0, +\rangle = |J, 0\rangle$ for $K = 0$ and $(|J, K, +\rangle, |J, K, -\rangle)$ for $K > 0$, with $\varepsilon = 2\pi/n$.

Generating functions	Group operations			
\mathcal{D}_{nh} (n even):	E	$R_+ = C_n$	$R'_+ = i$	$R_- = C_2^{(x)}$
$ J, 0, +\rangle$	1	1	1	1
$\begin{pmatrix} J, K, +\rangle \\ J, K, -\rangle \end{pmatrix}$	$\begin{pmatrix} 1 & 0 \\ 0 & 1 \end{pmatrix}$	$\begin{pmatrix} \cos K\varepsilon & -\sin K\varepsilon \\ \sin K\varepsilon & \cos K\varepsilon \end{pmatrix}$	$\begin{pmatrix} 1 & 0 \\ 0 & 1 \end{pmatrix}$	$\begin{pmatrix} 1 & 0 \\ 0 & -1 \end{pmatrix}$
\mathcal{D}_{nh} (n odd):	E	$R_+ = C_n$	$R'_+ = \sigma_h$	$R_- = C_2^{(x)}$
$ J, 0, +\rangle$	1	1	1	$(-1)^J$
$\begin{pmatrix} J, K, +\rangle \\ J, K, -\rangle \end{pmatrix}$	$\begin{pmatrix} 1 & 0 \\ 0 & 1 \end{pmatrix}$	$\begin{pmatrix} \cos K\varepsilon & -\sin K\varepsilon \\ \sin K\varepsilon & \cos K\varepsilon \end{pmatrix}$	$\begin{pmatrix} (-1)^K & 0 \\ 0 & (-1)^K \end{pmatrix}$	$\begin{pmatrix} (-1)^J & 0 \\ 0 & -(-1)^J \end{pmatrix}$

4.5 Chapter Summary

The \mathcal{D}_{nh} and $\mathcal{D}_{\infty h}$ symmetry groups have been introduced in this chapter, along with their correspondence to each other. Character tables, generating operations and irreducible representation transformation matrices for \mathcal{D}_{nh} of general integer odd or even n have been presented. The implementation of these symmetry groups in TROVE and a numerical example for $^{12}\text{C}_2\text{H}_2$ will be presented in Section 7.1.2.

Table 4.11: Irreducible representation transformation matrices of the \mathcal{D}_{nh} group for n even, generated by the rotational basis functions $(|J, K, +\rangle, |J, K, -\rangle)$ for $K > 0$ [189]. $\varepsilon = \frac{2\pi}{n}$, r is an integer used to identify the group operations, and $1 \leq K \leq \frac{n}{2} - 1$.

	ε_r	r	E_{Kg}	E_{Ku}
E			$\begin{pmatrix} 1 & 0 \\ 0 & 1 \end{pmatrix}$	$\begin{pmatrix} 1 & 0 \\ 0 & 1 \end{pmatrix}$
C'_n	$rK\varepsilon$	$1 \dots n-1$	$\begin{pmatrix} \cos \varepsilon_r & -\sin \varepsilon_r \\ \sin \varepsilon_r & \cos \varepsilon_r \end{pmatrix}$	$\begin{pmatrix} \cos \varepsilon_r & -\sin \varepsilon_r \\ \sin \varepsilon_r & \cos \varepsilon_r \end{pmatrix}$
C'_2	$2rK\varepsilon$	$0 \dots \frac{n}{2} - 1$	$(-1)^K \begin{pmatrix} \cos \varepsilon_r & \sin \varepsilon_r \\ \sin \varepsilon_r & -\cos \varepsilon_r \end{pmatrix}$	$(-1)^K \begin{pmatrix} \cos \varepsilon_r & \sin \varepsilon_r \\ \sin \varepsilon_r & -\cos \varepsilon_r \end{pmatrix}$
C''_2	$(2r+1)K\varepsilon$	$0 \dots \frac{n}{2} - 1$	$(-1)^K \begin{pmatrix} \cos \varepsilon_r & \sin \varepsilon_r \\ \sin \varepsilon_r & -\cos \varepsilon_r \end{pmatrix}$	$(-1)^K \begin{pmatrix} \cos \varepsilon_r & \sin \varepsilon_r \\ \sin \varepsilon_r & -\cos \varepsilon_r \end{pmatrix}$
i			$\begin{pmatrix} 1 & 0 \\ 0 & 1 \end{pmatrix}$	$\begin{pmatrix} -1 & 0 \\ 0 & -1 \end{pmatrix}$
σ_h			$(-1)^K \begin{pmatrix} 1 & 0 \\ 0 & 1 \end{pmatrix}$	$-(-1)^K \begin{pmatrix} 1 & 0 \\ 0 & 1 \end{pmatrix}$
σ_v	$2rK\varepsilon$	$0 \dots \frac{n}{2} - 1$	$(-1)^K \begin{pmatrix} \cos \varepsilon_r & \sin \varepsilon_r \\ \sin \varepsilon_r & -\cos \varepsilon_r \end{pmatrix}$	$-(-1)^K \begin{pmatrix} \cos \varepsilon_r & \sin \varepsilon_r \\ \sin \varepsilon_r & -\cos \varepsilon_r \end{pmatrix}$
σ_d	$(2r+1)K\varepsilon$	$0 \dots \frac{n}{2} - 1$	$(-1)^K \begin{pmatrix} \cos \varepsilon_r & \sin \varepsilon_r \\ \sin \varepsilon_r & -\cos \varepsilon_r \end{pmatrix}$	$-(-1)^K \begin{pmatrix} \cos \varepsilon_r & \sin \varepsilon_r \\ \sin \varepsilon_r & -\cos \varepsilon_r \end{pmatrix}$
$S_n^{(r)}$	$rK\varepsilon$	$1 \dots \frac{n}{2} - 1,$ $\frac{n}{2} + 1 \dots n - 1^a$	$(-1)^K \begin{pmatrix} \cos \varepsilon_r & -\sin \varepsilon_r \\ \sin \varepsilon_r & \cos \varepsilon_r \end{pmatrix}$	$-(-1)^K \begin{pmatrix} \cos \varepsilon_r & -\sin \varepsilon_r \\ \sin \varepsilon_r & \cos \varepsilon_r \end{pmatrix}$

^a $r = 0$ and $r = n/2$ are omitted from this list because $S_n^{(0)} = \sigma_h$ and $S_n^{(n/2)} = i$.

Table 4.12: Irreducible representation transformation matrices of the \mathcal{D}_{nh} group for n odd, generated by the rotational basis functions ($|J, K, +\rangle, |J, K, -\rangle$) for $K > 0$ [189]. E'_K and E''_K functions have even and odd K , respectively (Table 4.7), and so the present table has been simplified accordingly. $\varepsilon = \frac{2\pi}{n}$, r is an integer used to identify the group operations, and $1 \leq K \leq \frac{n-1}{2}$.

	ε_r	r	E'_K	E''_K
E			$\begin{pmatrix} 1 & 0 \\ 0 & 1 \end{pmatrix}$	$\begin{pmatrix} 1 & 0 \\ 0 & 1 \end{pmatrix}$
C_n^r	$rK\varepsilon$	$1 \dots n-1$	$\begin{pmatrix} \cos \varepsilon_r & -\sin \varepsilon_r \\ \sin \varepsilon_r & \cos \varepsilon_r \end{pmatrix}$	$\begin{pmatrix} \cos \varepsilon_r & -\sin \varepsilon_r \\ \sin \varepsilon_r & \cos \varepsilon_r \end{pmatrix}$
C_2'	$rK\varepsilon$	$0 \dots n-1$	$(-1)^J \begin{pmatrix} \cos \varepsilon_r & \sin \varepsilon_r \\ \sin \varepsilon_r & -\cos \varepsilon_r \end{pmatrix}$	$(-1)^J \begin{pmatrix} \cos \varepsilon_r & \sin \varepsilon_r \\ \sin \varepsilon_r & -\cos \varepsilon_r \end{pmatrix}$
σ_h			$\begin{pmatrix} 1 & 0 \\ 0 & 1 \end{pmatrix}$	$\begin{pmatrix} -1 & 0 \\ 0 & -1 \end{pmatrix}$
σ_v	$rK\varepsilon$	$0 \dots n-1$	$(-1)^J \begin{pmatrix} \cos \varepsilon_r & \sin \varepsilon_r \\ \sin \varepsilon_r & -\cos \varepsilon_r \end{pmatrix}$	$(-1)^J \begin{pmatrix} \cos \varepsilon_r & \sin \varepsilon_r \\ \sin \varepsilon_r & -\cos \varepsilon_r \end{pmatrix}$
$S_n^{(r)}$	$rK\varepsilon$	$1 \dots n-1$	$\begin{pmatrix} \cos \varepsilon_r & -\sin \varepsilon_r \\ \sin \varepsilon_r & \cos \varepsilon_r \end{pmatrix}$	$\begin{pmatrix} \cos \varepsilon_r & -\sin \varepsilon_r \\ \sin \varepsilon_r & \cos \varepsilon_r \end{pmatrix}$

Chapter 5

MARVEL Analysis of the Ro-vibrational Energy Levels of $^{12}\text{C}_2\text{H}_2$

Experimentally determined rotation-vibration energy levels provide an important component of the calculations of ro-vibrational spectra in order to implement the semi-empirical methods that are typically employed by the ExoMol group. This includes the refinement of the potential energy surface to experimental data (see Section 9.2), the empirical basis set correction (EBSC), which involves a shifting of band centres to experimental values (see Section 9.3), and in the comparison of *ab initio* results to experimental data to enable a determination of accuracy, often termed “obs-calc”¹ (see Chapter 8).

The work outlined in this chapter is based on the publication of Chubb *et al.* [56] and constitutes the largest compilation and analysis of published experimental data on rotation-vibration transitions for the ground electronic states of the main isotopologue of acetylene, $^{12}\text{C}_2\text{H}_2$. 37,813 measured transitions from 60 publications are considered. The analysis has resulted in the determination of 6013 *ortho* and 5200 *para* rotation-vibration energy levels for $^{12}\text{C}_2\text{H}_2$ using the Measured Active Rotational-Vibrational Energy Levels

¹This is shorthand for “observation minus calculation”, which is often shortened further to “o-c”.

(MARVEL) technique. The distinct networks linking *ortho* and *para* states are considered separately, with 20,717 *ortho* and 17,096 *para* transitions verified. The MARVEL results are compared with alternative compilations based on the use of effective Hamiltonians.

The underlying theory used for the MARVEL study is outlined in Section 5.1. Section 5.2 presents and discusses the experimental sources used. Results are given in Section 5.3 and discussed in Section 5.4, along with comparisons with recent empirical databases from Amyay *et al.* [46] (henceforth 16AmFaHe), Lyulin and Campargue [45] (henceforth 17LyCa) and Lyulin and Perevalov [44] (henceforth 17LyPe), which builds on their earlier work [210], all of which only became available while the present study was being undertaken. This is followed by a summary in Section 5.7 and the structure of the supplementary data in Section 5.8, which is included as part of the publication associated with this chapter [56].

5.1 MARVEL Theory

The Measured Active Rotational-Vibrational Energy Levels (MARVEL) procedure [211, 212] is based on the theory of spectroscopic networks [213, 214] and is principally based on earlier work by Flaud *et al.* [215] and Watson [216, 217]. MARVEL can be used to critically evaluate and validate experimentally-determined transition wavenumbers and uncertainties collected from the literature. It inverts the wavenumber information to obtain accurate energy levels with an associated uncertainty. MARVEL has been successfully used to evaluate the energy levels for molecules, such as $^{12}\text{C}_2$ [218], $^{48}\text{Ti}^{16}\text{O}$ [219], water vapour [220, 221, 222, 223, 224], H_3^+ [225], H_2D^+ and D_2H^+ [226], $^{14}\text{NH}_3$ [227, 228], and $^{12}\text{C}_2\text{H}_2^{16}\text{O}$ [229]. To be useful for MARVEL, measured transitions must have an associated uncertainty and be assigned. This means that each energy level resulting from the study must possess a unique set of quantum numbers. It should be noted that while MARVEL requires uniqueness it does not require these quantum numbers to be strictly correct, or indeed

even meaningful, beyond obeying rigorous selection rules; these assignments simply act as labels for each state. Nevertheless, it greatly aids comparisons with other data if sensible values are used.

The theory behind the MARVEL procedure will be summarised here, with a full account given in Refs. [211, 212, 215]. The input to the MARVEL algorithm is the set of experimental data which has been collected from the literature, and should include the transition wavenumber (line position), associated uncertainty, and labelled upper and lower energy levels. It also needs to contain a unique reference tag, so that a line of data relating to a particular transition is identifiable. Using this information, a series of linear equations is built, with each equation of the form:

$$\sigma_i = E_{j1(i)} - E_{j2(i)}, \quad (5.1)$$

where σ_i is the transition wavenumber and $E_{j1(i)}$ and $E_{j2(i)}$ are the associated upper and lower energy levels, respectively. The measurement uncertainty associated with a given transition is given by δ_i . All terms are typically in units of wavenumbers (cm^{-1}). Generally, the number of transitions, N_t is much larger than the number of energy levels to be determined, N_l , leading to an over-determined system of linear equations. This series of linear equations is converted to matrix form and a weighted least squares fitting method is used to determine the experimental values of the energy levels, E_j^{exp} , with the weights, g_i , initially related to the uncertainties in the measurements, δ_i , via

$$g_i = \frac{1}{\delta_i^2}. \quad (5.2)$$

As the procedure iterates, a robust weighting algorithm is used [216], with the weights updated each time:

$$g_i = \frac{1}{\delta_i^2 + \alpha \Delta_i^2}. \quad (5.3)$$

Here, α is a positive number ($\leq \frac{1}{3}$), chosen for the given problem [211], and Δ_i is the difference between the original measured transition, σ_i , and the computed

transition:

$$\Delta_i = \sigma_i - (E_{j1(i)}^{exp} - E_{j2(i)}^{exp}). \quad (5.4)$$

This leads to an uncertainty associated with each determined energy level; if $\Delta_i > \delta_i$, then MARVEL outputs suggestions for updates to the measured uncertainty δ_i , based on Δ_i . If this is an acceptably small increase then the new value should replace the original in the MARVEL input and the procedure run again. If $\Delta_i \gg \delta_i$, then it is likely that the transition has either been misassigned or the line position is incorrect; in this case the line in the input file should be removed (a minus sign in front of the transition will indicate that MARVEL should ignore that line of data) and MARVEL should be run again in order to get a new set of experimentally determined energy levels and associated uncertainties. The data set is said to be self-consistent when $\Delta_i \leq \delta_i$, for all i , i.e. when all transitions and deduced energy levels in the data-set are in agreement with one another.

5.1.1 Quantum Number Labelling

The quantum number assignments that were used in the MARVEL analysis are all outlined in Section 3.1 and summarised in Table 3.1. Sections 3.3, 3.4, 3.2 and 3.5 give further details. It should be noted that for a linear molecule such as acetylene, K is also equal to the total vibrational angular momentum quantum number, $|L| = |\ell_4 + \ell_5|$ (within the $(3N - 5)$ approach; see Section 7.1), and therefore K is sometimes also referred to as the total vibrational angular momentum. It was therefore only necessary to include one of these two labels, K , in the MARVEL analysis. All other quantum number labels in the MARVEL analysis are given in the same order as in Table 3.1. The assignments were taken from the original data sources where possible, with any exceptions noted in Section 5.2.1 and 5.2.2: particular reference should be made to the general comments (1a) and (1b) in Section 5.2.2. The symmetry labels of the vibrational states ($\Sigma_{u/g}^{+/-}$, $\Pi_{u/g}$, $\Delta_{u/g}$, ...; see Section 3.2) have been added to the end of the output energy files (see Table 5.5 and the supplementary material of the publication associated with this chapter [56]) to further aid

comparisons of the data against other sources.

5.2 Experimental Sources

The spectroscopy of acetylene has long been studied in the laboratory and a large number of experimentally determined transition frequencies can therefore be found in the literature for the main isotopologue, $^{12}\text{C}_2\text{H}_2$. As part of this study a rigorous and comprehensive search for all useable spectroscopic data for $^{12}\text{C}_2\text{H}_2$ was undertaken. This includes the transition frequency (in cm^{-1}) and associated uncertainty, along with quantum number assignments for both the upper and lower energy states. A unique reference label is assigned to each transition, which is required for MARVEL input. This reference indicates the data source, table (or page) and line number that the transition originated from. The data source tag is based on the notation employed by the IUPAC task group on water [221, 230] with an adjustment discussed below. The associated uncertainties were taken from the experimental data sources where possible, but it was necessary to increase many of these in order to achieve consistency with the same transition in alternative data sources. As noted by Lyulin and Perevalov [210], these sources often provide overall uncertainties for the strongest lines in a vibrational band which may underestimate the uncertainty associated with some or all of the weaker lines. It is also possible that some transitions have been misassigned or are due to blended lines, which will have a shifted transition wavenumber value. Herman and co-workers have presented a number of reviews of the behaviour of acetylene in $X^1\Sigma_g^+$ ground electronic state [52, 53, 54], which were particularly useful in this collation of data. Besides summarising the status of rotation-vibration spectroscopy of the system, these reviews also give insight into the internal dynamics of the system.

60 sources of experimental data were considered in this MARVEL study. Two of the data compilations mentioned in the introduction to this chapter [46, 45] contain data from multiple other sources, some of which were not

Table 5.1: Extract from the MARVEL input file for the *ortho* transitions. The full file is supplied as part of the supplementary information of the associated publication [56]. All transition energy term values and uncertainties (unc) are in units of cm^{-1} .

Energy	Unc	Upper assignment	Lower assignment	Ref
1248.2620	0.0005	0 0 0 1 1 1 -1 0 34 e ortho	0 0 0 0 0 0 0 0 35 e ortho	00Vander_11
1252.8546	0.0005	0 0 0 1 1 1 -1 0 32 e ortho	0 0 0 0 0 0 0 0 33 e ortho	00Vander_12
1257.4230	0.0005	0 0 0 1 1 1 -1 0 30 e ortho	0 0 0 0 0 0 0 0 31 e ortho	00Vander_14
1261.9694	0.0005	0 0 0 1 1 1 -1 0 28 e ortho	0 0 0 0 0 0 0 0 29 e ortho	00Vander_16
1266.4970	0.0005	0 0 0 1 1 1 -1 0 26 e ortho	0 0 0 0 0 0 0 0 27 e ortho	00Vander_18
1271.0098	0.0005	0 0 0 1 1 1 -1 0 24 e ortho	0 0 0 0 0 0 0 0 25 e ortho	00Vander_110
1275.5122	0.0005	0 0 0 1 1 1 -1 0 22 e ortho	0 0 0 0 0 0 0 0 23 e ortho	00Vander_111

directly available. Data taken from these compilations are given a tag based on that used in the compilation along with the original reference given in Table 5.2. After processing, 59 sources were used in the final data set. The data from more recent papers are generally provided in digital format, but those from some of the older papers had to be processed through digitalisation software, or even manually entered in the worst cases. After digitalisation the data were converted to MARVEL format; an example of the input file in this format is given in Table 5.1; the full file can be found in the supplementary data of the associated publication [56].

Table 5.2 gives a summary of all the data sources used in this work, along with the wavelength range, number of transitions, number of vibrational bands, the approximate temperature of the experiment and comments, which can be found in Section 5.2.1. Table 5.3 gives those data sources which were considered but not used, with comments on the reasons. The reference label given in these tables corresponds to the unique labels in the MARVEL input files, given in the supplementary data of Ref. [56] and illustrated in the last column of Table 5.1. As transitions do not occur between *ortho* and *para* states, they form two completely separate components of the main spectroscopic network, with no links between them. All input and output files supplied in the supplementary

data to the associated publication of this work [56] are split into either *ortho* or *para*.

Table 5.2: Data sources used in this study with wavelength range, numbers of transitions and approximate temperature of the experiment. A/V stands for the number of transitions analysed/verified. 'RT' stands for room temperature. See section 5.2.1 for the notes.

Tag	Ref.	Range (cm ⁻¹)	A/V	Bands	Temp	Note
09YuDrPe	[231]	29-55	20/20	5	RT	
16AmFaHe_kab91	[232]	61-1440	3233/3233	47	RT	
16AmFaHe_amy10	[233]	63-7006	1232/1232	36	RT	
11DrYu	[234]	85-92	20/20	7	RT	
17JaLyPe	[235]	429-592	627/627	9	RT	
81HiKa	[236]	628-832	684/684	5	RT	(3a)
93WeBlNa	[237]	632-819	1610/1609	13	RT	(3b)
00MaDaCl	[238]	644-820	77/77	1	RT	
01JaClMa	[239]	656-800	355/355	4	RT	
50BeNi	[240]	671-4160	500/0	13	RT	(3c)
16AmFaHe_gom10	[241]	1153-1420	27/27	3	RT	
16AmFaHe_gom09	[242]	1247-1451	66/66	8	RT	
00Vander	[243]	1248-1415	64/64	2	RT	
16AmFaHe_amy09	[91]	1253-3422	3791/3777	57	Up to 1455 K	(3d)
03JaMaDa	[177]	1810-2235	486/486	14	RT	
03JaMaDab	[244]	3207-3358	109/109	2	RT	
16AmFaHe_jac02	[180]	1860-2255	150/150	3	RT	
72Pliva	[192]	1865-2598	1016/1015	15	RT	
16AmFaHe_ber98	[245]	1957-1960	19/19	1	RT	(3e)
16AmFaHe_jac07	[246]	2515-2752	148/148	3	RT	
16AmFaHe_pal72	[247]	2557-5313	42/42	3	RT	
16AmFaHe_vda93	[248]	2584-3364	499/499	5	RT	
93DcSaJo	[249]	2589-2760	372/372	3	RT	
82RiBaRa	[87]	3140-3399	1789/1788	21	RT and 433 K	
16AmFaHe_sarb95	[250]	3171-3541	401/401	8	RT	
06LyPeMa	[251]	3182-3327	167/167	13	RT	

Table 5.2: Data sources used in this study with wavelength range, numbers of transitions and approximate temperature of the experiment. A/V stands for the number of transitions analysed/verified. 'RT' stands for room temperature. See section 5.2.1 for the notes.

Tag	Ref.	Range (cm ⁻¹)	A/V	Bands	Temp	Note
16AmFaHe_man05	[252]	3185-3355	288/288	5	RT	
16AmFaHe_sara95	[253]	3230-3952	424/424	5	RT	
16AmFaHe_ber99	[254]	3358-3361	21/21	1	RT	(3e)
16AmFaHe_lyub07	[255]	3768-4208	668/668	8	RT	
16AmFaHe_gir06	[256]	3931-4009	91/91	10	RT	
16AmFaHe_dcu91	[257]	3999-4143	251/251	6	RT	
72BaGhNa	[258]	4423-4791	472/408	8	RT	(3f)
16AmFaHe_lyua07	[259]	4423-4786	440/440	8	RT	
16AmFaHe_lyu08	[183]	5051-5562	320/320	7	RT	
16AmFaHe_kep96	[260]	5705-6862	1957/1957	30	RT	
17LyCa	[45]	5852-8563	4941/4941	108	RT	(3g)
16AmFaHe_rob08	[261]	5885-6992	568/568	20	RT	
07TrMaDa	[262]	6299-6854	546/546	13	RT	(3h)
16AmFaHe_lyu09	[263]	6300-6666	89/89	5	RT	
16KaNaVa	[264]	6386-6541	19/19	2	RT	(3i)
16AmFaHe_kou94	[265]	6439-6629	73/73	1	RT	
15TwCiSe	[266]	6448-6564	135/135	2	RT	
02HaVa	[267]	6448-6685	271/271	4	RT	
77BaGhNa	[268]	6460-6680	860/859	15	RT	(3j)
05EdBaMa	[269]	6472-6579	41/41	1	RT	
13ZoGiBa	[270]	6490-6609	37/37	1	RT	
00MoDuJa	[271]	6502-6596	36/36	1	RT	
96NaLaAw	[272]	6502-6596	36/36	1	RT	
16AmFaHe_amy11	[273]	6667-7868	2259/2256	79	RT	(3k)
15LyVaCa	[184]	7001-7499	2471/2471	29	RT	(3l)
09JaLaMa	[274]	7043-7471	233/233	4	RT	
02VaElBr	[275]	7062-9877	626/626	11	RT	(3m)
16LyVaCa	[276]	8283-8684	627/627	14	RT	(3n)
17BeLyHu	[277]	8994-9414	432/432	11	RT	

Table 5.2: Data sources used in this study with wavelength range, numbers of transitions and approximate temperature of the experiment. A/V stands for the number of transitions analysed/verified. 'RT' stands for room temperature. See section 5.2.1 for the notes.

Tag	Ref.	Range (cm ⁻¹)	A/V	Bands	Temp	Note
89HeHuVe	[278]	9362-10413	657/657	14	RT	(3o)
93SaKa	[279]	12428-12538	91/73	1	RT	(3p)
03HeKeHu	[181]	12582-12722	60/60	1	RT	
92SaKa	[280]	12904-13082	216/212	3	RT	(3q)
94SaSeKa	[281]	13629-13755	53/53	1	<RT (223 K)	(3r)
Total		29-13755	37813/37206			

Table 5.3: Data sources considered but not used in this work.

Tag	Ref.	Comments
16AmFaHe_abb96	[282]	0 transitions in 16AmFaHe; data not available in original paper.
16AmFaHe_eli98	[283]	0 transitions in 16AmFaHe; data not available in original paper.
72Plivaa	[284]:	Energy levels only
02MeYaVa	[285]	No suitable data
01MeYaVa	[286]	No suitable data
99SaPeHa	[287]	No suitable data
97JuHa	[288]	No suitable data
93ZhHa	[289]	No suitable data
93ZhVaHa	[290]	No suitable data
91ZhVaKa	[291]	No suitable data
13SiMeVa	[292]	No suitable data
83ScLeKl	[293]	No assignments given

5.2.1 Comments on the Experimental Sources in Table 5.2

(3a) 81HiKa [236] has an apparent misprint in column 2 of their Table 6: the R(19) line should be 780.2601 cm^{-1} not 790.2601 cm^{-1} , as confirmed by 01JaClMa [239], and in column 5 of their Table 4: the Q(3) line should be 728.9148 cm^{-1} not 729.9148 cm^{-1} , also confirmed by 01JaClMa [239].

(3b) 93WeBlNa_page14_l38 from 93WeBlNa [237] is not consistent with other data sources. It was marked in the original dataset as a transition that the authors did not include in their analysis and so was removed from the present dataset.

(3c) 50BeNi [240] was deemed too unreliable to use in the final dataset: data are directly contradicted by other sources.

(3d) Many of the transitions included from 16AmFaHe_amy09 [91] are not duplicated in any other source. While this means they represent a valuable source of data, and have thus been kept in the MARVEL dataset, the fact that there is no other experimental data to back them up means they should be treated with some degree of caution. As stated in the original paper, modelling such a high temperature region is a challenge. There are a small number of transitions - 14 out of 3791 - that do not match those from other data sources and were removed from the present dataset.

(3e) Note that 16AmFaHe_ber98 [245] and 16AmFaHe_ber99 [254] are Raman spectra and so the transitions do not follow the selection rules detailed in Section 3.5 of this paper.

(3f) 72BaGhNa [258] has a band labelled $(0013^10^0)^1 - (0001^10^0)^1$ (see Section 3.1 for this quantum number labelling definition) which is not consistent with other data sources. After MARVEL analysis it was found that the band labelled $(0104^01^1)^1 - (0001^10^0)^1$ gave energies consistent with those labelled $(0013^10^0)^1 - (0001^10^0)^1$ in other data sources (16AmFaHe_lyua07, 16AmFaHe_lyu08). Bands including $(0104^01^1)^1$ are not present in other data sources. The labelling of these bands were swapped accordingly. All other

bands from this dataset were included, with the exception of the single transition labelled 72BaGhNa_table2_c2_l32, which was not consistent with other datasets.

(3g) 17LyCa [45] provides a collection of data recorded in Grenoble using cavity ring down spectroscopy from several papers. 15LyVaCa (FTS15 in the notation of 17LyCa) [184], 16LyVaCa (FTS16) [276] and 17BeLyHu (FTS17) [277] were all already included as separate files in the present dataset and so were removed from the 17LyCa [45] dataset. The remaining data, CRDS13 [294], CRDS14 [295] and CRDS16 [296] are all included in the final dataset with the tag '17LyCa'. See comment (3l).

(3h) 07TrMaDa [262] contained a band labelled $2\nu_2 + (\nu_4 + 3\nu_5)_+$. ℓ_4 and ℓ_5 were assigned as 1 and -1 respectively, to be consistent with the labelling of 16AmFaHe_kep96.

(3i) Full data for 16KaNaVa [264] was provided in digital format from the corresponding author (private communication, Juho Karhu).

(3j) 77BaGhNa_table3_l205 of 77BaGhNa [268] does not fit with the same transition in two other sources.

(3k) 16AmFaHe_amy11 [273] includes a band $((1000^06^6) - (0000^00^0)^0)$ which has transitions from $J = 0$ to $J = 10, 11, 12$. These are not physical and so were removed from the dataset. There is one other transition which was removed which was found to be inconsistent with the other datasets.

(3l) There were previously some differences in the authors approach to labelling levels for 15LyVaCa [184] and 17LyCa [45], see comment (3g) (Alain Campargue, private communication). This was partly to allow all bands to have unique labelling, as duplicate labels were provided in 15LyVaCa as indicated by ** or * superscripts. These bands were relabelled to fit with other data sources, for example 16AmFaHe_amy11 [273]. The authors of 17LyCa have since made amendments to their published dataset (Alain Campargue, private communication). Table 5.4 summarises the changes in labelling between 15LyVaCa, the current version of 17LyCa_FTS15 (see supplementary

data of [45]) and this work.

(3m) 02VaElBr [275] is missing one band labelling in the footnote to their Table 3. The missing label for the penultimate level is $I = (v_1v_2v_3v_4^l v_5^l)^K = (0020^0 1^1)^1$. Full data was provided in digital format from the corresponding author (Jean Vander Auwera, private communication).

(3n) 16LyVaCa [276] has duplicate lines in the $(1110^0 0^0)^0$ band. Those which were inconsistent with other sources were removed and thus not included in the final data set. It is possible that they should be re-assigned.

(3o) The assignments given for the band labelled $(0122^0 2^0)^0 - (0000^0 0^0)^0$ in 89HeHuVe [278] require the upper state to have the parity of an f-level, which is unphysical if both $\ell_4=0$ and $\ell_5=0$. There can be no e/f splitting in this case. It was assumed that this upper state should be labelled $(0122^2 2^{-2})^0$. These reassigned transitions were amended and included in the present dataset.

(3p) Table 1 of 93SaKa [279] has duplicates for the $e \leftrightarrow e$ transitions in the $(2021^1 0^0)^1 - (0000^0 1^1)^1$ vibrational band. Those which are inconsistent with other sources were removed and thus not included in the final data set.

(3q) 92SaKa [280] contains some duplicate lines which have been assigned identical quantum numbers. Those which are inconsistent with other sources were removed and thus not included in the final data set.

(3r) 94SaSeKa [281] gives two tables of data but only one is assigned with vibrational quantum numbers, so data from the other table was not considered as part of this work.

Table 5.4: Changes in labelling between 15LyVaCa [184], 17LyCa_FTS15 [45] and this work, in the form $(v_1v_2v_3v_4^l v_5^l)^K$. See comment (3l) in the text.

15LyVaCa	17LyVa_FTS15	This work
$(0204^2 1^{-1})^{1**}$	$(0113^1 0^0)^1$	$(0204^1 1^0)^1$
$(0113^1 0^0)^1$	$(0204^0 1^1)^1$	$(0113^1 0^0)^1$
$(1102^0 1^1)^1$	$(1102^0 1^1)^1$	$(1102^1 1^0)^1$

$(1102^2 1^{-1})^{1**}$	$(0202^2 3^{-1})^1$	$(1102^0 1^1)^1$
$(1102^2 1^{-1})^{1*}$	$(1102^2 1^{-1})^1$	$(1102^2 1^{-1})^1$

5.2.2 General Comments

A number of general issues had to be dealt with before consistent networks could be obtained.

(1a) 16AmFaHe [46] released a collation and analysis of experimental data in the middle of the collation and analysis stage of this work. The entire database was formatted into MARVEL format so it could subsequently be run through the software and combined with the other experimental sources in the MARVEL dataset. Some of the experimental sources featured in the 16AmFaHe database paper had already been collated and formatted to MARVEL format prior to its publication. These are 03JaMaDa [177], 91KaHeDi [232], 06LyPeMa [251], 07LyPeGu [259], 82RiBaRa [87], 02VaElBr [275] and 00MoDuJa [271]. The data included in the present study come from the original datasets for these papers and not from 16AmFaHe. A few of the sources that were cited in 16AmFaHe were not included in the final dataset of this work. There were 0 transitions in 16AmFaHe from Refs. [282] (abb96), [283] (eli98) or [234] (drou11); the data for Ref. [234] were taken from the original paper (see 11DrYu in Table 5.2), but there were no data obviously available in the original papers for the other two sources. The quantum number labelling was kept consistent with that of 16AmFaHe as much as possible (see comment (1b) for an exception).

(1b) Many of the ℓ_4 and ℓ_5 assignments were either inconsistent between different sources, were not given in the original data (often only the total $K = |\ell_4 + \ell_5|$ is given), or were inconsistent between data in the same dataset. For example, the bands with upper energies labelled $(v_1 v_2 v_3 v_4^{\ell_4} v_5^{\ell_5})^K = (0002^* 1^*)^1$, $(1102^* 1^*)^1$ or $(0102^* 1^*)^1$ in 16AmFaHe. Using simple combination differences, with the known lower value and given transition wavenumber, there was found to be more than one value for the upper energy. It is assumed

that this duplication of quantum numbers for different states is down to the different method of analysis used in 16AmFaHe, which does not require a completely unique set. For example, for the upper level $(1102^2 1^{-1})^1$, $J=2$, e , there are two transitions which give as upper energy level of 7212.93 cm^{-1} (from 16AmFaHe_kep96) and three that give 7235.29 cm^{-1} (from 16AmFaHe_vda02 and 16AmFaHe_rob08). These same two energies can be found in multiple other sources (07TrMaDa, 15LyVaCa, 77BaGhNa, 02VaElBr), but the ℓ_4 and ℓ_5 assignment was inconsistent for states of the same upper energy. The decision was made to batch them together and assign the first energy level (7212.94 cm^{-1} in this example) as $(1102^2 1^{-1})^1$ and the second (7235.29 cm^{-1} in this example) as $(1102^0 1^1)^1$. The same logic was applied to other bands with $K = |\ell_4 + \ell_5| = 1$.

(1c) The e/f notation (see Section 3.3) was mostly specified in experimental papers, but some required additional investigation in order to assign them in such a way as to be consistent with other papers. The c/d notation in Ref. [192], for example, is analogous to the e/f notation used in this work.

(1d) All transitions which were considered but not processed in the final dataset are labelled with `_ct` at the end of the reference and have a minus sign in front of the transition frequency, at the start of the file. MARVEL software ignores any line with a negative wavenumber.

(1e) The *ortho/para* notation was often not specified in the experimental papers, but can easily be determined via the logic of Section 3.4.

5.2.3 Other Comments

The following are sources of the acetylene data in the HITRAN database up to HITRAN-2012 ([244, 132, 297, 298]): 16AmFaHe_gom09 [242], 16AmFaHe_gom10 [241], 96NaLaAw [272], 05EdBaMa [269], 16AmFaHe_lyua07 [259], 16AmFaHe_jac07 [246], 16AmFaHe_jac09 [274], 00Vander [243], 02HaVa [267], 03JaMaDab [244], 16AmFaHe_kab91 [232], 72Pliva [192], 03JaMaDa [177], 82RiBaRa [87], 16AmFaHe_vda93 [248].

Additional data included in HITRAN-2016 [176], which was released after the work undertaken in this Chapter, are: 16LyPe [210], 11DrYu [234], 17JaLyPe [235] (with 17LyCa [45] under consideration for future inclusion [176]).

5.3 Results

The MARVEL website (<http://kkrk.chem.elte.hu/marvelonline>) has a version of MARVEL which can be run online. The variable NQN (number of quantum numbers) is 11 in the case of acetylene, given in Table 3.1. These are required for both the lower and upper levels, as illustrated in Table 5.1.

All energies are measured from the zero point energy (ZPE). This is the energy of the ground ro-vibrational state, which is given a relative energy of 0 and is included in the *para* set of energy levels. The *ortho* set of energies therefore needs a ‘magic number’ to be added to all the MARVEL *ortho*-symmetry energies. Here the magic number was taken as the ground vibrational $(0000^00^0)^0$, $J = 1$ state of 16AmFaHe [46] who determined the value $2.3532864 \text{ cm}^{-1}$, see Table 5.7 below. The output for the *ortho* energies in the supplementary data of [56], and the extract of the output file in Table 5.5, all have this magic number added for the main spectroscopic network. The main spectroscopic network in the *para* output does not require a magic number as it contains the ground ro-vibrational level, $(0000^00^0)^0$, $J = 0$. There are a small number (284 for *ortho* and 119 for *para*) of energy levels which are not joined to the main network. If more experimental transitions became available in the future it would be possible to link these to the main network.

A total of 37,813 transitions were collated and considered (20,717 *ortho* and 17,096 *para*) from the data sources detailed in Section 5.2. Of those 607 were found to be inconsistent with others (353 *ortho* and 254 *para*) and thus removed from the final data set, leaving a total of 37,206 transitions used as input into MARVEL (20,364 *ortho* and 16,842 *para*). A plot of energy as a function of rotational quantum number, J , was made for each vibrational band as a check that quantum numbers had been assigned consistently. Figures 5.1

Table 5.5: Extract from the MARVEL output file for the *ortho* transitions. The full file is supplied as part of the supplementary information to the associated publication [56]. All energy term values and uncertainties are in units of cm^{-1} .

Assignment										Energy	Unc	Num Trans	u/g	Symmetry		
0	0	0	0	0	0	0	0	0	1	e	ortho	2.35329	0.00003	204	g	sigma_g_plus
0	0	0	0	0	0	0	0	0	3	e	ortho	14.11952	0.00002	289	g	sigma_g_plus
0	0	0	0	0	0	0	0	0	5	e	ortho	35.29793	0.00002	306	g	sigma_g_plus
0	0	0	0	0	0	0	0	0	7	e	ortho	65.88710	0.00002	298	g	sigma_g_plus
0	0	0	0	0	0	0	0	0	9	e	ortho	105.88501	0.00002	306	g	sigma_g_plus
0	0	0	0	0	0	0	0	0	11	e	ortho	155.28899	0.00002	306	g	sigma_g_plus
0	0	0	0	0	0	0	0	0	13	e	ortho	214.09576	0.00002	306	g	sigma_g_plus
0	0	0	0	0	0	0	0	0	15	e	ortho	282.30144	0.00002	310	g	sigma_g_plus
0	0	0	0	0	0	0	0	0	17	e	ortho	359.90150	0.00002	294	g	sigma_g_plus
0	0	0	0	0	0	0	0	0	19	e	ortho	446.89078	0.00003	282	g	sigma_g_plus
0	0	0	0	0	0	0	0	0	21	e	ortho	543.26353	0.00002	274	g	sigma_g_plus
0	0	0	1	1	0	0	1	1	1	e	ortho	614.04436	0.00018	98	g	pi_g
0	0	0	1	1	0	0	1	2	2	f	ortho	618.77696	0.00013	133	g	pi_g

and 5.2 show this for each vibrational band, for the *ortho* and *para* states respectively. Figures 5.3 and 5.4 illustrate the *ortho* and *para* components of the principal spectroscopic network, respectively. The nodes are energy levels and the edges the transitions between them, with the colours representing Num Trans, the number of transitions linked to each energy level. These figures were produced using algorithms from gephi, an open source network visualisation software [299]. Different algorithms can be used to present these networks in a variety of ways. Figure 5.5, for example, gives alternative representations of the structure of the experimental spectroscopic network. These figures highlight the intricate relationships between different energy levels and illustrate how the variety of sources collated in this work link together. If transition intensities were to be included as weights in the spectroscopic network it could aid in the determination of transitions which should preferentially be investigated in new experiments [213].

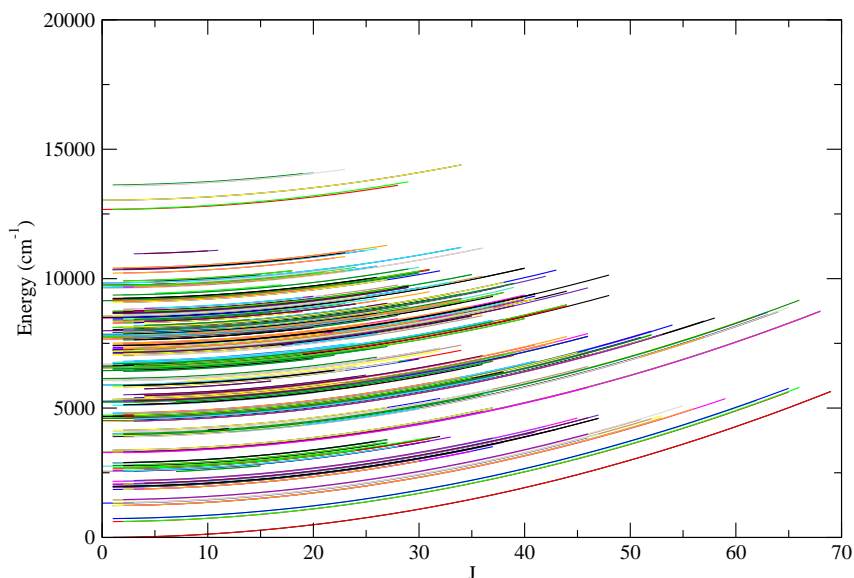


Figure 5.1: MARVEL energy levels (cm^{-1}) as a function of rotational quantum number, J , for all the vibrational energy bands in the *ortho* component of the principal spectroscopic network analysed in this paper.

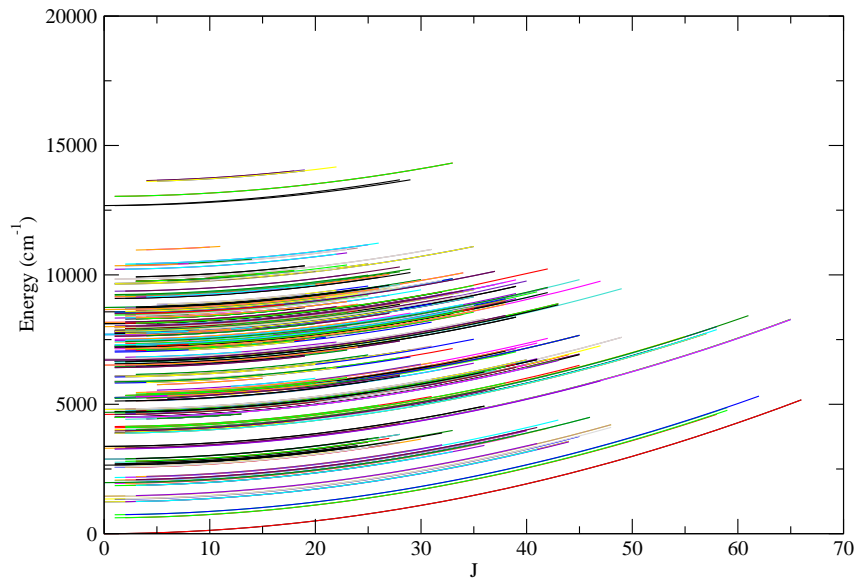


Figure 5.2: MARVEL energy levels (cm^{-1}) as a function of rotational quantum number, J , for all the vibrational energy bands in the *para* component of the principal spectroscopic network analysed in this paper.

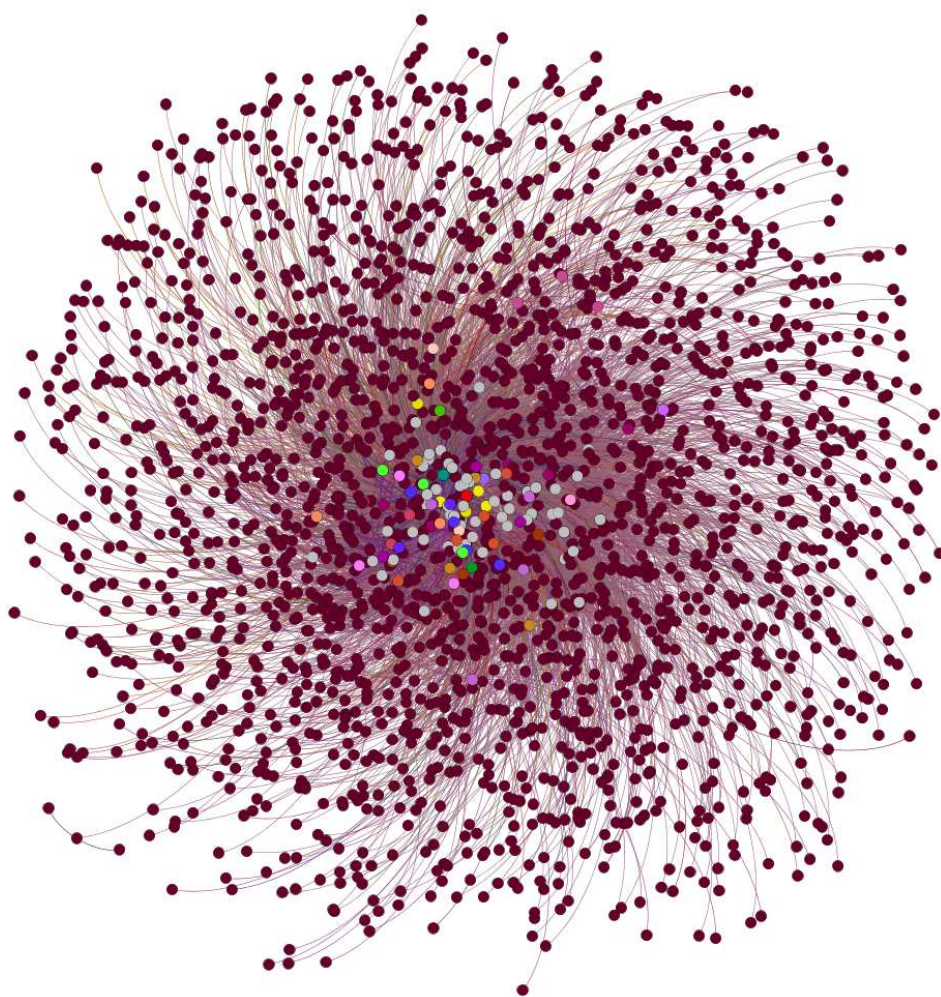


Figure 5.3: A representation of the *Ortho* component of the principal spectroscopic network of $^{12}\text{C}_2\text{H}_2$ produced using MARVEL input data.

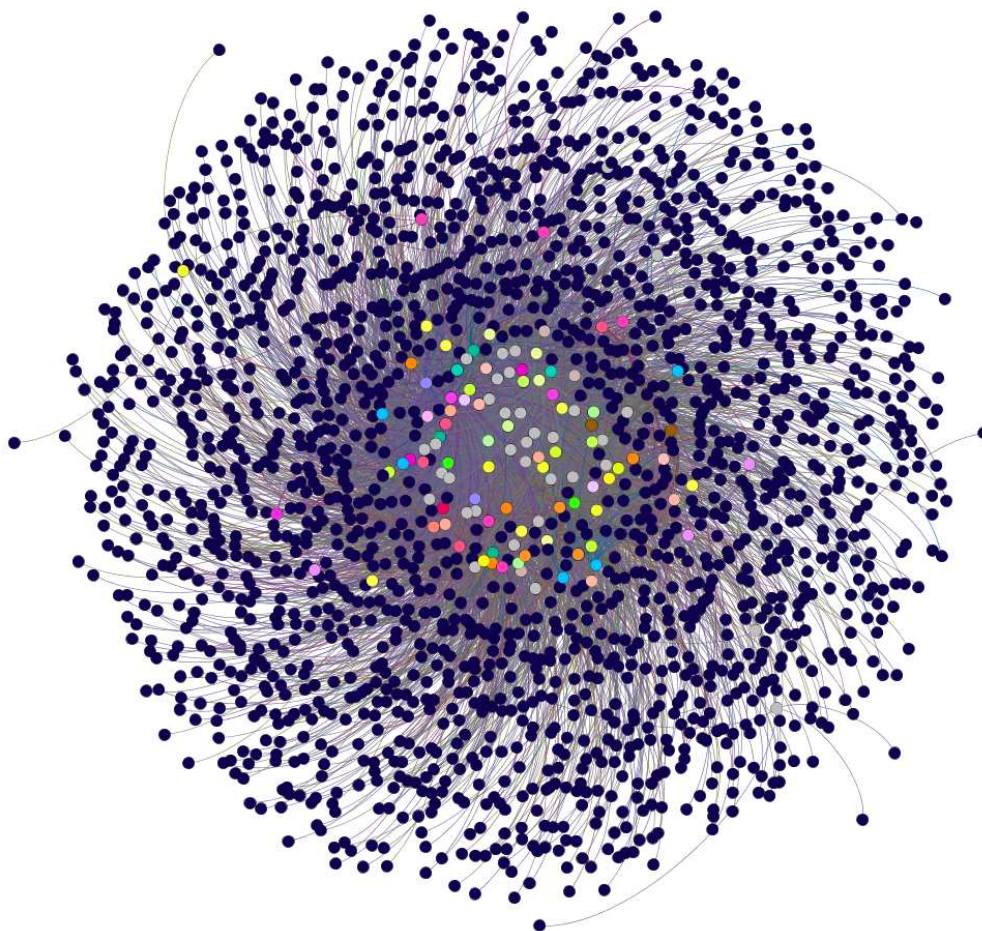


Figure 5.4: A representation of the *Para* component of the principal spectroscopic network of $^{12}\text{C}_2\text{H}_2$ produced using MARVEL input data.

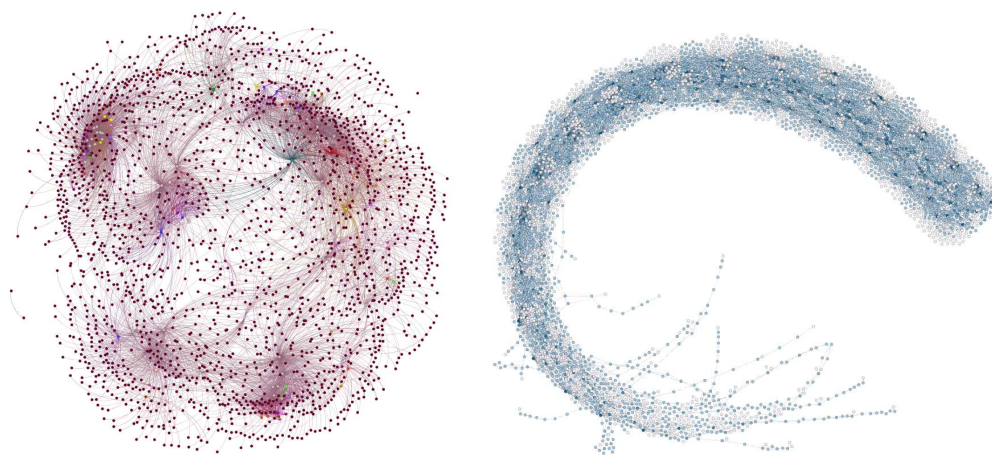


Figure 5.5: Alternative *ortho* (left) and *para* (right) components of the spectroscopic network of $^{12}\text{C}_2\text{H}_2$ produced using MARVEL input data.

Table 5.6 gives the vibrational ($J=0$) energies resulting from the MARVEL analysis, with associated uncertainty, vibrational assignment and the number of transitions (Num Trans) which were linked to the particular energy level. The higher the number of transitions the more certainty can be given to the energy value. See comment (3o) of Section 5.2.1 relating to the band $(0122^2 2^{-2})^0$ which may not have the correct assignment.

Table 5.6: Vibrational energy levels (cm^{-1}) from the MARVEL analysis of $^{12}\text{C}_2\text{H}_2$.

$(v_1 v_2 v_3 v_4^{\ell_4} v_5^{\ell_5})^K$	e/f	State	MARVEL Energy (cm^{-1})	Uncertainty (cm^{-1})	Num Trans
$(0000^0 0)^0$	<i>e</i>	<i>para</i>	0	0.00005	85
$(0002^0 0)^0$	<i>e</i>	<i>para</i>	1230.39030	0.00028	10
$(0001^1 1^{-1})^0$	<i>e</i>	<i>ortho</i>	1328.07000	0.00016	19
$(0001^1 1^{-1})^0$	<i>f</i>	<i>para</i>	1340.55068	0.00078	9
$(0000^0 2^0)^0$	<i>e</i>	<i>para</i>	1449.11236	0.00059	10
$(0100^0 0)^0$	<i>e</i>	<i>para</i>	1974.31662	0.00300	1
$(0003^1 1^{-1})^0$	<i>e</i>	<i>ortho</i>	2560.59000	0.00100	3
$(0002^2 2^{-2})^0$	<i>e</i>	<i>para</i>	2648.01447	0.00200	1
$(0001^1 3^{-1})^0$	<i>e</i>	<i>ortho</i>	2757.80000	0.00095	3
$(0000^0 4^0)^0$	<i>e</i>	<i>para</i>	2880.22008	0.00200	1
$(0101^1 1^{-1})^0$	<i>e</i>	<i>ortho</i>	3281.90000	0.00087	5

$(0010^00^0)^0$	<i>e</i>	<i>ortho</i>	3294.84000	0.00095	4
$(0101^11^{-1})^0$	<i>f</i>	<i>para</i>	3300.63559	0.00384	2
$(1000^00^0)^0$	<i>e</i>	<i>para</i>	3372.83899	0.00800	1
$(0103^11^{-1})^0$	<i>e</i>	<i>ortho</i>	4488.84000	0.00060	2
$(0012^00^0)^0$	<i>e</i>	<i>ortho</i>	4508.01000	0.00133	4
$(0102^22^{-2})^0$	<i>f</i>	<i>ortho</i>	4599.77000	0.00195	2
$(0011^11^{-1})^0$	<i>e</i>	<i>para</i>	4609.34105	0.00295	3
$(0011^11^{-1})^0$	<i>f</i>	<i>ortho</i>	4617.93000	0.00254	4
$(1001^11^{-1})^0$	<i>e</i>	<i>ortho</i>	4673.63000	0.00089	3
$(1001^11^{-1})^0$	<i>f</i>	<i>para</i>	4688.84649	0.00570	1
$(0101^13^{-1})^0$	<i>e</i>	<i>ortho</i>	4710.74000	0.00900	1
$(0010^02^0)^0$	<i>e</i>	<i>ortho</i>	4727.07000	0.00060	3
$(1000^02^0)^0$	<i>e</i>	<i>para</i>	4800.13729	0.00030	1
$(0201^11^{-1})^0$	<i>e</i>	<i>ortho</i>	5230.23000	0.00500	1
$(0110^00^0)^0$	<i>e</i>	<i>ortho</i>	5260.02000	0.00166	2
$(0103^13^{-1})^0$	<i>e</i>	<i>ortho</i>	5893.26000	0.00500	1
$(1001^13^{-1})^0$	<i>e</i>	<i>ortho</i>	6079.69000	0.00186	2
$(0010^04^0)^0$	<i>e</i>	<i>ortho</i>	6141.13000	0.00500	1
$(0112^00^0)^0$	<i>e</i>	<i>ortho</i>	6449.11000	0.00300	1
$(1102^00^0)^0$	<i>e</i>	<i>para</i>	6513.99145	0.00400	1
$(1010^00^0)^0$	<i>e</i>	<i>ortho</i>	6556.46000	0.00005	4
$(1101^11^{-1})^0$	<i>e</i>	<i>ortho</i>	6623.14000	0.00596	2
$(0110^02^0)^0$	<i>e</i>	<i>ortho</i>	6690.58000	0.00600	1
$(2000^00^0)^0$	<i>e</i>	<i>para</i>	6709.02119	0.00186	2
$(1100^02^0)^0$	<i>e</i>	<i>para</i>	6759.23908	0.00500	1
$(0114^00^0)^0$	<i>e</i>	<i>ortho</i>	7665.44000	0.00500	1
$(0022^00^0)^0$	<i>e</i>	<i>para</i>	7686.07895	0.00100	1
$(0204^22^{-2})^0$	<i>e</i>	<i>para</i>	7707.27769	0.00200	1
$(1012^00^0)^0$	<i>e</i>	<i>ortho</i>	7732.79000	0.00265	4
$(0203^33^{-3})^0$	<i>e</i>	<i>ortho</i>	7787.32000	0.00500	1
$(0021^11^{-1})^0$	<i>e</i>	<i>ortho</i>	7805.00000	0.00094	3
$(1103^11^{-1})^0$	<i>e</i>	<i>ortho</i>	7816.01000	0.00500	1
$(1011^11^{-1})^0$	<i>f</i>	<i>ortho</i>	7853.28000	0.00600	1
$(1010^02^0)^0$	<i>e</i>	<i>ortho</i>	7961.82000	0.00383	3
$(2001^11^{-1})^0$	<i>e</i>	<i>ortho</i>	7994.39000	0.00129	2
$(2001^11^{-1})^0$	<i>f</i>	<i>para</i>	8001.20409	0.00494	2

$(2000^0 2^0)^0$	<i>e</i>	<i>para</i>	8114.36288	0.00185	3
$(1100^0 4^0)^0$	<i>e</i>	<i>para</i>	8164.55403	0.00400	1
$(1110^0 0^0)^0$	<i>e</i>	<i>ortho</i>	8512.06000	0.00021	3
$(1201^1 1^{-1})^0$	<i>e</i>	<i>ortho</i>	8556.59000	0.00500	1
$(1201^1 1^{-1})^0$	<i>f</i>	<i>para</i>	8570.32289	0.00500	1
$(2100^0 0^0)^0$	<i>e</i>	<i>para</i>	8661.14909	0.00500	1
$(0300^0 4^0)^0$	<i>e</i>	<i>para</i>	8739.81449	0.00500	1
$(0310^0 0^0)^0$	<i>e</i>	<i>ortho</i>	9151.73000	0.00500	1
$(0030^0 0^0)^0$	<i>e</i>	<i>ortho</i>	9639.86000	0.00772	2
$(1112^0 0^0)^0$	<i>e</i>	<i>ortho</i>	9668.16000	0.00772	2
$(0122^2 2^{-2})^0$	<i>f</i>	<i>ortho</i>	9741.62000	0.01500	1
$(0121^1 1^{-1})^0$	<i>e</i>	<i>ortho</i>	9744.54000	0.01500	1
$(2010^0 0^0)^0$	<i>e</i>	<i>ortho</i>	9835.17000	0.00772	2
$(1030^0 0^0)^0$	<i>e</i>	<i>ortho</i>	12675.70000	0.00050	1
$(3010^0 0^0)^0$	<i>e</i>	<i>ortho</i>	13033.30000	0.00500	1
$(2210^0 0^0)^0$	<i>e</i>	<i>ortho</i>	13713.80000	0.00300	1

5.4 Comparison to Other Derived Energy Levels

Table 5.7 compares the rotational energy levels of this work for the vibrational ground state, which are determined up to $J = 69$, with those obtained by 16AmFaHe [46] from an effective Hamiltonian fit to the observed data. In general the agreement is excellent. However, for the highest few levels with $J \geq 55$ differences are found which are significantly larger than the uncertainties of this work; the resulting levels are systematically below those of 16AmFaHe. This suggests that the effective Hamiltonian treatment used by 16AmFaHe becomes unreliable for these high J levels. It should be noted that data relating to these highly excited levels originated from 16AmFaHe_amy9, a high temperature experiment which has not been reproduced; see comment (3d), Section 5.2.1. It is interesting to note that a further comparison with rotational energies extrapolated as part of 17LyPe's ASD-1000 spectroscopic databank [44], also given in Table 5.7, yields differences of approximately the same magnitude but, in

contrast, consistently lower than this work.

Table 5.7: Comparison of pure rotational levels from the present MARVEL analysis of $^{12}\text{C}_2\text{H}_2$ with those of 16AmFaHe [46] and 17LyPe [44].

J	This work	Uncertainty	16AmFaHe	Difference	17LyPe	Difference	State
1	2.35329	0.00003	2.353286417	0.00000	2.3533	0.00001	<i>ortho</i>
2	7.05982	0.00003	7.059820210	0.00000	7.0598	-0.00002	<i>para</i>
3	14.11952	0.00002	14.119523294	0.00001	14.1195	-0.00002	<i>ortho</i>
4	23.53228	0.00003	23.532278547	0.00000	23.5322	-0.00008	<i>para</i>
5	35.29793	0.00002	35.297929811	0.00000	35.2978	-0.00013	<i>ortho</i>
6	49.41629	0.00003	49.416281896	-0.00001	49.4161	-0.00019	<i>para</i>
7	65.88710	0.00002	65.887100587	0.00000	65.8869	-0.00020	<i>ortho</i>
8	84.71012	0.00002	84.710112648	-0.00001	84.7098	-0.00032	<i>para</i>
9	105.88501	0.00002	105.885005832	0.00000	105.8846	-0.00041	<i>ortho</i>
10	129.41144	0.00003	129.411428888	-0.00001	129.4110	-0.00044	<i>para</i>
11	155.28899	0.00002	155.28899157	0.00001	155.2885	-0.00049	<i>ortho</i>
12	183.51727	0.00003	183.517264652	-0.00001	183.5167	-0.00057	<i>para</i>
13	214.09576	0.00002	214.095779933	0.00002	214.0951	-0.00066	<i>ortho</i>
14	247.02403	0.00003	247.024030258	0.00000	247.0233	-0.00073	<i>para</i>
15	282.30144	0.00002	282.301469525	0.00003	282.3007	-0.00074	<i>ortho</i>
16	319.92751	0.00003	319.927512702	0.00000	319.9266	-0.00091	<i>para</i>
17	359.9015	0.00002	359.901535847	0.00004	359.9006	-0.0009	<i>ortho</i>
18	402.22287	0.00003	402.22287612	0.00001	402.2219	-0.00097	<i>para</i>
19	446.89078	0.00003	446.890831804	0.00006	446.8898	-0.00098	<i>ortho</i>
20	493.90464	0.00003	493.904662324	0.00002	493.9036	-0.00104	<i>para</i>
21	543.26353	0.00002	543.263588267	0.00006	543.2625	-0.00103	<i>ortho</i>
22	594.96668	0.00004	594.966791406	0.00011	594.9657	-0.00098	<i>para</i>
23	649.01328	0.00003	649.013414717	0.00014	649.0123	-0.00098	<i>ortho</i>
24	705.40237	0.00004	705.402562408	0.00019	705.4015	-0.00087	<i>para</i>
25	764.13315	0.00003	764.133299944	0.00015	764.1322	-0.00095	<i>ortho</i>
26	825.20439	0.00004	825.204654067	0.00026	825.2037	-0.00069	<i>para</i>
27	888.61531	0.00003	888.615612828	0.00031	888.6147	-0.00061	<i>ortho</i>
28	954.36496	0.00005	954.365125617	0.00017	954.3642	-0.00076	<i>para</i>
29	1022.45167	0.00003	1022.452103183	0.00044	1022.4513	-0.00037	<i>ortho</i>
30	1092.87513	0.00005	1092.875417676	0.00029	1092.8747	-0.00043	<i>para</i>

31	1165.63343	0.00004	1165.633902667	0.00048	1165.6333	-0.00013	<i>ortho</i>
32	1240.72592	0.00017	1240.726353188	0.00043	1240.7259	-0.00002	<i>para</i>
33	1318.15099	0.00011	1318.151525765	0.00054	1318.1512	0.00021	<i>ortho</i>
34	1397.90769	0.00023	1397.908138445	0.00045	1397.9080	0.00031	<i>para</i>
35	1479.99435	0.00007	1479.994870843	0.00053	1479.9949	0.00055	<i>ortho</i>
36	1564.40979	0.00026	1564.410364167	0.00057	1564.4105	0.00071	<i>para</i>
37	1651.15189	0.00017	1651.153221265	0.00134	1651.1535	0.00161	<i>ortho</i>
38	1740.22038	0.00037	1740.222006657	0.00163	1740.2225	0.00212	<i>para</i>
39	1831.61393	0.00026	1831.615246582	0.00132	1831.6159	0.00197	<i>ortho</i>
40	1925.33058	0.00074	1925.331429031	0.00085	1925.3322	0.00162	<i>para</i>
41	2021.36757	0.00043	2021.369003793	0.00144	2021.3699	0.00233	<i>ortho</i>
42	2119.72439	0.0006	2119.726382499	0.00199	2119.7273	0.00291	<i>para</i>
43	2220.4006	0.00057	2220.401938666	0.00134	2220.4029	0.00230	<i>ortho</i>
44	2323.39201	0.00127	2323.394007739	0.00200	2323.3950	0.00299	<i>para</i>
45	2428.69912	0.00135	2428.70088714	0.00177	2428.7018	0.00268	<i>ortho</i>
46	2536.31702	0.00103	2536.320836316	0.00382	2536.3217	0.00468	<i>para</i>
47	2646.25026	0.00128	2646.252076785	0.00182	2646.2527	0.00244	<i>ortho</i>
48	2758.49217	0.00142	2758.492792187	0.00062	2758.4931	0.00093	<i>para</i>
49	2873.03874	0.00194	2873.041128336	0.00239	2873.0411	0.00236	<i>ortho</i>
50	2989.89046	0.00175	2989.895193269	0.00473	2989.8947	0.00424	<i>para</i>
51	3109.04649	0.00148	3109.05305730	0.00657	3109.0519	0.00541	<i>ortho</i>
52	3230.50478	0.00124	3230.512753073	0.00797	3230.5108	0.00602	<i>para</i>
53	3354.26378	0.00224	3354.272275619	0.00850	3354.2694	0.00562	<i>ortho</i>
54	3480.32661	0.0025	3480.329582411	0.00297	3480.3256	-0.00101	<i>para</i>
55	3608.67187	0.0025	3608.682593419	0.01073	3608.6772	0.00533	<i>ortho</i>
56	3739.32523	0.00118	3739.329191172	0.00396	3739.3223	-0.00293	<i>para</i>
57	3872.2553	0.00208	3872.267220814	0.01193	3872.2585	0.00320	<i>ortho</i>
58	4007.49264	0.0017	4007.494490165	0.00185	4007.4836	-0.00904	<i>para</i>
59	4144.99542	0.00118	4145.008769784	0.01335	4144.9955	0.00008	<i>ortho</i>
60	4284.80143	0.00181	4284.807793029	0.00636	4284.7918	-0.00963	<i>para</i>
61	4426.8772	0.00154	4426.889256124	0.01206	4426.8701	-0.00710	<i>ortho</i>
62	4571.24409	0.00142	4571.25081822	0.00673	4571.2281	-0.01599	<i>para</i>
63	4717.87442	0.00142	4717.890101462	0.01569	4717.8635	-0.01092	<i>ortho</i>
64	4866.79028	0.00232	4866.804691055	0.01441	4866.7736	-0.01668	<i>para</i>
65	5017.97095	0.00168	5017.992135336	0.02119	5017.9561	-0.01485	<i>ortho</i>
66	5171.43923	0.00366	5171.449945837	0.01072	5171.4085	-0.03073	<i>para</i>

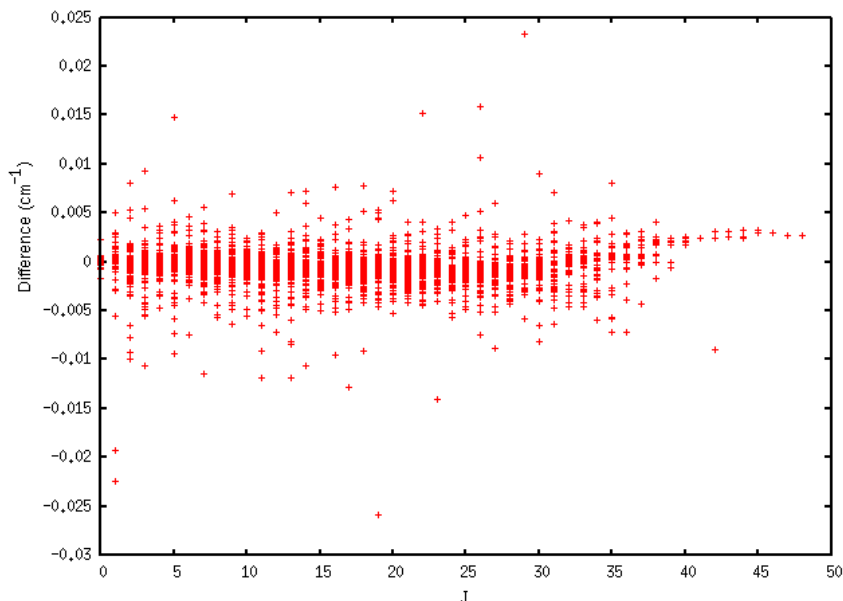


Figure 5.6: Differences between the energy term values given in 17LyCa [45] and this work as a function of rotational angular momentum quantum number, J .

67	5327.14526	0.00195	5327.175597358	0.03034	5327.1280	-0.01726	<i>ortho</i>
69	5645.38676	0.003	5645.420139428	0.03338	5645.3585	-0.02826	<i>ortho</i>

The supplementary data from 17LyCa [45] contains lower energy levels, frequency and assignments, from which upper energy levels can be calculated. Figure 5.6 gives the differences between the energies given in 17LyCa and this work as a function of J . The vast majority are within 0.005 cm^{-1} . Note that the difference in labelling of some bands has been taken into account when comparisons are made (see comment (3l) in Section 5.2.1 and comment (1b) in Section 5.2.2).

The energy levels given as supplementary data in annex 5 of 16AmFaHe [46] are separated into polyads which are characterised by a small number of quantum numbers; $N_{rmv} = 5v_1 + 3v_2 + 5v_3 + v_4 + v_5$, J , e/f symmetry and u/g symmetry. As there are more than one state defined by these quantum numbers, the only comparison that was possible to make was to match these and find the closest energy value within these bounds. As such, one cannot

be certain that bands have been matched correctly. 17LyCa compared what they could against 16AmFaHe's data but also could not find a reliable way to determine unambiguously which energy of each polyad block corresponds to their energy levels. Figure 5.7 gives the difference between the energies in this work and those matched with 16AmFaHe as a function of rotational angular momentum quantum number, J . 6160 out of the 11,154 energies differ by less than 0.01 cm^{-1} . However, this leaves 4994 energies with a difference of higher than 0.01 cm^{-1} . 2176 of these energies also appear in 17LyCa, so a comparison could be made between the three. Only 7 of the energies in the 17LyCa dataset are closer to 16AmFaHe than this work, and of those all are within 0.02 cm^{-1} with this work.

It should be noted, however, that the differences between this work and 16AmFaHe are largest for those energy levels with a low value of Num Trans (the number of transitions that link the energy state to other energies within the dataset); see figure 5.8. The vast majority of energy levels which only have one transition are not in the 17LyCa dataset. Many of these transitions came from the data source 16AmFaHe_amy09; see comment (3d) in Section 5.2.1. It would be of use to have more experimental data on transitions to these levels in order to confirm their validity. The entire band $(0122^22^{-2})^0$ has differences of over 900 cm^{-1} in comparison to the matched values in 16AmFaHe. This indicates that this band has been misassigned (see comment (3o) in Section 5.2.1)). It is uncertain currently as what it should be reassigned to. This band has been excluded from figures 5.7 and 5.8.

It should be made clear, as mentioned above, that those energy levels present in the input data which are only linked to the main spectroscopic network by one transition should be treated with caution; this is given as a parameter in the last column of the output files included in the supplementary data of Ref. [56]. It can be used, along with the uncertainties, as an indication of the reliability of each energy level. MARVEL only processes data given as input; it does not extrapolate to higher excitations.

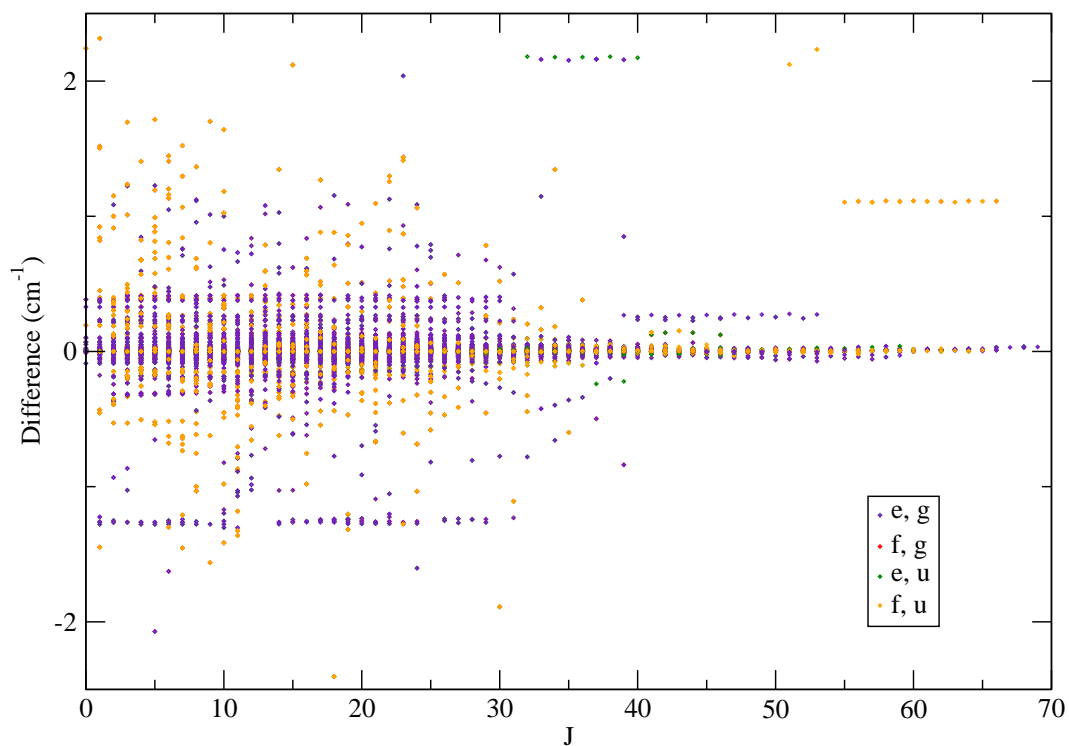


Figure 5.7: Deviations of energy levels in cm^{-1} between this work and 16Am-FaHe [46] as a function of rotational angular momentum quantum number, J . Different colours represent different designations of e/f and u/g .

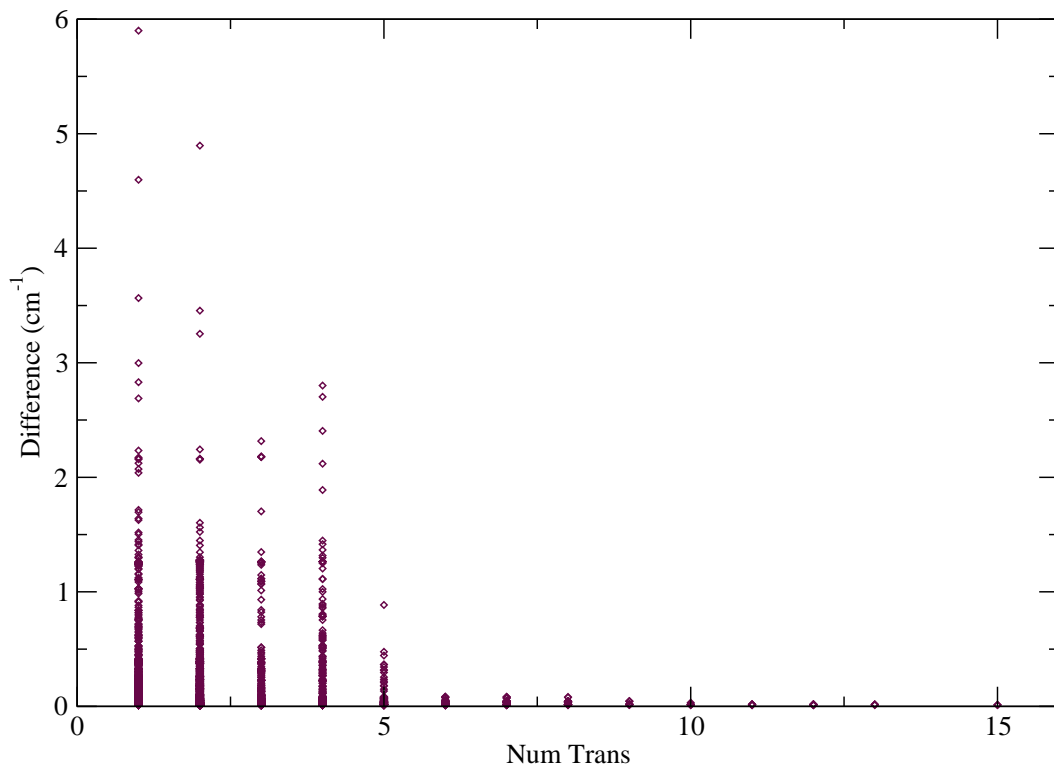


Figure 5.8: Deviations of energy levels in cm^{-1} between this work and 16Am-FaHe [46] as a function of the number of transitions that link to the energy level in the present dataset.

5.5 Comments and Updates Subsequent to the MARVEL Analysis

A recent very high accuracy lamb-dip study was undertaken by Tao *et al.* [300] into the $\nu_1 + 3\nu_3$ band. This same band was observed using high accuracy measurements by Liu *et al.* [301], a data source which was missed in the original MARVEL study. Inclusion of the data from these studies in the MARVEL data would give a slightly different set of energy levels for the $\nu_1 + 3\nu_3$ band, and alter the corresponding uncertainties. The only data for the $\nu_1 + 3\nu_3$ band which was included in the current MARVEL study was taken from 03HeKeHu [181], which, as the authors of Ref [300] point out, is likely to be less accurate than the measured values of Refs [301] and [300]. Further investigation into 03HeKeHu [181] shows that the line positions of their Ta-

ble 1 were actually calculated from spectroscopic constants based on previous studies, rather than measured directly. It is therefore apparent that these lines in the MARVEL dataset should be replaced with those from Liu *et al.* [301]. Tao *et al.* [300] compare their derived energy levels to those of Chubb *et al.* [56] and find an average difference of about 0.01cm^{-1} . The energy levels in the supplementary data of Chubb *et al.* [56] will therefore be off by approximately this amount for the $\nu_1 + 3\nu_3$ band. MARVEL studies typically need to be updated periodically as new experimental data is published, and there are plans for an online MARVEL database for this reason. $^{12}\text{C}_2\text{H}_2$ is expected to be re-analysed in due course, and studies which were missed in the original analysis such as Refs. [300, 301] will be included. Comparison to variational data, which were not available at the time of the original $^{12}\text{C}_2\text{H}_2$ MARVEL analysis, will also allow potentially misassigned transitions to be removed from the MARVEL dataset, and may help currently unpublished and unassigned data to be assigned. It should be noted that when only spectroscopic constants are provided, such as is the case for Ref. [302], this data cannot be used in a MARVEL study.

5.6 The MARVEL Analysis of $H_2^{32}S$

A MARVEL analysis was also recently conducted for $H_2^{32}S$, as detailed in Chubb *et al.* [143]. A total of 44 325 measured experimental rovibrational transitions of $H_2^{32}S$ from 31 publications were considered; 3969 *ortho* and 3467 *para* energy levels were determined as a result of this MARVEL analysis, as illustrated in Figure 5.9. Work is underway to update the existing ExoMol AYT2 states file and linelist based on the energy levels obtained as a result of this MARVEL study, outlined in Ref. [143].

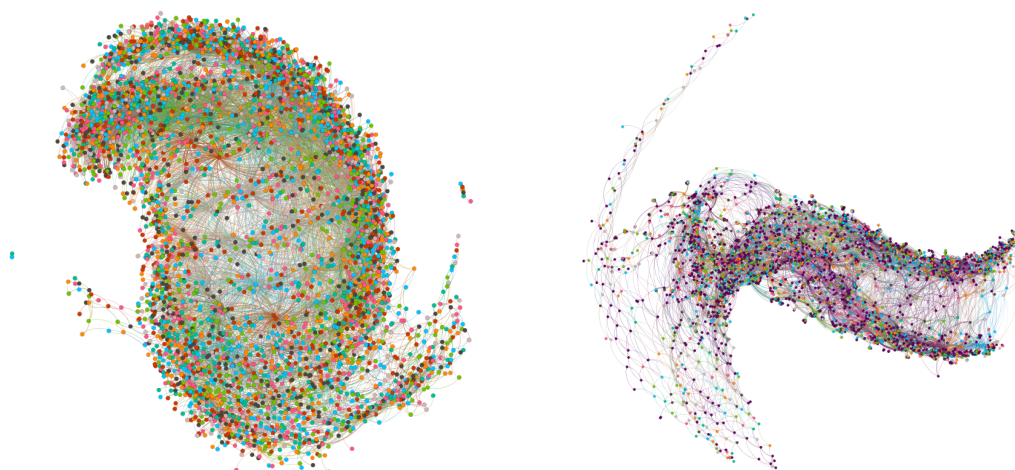


Figure 5.9: Representations of the *ortho* (left) and *para* (right) components of the experimental spectroscopic network of H_2^{32}S produced using MARVEL input data.

5.7 Chapter Summary

A total of 37,813 measured experimental transitions of $^{12}\text{C}_2\text{H}_2$ from 60 publications were considered in this work. From this 6013 *ortho* and 5200 *para* energy levels were determined using the MARVEL technique. These results were compared with alternative compilations based on the use of effective Hamiltonians. The resulting energy levels are being used in the process for calculating a high-accuracy, high-temperature linelist for acetylene (see Section 9.2).

A significant part of this work was performed in collaboration with pupils from Highams Park School in London, as part of a project known as ORBYTS (Original Research By Young Twinkle Students) [142]. The MARVEL studies of H_2^{32}S [143] (Section 5.6) and $^{48}\text{Ti}^{16}\text{O}$ [219] were also performed as part of the ORBYTS project and further studies on other key molecules will be published in due course, involving high-school students from the UK, Australia, and Hungary. A paper discussing the experiences of performing original research in collaboration with school children can be found elsewhere [141].

5.8 Supplementary Data

Please refer to the web version of Ref. [56] for access to the supplementary data. There are four files provided, as listed in Table 5.8. The column definitions are given in Table 5.9 for files 1 and 2 (MARVEL input files) and Table 5.10 for files 3 and 4 (MARVEL output files).

Table 5.8: Supplied supplementary data files.

File	Name
1	MARVEL_ortho_transitions_input.txt
2	MARVEL_para_transitions_input.txt
3	MARVELenergylevels_ortho_output.txt
4	MARVELenergylevels_para_output.txt

Table 5.9: Definition of columns in files 1 and 2.

Column	Label	Description
1	Energy (cm^{-1})	Transition wavenumber
2	Uncertainty (cm^{-1})	Associated uncertainty
	Upper assignments:	
3	ν_1	CH symmetric stretch (σ_g^+)
4	ν_2	CC symmetric stretch (σ_g^+)
5	ν_3	CH antisymmetric stretch (σ_u^+)
6	ν_4	Symmetric (trans) bend (π_g)
7	ℓ_4	Vibrational angular momentum associated with ν_4
8	ν_5	Antisymmetric (cis) bend (π_u)
9	ℓ_5	Vibrational angular momentum associated with ν_5
10	K	$= \ell_4 + \ell_5 $, total vibrational angular momentum
11	J	Rotational angular momentum
12	e/f	Symmetry relative to the Wang transformation (see Section 3.3)
13	<i>ortho/para</i>	Nuclear spin state (see Section 3.4)
	Lower assignments:	
14	ν_1	CH symmetric stretch (σ_g^+)
15	ν_2	CC symmetric stretch (σ_g^+)
16	ν_3	CH antisymmetric stretch (σ_u^+)
17	ν_4	Symmetric (trans) bend (π_g)
18	ℓ_4	Vibrational angular momentum associated with ν_4
19	ν_5	Antisymmetric (cis) bend (π_u)
20	ℓ_5	Vibrational angular momentum associated with ν_5
21	K	$= \ell_4 + \ell_5 $, total vibrational angular momentum
22	J	Rotational angular momentum
23	e/f	Symmetry relative to the Wang transformation (see Section 3.3)
24	<i>ortho/para</i>	Nuclear spin state (see Section 3.4)
25	Ref	Unique reference label (see Section 3.1)

Table 5.10: Definition of columns in files 3 and 4.

Column	Label	Description
1	ν_1	CH symmetric stretch (σ_g^+)
2	ν_2	CC symmetric stretch (σ_g^+)
3	ν_3	CH antisymmetric stretch (σ_u^+)
4	ν_4	Symmetric (trans) bend (π_g)
5	ℓ_4	Vibrational angular momentum associated with ν_4
6	ν_5	Antisymmetric (cis) bend (π_u)
7	ℓ_5	Vibrational angular momentum associated with ν_5
8	K	$= \ell_4 + \ell_5 $, total vibrational angular momentum
9	J	Rotational angular momentum
10	e/f	Symmetry relative to the Wang transformation (see Section 3.3)
11	<i>ortho/para</i>	Nuclear spin state (see Section 3.4)
12	Energy (cm^{-1})	MARVEL energy assignment
13	Uncertainty (cm^{-1})	MARVEL uncertainty
14	Num Trans	The number of transitions in the dataset which link to this state
15	u/g symmetry	See Section 3.2
16	Symmetry label	See Section 3.2

Chapter 6

The Singularity Issue for Linear Molecules

As will be shown in Section 6.3, some special consideration is required to handle the singularities¹ which would occur if standard Hamiltonians and number of internal coordinates are used in ro-vibrational calculations of linear molecules. Two general options exist: (i) the so-called $(3N - 6)$ -approach, which involves using the same form of the kinetic energy operator as in the non-linear case, while modifying the form of the wave function (more specifically, the basis set of functions used to represent the wave function of the system) and (ii) the so-called $(3N - 5)$ -approach, according to which the form of the kinetic energy operator (KEO) is modified by treating one of the rotations as part of the internal ‘vibrational’ modes, making $3N - 5$ in total (where N is the number of atoms).

In the first $(3N - 6)$ approach, it is necessary to carefully choose the form of the basis functions to ensure that when the wave function is acted on by the singular KEO of the system it cancels the singularity. A popular choice which is used in WAVR4 [303], DVR3D [34] and many other works [304, 305, 306, 307, 308, 38, 309, 310, 311, 312, 313, 314, 315] is the use of angular basis functions which include Legendre polynomials, such as spherical harmonics.

¹In this context, singularity refers to terms which become infinite due to a zero in the denominator.

An alternative form of the wave function for linear triatomic molecules was developed by Refs. [316], [317], which is not restricted to the use of spherical polar coordinates. This idea was originally formulated for triatomics but has been extended in this work for tetratomic molecules; see Section 7.2.

WAVR4 is an example of a computational method for ro-vibrational calculations capable of treating linear four-atomic molecules within the $3N - 6$ approach [303, 318] which uses finite basis representation (FBR) for the angular coordinates and a mixed FBR-DVR (where DVR stands for Discrete Variable Representation, see e.g. Refs. [34, 48]) basis for the radial motion. While accurate at low excitations of rotational energy, it is currently too computationally demanding to make it viable for use up to highly rotationally excited states [43, 319]. WAVR4 has been used to calculate the ro-vibrational energy levels and spectra of acetylene, up to rotational excitation $J = 1$ [303, 43] (with extrapolations to higher rotational excitations [43]). As stated in the papers, the program was specifically designed to deal with wide amplitude motion and isomerisations; the isomerisation from acetylene to vinylidene is expected to occur at around $15,000 \text{ cm}^{-1}$ above the acetylene ground state [40].

DVR3D is a code used by the ExoMol project which utilises the DVR (Discrete Variable Representation) method, based on Gauss-Jacobi and Gauss-Laguerre quadrature [34, 48], in the modelling of the ro-vibrational spectra of triatomic molecules and is capable of successfully handling linear molecules such as CO_2 [20, 36]. It is currently not suitable for dealing with linear molecules of more than three atoms.

The second ($3N - 5$) approach involves choosing appropriate coordinates to represent a linear molecule which do not lead to singular terms in the KEO. One of the best known examples of such a $3N - 5$ ro-vibrational Hamiltonian was published by Watson in 1968 [32], which uses normal coordinates and is still an important basis for a large amount of related work until the present day [320, 321, 322, 323, 324]. Its foundation is found in techniques developed by Ref. [325] for treating linear triatomic molecules in a doublet- Π electronic

state and the work by Refs. [326], [327], [325], in which the Hamiltonian is built in the classical form and transformed to the corresponding quantum operator form via the Podolsky trick [328] and employing the Eckart conditions [329]. An alternative form of the Hamiltonian, appropriate for linear molecules, was subsequently published by Watson [330], which deals with the angular momentum around the linear axis differently to the standard non-linear case. There are similarities here with the method that is employed in Section 7.1; the Euler angle describing rotation about the z -axis, i.e. χ (see Fig. 6.1), becomes undefined for a linear molecule, and so this rotational motion is effectively treated as vibrational instead.

6.1 Nuclear-Motion Routine TROVE

As aforementioned, TROVE (Theoretical ROVibrational Energies) [50, 51] is the principal software package for calculating the ro-vibrational spectra of medium to large (typically four atoms or more) polyatomic molecules as part of the ExoMol project. The nuclear motion Schrödinger equation and its solution were introduced in Section 2.3, which will be briefly mentioned here. The focus of this chapter, however, will primarily be on the construction of the kinetic energy operator (KEO), which is typically carried out numerically in TROVE, requiring no analytical pre-derivation. It is the construction of the KEO, when implemented in the same way as for non-linear molecules, which causes numerical issues for ro-vibrational calculations involving linear molecules.

For a reader interested in learning the in-depth, step-by-step process of running TROVE for ro-vibrational energy calculations of general polyatomic molecules, the TROVE manual [331] provides an excellent starting point. In summary, calculations in TROVE are performed sequentially, with the option to save a number of checkpoint files in order to be read back in during subsequent stages of the calculation, often necessary in order to make the process computationally viable. The potential energy, dipole moment and kinetic en-

ergy functions are all expanded as Taylor series and truncated at a specified order, with the potential energy and dipole moment functions given as input, and the kinetic energy function generated numerically on-the-fly. Basis sets are built from primitive 1D functions, processed through a double layer contraction scheme, and used to solve the vibrational ($J = 0$) problem. The resulting vibrational eigenfunctions can subsequently be used in the construction of a basis set for the $J > 0$ calculations. Making use of this $J = 0$ representation makes ro-vibrational calculations in TROVE far more efficient. See Section 7.1 for more details.

6.2 Ro-vibrational Calculations in TROVE

Ro-vibrational energies, E_{rv} , and wave-functions, Ψ_{rv} , are obtained using TROVE as a solution of the Schrödinger equation within the Born-Oppenheimer (B-O) approximation,

$$\hat{H}_{rv} \Psi_{rv} = E_{rv} \Psi_{rv}, \quad (6.1)$$

where \hat{H}_{rv} is the ro-vibrational Hamiltonian operator of the molecular system. Solving this variationally can be highly computationally demanding, especially for polyatomic molecules, with a general increase in time for systems with more atoms. With the B-O approximation comes the concept of potential energy surfaces; the Schrödinger equation should be solved for the motions of the nuclei moving in the potential created by the electrons, as described in Section 2.3. The nuclear Hamiltonian operator, \hat{H} is a sum of the kinetic energy operator and potential energy function,

$$\hat{H} = \hat{T} + V. \quad (6.2)$$

Note that the rv subscript will be dropped from now on, but focus is still on ro-vibrational operators, wavefunctions, and energy levels. In TROVE, these operators are expanded as a Taylor series around the minimum of the potential energy surface (i.e. the equilibrium geometry) or, alternatively, around a non-rigid configuration (for example, the “umbrella” motion that is known to occur

in NH_3 [332]), in terms of a suitable set of internal coordinates, ξ_i . For example, in the case of the potential energy function [50]:

$$V(\boldsymbol{\xi}) = \sum_{i,j,k,\dots} f_{ijk\dots} \xi_1^i \xi_2^j \xi_3^k \dots, \quad (6.3)$$

where $f_{ijk\dots}$ are expansion coefficients. This is appropriate as long as only the region around one minimum of the system is being considered, as is the case for C_2H_2 (the isomerisation of acetylene to vinylidene is not considered here). Typically this expansion is truncated around the 6th or 8th order term. A more in depth account of this can be found in Chapter 8 (see also Ref. [50]).

6.3 Construction of the Kinetic Energy Operator in TROVE

In order to fully understand why an amendment is required for calculations involving linear molecules using TROVE, it is necessary to look at the method used to solve for the ro-vibrational energies of non-linear molecules. Though the variational method of TROVE is specifically considered here, the conclusions are general enough to be applicable to other nuclear motion programs.

The minimum number of coordinates required to describe the motions of any general molecule is $3N$, where N is the number of atoms in the system: for a non-linear molecule this breaks down as 3 to describe the position of the center of mass of the molecule (which is also the center of the molecular frame with respect to the laboratory frame (Figure 6.1)) and 3 to describe the orientation of this frame (typically Euler angles in conjunction with the Eckart conditions [333]; see Figure 6.1), leaving $M = 3N - 6 = 6$ variables to describe the internal, vibrational motions of the molecule, i.e. the stretches, bends and dihedrals (see e.g. Figure 6.2). For linear molecules, this is not necessarily the case, as will be seen below.

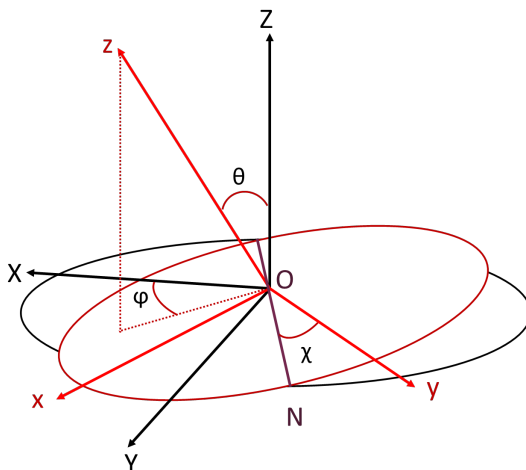


Figure 6.1: The Euler angles describing the orientation of the molecular (x, y, z) axis (red) from the laboratory (X, Y, Z) axis (black). Here, θ is the angle between the Z and z axes, ϕ is the angle from X to the projection of z on the $X - Y$ plane, and χ is the angle between from ON (purple) to the y -axis (where O is the origin of both axes and ON defines the node line, which is the intersection of the $X - Y$ and the $x - y$ planes. ON is also perpendicular to both the z and Z axes. χ is therefore the azimuthal angle about the z -axis).

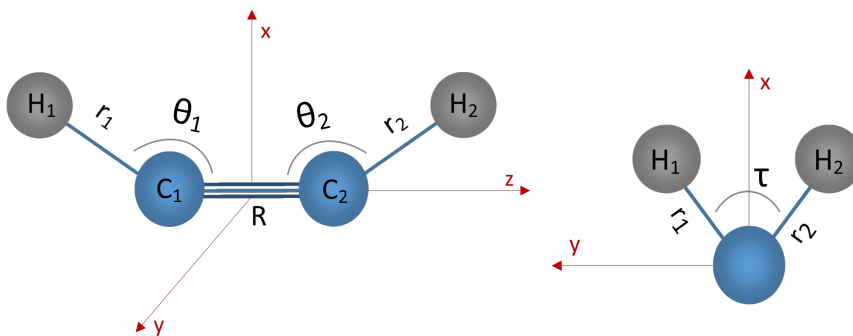


Figure 6.2: The geometry of HCCH as described using $3N - 6$ internal curvilinear coordinates ξ ($R, r_1, r_2, \theta_1, \theta_2$ and τ)

The form of the KEO used in TROVE [50], \hat{T} , is given by

$$\hat{T} = \frac{1}{2} \sum_{\lambda, \mu=1}^{M+3} \hat{p}_{\lambda}^{\dagger} G_{\lambda\mu}(\xi) \hat{p}_{\mu} + U(\xi), \quad (6.4)$$

in terms of vibrational coordinates, $\boldsymbol{\xi} = \{\xi_1 \dots \xi_M\}$, angular momentum operators of the form $\hat{p}_{\lambda=1 \dots M+3} = \{-i\hbar \partial / \partial \xi_1 \dots -i\hbar \partial / \partial \xi_M, \hat{J}_x, \hat{J}_y, \hat{J}_z\}$ (the momenta operators conjugate to the internal coordinates, along with three, x, y, z , components of the total angular momentum operator, \hat{J}), and the pseudopotential function, $U(\boldsymbol{\xi})$. M is the number of internal (vibrational) degrees of freedom, typically $3N - 6 = 6$ for non-linear molecules.

$G_{\lambda\mu}(\boldsymbol{\xi})$ is a kinetic factor which is also known as the kinetic energy \mathbf{G} -matrix, typically of dimensions $M + 3$, corresponding to the total number of ro-vibrational degrees of freedom. There is coupling between the rotational and vibrational motion, but the translational motion is always separable and so can be removed from these calculations. If this were not the case then nuclear motion calculations would be unattainably difficult, as this translational motion essentially leads to a continuous spectrum (see e.g. Ref. [309]).

Using the nomenclature of Sørensen [334], each element of $G_{\lambda\mu}(\boldsymbol{\xi})$ is given by:

$$G_{\lambda\mu}(\boldsymbol{\xi}) = \sum_{i=1}^N \frac{1}{m_i} \sum_{\alpha=x,y,z} s_{\lambda,i\alpha} s_{\mu,i\alpha}, \quad (6.5)$$

where $s_{\lambda,i\alpha}$ is the Jacobian \mathbf{s} -matrix ($\lambda = 1 \dots M + 3$), which can be found via inversion of another matrix, called the Jacobian \mathbf{t} -matrix. This is defined in three parts, associated with the M vibrational, 3 rotational and 3 translational coordinates. These are given respectively [334] by:

$$t_{i\alpha,\lambda} = \frac{\partial r_{i\alpha}}{\partial \xi_\lambda}, \quad (6.6)$$

$$t_{i\alpha,M+\beta} = \sum_{\lambda=x,y,z} \varepsilon_{\alpha\beta\gamma} r_{i\gamma} \quad (\beta = x, y, z), \quad (6.7)$$

$$t_{i\alpha,M+3+\beta} = \delta_{\alpha\beta} \quad (\beta = x, y, z). \quad (6.8)$$

Here $r_{i\alpha}$ defines the Cartesian coordinates, $\alpha=x,y,z$, of each atom, $i = 1 \dots N$, with respect to the center of mass of the system (body-fixed); ξ_λ is the λ^{th} vibrational coordinate and $\varepsilon_{\alpha\beta\gamma}$ is the fully antisymmetric Levi-Civita tensor.

The \mathbf{s} -matrix is defined by

$$s_{\kappa,i\alpha} = \frac{\partial \xi_\kappa}{\partial r_{i\alpha}}, \quad (6.9)$$

where ξ_κ is a generalised coordinate ($\kappa = 1, \dots, 3N$) consisting of the translational, vibrational and rotational coordinates. The \mathbf{s} -matrix is related to the \mathbf{t} -matrix by the chain rule:

$$\sum_{i,\alpha} s_{k,i\alpha} t_{i\alpha,\mu} = \delta_{k\mu}. \quad (6.10)$$

In order to build the kinetic energy operator expansion, TROVE was originally programmed such that the \mathbf{t} -matrix is first generated, before being numerically inverted as in Eq. (6.10) to obtain the rotational and vibrational elements of the \mathbf{s} -matrix as expansions in terms of ξ_k , and in turn used to build the \mathbf{G} -matrix expansions. However, improvements have been made (prior to the work undertaken in this thesis) since Ref. [50] to reflect a method demonstrated by Sørensen [334] which reduces the size of the matrices that are required to be inverted; these improvements will be outlined here.

Sørensen [334] makes use of a matrix of so-called ‘‘constraint vectors’’ \mathbf{c} , which in the Eckart embedding (as implemented in TROVE) are given by

$$c_{g,i\alpha} = m_i \sum_{\beta} \epsilon_{g\alpha\beta} r_{i\beta}^e, \quad (6.11)$$

where $g = x, y, z$, $r_{i\beta}^e$ is a β -Cartesian ($\beta = x, y, z$) component of the nucleus i at the equilibrium configuration and $\epsilon_{g\alpha\beta}$ is the fully antisymmetric Levi-Civita tensor. These constraint vectors can be combined with the rotational \mathbf{t} -vectors to form a new 3×3 matrix,

$$J_{gg'} = \sum_{i\alpha} c_{g,i\alpha} t_{g',i\alpha}, \quad (6.12)$$

which can be inverted to give $\eta_{gg'}$. That is, $\eta_{gg'}$ and $J_{gg'}$ are related as follows

$$\sum_{g,g''} \eta_{g,g''} J_{g''g'} = \delta_{gg'}, \quad (6.13)$$

where $g, g' = x, y, z$. Once $\eta_{gg'}$ and $c_{g,i\alpha}$ have been found, they can be used to form the rotational part of the \mathbf{s} -matrix

$$s_{g,i\alpha} = \sum_{g'} \eta_{gg'} c_{g',i\alpha}. \quad (6.14)$$

Here, the $\eta_{gg'}$ coefficients are common to all atoms, reducing the number of elements required to be evaluated; only inversion of the 3×3 (4×4 for non-rigid representations [334, 50]) \mathbf{J} -matrix (Eq. (6.12)) is required. It is for this reason the method has been implemented in TROVE.

In the case of Eckart embedding, the \mathbf{J} -matrix is linear in $r_{i\alpha}$ [334]. The $\boldsymbol{\eta}$ -matrix is expanded as a Taylor series in terms of the vibrational coordinates ξ_λ ,

$$\eta_{gg'} = \sum_{i,j,k,\dots} \eta_{i,j,k,\dots}^{gg'} \xi_1^i \xi_2^j \xi_3^k \dots, \quad (6.15)$$

and solved iteratively for the coefficients by inverting the \mathbf{J} -matrix of Eq. (6.12).

Once the rotational part of the \mathbf{s} -matrix has been found in this way, the vibrational part can be found as follows.

TROVE's default choice is to use linearised internal coordinates describing the vibrational motion of the molecule. The \mathbf{t} - and \mathbf{s} -matrices are simplified by the linear transformation between Cartesian and linearised (rectilinear) coordinates ξ_λ^{lin} :

$$r_{i\alpha} = r_{i\alpha}^e + \sum_{\lambda} A_{i\alpha,\lambda} \xi_\lambda^{\text{lin}}, \quad (6.16)$$

$$\xi_\lambda^{\text{lin}} = \sum_{i,\alpha} B_{\lambda,i\alpha} (r_{i\alpha} - r_{i\alpha}^e), \quad (6.17)$$

where $A_{i\alpha,\lambda}$ and $B_{\lambda,i\alpha}$ ($i = 1 \dots N$, $\alpha = x, y, z$, $\lambda = 1 \dots M$) are matrices of coefficients defining the direct and inverse transformation between the Cartesian and linearised coordinates. The linearised coordinates are obtained by linearisation (Taylor expanding in terms of Cartesian displacements and truncating at the linear term) of the geometrically defined coordinates (GMD) such as bond lengths, inter-bond angles and dihedral angles with respect to the Cartesian displacement from the equilibrium configuration [189]. The elements of the linearised \mathbf{B} -matrix are defined as the first derivatives of the Cartesian positions $r_{i\alpha}$ with respect to the GMD coordinates taken at the equilibrium and thus coincide with the vibrational elements of the \mathbf{s} -matrix in Eq. (6.9) at the equilibrium:

$$B_{\lambda,i\alpha} = s_{\lambda,i\alpha}^e. \quad (6.18)$$

The elements of the \mathbf{A} -matrix are subject to the constraints of the center of mass, Eckart, and orthogonality conditions:

$$\sum_{i\alpha} B_{\lambda,i\alpha} A_{i\alpha,\lambda'} = \delta_{\lambda\lambda'}, \quad (6.19)$$

see Ref. [50] for details. In this case, the \mathbf{J} -matrix in Eq. (6.12) becomes a simple linear function of $\xi_{\lambda}^{\text{lin}}$. The vibrational part of \mathbf{s} is also simplified. According to Sørensen [334] it is now given by

$$s_{\lambda,i\alpha}^{\text{vib}} = s_{\lambda,i\alpha}^{\text{e}} - \sum_{g,\lambda'} \xi_{\lambda'}^{\text{lin}} \zeta_{\lambda',\lambda}^g s_{g,i\alpha}^{\text{rot}}, \quad (6.20)$$

which makes use of the rotational part of the \mathbf{s} -matrix, $s_{g,i\alpha}^{\text{rot}}$, and where $\zeta_{\lambda',\lambda}^g$ are the Coriolis coefficients

$$\zeta_{\lambda',\lambda}^g = \sum_{i\alpha,\beta} \epsilon_{g,\alpha,\beta} A_{i\alpha,\lambda'} B_{\lambda,i\alpha}. \quad (6.21)$$

It can clearly be seen that if the determinant of the \mathbf{t} -matrix which is used to build the KEO involves any bending angles it will tend to zero at linearity and therefore inversion of this matrix in the process described above will lead to singular terms. For example, for the $3N - 6$ coordinates illustrated in Fig. 6.2, the determinant of the \mathbf{t} -matrix becomes singular at the linear geometry:

$$\det(\mathbf{t}) = 2 \sin(\theta_1) \sin(\theta_2) R^2 r_1^2 r_2^2. \quad (6.22)$$

It should be noted that TROVE is now capable of working with geometrically defined coordinates as described in Ref. [51]. Although the current implementation described in this thesis is based on linearised coordinates only (see Section 7.1), it is possible to extend it to be compatible with such geometrically defined coordinates.

6.4 Chapter Summary

Two different approaches to dealing with linear molecules in ro-vibrational energy calculations are introduced in this chapter, which will be explored in Chapter 7. The $(3N - 5)$ approach, which is now fully implemented in

TROVE, is investigated in Section 7.1, and the $(3N - 6)$ approach, is outlined in Section 7.2. The latter is the numerical method used in the variational calculations presented in Chapter 8. A discussion and comparison between the two approaches can be found in Chapter 10. The general formulation of the kinetic energy operator, as it is implemented for non-linear molecules, has been outlined in this chapter. This is necessary in order to understand the singularity issue for linear molecules and why novel approaches to dealing with them are required.

Chapter 7

Approaches to Dealing with Linear Molecules

Two approaches to handling linear molecules in ro-vibrational calculations were introduced in Chapter 6 and will be investigated in more detail in this chapter: $(3N - 5)$ and $(3N - 6)$. While the idea behind the $(3N - 6)$ approach is to select a form of the wave function which removes the singularity in the Hamiltonian (which was shown in Section 6.3 to occur if standard Hamiltonians and number of internal coordinates are used in ro-vibrational calculations), the $(3N - 5)$ approach makes use of a KEO which is already non-singular.

7.1 The $(3N - 5)$ -approach to Dealing with Linear Molecules

As demonstrated in Chapter 6, the singularity issue in the KEO is associated with some of the angles used to describe the system becoming undefined at linearity. According to the $(3N - 5)$ approach, one of the rotational angles must be combined with the vibrational modes (the Euler angle describing the rotation of the molecule around the z axis, χ (see Fig. 6.1)). Therefore, an extended set of the internal coordinates is defined to cover all vibrations as well as this rotation motion; $(3N - 5)$ coordinates. This chapter outlines this approach which has now been implemented in TROVE to construct a $(3N - 5)$ -type kinetic energy operator (KEO) as part of TROVE's numerical 'on-the-fly'

methodology. This approach was employed in the variational calculations of Chapter 8.

7.1.1 The Coordinate System and KEO

In the case of $^{12}\text{C}_2\text{H}_2$, the common choice of the $3N - 6$ curvilinear (GDC) coordinates includes $R \equiv r_{\text{CC}}$, $r_1 \equiv r_{\text{CH}_1}$, $r_2 \equiv r_{\text{CH}_2}$, $\theta_1 \equiv \theta_{\text{CCH}_1}$, $\theta_2 \equiv \theta_{\text{CCH}_2}$, and $\tau \equiv \tau_{\text{HCCH}}$ (see Fig. 6.2). Thus, apart from the Euler angle χ (see Fig. 6.1), another ‘singular’ coordinate is τ , describing the torsional motion of the molecule; τ is undefined if either of the θ s become 180° , while χ is undefined for the linear configuration $\theta_1 = \theta_2 = 180^\circ$. Using any of these coordinates would introduce a singularity in the kinetic energy operator, even in the $(3N - 5)$ approach.

Singularity-free coordinates can be defined as follows. The equilibrium configuration $r_{i\alpha}^e$ of a linear molecule is set along the molecular z -axis (centered at $z = 0$), as shown in Figure 6.2. The positions of the H_1 and H_2 atoms are given by their (rectilinear) Cartesian x and y displacements relative to the equilibrium linear configuration (subject to the center of mass and Eckart conditions), supplemented by the bond length between the two carbon atoms, R and the two carbon-hydrogen bonds lengths, r_1 and r_2 . These seven coordinates ξ_λ ($\Delta x_1, \Delta y_1, \Delta r_1, \Delta x_2, \Delta y_2, \Delta r_2$ and ΔR , where $\Delta x_i = r_{ix}$ and $\Delta y_i = r_{iy}$ ($i = 1, 2$)) provide an (almost) unambiguous description of any instantaneous configurations of $^{12}\text{C}_2\text{H}_2$ including the linear geometry; such a choice is not ideal to describe the vibrational motion of the molecule as the bond lengths r_1 and r_2 become ambiguous for the configurations with $\theta_i > 90^\circ$ and $\theta_i < 90^\circ$. As will be seen below, the linearised version of this set of coordinate does not have this problem.

Based on these seven coordinates ξ_λ , seven linearised coordinates can be defined as follows. For the three stretching modes ξ_1^{lin} , ξ_2^{lin} and ξ_3^{lin} the linearised versions of the bond length displacements ΔR , Δr_1 , and Δr_2 are used. The linearisation is defined by Taylor expanding the coordinates in terms of the Cartesian displacements $\Delta x_i, \Delta y_i, \Delta z_i$ ($i = 1, 2, 3, 4$) and truncating after the linear terms, as in Section 6.3.

The four rectilinear bending modes ξ_4^{lin} , ξ_5^{lin} , ξ_6^{lin} and ξ_7^{lin} are defined as the Δx_i and Δy_i ($i = 1, 2$) Cartesian components of the hydrogen atoms, H_1 and H_2 as follows:

$$\xi_4^{\text{lin}} = \Delta x_1, \quad \xi_5^{\text{lin}} = \Delta y_1, \quad (7.1)$$

$$\xi_6^{\text{lin}} = \Delta x_2, \quad \xi_7^{\text{lin}} = \Delta y_2. \quad (7.2)$$

Refs. [335, 314] give an alternative representation where the $\sin \theta_i$ projection on x_i and y_i are used. Technically, the x and y projections of the vectors, CH_1 and CH_2 onto the molecular \vec{e}_x and \vec{e}_y axes are defined using the normals \vec{n}_1 and \vec{n}_2 to the CCH_1 and CCH_2 planes, respectively:

$$\begin{aligned} \Delta x_1 &= -(\vec{e}_y \cdot \vec{n}_1), & \Delta y_1 &= (\vec{e}_x \cdot \vec{n}_1), \\ \Delta x_2 &= (\vec{e}_y \cdot \vec{n}_2), & \Delta y_2 &= -(\vec{e}_x \cdot \vec{n}_2), \end{aligned} \quad (7.3)$$

where the normals \vec{n}_i ($i = 1, 2$) are given by:

$$\vec{n}_i = \frac{[\vec{R} \times \vec{r}_i]}{R r_i}. \quad (7.4)$$

An illustration of these coordinates is given in Figure 7.1.

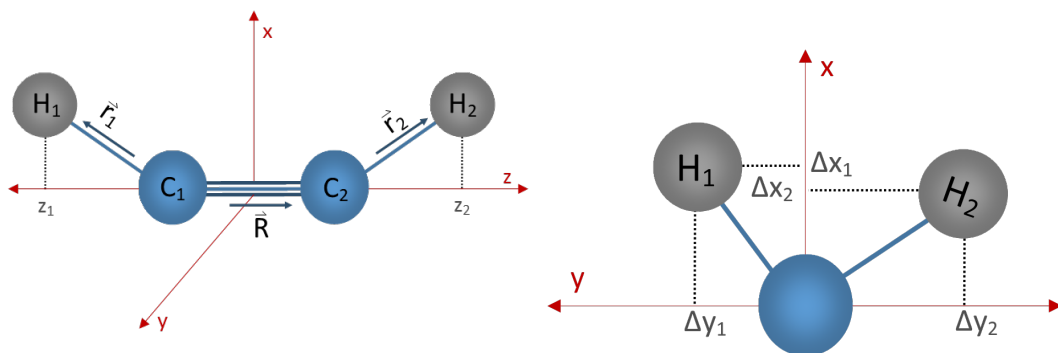


Figure 7.1: HCCH as described using the $3N - 5$ coordinates employed in TROVE (see text). \vec{R} is the vector (of length R) pointing from the first to the second carbon atom, C_1 to C_2 , while \vec{r}_i are the two CH_i bond vectors (of lengths r_i). The Δx_1 , Δx_2 , Δy_1 and Δy_2 notation of this diagram and Eq. (7.3) is to reflect the Cartesian projections of the CH_i bond vectors.

The molecular xyz-body fixed system is chosen according to the Eckart conditions [50] (see Figure 6.1) and for this choice of coordinates the coordinate transformation in Eq. (6.16) is given by:

$$r_{i,x} = (A_{i,x,4} \xi_4^{\text{lin}} + A_{i,x,6} \xi_6^{\text{lin}}), \quad (7.5)$$

$$r_{i,y} = (A_{i,y,5} \xi_5^{\text{lin}} + A_{i,y,7} \xi_7^{\text{lin}}), \quad (7.6)$$

$$r_{i,z} = r_{i,z}^e + (A_{i,z,1} \xi_1^{\text{lin}} + A_{i,z,2} \xi_2^{\text{lin}} + A_{i,z,3} \xi_3^{\text{lin}}), \quad (7.7)$$

where the property $r_{ix}^e = r_{iy}^e = 0$ is taken into account. The matrix elements $A_{i\alpha,\lambda}$ (see Eq. (6.16)) are provided as part of the supplementary material of Ref. [24]. Thus, the rectilinear bending coordinates ξ_4^{lin} , ξ_6^{lin} and ξ_5^{lin} , ξ_7^{lin} are always directed along the x and y axes, respectively (Eq. (7.3)), while ξ_1^{lin} , ξ_2^{lin} , and ξ_3^{lin} (i.e. ΔR^{lin} , Δr_1^{lin} and Δr_2^{lin}) are along the z axis. Thus the stretching linearized coordinates ξ_2^{lin} , and ξ_3^{lin} do not have the aforementioned ambiguous configuration when $\theta_i > 90^\circ$ and $\theta_i < 90^\circ$. They are, however, less physically intuitive as they do not support the chemical bonding between the atoms.

It is important to note that in this coordinate system the angular momentum defined by the remaining two Euler angles is conserved and thus all the standard commutation properties (with standard matrix elements of $\hat{\mathbf{J}}$) will still apply. This is not an obvious conclusion; see, for example, the discussion by Howard and Moss [336], Sørensen [334] or Watson [337], who obtained different commutation relations for the corresponding \hat{J}_x , \hat{J}_y , and \hat{J}_z components. However Hougen [325] and Howard and Moss [336] have shown that the normal commutation relations can be always restored via a suitable unitary transformation of the eigenfunctions. The consequence of this conclusion is that the standard procedure to build a KEO (e.g. based on the \mathbf{s} - and \mathbf{t} -matrices as described in Section 6.3) can be used with the only amendment being to remove the z -component, which thus causes the \hat{J}_z terms to disappear in the KEO (Eq. (6.4)). The TROVE approach [50] (Section 6.3) is employed for the process of building the kinetic energy operator, where the z -components of all matrices (\mathbf{t} , \mathbf{s} , \mathbf{G}) are set to zero. In other words, the angular momentum

about the molecular axis is treated as purely vibrational, known as the Sayvetz condition for linear molecules [337]. The $(3N - 5)$ treatment requires that the condition $K = L$ is fulfilled (see, for example, Refs. [330], [338]), where K is the z -projection of the rotational angular momentum and L is the vibrational angular momentum, otherwise nonphysical states would be included in the basis set and the solution.

7.1.2 Symmetrisation using the TROVE $(3N - 5)$ -approach

The use of \mathcal{D}_{nh} as opposed to $\mathcal{D}_{\infty h}$ symmetry is a practical alternative for numerical calculations involving centrosymmetric linear molecules such as $^{12}\text{C}_2\text{H}_2$. The transformation matrices for the \mathcal{D}_{nh} group were outlined in Chapter 4. The symmetrisation procedure of TROVE [50, 51], based on a set of “reduced” vibrational eigenvalue problems with simplified Hamiltonians, is outlined in this section, along with a general subroutine which has been implemented in TROVE to automatically generate all transformation matrices associated with the irreducible representations of a symmetry group \mathcal{D}_{nh} for a given n , for use in calculations involving linear molecules. The solutions of the eigenvalue problems resulting from the TROVE symmetrisation procedure are also extended to include the classification of basis-set functions using ℓ , the eigenvalue (in units of \hbar) of the vibrational angular momentum operator \hat{L}_z . This facilitates the symmetry adaptation of the basis set functions in terms of the irreducible representations of \mathcal{D}_{nh} .

In a given TROVE calculation, the required extent of the rotational excitation is ideally defined by the maximum value J_{\max} of the angular momentum quantum number J . For a linear molecule, only combinations with $k = \ell$ are physically meaningful, where k is the z -axis-projection of the rotational angular momentum quantum number and ℓ is the vibrational angular momentum quantum number, as part of the $3N - 5$ -approach to linear molecules. The maximum values of $|k|$ and $|\ell|$, K_{\max} and L_{\max} , respectively, are then $K_{\max} = L_{\max} = J_{\max}$. However, in practise the numerical calculations are computation-

ally limited by the total number of quanta representing vibrational bending modes, which controls the maximum value for $|\ell|$, and thus $|k|$. The group \mathcal{D}_{nh} suitable for symmetry classification of ro-vibrational states has an n -value determined by $K_{\max} = L_{\max}$; $n=2L_{\max}+1$ for odd- n and $n=2L_{\max}+2$ for even- n .

It has already been mentioned that the use of a symmetry-adapted ro-vibrational basis set can considerably reduce the size of the Hamiltonian matrix which is to be diagonalised numerically in ro-vibrational energy calculations. This is due to the useful property that the matrix elements between basis functions of different symmetry are zero by definition:

$$\langle \Psi_{\mu}^{J, \Gamma_s, \alpha} | H^{rv} | \Psi_{\mu'}^{J, \Gamma_t, \alpha'} \rangle = H_{\mu, \mu'} \delta_{s,t} \delta_{\alpha, \alpha'}, \quad (7.8)$$

where Γ_s and Γ_t give the irreducible representations (irreps) of \mathcal{D}_{nh} that the basis functions, $\Psi_{\mu}^{J, \Gamma_s, \alpha}$ and $\Psi_{\mu'}^{J, \Gamma_t, \alpha'}$, transform according to, and α and α' represent their degenerate components (if present). The block diagonal structure of a Hamiltonian matrix in the \mathcal{D}_{nh} irreducible representation is given in Figure 7.2; the symmetry blocks of non-vanishing matrix elements can be diagonalised separately.

In addition to the matrix becoming block-diagonal according to the symmetries of the basis functions, the resulting eigenfunctions are automatically symmetrised and can be labelled by the irrep that they generate. Without this labelling, the calculations would produce redundant energies, there would be no way to determine the appropriate nuclear-spin statistics to be applied to a given state, and it would be impossible to identify the rotation-vibration transitions allowed by symmetry selection rules [189]. In particular, the nuclear spin-statistical weight factors g_{ns} entering into intensity calculations (for $^{12}\text{C}_2\text{H}_2$ the spin-statistical weight factors are 1 for Σ_g^+ and Σ_u^- (*para*) ro-vibrational states and 3 for Σ_g^- and Σ_u^+ (*ortho*) states) would be unable to be allocated to individual states. There are no allowed electric dipole transitions between *ortho* and *para* states [56, 15]. Allocating symmetries to each state also makes processes such as refinement (for which comparison against experimental energy levels is required; see Section 9.2.1) far easier.

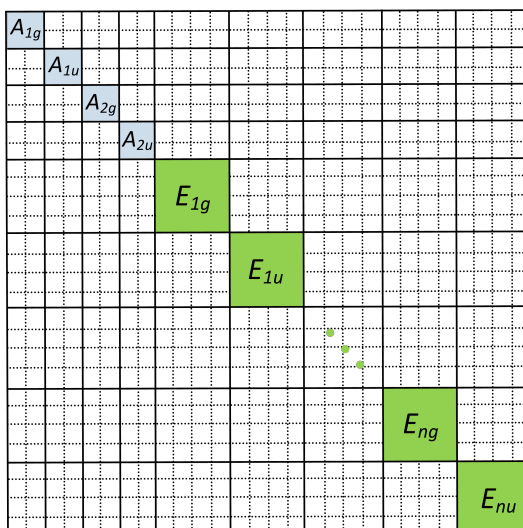


Figure 7.2: The block diagonal structure of a Hamiltonian matrix in the \mathcal{D}_{nh} irreducible representation. The empty (white) cells indicate blocks of vanishing matrix elements. It should be noted that, although \mathbf{B} -symmetries will be present for even values of n , they are not physical and do not appear as a block of matrix elements to be diagonalised.

The symmetrisation is achieved by utilising the fact that each of these Hamiltonian operators commute with the operations in the symmetry group of the molecule in question [200], so that eigenfunctions of a reduced vibrational Hamiltonian generate irreducible representations of the symmetry group. Consequently, a symmetry-adapted ro-vibrational basis set can be obtained numerically by solving the eigenvalue problems for the reduced Hamiltonians; the vibrational basis functions are products of the eigenfunctions thus obtained.

TROVE uses a general numerical symmetrisation approach to build a symmetry adapted basis set, recently outlined in Ref. [200], which will be summarised here. It utilises the concept of a sum-of-product basis set, with the ro-vibrational basis functions (prior to symmetrisation) given by:

$$\Phi_{k,v,l}^J(\theta, \phi, \chi, \xi_1, \xi_2 \dots \xi_M) = |J, k, m\rangle \phi_{n_1}(\xi_1) \phi_{n_2}(\xi_2) \dots \phi_{n_N}(\xi_M), \quad (7.9)$$

with one-dimensional (1D) vibrational basis functions $\phi_{n_i}(\xi_i)$ (where ξ_i is a generalised vibrational coordinate) and rigid-rotor (spherical harmonics) ro-

tational basis functions $|J, k, m\rangle$, where J is the rotational angular momentum quantum number, and k and m are the quantum numbers describing its projections on the molecular z and laboratory Z axes, respectively (with m commonly dropped or taken as $m = 0$ in the absence of an external electric field, as is the case in this work).

According to the TROVE symmetrisation technique [200], the symmetry adapted vibrational basis functions are formed from linear combinations of the products of the 1D vibrational basis functions $\phi_{n_i}(\xi_i)$ as follows. For calculations involving $^{12}\text{C}_2\text{H}_2$ in TROVE, the vibrational part of the basis set of Eq. (7.9) is divided into three symmetry-independent vibrational sub-spaces:

$$CC - stretch : \phi_{n_1}^{(1D)}(\xi_1^{\text{lin}}) = \phi_{n_1}(\xi_1^{\text{lin}}), \quad (7.10)$$

$$CH - stretches : \phi_{n_2 n_3}^{(2D)}(\xi_2^{\text{lin}}, \xi_3^{\text{lin}}) = \phi_{n_2}(\xi_2^{\text{lin}})\phi_{n_3}(\xi_3^{\text{lin}}), \quad (7.11)$$

$$Bends : \phi_{n_4 n_5 n_6 n_7}^{(4D)}(\xi_4^{\text{lin}}, \xi_5^{\text{lin}}, \xi_6^{\text{lin}}, \xi_7^{\text{lin}}) = \phi_{n_4}(\xi_4^{\text{lin}})\phi_{n_5}(\xi_5^{\text{lin}})\phi_{n_6}(\xi_6^{\text{lin}})\phi_{n_7}(\xi_7^{\text{lin}}), \quad (7.12)$$

where $n_1 \dots n_7$ relate to the vibrational modes of acetylene as used in the TROVE approach; Table 3.1 of Section 3.1 gives the typical quantum numbers used to describe the rotational and vibrational states of $^{12}\text{C}_2\text{H}_2$, with their relationship to the quantum numbers used in TROVE given in Table 7.1.

For the stretching primitive basis functions, $\phi_{n_1}(\xi_1)$, $\phi_{n_2}(\xi_2)$ (Eq. 7.10) and $\phi_{n_3}(\xi_3)$ (Eq. 7.11), the eigenfunctions of the corresponding 1D reduced stretching Hamiltonian operators $\hat{H}_i^{(1D)}$ are used, obtained using the Numerov-Cooley approach [50, 339, 340]. The bending basis functions, $\phi_{n_4}(\xi_4) \dots \phi_{n_7}(\xi_7)$ (Eq. 7.12), on the other hand, are formed from 1D Harmonic oscillator functions (the harmonic constants $\tilde{\omega}_i$ are obtained from the corresponding second derivatives of $V(\boldsymbol{\xi})$ at the equilibrium geometry). Each invariant sub-space is then processed through the corresponding reduced Schrödinger equation (1D, 2D and 4D, respectively). The reduced Hamiltonians $\hat{H}^{(ND)}$ ($N = 1, 2, 4$) are

Table 7.1: Quantum numbers used to classify the energy states of $^{12}\text{C}_2\text{H}_2$ in TROVE. See Table 3.1 for description of the experimental quantum numbers.

TROVE	Standard quantum numbers (see Table 3.1)
n_1 CC-stretch (1D)	ν_2
n_2, n_3 CH-stretches (2D)	$\nu_1 + \nu_3$
n_4, n_5, n_6, n_7 Bends (4D)	$\nu_4 + \nu_5$
L	Total vibrational angular momentum, $L = \ell_4 + \ell_5 $
$K = k $	Rotational quantum number; z-projection of the rotational angular momentum
J	Quantum number associated with rotational angular momentum, \mathbf{J} .
Γ_{vib}	Vibrational symmetry
Γ_{rot}	Rotational symmetry
Γ	Total symmetry, $\Gamma_{\text{vib}} \otimes \Gamma_{\text{rot}}$, can be related to <i>e/f</i> and <i>ortho/para</i> (see Chapter 3 for definitions)

constructed by averaging the total vibrational Hamiltonian operator $\hat{H}^{(J=0)}$ over the other ground vibrational basis functions. For example, $\hat{H}^{(4D)}$ is given by:

$$\hat{H}^{(4D)} = \langle 0 | \langle 0, 0 | \hat{H}^{(J=0)} | 0, 0 \rangle | 0 \rangle, \quad (7.13)$$

where $|0\rangle = \phi_0^{(1D)}(\xi_1)$ and $|0, 0\rangle = \phi_{0,0}^{(2D)}(\xi_2, \xi_3)$. The eigenfunctions obtained are classified according to the \mathcal{D}_{nh} point group symmetry, as outlined in Chapter 4 (as opposed to infinite-order $\mathcal{D}_{\infty h}$ point group). The symmetrised eigen-solution of the bending sub-space (Eq. 7.12) leads to a solution of the 4D isotropic oscillator in the $\mathcal{D}_{\infty h}$ representation.

According to the idea of the so-called complete set of commuting operators (CSCO) [200] which the TROVE symmetrisation approach is based on, the eigenfunctions of the reduced operator $\hat{H}^{(ND)}$ must transform according to one of the irreps of the symmetry group of the system, since $\hat{H}^{(ND)}$ commutes with the symmetry operators of this group. Thus the symmetrisation of the basis set is generated automatically by solving the appropriate eigenvalue problem, provided that the corresponding irreps have been determined. To this end, TROVE applies the symmetry operators of the appropriate group to the eigenfunctions and analyses their transformation properties on a set of

sampled geometries (usually 40-60). Some states of the same energy (either with accidental or actual degeneracy) may appear as random mixtures of each other, and have to be processed simultaneously and even further reduced to irreps, if necessary (see Section 7.1.3 for an example).

Applying this procedure to stretching functions gives rise to *A*-type symmetries: e.g. for \mathcal{D}_{nh} (even n), the eigenfunctions of $\hat{H}^{(1D)}$ span the A_{1g} irrep, while the eigenfunctions of $\hat{H}^{(2D)}$ span the A_{1g} and A_{2u} irreps.

The 4D bending basis set, based on the 1D harmonic oscillators of Eq. (7.12), has the disadvantage of being extremely degenerate: combinations of $\phi_{n_4 n_5 n_6 n_7}^{(4D)}$ give rise to large clusters of the same energies. According to the TROVE symmetrisation approach these combinations must be processed together, which makes this process extremely slow. In order to facilitate this step the 4D bending sets (Eq. (7.12)) are first transformed to become eigenfunctions of the vibrational angular momentum operator,

$$\hat{L}_z = \sum_{\lambda, \lambda'} \xi_{\lambda}^{\text{lin}} \zeta_{\lambda, \lambda'}^z \hat{p}_{\lambda'} \quad (7.14)$$

where p_{λ} is a vibrational momentum operator, $\zeta_{\lambda, \lambda'}^z$ are Coriolis coefficients [334], and $\xi_{\lambda}^{\text{lin}}$ are linearised internal coordinates.

TROVE is equipped to compute matrix elements of quadratic forms, therefore \hat{L}_z^2 is used instead of \hat{L}_z . Using the $\phi_{n_4 n_5 n_6 n_7}^{(4D)}$ basis functions eigenfunctions of \hat{L}_z^2 are found by diagonalising the matrix formed by combinations of the 4D bending basis set of Eq. (7.12):

$$\langle \phi_{n_4 n_5 n_6 n_7}^{(4D)} | \hat{L}_z^2 | \phi_{n'_4 n'_5 n'_6 n'_7}^{(4D)} \rangle. \quad (7.15)$$

The eigenfunctions of \hat{L}_z^2 are consequently characterised by their vibrational angular momentum $\ell = |\ell| = \sqrt{\ell^2}$ and can thus be divided into independent sub-sets with different symmetry properties: the $L = 0$ sub-set must be a mixture of *A*-type functions, while the $L > 0$ sub-sets consist of the E_L -type irreps (E_{Lg} and E_{Lu}). These mixtures are then further reduced to irreps using the TROVE symmetrisation scheme outlined above, in which the reduced 4D-eigenvalue problem, using the eigenfunctions of \hat{L}_z^2 as the basis set, is solved

for a 4D isotropic harmonic oscillator Hamiltonian:

$$\hat{H}^{4D} = \frac{1}{2} (\hat{p}_4^2 + \hat{p}_5^2 + \hat{p}_6^2 + \hat{p}_7^2) + \frac{1}{2} \lambda (\xi_4^2 + \xi_5^2 + \xi_6^2 + \xi_7^2), \quad (7.16)$$

where λ is a constant related to the standard harmonic oscillator constant (see Sections 10.4.3 and 11.3.2 of Ref [189]) and \hat{p}_i are the vibrational momenta, conjugate to generalised vibrational coordinates ξ_i . Thus eigenfunctions are obtained which can be divided into sub-sets of the same energies and values of ℓ . It also facilitates another important constraint for the $(3N - 5)$ approach to linear molecules; that the rotation and vibrational basis sets need to be coupled according to the linear molecule angular momentum rule $k = \ell$ (see, for example, Refs. [330, 338], and earlier in this chapter), where $K = |k|$, which requires the states to be classified by L . The maximum value for $L_{\max} = K_{\max}$ is specified as an input into the TROVE numerical routine. These sub-sets must transform independently, thereby significantly decreasing the time spent on the symmetry sampling step by breaking the symmetry space into small sets and making numerical calculations more computationally viable. Although the \hat{L}_z^2 -diagonalisation step is not strictly necessary for the general TROVE symmetrisation procedure that follows it, this increase in efficiency is a big advantage.

As a result of applying the procedure described above, a symmetry-adapted vibrational basis set $\Phi_{v,L}^{\Gamma_{\text{vib}},\alpha}$ is generated. Here Γ_{vib} is the irrep of the basis function according to \mathcal{D}_{nh} , and α indicates a degenerate component in the case of 2D irreps.

The symmetry-adapted rotational basis set in TROVE is represented by:

$$|J, K, \tau\rangle^{\Gamma_{\text{rot}}} = \frac{i^\sigma}{\sqrt{2}} \left[|J, K\rangle + (-1)^{J+K+\tau} |J, -K\rangle \right], \quad (7.17)$$

where $K = 0$ is a special case, given by:

$$|J, 0, \tau\rangle^{\Gamma_{\text{rot}}} = |J, 0\rangle. \quad (7.18)$$

Here $|J, k\rangle$ is a rigid rotor wavefunction, with the Z-projection of the rotational quantum number m omitted here. $\tau (= 0, 1)$ is a parameter used to define

the parity of a state, where $\sigma = (K \bmod 3)$ for $\tau = 1$ and $\sigma = 0$ for $\tau = 0$ (see [341, 342, 200]). The irreps Γ_{rot} of these functions are listed in Table 7.2, where τ defines their degenerate component. The symmetry properties of $|J, K, \tau\rangle^{\Gamma_{rot}}$ can be derived from those of $|J, k\rangle$ using the method described in Ref. [55].

Table 7.2: Symmetries of the symmetrised rotational basis set used by TROVE, Eqs. (7.17), 7.18 for different combinations of J , K and τ (where $\tau (= 0, 1)$ and $K = |k|$); each 2D representation E_{Kg} state has an a and b component, represented by the different values of τ . See Table 4.7 for an explanation of the differing notation of Γ_{rot} for even and odd values of n .

K	τ	Γ_{rot}	
		Even n	Odd n
0	0	A_{1g}	A'_1
	1	A_{2g}	A'_2
> 0, odd	0	E_{kgb}	E''_{kb}
	1	E_{kga}	E''_{ka}
> 0, even	0	E_{kga}	E'_{ka}
	1	E_{kgb}	E'_{kb}

The vibrational basis set is then processed through a double-layered contraction scheme [200], where (i) symmetrically independent modes are combined and used to solve reduced Hamiltonian problems resulting in symmetrised combinations of the corresponding basis functions and (ii) then used to solve the vibrational ($J = 0$) problem. The final contracted TROVE basis functions are given by symmetrised products of the rotational and vibrational basis functions,

$$\Phi_{v,L,K}^{J,\Gamma} = \Phi_{v,l}^{\Gamma_{vib}} \otimes |J, K, \Gamma_{rot}\rangle. \quad (7.19)$$

Here, $\Phi_{v,l}^{\Gamma_{vib}}$ is a vibrational ($J = 0$) eigenfunction of the pure vibrational (of generic vibrational quantum number ν) Hamiltonian \hat{H}_{vib} which transforms according to the Γ_{vib} irreducible representation (irrep) [333]. Note that

$K = |k| = L$ according to the $(3N - 5)$ approach to angular momentum in linear molecules (see, for example, Ref. [330], [338]), which ensures no nonphysical states are included in the basis set and corresponding solution. $|J, K, \Gamma_{\text{rot}}\rangle$ is a symmetrised linear combination of rotational basis functions which transform according to the Γ_{rot} irrep and Γ_s is one of the irreps of the direct product $\Gamma_{\text{vib}} \otimes \Gamma_{\text{rot}}$. Equation (7.19) gives the final contracted symmetrised TROVE ro-vibrational basis functions. Further details on the general symmetrisation approach in TROVE can be found in Ref. [200], with updates for linear molecules outlined in this Chapter (based on Chubb *et al.* [55]).

As mentioned in Chapter 4, for a linear molecule such as HCCH both the vibrational $\Phi_{v,l}^{\Gamma_{\text{vib}}}$ and rotational $|J, K, \Gamma_{\text{rot}}\rangle$ basis functions must transform according to the infinite molecular point group $\mathcal{D}_{\infty\text{h}}$, while the total nuclear-rotation-vibration eigenfunction spans a four-dimensional irrep of the finite $\mathcal{D}_{\infty\text{h}}(\text{M})$ molecular symmetry group, or isomorphic to it [55]. The latter constraint can also be interpreted within the irreps of the point group $\mathcal{D}_{\infty\text{h}}$ as follows. The $\mathcal{D}_{\infty\text{h}}$ point group spans the following irreps: $A_{1g}, A_{2g}, A_{1u}, A_{2u}, E_{1g}, E_{1u}, \dots, E_{k(g/u)}$ ($k = 1, 2, \dots, \infty$). The rotational and vibrational basis symmetries Γ_{vib} and Γ_{rot} spanning these irreps can also be associated with the corresponding value of the projection of the angular momenta (vibrational L or rotational K) on the z axis: the A -type irreps are those with a zero value of L (or K), while the E_k irreps are characterised by the angular momentum quantum number K . Hence, both $\Phi_{v,l}^{\Gamma_{\text{vib}}}$ and $|J, K, \Gamma_{\text{rot}}\rangle$ can span any irreps with the corresponding value of the angular momentum, L or K , while the total nuclear-rotation-vibration function in Eq. (7.19) can span only the A -type irreps Γ of $\mathcal{D}_{\infty\text{h}}$.

The model outlined in this section, along with the potential energy function given in Section 8.2, and dipole moment function given in Section 8.3 were used in the calculation of the *ab initio* line list given in Section 8.4.

7.1.3 Numerical Example of Basis Set Symmetrisation

As an illustration of the practical application of the finite \mathcal{D}_{nh} group being used in place of $\mathcal{D}_{\infty h}$, an example of the construction of the vibrational basis set in case of the linear molecule $^{12}\text{C}_2\text{H}_2$ is given here. The implementation of the $(3N - 5)$ coordinates approach in TROVE is used here and a set of seven vibrational coordinates is thus used for $^{12}\text{C}_2\text{H}_2$: ΔR , Δr_1 , Δr_2 , Δx_1 , Δy_1 , Δx_2 , Δy_2 , as illustrated in Figure 7.1. The transformation matrices defining their symmetry properties are listed in Table 7.3 (with even n used in this example). These relate to the symmetry operations of Table 4.4, and the general irrep transformation matrices for \mathcal{D}_{nh} of even n given in Table 4.11. The two-component vectors $\vec{\rho}_1 = (\Delta x_1, \Delta y_1)^T$ and $\vec{\rho}_2 = (\Delta x_2, \Delta y_2)^T$ transform as E_{1u} , with the corresponding 2D transformation matrices from Table 4.11.

Table 7.3: Transformation matrices based on those of Table 4.11 for the \mathcal{D}_{nh} (n even) group (relating to the symmetry operations of Table 4.4), where n is even, for transforming the set of 7 vibrational coordinates ($\xi = \{R, r_1, r_2, \Delta x_1, \Delta y_1, \Delta x_2, \Delta y_2\}$, as illustrated in Figure 7.1) used in the calculations of Chapter 8. m is an integer for the bounds given for each operation, used to form ϵ_m , where $\epsilon = \frac{2\pi}{n}$ in all cases. The transformation is given in terms of two-component vectors $\vec{\rho}_1 = (\Delta x_1, \Delta y_1)^T$ and $\vec{\rho}_2 = (\Delta x_2, \Delta y_2)^T$, which transform as E_{1u} with the corresponding transformation matrices $\mathbf{M}_R^{E_{1u}}$ (with R denoting the general group operation) from Table 4.11.

Irrep	ϵ_m	m	Transformation matrix						Transformation	
E			1	0	0	0	0	0	0	ΔR
			0	1	0	0	0	0	0	Δr_1
			0	0	1	0	0	0	0	Δr_2
			0	0	0	1	0	0	0	$\vec{\rho}_1$
			0	0	0	0	1	0	0	
			0	0	0	0	0	1	0	$\vec{\rho}_2$
			0	0	0	0	0	0	1	
C_n^m	$m\epsilon$	$1 \dots n - 1$	1	0	0	0	0	0	0	ΔR
			0	1	0	0	0	0	0	Δr_1
			0	0	1	0	0	0	0	Δr_2

			0 0 0 $\cos \phi_n$ $-\sin \phi_n$ 0 0	$\mathbf{M}_{C_n^r}^{E_{1u}}(\epsilon_m) \cdot \vec{\rho}_1$
			0 0 0 $\sin \phi_n$ $\cos \phi_n$ 0 0	
			0 0 0 0 0 $\cos \phi_n$ $-\sin \phi_n$	$\mathbf{M}_{C_n^r}^{E_{1u}}(\epsilon_m) \cdot \vec{\rho}_2$
			0 0 0 0 0 $\sin \phi_n$ $\cos \phi_n$	
C_2'	$2m\epsilon$	$0 \dots \frac{n}{2} - 1$	1 0 0 0 0 0 0	ΔR
C_2''	$\epsilon(2m+1)$	$0 \dots \frac{n}{2} - 1$	0 0 1 0 0 0 0	Δr_2
			0 1 0 0 0 0 0	Δr_1
			0 0 0 0 0 $\cos \phi_n$ $\sin \phi_n$	$\mathbf{M}_{C_2'}^{E_{1u}}(\epsilon_m) \cdot \vec{\rho}_2$
			0 0 0 0 0 $\sin \phi_n$ $-\cos \phi_n$	
			0 0 0 $\cos \phi_n$ $\sin \phi_n$ 0 0	$\mathbf{M}_{C_2''}^{E_{1u}}(\epsilon_m) \cdot \vec{\rho}_1$
			0 0 0 $\sin \phi_n$ $-\cos \phi_n$ 0 0	
i			1 0 0 0 0 0 0	ΔR
			0 0 1 0 0 0 0	Δr_2
			0 1 0 0 0 0 0	Δr_1
			0 0 0 0 0 0 -1 0	$-\vec{\rho}_2$
			0 0 0 0 0 0 0 -1	
			0 0 0 -1 0 0 0 0	$-\vec{\rho}_1$
			0 0 0 0 -1 0 0 0	
σ_h			1 0 0 0 0 0 0	ΔR
			0 0 1 0 0 0 0	Δr_2
			0 1 0 0 0 0 0	Δr_1
			0 0 0 0 0 0 1 0	$\vec{\rho}_2$
			0 0 0 0 0 0 0 1	
			0 0 0 1 0 0 0 0	$\vec{\rho}_1$
			0 0 0 0 1 0 0 0	
σ_d	$\epsilon(2m+1)$	$0 \dots \frac{n}{2} - 1$	1 0 0 0 0 0 0 0	ΔR
σ_v	$2m\epsilon$	$0 \dots \frac{n}{2} - 1$	0 1 0 0 0 0 0 0	Δr_1
			0 0 1 0 0 0 0 0	Δr_2
			0 0 0 $\cos \phi_n$ $\sin \phi_n$ 1 0	$\mathbf{M}_{\sigma_{d/v}}^{E_{1u}}(\epsilon_m) \cdot \vec{\rho}_1$
			0 0 0 $\sin \phi_n$ $-\cos \phi_n$ 0 1	
			0 0 0 1 0 $\cos \phi_n$ $\sin \phi_n$	$\mathbf{M}_{\sigma_{d/v}}^{E_{1u}}(\epsilon_m) \cdot \vec{\rho}_2$
			0 0 0 0 1 $\sin \phi_n$ $-\cos \phi_n$	
S_n^i	$m\epsilon$	$1 \dots n - 2$	1 0 0 0 0 0 0 0	ΔR
			0 0 1 0 0 0 0 0	Δr_2
			0 1 0 0 0 0 0 0	Δr_1
			0 0 0 0 0 0 $\cos \phi_n$ $-\sin \phi_n$	$\mathbf{M}_{S_n^i}^{E_{1u}}(\epsilon_m) \cdot \vec{\rho}_2$

			0	0	0	0	0	$\sin \phi_n$	$\cos \phi_n$	$\mathbf{M}_{S_n}^{E_{1u}}(\boldsymbol{\varepsilon}_m) \cdot \vec{\rho}_1$
			0	0	0	$\cos \phi_n$	$-\sin \phi_n$	0	0	
			0	0	0	$\sin \phi_n$	$\cos \phi_n$	0	0	

An example of building a symmetry adapted basis set for the 4D bending function of Eq. (7.12) using the TROVE symmetrisation approach for linear molecules is given. In this example, the size of the primitive basis sets was controlled by the polyad number

$$P = 2n_1 + n_2 + n_3 + n_4 + n_5 + n_6 + n_7 \leq P_{\max}, \quad (7.20)$$

with $P_{\max}=2$. Here, the quantum numbers n_k for $k=1 \dots 7$ correspond to the vibrational primitive functions $\phi_{n_k}(\xi_k)$, in the TROVE quantum number notation of Table 7.1.

Using the 4D reduced Hamiltonian in Eq. (7.13) with this small basis set, the following contracted eigenfunctions are obtained (with only the first seven given here for illustration purposes):

$$\Psi_1^{L=0} = -0.9793 |0000\rangle - 0.0095(|2000\rangle + |0200\rangle + |0020\rangle + |0002\rangle) + 0.1425(|1010\rangle + |0101\rangle),$$

$$\Psi_2^{L=1} = \frac{1}{\sqrt{2}}(|1000\rangle - |0010\rangle),$$

$$\Psi_3^{L=1} = \frac{1}{\sqrt{2}}(|0100\rangle - |0010\rangle),$$

$$\Psi_4^{L=1} = \frac{1}{\sqrt{2}}(|1000\rangle + |0100\rangle),$$

$$\Psi_5^{L=1} = \frac{1}{\sqrt{2}}(|0100\rangle + |0010\rangle),$$

$$\Psi_6^{L=2} = -0.3505(|2000\rangle - |0200\rangle + |0020\rangle - |0002\rangle) + 0.4957(|1010\rangle - |0101\rangle) + 0.0651(|1100\rangle - |1001\rangle - |0110\rangle + |0011\rangle),$$

$$\Psi_7^{L=2} = 0.0460(|2000\rangle - |0200\rangle + |0020\rangle - |0002\rangle) - 0.0651(|1010\rangle - |0101\rangle) + 0.4957(|1100\rangle - |1001\rangle - |0110\rangle + |0011\rangle),$$

One can see that after this step some of the eigenfunctions ($\Psi_1, \Psi_2, \Psi_3, \Psi_4$ and Ψ_5) are already in the form of an irreducible representation, while Ψ_6 and Ψ_7 need to be further reduced.

In order to define the L -values, the matrix elements of \hat{L}_z are computed as in Eqs. (7.14) and (7.15). In this example, the sets with degenerate eigenvalues and identical L values are: $\{\Psi_1^{L=0}\}$ ($\tilde{E}_1 = 0 \text{ cm}^{-1}$), $\{\Psi_2^{L=1}, \Psi_3^{L=1}\}$ ($\tilde{E}_2 = 636.11 \text{ cm}^{-1}$), $\{\Psi_4^{L=1}, \Psi_5^{L=1}\}$ ($\tilde{E}_3 = 763.12 \text{ cm}^{-1}$), $\{\Psi_6^{L=2}, \Psi_7^{L=2}\}$ ($\tilde{E}_4 = 1215.84 \text{ cm}^{-1}$). The pair of eigenfunctions $\Psi_2^{L=1}$ and $\Psi_3^{L=1}$, for example, both have $L = 1$ and are also degenerate with the eigenvalue 636.11 cm^{-1} ($\pm 10^{-12}$). All degenerate states are combined into the same set and are assumed to share symmetry transformation properties, now with the additional constraint that those states in the same set must also possess the same value of L . For the present example, this gives the following symmetries and L -values: $\{\Psi_1^{L=0}\}^{A_{1g}}$, $\{\Psi_2^{L=1}, \Psi_3^{L=1}\}^{E_{1g}}$, $\{\Psi_4^{L=1}, \Psi_5^{L=1}\}^{E_{1u}}$, $\{\Psi_6^{L=2}, \Psi_7^{L=2}\}^{E_{2g}}$.

The irreducible form of the wavefunctions Ψ_6, Ψ_7 is now given by:

$$\begin{aligned}\Psi_6^{L=2} &= \frac{\sqrt{2}}{4}(|2000\rangle - |0200\rangle + |0020\rangle - |0002\rangle) - \frac{1}{2}(|1010\rangle - |0101\rangle), \\ \Psi_7^{L=2} &= \frac{1}{2}(|1100\rangle - |1001\rangle - |0110\rangle + |0011\rangle).\end{aligned}$$

7.1.4 Even vs. Odd \mathcal{D}_{nh} Symmetries

For the example calculations using even vs odd \mathcal{D}_{nh} that are outlined below the primitive and contracted basis sets were controlled by the polyad number as given by Eq. (8.13), with $P_{\max}=8$ for the primitive basis set and reduced to 6 after contraction (see Refs. [50, 24] for more details).

The finite \mathcal{D}_{nh} groups were used here, with a value of n large enough to cover all required excitations of the vibrational angular momentum $L = |\ell|$ up to up L_{\max} and of the rotational quantum number K up to K_{\max} (with the constraint $L_{\max} = K_{\max}$) such that $n = 2L_{\max} + 1$ or $n = 2L_{\max} + 2$ (depending on whether n is odd or even, respectively). For example, in order to be able to cover the rotational excitation up to $K = 10$ (E_{10g} and E_{10u}), it is necessary to use at least the \mathcal{D}_{21h} symmetry.

Even though odd and even values of n lead to different symmetry operations (see Table 4.4), both lead to the same resulting eigenvalues energies in the TROVE calculations, with example energies and assignments given in Ta-

ble 7.4, on the condition that $n \geq 2L_{\max} + 1$ (odd n) or $n \geq 2L_{\max} + 2$ (even n). For a maximum value of the z -projection of the vibrational angular momentum, $L_{\max} = K_{\max} = 4$, different values of n were used for \mathcal{D}_{nh} in the symmetrisation approach described in Section 7.1.2.

Table 7.4: An example of some rotational, vibrational and ro-vibrational assignments (see Section 3.1 for the meaning of these assignments) with associated symmetries (Γ_r , Γ_v and Γ_{r-v} , respectively) from ro-vibrational calculations using TROVE of $^{12}\text{C}_2\text{H}_2$ using different (even/odd) values of n for \mathcal{D}_{nh} . In each case $L_{\max} = 4$. The energies are identical for symmetries of higher n than those shown here, but converge towards the experimental values as the polyad number (Eq. 8.13) is increased; a low value is used here for demonstration purposes.

Energy (cm^{-1})	J	K	τ	$\nu_1 \nu_2 \nu_3 \nu_4^l \nu_5^l$	\mathcal{D}_{12h}			\mathcal{D}_{13h}		
					Γ_{r-v}	Γ_r	Γ_v	Γ_{r-v}	Γ_r	Γ_v
2.356491	1	0	1	0000 ⁰ 0 ⁰	A_{2g}	A_{2g}	A_{1g}	A'_2	A'_2	A'_1
625.810547	1	1	1	0001 ¹ 0 ⁰	A_{2g}	E_{1g}	E_{1g}	A'_2	E''_1	E''_1
1283.603736	1	0	1	0002 ⁰ 0 ⁰	A_{2g}	A_{2g}	A_{1g}	A'_2	A'_2	A'_1
7.069433	2	0	0	0000 ⁰ 0 ⁰	A_{1g}	A_{1g}	A_{1g}	A'_1	A'_1	A'_1
630.518518	2	1	1	0001 ¹ 0 ⁰	A_{1g}	E_{1g}	E_{1g}	A'_1	E''_1	E''_1
1276.518756	2	2	0	0002 ² 0 ⁰	A_{1g}	E_{2g}	E_{2g}	A'_1	E'_2	E'_2

If a lower value than $n = 2L_{\max} + 1$ (for odd n) or $n = 2L_{\max} + 2$ (for even n) is used, then the symmetrisation procedure will lead to the wrong classification of states, resulting in, for example, the wrong nuclear statistics in intensity calculations. Ideally the maximum value of $L_{\max} = K_{\max}$ would be limited by $K_{\max} = J_{\max}$, however, it should be noted that in practise numerical calculations are limited by the maximum number of vibrational bending quanta which can be included in calculations, giving a limit on L_{\max} . This is therefore referred to as the deciding factor in what n for \mathcal{D}_{nh} to use.

7.2 The $(3N - 6)$ -approach to Dealing with Linear Molecules

The $3N - 6$ -approach builds upon the ideas and methodology set out by Bunker and Jensen [333, 343] which are based upon a linear triatomic molecule, CH_2 [343]. Here, this concept is extended to symmetric tetratomic molecule $^{12}\text{C}_2\text{H}_2$.

The KEO for a linear molecule (see Section 6.3, Equation (6.4)) in terms of the $3N - 6$ vibrational coordinates ξ (R , r_1 , r_2 , θ_1 , θ_2 and τ) illustrated in Figure 6.2 contains singular terms with negative exponents for coordinates describing bending vibrations. This is demonstrated by the determinant of the \mathbf{t} -matrix of Equation 6.6 as written in terms of this set of $3N - 6$ curvilinear coordinates for $^{12}\text{C}_2\text{H}_2$:

$$\det(\mathbf{t}) = 2 \sin(\theta_1) \sin(\theta_2) R^2 r_1^2 r_2^2. \quad (7.21)$$

It can clearly be seen that if this determinant involves any bending angles, as it does here, it will tend to zero at linearity and therefore inversion of this matrix in the process of building the KEO, as described in Section 6.3, will lead to singular terms.

For the remainder of this section, the bending angles will be referred to as α_1, α_2 instead of θ_1, θ_2 (as given in Figure 6.2) which are related by $\alpha_1 = \pi - \theta_1$, $\alpha_2 = \pi - \theta_2$.

As the bending vibrational coordinates, α_1, α_2 , approach zero at the linear geometry of acetylene, τ and χ (the torsional coordinate of Figure 6.2 and the Euler angle describing rotation about the molecule-fixed z -axis of Figure 6.1, respectively) become undefined. As a result, the terms of the KEO G -matrix which describe vibrations with respect to the τ and χ coordinates, along with part of the pseudopotential U , diverge as $1/\alpha_1^2$ or $1/\alpha_2^2$ at small values of the α_1 or α_2 bending coordinates.

For example, the $1/\alpha_1^2$ -divergent terms of the KEO for acetylene can be

collected together into the expression

$$T_{\text{sing}}^{(1)} = \frac{1}{\sin^2 \alpha_1} \left(-\frac{\hbar^2}{2} G_{\tau\tau}^{(1)} \frac{\partial^2}{\partial \tau^2} - \frac{i\hbar}{2} [G_{\tau\chi}^{(1)} + G_{\chi\tau}^{(1)}] \frac{\partial}{\partial \tau} \hat{J}_z + \frac{1}{2} G_{\chi\chi}^{(1)} \hat{J}_z^2 + U^{(1)} \right), \quad (7.22)$$

where the singular parts of the expressions for elements of vibrational $G_{\tau\tau}^{(1)}$, rotational $G_{\chi\chi}^{(1)}$ and Coriolis $G_{\tau\chi}^{(1)}$ and $G_{\chi\tau}^{(1)}$ matrices and pseudopotential $U^{(1)}$ are independent of α_1 , α_2 and τ . In practical calculations, these are replaced by constant values computed at the equilibrium. An expression similar to Eq. (7.22) can be obtained for $T_{\text{sing}}^{(2)}$ by collecting terms in the total KEO with a $1/\sin^2 \alpha_2$ factor. The explicit analytic expressions for $T_{\text{sing}}^{(1)}$ and $T_{\text{sing}}^{(2)}$, in the coordinate system as shown in Figure 6.2, can be derived using the script which is provided as supplementary information of Ref. [24].

The basis functions $\phi_1(\alpha_1)$ and $\phi_2(\alpha_2)$ now need to be formulated in such a way that they exactly cancel the divergence of the KEO in the vicinity of the linear geometry. From the pragmatic point of view of numerical calculations, the basis functions must be chosen such that they eliminate the singularity in the respective matrix elements. The most evident approach is to cancel the singularity in each term in Eq. (7.22) individually by using the form $\phi_1(\alpha_1) \sim \alpha_1$ and $\phi_2(\alpha_2) \sim \alpha_2$. This is satisfied, for example, by choosing the Legendre orthogonal polynomials as a basis, which approach zero linearly. For this reason, Legendre based polynomials have been employed as a suitable basis functions for solving the bending problem in many variational ro-vibrational approaches [304, 305, 306, 307, 308, 38, 309, 310, 311, 312, 313].

Here, an alternative approach, developed in Refs. [333], [343] for triatomic molecules, is followed, which attempts to find the exact form of the bending wave function in the vicinity of the linear geometry. It is based on the fact that since neither the energy nor the wave function can be singular, the Hamiltonian operator acting on a wave function has to produce a non-singular function as well. Therefore, the divergence of $T_{\text{sing}}^{(1)}$ and $T_{\text{sing}}^{(2)}$ must be exactly cancelled by other terms in the ro-vibrational Hamiltonian; the kinetic energy operators for the α_1 and α_2 vibrations. This can only be so if the wave function $\phi_{v_1}(\alpha_1)$

satisfies the equation

$$-\frac{\hbar^2}{2}G_{\alpha_1\alpha_1}\frac{\partial^2\phi_{v_1}(\alpha_1)}{\partial\alpha_1^2}+T_{\text{sing}}^{(1)}\phi_{v_1}(\alpha_1)=0 \quad \text{at } \alpha_1=0, \quad (7.23)$$

with a similar expression for $\phi_{v_2}(\alpha_2)$. If the basis functions for χ and τ coordinates is chosen to be $\phi_k(\chi) = (2\pi)^{-1/2}e^{ik\chi}$ and $\phi_t(\tau) = (2\pi)^{-1/2}e^{it\tau}$ (k and t are quantum numbers associated with χ and τ , respectively), the integration of Eq.(7.23) over the χ and τ variables yields

$$G_{\alpha_1\alpha_1}\frac{\partial^2\phi_{v_1}(\alpha_1)}{\partial\alpha_1^2}-\frac{1}{\sin^2\alpha_1}\left(t^2G_{\tau\tau}^{(1)}+kt\left[G_{\tau\chi}^{(1)}+G_{\chi\tau}^{(1)}\right]+k^2G_{\chi\chi}^{(1)}+\frac{2}{\hbar^2}U^{(1)}\right)\phi_{v_1}(\alpha_1)=0. \quad (7.24)$$

The solution of this equation implies that for small α_1 the wave function behaves as

$$\psi_{v_1}(\alpha_1) \sim (1 - \cos^2 \alpha_1)^{1/4} L_{n_1}^{m_1}(\cos \alpha_1), \quad (7.25)$$

where $L_{n_1}^{m_1}(\cos \alpha_1)$ is the associated Legendre function of the first kind, a solution to the associated Legendre differential equation [344] with

$$n_1 = -\frac{1}{2} \quad (7.26)$$

$$m_1(k, t) = \sqrt{\frac{1}{4} + \frac{t^2 G_{\tau\tau}^{(1)} + kt \left[G_{\tau\chi}^{(1)} + G_{\chi\tau}^{(1)} \right] + k^2 G_{\chi\chi}^{(1)} + 2U^{(1)}/\hbar^2}{G_{\alpha_1\alpha_1}}}. \quad (7.27)$$

Similar expressions can be obtained for $\psi_{v_2}(\alpha_2)$. At small values of the argument α_1 , the wave function in Eq. 7.25 can be reduced to the expression

$$\psi_{v_1}(\alpha_1) \sim \alpha_1^{\frac{1}{2} \pm m_1(k, t)}, \quad (7.28)$$

where plus and minus signs indicate two solutions for α_1 varying in the positive $[0, \pi]$ and the negative $[0, -\pi]$ directions, respectively. From Eq. (7.28) it follows that bending basis functions are intrinsically coupled with the torsional and k -type rotational molecular motions through parametric dependence on the respective quantum numbers, k and t . More importantly, the bending wave function of a linear molecule behaves as a square root function and forms a non-differentiable cusp at the linear geometry, as illustrated in Figure 7.3.

This linearity-cusp in the wave function is not well reproduced by the commonly used expansions in terms of Legendre polynomials, and, furthermore, convergence towards the exact minimum point of the solution of Eq. (7.28) is slow, as can also be seen in Figure 7.3. Other recent works (for example, Refs. [207, 345]), have also come to the conclusion that the form of the bending wave function of a linear molecule has zero amplitude at $\rho = 0$, as in Figure 7.3.

Work is in progress to implement the approach outlined in this section in to TROVE. The presently implemented automatic numerical approach for building the power series expansion of the KEO is not capable of treating terms with negative exponents, which is the main obstacle to generalisation of the present method. For grid-based approaches, however, the implementation of the present method should be straightforward. Currently, the KEO is built externally using symbolic algebra packages, and read in to TROVE.

It is thought that this approach could be applied to any chain tetratomic molecule and easily extended to polyatomic molecules with more than four atoms, such as linear molecule cyanoacetylene, C_3HN , for example (which is potentially important in exoplanet atmospheres [346] and in investigating that of Titan [347]), or Propynylidyne, C_3H , [348, 349]. It will be interesting to test it also on chain molecules with relatively high barrier to linearity, e.g., H_2O_2 , [350, 15] to see if the exact cusp conditions in Eq. (7.28) will be relevant for the basis set convergence of the variational results.

7.3 Chapter Summary

The $(3N - 5)$ and $(3N - 6)$ approaches to dealing with linear molecules in ro-vibrational energy calculations have been outlined in this chapter. The symmetry of a centrosymmetric linear molecule was a big part of the implementation of the $(3N - 5)$ approach, which has been fully implemented into TROVE (see Chapter 4 for more general background on the symmetry of centrosymmetric linear molecules) and is valid for any linear molecule. The general numerical symmetrisation approach used by TROVE to build symmetry-adapted basis

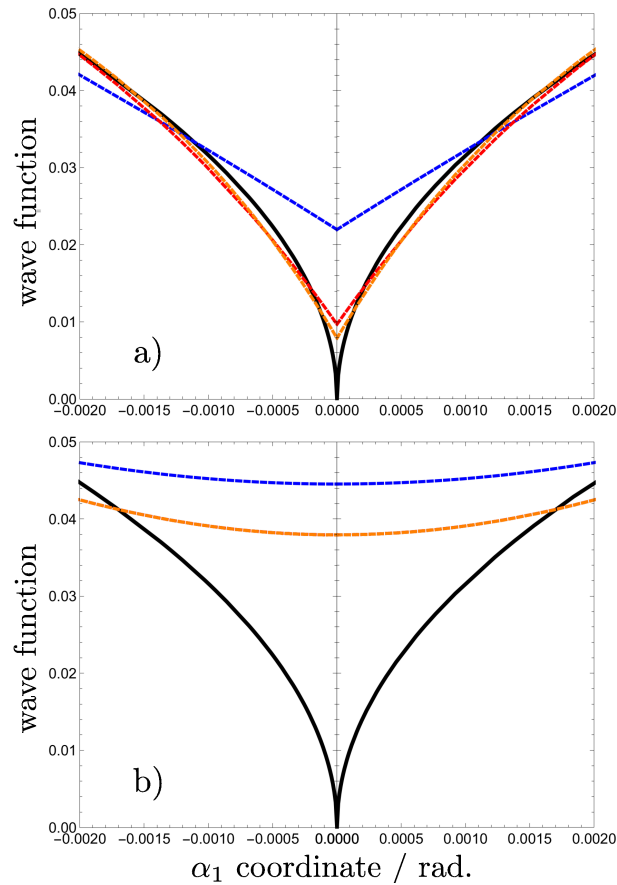


Figure 7.3: Comparison of the exact bending wave function given by Eq. (7.28) with $k, t = 0$ (black line in both panels), with least squares fits of standard Legendre polynomial series truncated at; $n_{\max} = 2$ (blue), 6 (red), and 10 (orange), for $L_n(\alpha)$ (panel a) and $L_n(\cos \alpha)$ (panel b). The fit was done on an equidistant grid of α_1 values from $\alpha_1 = 0$ to 1 degree. Figure reprinted with permission from Ref. [24].

sets [200] has been extended to be compatible with centrosymmetric linear molecules such as $^{12}\text{C}_2\text{H}_2$. This type of molecule is formally described by the $\mathcal{D}_{\infty\text{h}}$ symmetry group, but as TROVE can only work with finite symmetries a finite \mathcal{D}_{nh} (with arbitrary user-defined n) is used instead, with a value of n large enough to cover all required excitations (up to $L_{\text{max}} = K_{\text{max}}$), such that $n = 2L_{\text{max}} + 1$ or $n = 2L_{\text{max}} + 2$ [55] (depending on whether n is odd or even). The TROVE symmetrisation scheme was extended by including the vibrational angular momentum operator \hat{L}_z into the set of commuting operators, allowing the classification of basis sets based on vibrational angular momentum quantum number, L .

The $(3N - 6)$ approach to dealing with linear molecules has also been investigated. Although it is not currently fully implemented into TROVE, work is in progress with this aim in mind. There is also potential for implementation into general nuclear motion routines. A full comparison of this method against the $(3N - 5)$ approach, regarding calculation time and accuracy, would be an interesting investigation to make.

Chapter 8

Variational Calculations of Acetylene

8.1 *Ab Initio* Calculations (MOLPRO)

Ab initio electronic structure calculations were introduced in Section 2.3. The electronic structure package MOLPRO [110] was used to solve, on a large grid of nuclear geometries, the electronic energy of Eq. (2.9), and the dipole moment which is required for calculations of transition strength (Eq. (2.12)). The resulting grid of electronic energies and dipole moments were used in the construction of potential energy surfaces (PES) and a dipole moment surface (DMS) for C_2H_2 , with details given in Sections 8.2 and 8.3, respectively.

8.2 Potential Energy Surfaces

Potential energy surfaces for acetylene are generally either local, appropriate for describing ro-vibrational motion close to the linear equilibrium structure [351, 335, 352, 353, 354], or they are designed to be more global [355, 42, 356, 310] in order to properly describe the isomerisation to vinylidene at around $15,000\text{ cm}^{-1}$ [109, 40]. The set of coordinates used to describe the potential are to some extent determined by this choice; curvilinear coordinates have been thought to represent a non-isomerising potential energy surface (PES) more smoothly than rectilinear [357, 109], though the difference is small in the region very close to equilibrium geometry; while coordinates such as diatom-diatom

are thought to handle the isomerisation process more appropriately [38].

The use of a Taylor series expansion in an appropriate set of coordinates to represent the potential can only be justified for the local surfaces, restricted to accurately describe the area around one potential minimum only at which the expansion is taken; a linear configuration in this case. This is the approach which has been taken in this work (the isomerisation to vinylidene is not considered here). The Taylor series expansion of a PES is often truncated at 4th, 6th or 8th order.

8.2.1 Linearised ($3N - 5$) Potential Energy Surface

In the TROVE rigid approach, all components of the Hamiltonian operator are represented as a Taylor expansion in terms of linearised coordinates (or some 1D functions of them) around the equilibrium configuration, leading to a sum-of-product form designed to facilitate the matrix elements calculations via 1D-integrals. This includes the potential energy function $V(\boldsymbol{\xi})$. Since the PES is usually provided in terms of some different user-chosen curvilinear coordinates, TROVE uses a numerical finite difference method (with quadruple-precision) to re-expand $V(\boldsymbol{\xi})$ in terms of the TROVE-coordinates ξ_λ^{lin} .

The geometrically defined coordinates $\boldsymbol{\xi}$ (R , r_1 , r_2 , θ_1 , θ_2 and τ) used to sample the *ab initio* PES were transformed to the linearised TROVE coordinates ξ_λ^{lin} using the Cartesian coordinate representation as an intermediate via the chain:

$$\boldsymbol{\xi} \rightarrow \{\mathbf{r}_i\} \rightarrow \boldsymbol{\xi}^{lin}, \quad (8.1)$$

with the transformation from $\boldsymbol{\xi}^{lin} \rightarrow \{\mathbf{r}_i\}$ given by Eqs. (7.5–7.7) via the \mathbf{A} -matrix representation. Here $\{\mathbf{r}_i\}$ represents the Cartesian coordinates of an atom i in the molecular coordinate system defined using the Eckart-frame. This transformation is under-defined since there are only six coordinates ξ_λ being used to obtain seven ξ_μ^{lin} . As an additional condition we use the requirement that the x -axis should bisect the dihedral τ angle. Since the potential expansion is built to be invariant for any rotation around the z axis, this requirement does not affect the expansion parameters.

For C₂H₂ it was found that this numerical re-expansion procedure can behave very unstably, leading to extremely large expansion parameters and numerical instability. This is apparently related to the fact that if the C₂H₂ potential function is represented in the original *ab initio* coordinates, it effectively depends on six ($3N - 6$) vibrational coordinates only, but in TROVE it is represented in terms of seven ($3N - 5$) dependent coordinates. The expansion parameters are therefore strongly correlated, which leads to a numerical instability in the finite differences.

It was therefore decided to avoid the TROVE re-expansion by preparing the PES in terms of the TROVE linearised coordinates ξ^{lin} directly (see Section 7.1.1). Thus, the potential energy function of C₂H₂ currently used in TROVE is given by:

$$V(\boldsymbol{\chi}) = \sum_{i,j,k,\dots} f_{i,j,k,\dots} \chi_1^i \chi_2^j \chi_3^k \dots, \quad (8.2)$$

where χ_λ are given by:

$$\begin{aligned} \chi_1 &= 1 - \exp\left(-a \Delta R^{\text{lin}}\right), \\ \chi_2 &= 1 - \exp\left(-b \Delta r_1^{\text{lin}}\right), \\ \chi_3 &= 1 - \exp\left(-b \Delta r_2^{\text{lin}}\right), \\ \chi_4 &= \Delta x_1, \\ \chi_5 &= \Delta y_1, \\ \chi_6 &= \Delta x_2, \\ \chi_7 &= \Delta y_2. \end{aligned} \quad (8.3)$$

Here a and b are two Morse parameters and the displacements are taken from the equilibrium values of R , r_1 and r_2 , respectively. The equilibrium values (at the linear configuration) of x_i and y_i ($i = 1, 2$) are zero.

As discussed in Section 7.1, the ground electronic state of acetylene has an equilibrium structure of linear configuration and is therefore part of the $\mathcal{D}_{\infty h}$ point group. The potential energy must therefore be invariant under the action of operations which are a part of this group, e.g. to any rotation around

z. As TROVE tends to use discrete symmetries (see Section 7.1.2), this is achieved by making it invariant to the operations of \mathcal{D}_{nh} instead. While the process of symmetrising the ro-vibrational basis set requires \mathcal{D}_{nh} with a value for n such that $n \geq 2L_{\max} + 1$ (odd n) or $n \geq 2L_{\max} + 2$ (even n) [55], the same constraint does not need to be applied to the symmetrisation of parameters to be used in the potential energy or dipole moment fitting routines. Instead, the required n for \mathcal{D}_{nh} appears to be related to the expansion order of the potential; for a potential expanded up to 8^{th} order, for example, a symmetry of \mathcal{D}_{12h} is sufficient, with identical results for higher values of n . The operations of the \mathcal{D}_{12h} group were therefore used to form the symmetrised $3N - 5$ potential energy function, expanded up to 8^{th} order.

The *ab initio* electronic structure calculations used in this work were performed using MOLPRO [110] at a CCSD(T)-F12c level of theory (this has a computational cost close to that of conventional CCSD, while retaining the accuracy of CCSD(F12) [358]) for the PES with a VQZ-F12 basis set [359, 360]. They were carried out on a grid of 66 000 points spanning the 6D nuclear-geometry coordinate space up to $50\,000\text{cm}^{-1}$, defined by a set of 6 curvilinear bond length and bond angle coordinates (as given in Figure 6.2).

When fitting $V(\boldsymbol{\xi})$ in Eq. (8.2)-(8.3) to the *ab initio* energies, each grid point i was weighted using the method outlined in Ref. [361], with a higher weight, w_i , given to points with lower energy:

$$w_i = \frac{s_i}{\tilde{E}_i^w}, \quad (8.4)$$

$$s_i = \frac{\{\tanh[-\alpha(V_i - V^{\text{top}})] + 1.002002002\}}{2.002002002}, \quad (8.5)$$

$$\tilde{E}_i^w = \max(V_{\max}, V_i). \quad (8.6)$$

Here, V_i is the potential energy, in cm^{-1} , above the equilibrium value for each point i , α is a parameter which can be varied, V^{top} is the ‘switching energy’, with s_i switching between 0.001 for energies much above V^{top} and 1 for those

much below, and \tilde{E}_i^w is included in order to avoid low energy noise being too much of an influence, giving a bias against points below V_{max} . In the case of the linearised $(3N - 5)$ *ab initio* potential energy fit used in this work, the following parameters were used: $\alpha = 6 \times 10^{-4} \text{ cm}^{-1}$, $V_{top} = 20\,000 \text{ cm}^{-1}$, $V_{max} = 6000 \text{ cm}^{-1}$.

A least squares fitting routine was used to fit the coefficients $f_{i,j,k,\dots}$ in Eq. (8.2) to the *ab initio* energies, using a grid of 46 986 *ab initio* points covering up to $14\,000 \text{ cm}^{-1}$, weighted as in Eq. (8.4)-(8.6), with a weighted root-mean-square (*rms*) error of 3.98 cm^{-1} and an un-weighted *rms* of 15.65 cm^{-1} , using 358 symmetrised parameters expanded up to 8th order. The potential energy function is provided as supplementary material to Ref. [24] as a Fortran program.

The Born Oppenheimer Diagonal Correction (BODC) is usually neglected in the Born-Oppenheimer approximation. It has been shown that the worst case for the BODC, for H_2 , gives a correction of 16 cm^{-1} , whereas for acetylene this is estimated to be less than 1 cm^{-1} (Refs. [362], [363]). This has not been taken into account in the present work, but for greater spectroscopic accuracy this and other higher order corrections [364] could be taken into account in the future.

8.2.2 Non-Linearised $(3N - 5)$ Potential Energy Surface

Different coordinates were explored with which to represent the potential function. The $(3N - 5)$ fit was found to improve when bond lengths (R , r_1 and r_2) instead of linearised coordinates (R^{lin} , r_1^{lin} and r_2^{lin}) were used for the z -coordinates (with a weighted *rms* error of 0.69 cm^{-1} and an un-weighted *rms* of 7.40 cm^{-1} for the same grid of weighted *ab initio* points up to $14\,000 \text{ cm}^{-1}$); see Figure 8.1 for the residuals of both $(3N - 5)$ fits (using linearised and non-linearised coordinates) as a function of energy. As mentioned above, this choice has a degeneracy in the definition of an instantaneous geometry for the interbond angles $\theta_i < 90^\circ$ and $> 90^\circ$. It should be noted that the $\theta_i > 90^\circ$ geometries are found to occur at energies less than the isomerisation to vinylidene at around $15,000 \text{ cm}^{-1}$ (Refs. [109], [40]) and are therefore likely to be impor-

tant for ro-vibrational calculations. The linearised-coordinate alternative does not have this degeneracy issue, though it does have the aforementioned problem with being less intuitive in modelling vibrational stretches. Nevertheless, the linearised-coordinate fit to the potential energy function of Eq. (8.4)-(8.6) is reasonable and the use of a potential function which has been fit using linearised coordinates avoids any re-expansion, as these are exactly the coordinates which are used by TROVE. This makes this potential function suited for use with TROVE, but not particularly useful for the community. A PES fitted using the standard six curvilinear coordinates R , r_1 , r_2 , θ_1 , θ_2 , and τ , with the χ -expansion variables (see Section 8.2.3) is therefore also provided as supplementary data for the publication associated with this work, Ref. [24].

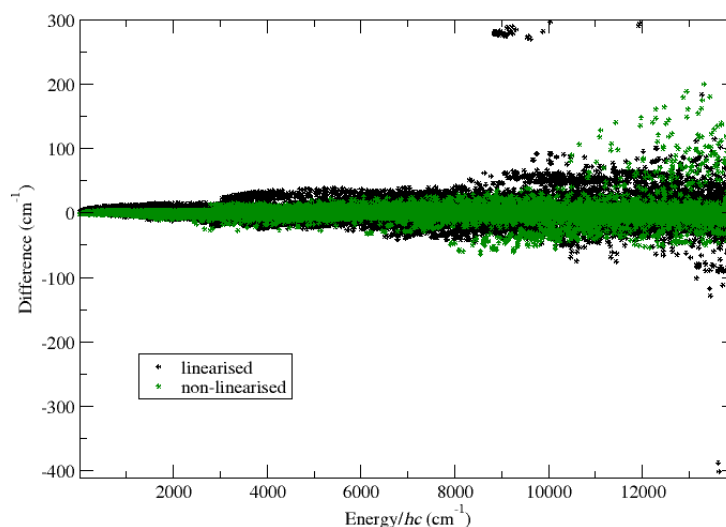


Figure 8.1: A comparison of the residuals of the $(3N - 5)$ linearised coordinate PES fit with the $(3N - 5)$ non-linearised coordinate PES fit using the same grid of *ab initio* points

8.2.3 $(3N - 6)$ Potential Energy Surface

A Fortran least squares fitting routine was used to fit the *ab initio* points described in Section 8.2.1 to functions of a Morse-oscillator form, as given

below for the $3N - 6$ set of internal valence coordinates (which are illustrated in Figure 6.2):

$$V(\mathbf{y}) = \sum_{i,j,k,\dots} F_{i,j,k,\dots} y_1^i y_2^j y_3^k \dots, \quad (8.7)$$

where

$$\begin{aligned} y_1 &= 1 - e^{-a_1(R-R_e)}, \\ y_2 &= 1 - e^{-a_2(r_1-r_e)}, \\ y_3 &= 1 - e^{-a_2(r_2-r_e)}, \\ y_4 &= \sin \theta_1, \\ y_5 &= \sin \theta_2, \\ y_6 &= \cos \tau. \end{aligned} \quad (8.8)$$

The use of Morse functions for the stretches has been shown to give a more accurate representation on the condition that the two atoms involved are suitably light [38, 365], as is the case for the bonds in the acetylene molecule. Care was taken to comply with the relevant symmetry constraints on the expansion coefficients $F_{i,j,k,\dots}$, for example if either of the bending angles were being expanded to the power of zero then the dihedral angle, τ should not be expanded to any power greater than zero, as for linear geometries it is undefined.

The same grid of 46 986 *ab initio* points are used as for the $3N - 5$ potential of Section 8.2.1, weighted as per Eq. (8.4–8.6), with the same weighting parameters and equilibrium values used as in the $(3N - 5)$ fit. The $(3N - 6)$ fit, with the potential function expanded and truncated at 8th order, gives a weighted *rms* error of 1.30 cm^{-1} and an un-weighted *rms* of 1.49 cm^{-1} , up to 14,000 cm^{-1} using 927 parameters. Again, the potential energy function is provided as supplementary material for Ref. [24] as a Fortran program. As can be seen in Figure 8.2, the residuals are smaller than for the fit using the $(3N - 5)$ linearised coordinates, with an increase as a function of *ab initio* energy, as would be expected as a result of the weighting of Eq. (8.4-8.6). The better fit to the *ab initio* energies using the $(3N - 6)$ model is due to the curvilinear coordinates being chemically more intuitive to describe the internal stretching

and bending motion of the molecule than the rectilinear-type coordinates. As described previously, the re-expansion of this $3N - 6 = 6$ dimensional surface in terms of the set of $3N - 5 = 7$ coordinates used in TROVE is not currently stable, which is why this potential fit is not used in the calculations of Section 8.4, but it may be of use with other general nuclear motion routines, including the curvilinear version of TROVE; this version of the potential was used in testing the $(3N - 6)$ model outlined in Section 7.2.

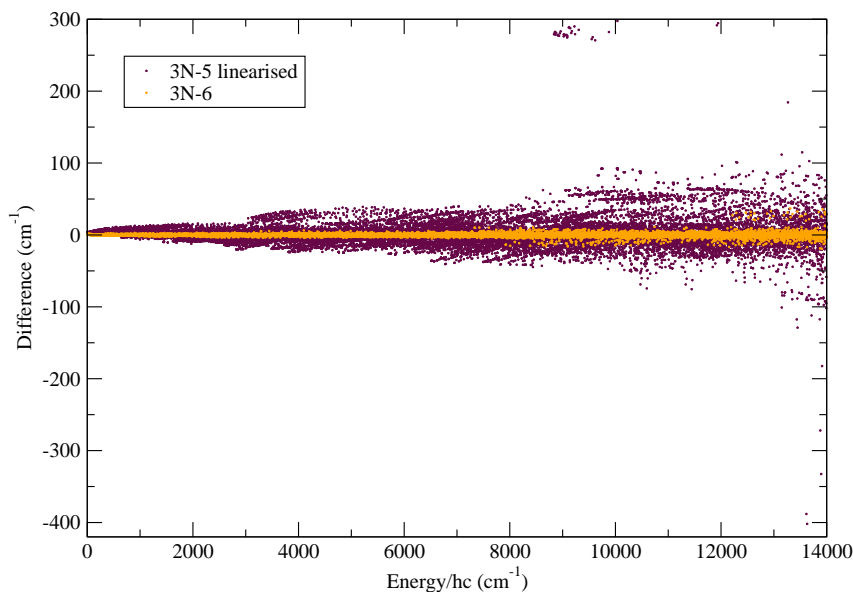


Figure 8.2: A comparison of the residuals of the $(3N - 5)$ linearised coordinate PES fit of Section 8.2.1 with the $(3N - 6)$ coordinate PES fit, both expanded up to 8th order and using the same equilibrium values and the same grid of *ab initio* points

8.3 Dipole Moment Surfaces: $(3N - 5)$ Linearised Coordinates

The *ab initio* electric dipole moment components, μ_α ($\alpha=x,y,z$), were computed using the finite difference method in MOLPRO, on a grid of 66 000 points spanning the 6D nuclear-geometry coordinate space covering up to 50 000 cm^{-1} , defined by a set of $3N - 6 = 6$ curvilinear bond length and bond angle coor-

ordinates (as given in Figure 6.2), at CCSD(T) level of theory and using an aug-cc-PVQZ basis set. The dipole moment surface was fit using the same set of $3N - 5$ coordinates as for the $3N - 5$ potential of Section 8.2.1 (as illustrated in Figure 7.1) to the following function:

$$\mu_x(\boldsymbol{\chi}) = \sum_i F_{i,j,k,\dots}^x \chi_1^i \chi_2^j \chi_3^k \dots, \quad (8.9)$$

$$\mu_y(\boldsymbol{\chi}) = \sum_i F_{i,j,k,\dots}^y \chi_1^i \chi_2^j \chi_3^k \dots, \quad (8.10)$$

$$\mu_z(\boldsymbol{\chi}) = \sum_i F_{i,j,k,\dots}^z \chi_1^i \chi_2^j \chi_3^k \dots. \quad (8.11)$$

where χ_λ are given by:

$$\chi_1 = \Delta R^{\text{lin}}, \quad (8.12)$$

$$\chi_2 = \Delta r_1^{\text{lin}},$$

$$\chi_3 = \Delta r_2^{\text{lin}},$$

$$\chi_4 = \Delta x_1,$$

$$\chi_5 = \Delta y_1,$$

$$\chi_6 = \Delta x_2,$$

$$\chi_7 = \Delta y_2.$$

Use was made of discrete symmetries (see Section 7.1.2), and the three components of the dipole were expanded up to 7th order and symmetrised according to the operations of \mathcal{D}_{12h} (\mathcal{D}_{12h} is sufficient for the same reasons as the $3N - 5$ potential energy symmetrisation of Section 8.2.1). The three Cartesian components of the dipole moment, μ_x , μ_y , μ_z , transform differently to one another (μ_x and μ_y as E_{1u} and μ_z as A_{2u} for $D_{nh}(M)$): [333] the μ_x and μ_y components share the corresponding expansion parameters, while that the parameters for the μ_z component are independent.

Figure 8.3 gives the residuals of the dipole moment surface fit up to 14,000 cm^{-1} (for the x , y and z -components of the dipole) using the $(3N - 5)$ linearised coordinates described in Section 8.2.1 and illustrated in Figure 7.1.

The overall *rms* of the fit up to $14,000\text{ cm}^{-1}$ was 0.54×10^{-3} Debye (weighted with the same parameters as the potential energy fits, as per Eq (8.4)-(8.6)), and 0.75×10^{-3} Debye (unweighted), on a grid of 46 714 *ab initio* points, using 459 symmetrised parameters (259 and 200 for the *x/y* and *z* components, respectively). The dipole moment function is provided as supplementary material to Ref. [24] as a Fortran program.

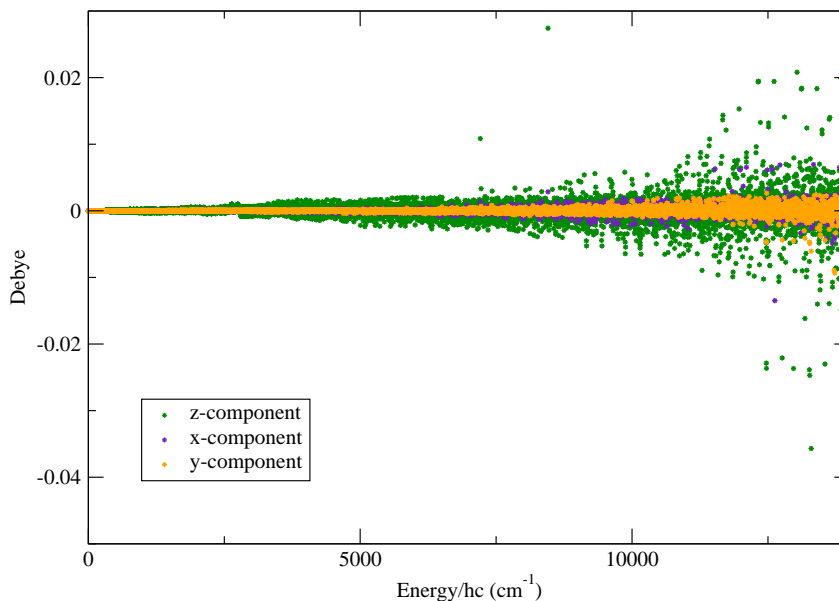


Figure 8.3: Residuals of the dipole moment surface fit up to $14,000\text{ cm}^{-1}$ (for the *x*, *y* and *z*-components of the dipole) using the set of $(3N - 5)$ linearised coordinates of Figure 7.1.

8.4 *Ab initio* Line List

8.4.1 Variational Calculations

The $(3N - 5)$ model outlined in Section 7.1 has been fully implemented in TROVE. Here, we give an application to $^{12}\text{C}_2\text{H}_2$ in the form of an *ab initio* line list, with a spectra calculated at 296 K in order to compare to available data. The calculated *ab initio* potential energy and dipole moment surfaces used for this linelist are presented in Sections 8.2.1 and 8.3.

The polyad number for acetylene is typically given by that of Eq. (3.9).

However, due to a slower than expected convergence of the stretches, most likely due to the linearised coordinates that are employed, a different definition of polyad number was used to control the size of the primitive and contracted basis sets in Eq (7.9):

$$P = 2n_1 + n_2 + n_3 + n_4 + n_5 + n_6 + n_7 \leq P_{\max}, \quad (8.13)$$

with $P_{\max}=18$ for the primitive basis set and reduced to 16 after contraction. Here, the vibrational modes are given in TROVE notation, with n_1 corresponding to the excitation of the C–C stretching mode, n_2 and n_3 representing the C–H₁ and C–H₂ stretching modes and n_4 , n_5 , n_6 and n_7 representing the bending modes. The stretching primitive basis functions $\phi_{n_1}(\xi_1)$, $\phi_{n_2}(\xi_2)$ and $\phi_{n_3}(\xi_3)$ are generated using the Numerov-Cooley approach [50, 339, 340] as eigenfunctions of the corresponding 1D reduced stretching Hamiltonian operators $\hat{H}_i^{(1D)}$, obtained by freezing all other degrees of freedom at their equilibrium values in the $J = 0$ Hamiltonian. For the bending basis functions, $\phi_{n_4}(\xi_4), \dots, \phi_{n_7}(\xi_7)$, 1D Harmonic oscillators are used. These basis sets are then divided into three sub-groups:

$$\phi_{n_1}^{(1D)}(\xi_1) = \phi_{n_1}(\xi_1), \quad (8.14)$$

$$\phi_{n_2 n_3}^{(2D)}(\xi_2, \xi_3) = \phi_{n_2}(\xi_2) \phi_{n_3}(\xi_3), \quad (8.15)$$

$$\phi_{n_4 n_5 n_6 n_7}^{(4D)}(\xi_4, \xi_5, \xi_6, \xi_7) = \phi_{n_4}(\xi_4) \phi_{n_5}(\xi_5) \phi_{n_6}(\xi_6) \phi_{n_7}(\xi_7). \quad (8.16)$$

The corresponding eigenvalue problems are solved for the three reduced Hamiltonian operators using these basis sets: stretching $\hat{H}^{(1D)}$ and $\hat{H}^{(2D)}$, and bending $\hat{H}^{(4D)}$. The reduced Hamiltonians $\hat{H}^{(ND)}$ ($N = 1, 2, 4$) are constructed by averaging the total vibrational Hamiltonian operator $\hat{H}^{(J=0)}$ over the other ground vibrational basis functions, see Ref. [55] and Section 7.1.2.

Energy cutoffs of 50,000 cm⁻¹ and 30,000 cm⁻¹ were set for the primitive and contracted matrices (see Section 7.1.2), respectively, while the overall energy cutoff was set to 18,000 cm⁻¹. The $\mathcal{D}_{24h}(M)$ molecular symmetry group

was used, which includes irreducible representations A_{1g} , A_{2g} , B_{1g} , B_{2g} , A_{1u} , A_{2u} , B_{1u} , B_{2u} , E_{1g} , E_{1u} , E_{2g} , E_{2u} ... E_{11g} , E_{11u} . As mentioned previously, only the A-type symmetry ro-vibrational states are allowed by nuclear statistics; the statistical weights are 1 for A_{1g} and A_{1u} (para), 3 for A_{2g} and A_{2u} (ortho), and 0 for everything else [56, 191]. The kinetic energy and potential energy expansions are truncated at 2nd and 8th order, respectively (the kinetic energy terms of higher than 2nd order appear to contribute very little to the calculated ro-vibrational energies, with expansion to higher orders becoming more computationally demanding). The maximum value for the z-projection of the vibrational angular momentum, $K_{\max} = L_{\max}$, used to build the multidimensional basis sets was 8. The equilibrium bond lengths were set to 1.20498127 Å and 1.053024743 Å for the C-C and C-H bonds, respectively. Calculations were performed up to a maximum value of $J=58$, with transitions calculated up to 10,000 cm⁻¹, with a maximum lower energy of 4,000 cm⁻¹ and a maximum higher energy of 14,000cm⁻¹ (transitions to higher J were not within this energy window), in order for a comparison to be made against a recent line list detailed below. These calculations have resulted in an *ab initio* linelist consisting of 13.9 million transitions between 2.7 million states.

8.4.2 Comparison to Other Data

A recent line list, ASD-1000 [44], has been calculated by Lyulin and Perevalov up to 10,000 cm⁻¹ and $J=100$, based on the use of an effective Hamiltonian fit to experimental data and extrapolated to higher energies. The energies and intensities at room-temperature agree reasonably well with those in the HITRAN-2016 [88] database (see Refs. [44], [45] for detailed comparisons), and ASD-1000 has been used to update the 2016 HITRAN release in the low energy region [88, 235]. Figure 8.4 gives a comparison of the linear-TROVE *ab initio* room-temperature line list with ASD-1000, and Figure 8.5 shows a comparison of this work against the data for ¹²C₂H₂ in HITRAN-2016 [88], both at a temperature of 296 K. Figures 8.6 and 8.7 give more detailed comparisons of the fundamental ν_3 and ν_5 bands with data from HITRAN-2016 [88], again

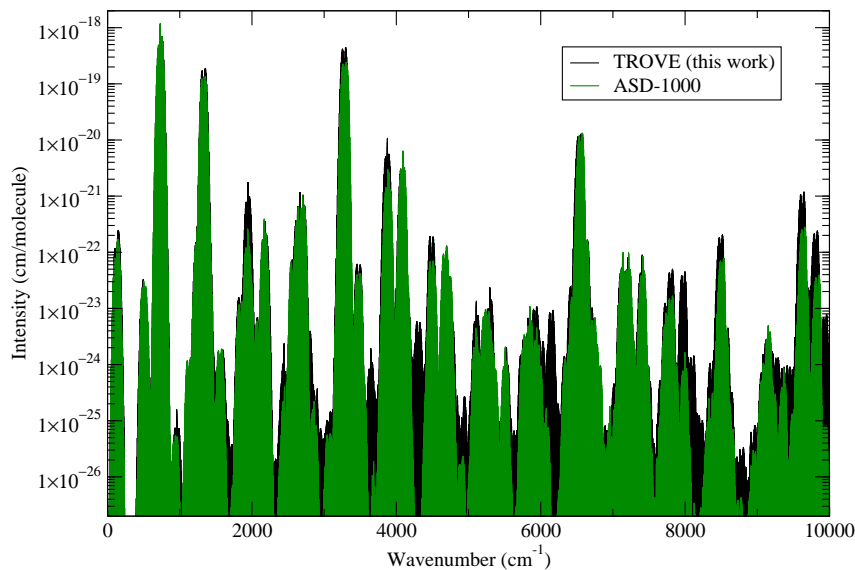


Figure 8.4: Comparison of TROVE room-temperature *ab initio* spectrum (with linearised coordinates, up to 8th order expansion) with ASD-1000 [44], up to 10,000 cm⁻¹ (TROVE calculations up to $J=58$; transitions to higher J were not within the specified energy window of below 10,000 cm⁻¹).

just giving stick spectra at room-temperature. No broadening coefficients or refinement of the *ab initio* potential energy surface to experimentally determined energies have been considered at this stage. Table 8.1 gives a comparison of the fundamental and some combination vibrational band centers of this work against those presented in Ref. [43] (calculated \tilde{E}^{calc} and experimental \tilde{E}^{obs}) and Table 8.2 gives a comparison of band intensities from this work with those presented in Ref. [366].

8.4.3 Discussion of Results

A refinement procedure on the equilibrium bond-length geometry can vastly improve the accuracy of the rotational transitions, but generally is balanced by a loss of accuracy on the vibrations [368]. The calculations outlined in this chapter have had the equilibrium bond-length geometry adjusted using the Newton method to give a good rotational structure, which may have negatively affected the vibrational band centers. Fortunately, there are other methods which can improve this, such as empirically refining the potential energy surface

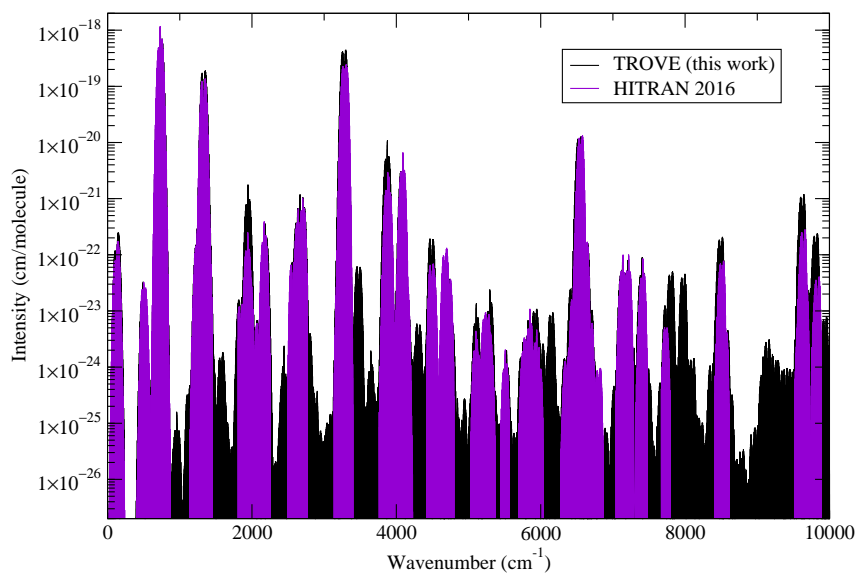


Figure 8.5: Comparison of the TROVE room-temperature *ab initio* spectrum (using linearised coordinates, up to 8th order expansion) with the ¹²C₂H₂ data from HITRAN-2016 [88], up to 10,000 cm⁻¹ (TROVE calculations up to $J = 58$; transitions to higher J were not within the specified energy window of below 10,000 cm⁻¹).

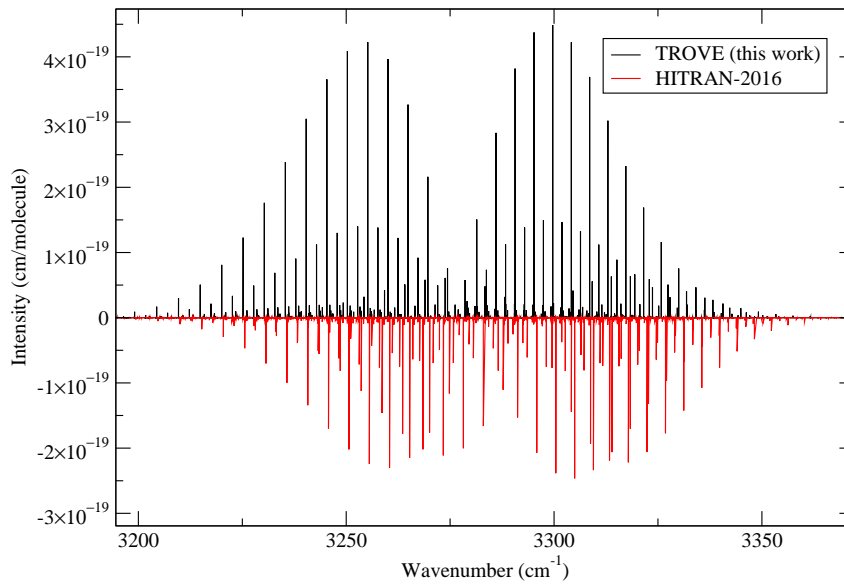


Figure 8.6: Comparison of the region around the ν_3 band from the TROVE room-temperature *ab initio* spectrum (using linearised coordinates, up to 8th order expansion) with the same band using $^{12}\text{C}_2\text{H}_2$ data from HITRAN-2016 [88].

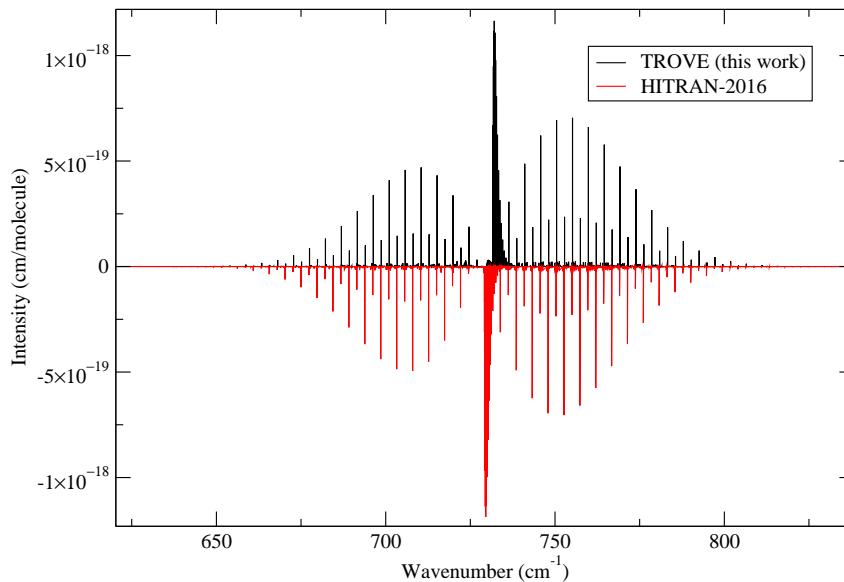


Figure 8.7: Comparison of the ν_5 band from the TROVE room-temperature *ab initio* spectrum (using linearised coordinates, up to 8th order expansion) with the same band using $^{12}\text{C}_2\text{H}_2$ data from HITRAN-2016 [88].

Table 8.1: Comparison of the *ab initio* (before refinement) fundamental and some combination vibrational band centers of this work against the calculated energy term values \tilde{E}^{calc} (cm^{-1}) presented in Urru *et al.* [43] and experimental energy term values \tilde{E}^{obs} (cm^{-1}) from Refs. [302], [56] and [43]. The obs.-calc. value given is the difference between \tilde{E}^{obs} and \tilde{E}^{calc} (cm^{-1}) (this work).

Band	Symmetry	\tilde{E}^{obs}	\tilde{E}^{calc} [43]	\tilde{E}^{calc} (this work)	obs.-calc.
ν_4^1	E_{1g} / Π_g	611.69 ^a	602.9	610.55	1.14
ν_5^1	E_{1u} / Π_u	729.15 ^a	722.2	732.78	-3.63
$2\nu_4^0$	A_{1g} / Σ_g^+	1230.39 ^b	1203.5	1226.89	3.5
$(\nu_4 + \nu_5)^0$	A_{2u} / Σ_u^+	1328.07 ^b	1311.6	1330.73	-2.66
$2\nu_5^0$	A_{1g} / Σ_g^+	1449.11 ^b	1448.6	1455.01	-5.9
ν_2^0	A_{1g} / Σ_g^+	1974.32 ^b	1950.7	1974.47	-0.15
ν_3^0	A_{2u} / Σ_u^+	3294.84 ^b	3241.1	3295.36	-0.52
ν_1^0	A_{1g} / Σ_g^+	3372.84 ^b	3371.1	3365.04	7.8
$\nu_3 + \nu_4^1$	E_{1u} / Π_u	3898.3 ^c	3867.7	3899.69	-1.39

^aRef. [302]; ^bRef. [56]; ^cRef. [43]

[369] or employing the empirical basis set correction (EBSC) [21], where the calculated vibrational band centers are replaced by their experimental values. These will both be addressed in Chapter 9.

As expected, there is some obvious shifting of the band centers of the calculated linelist when compared to HITRAN-2016, as illustrated in Figures 8.6 and 8.7, but the overall rotational structure is good. As can be seen in Table 8.1, the ν_1 band gives the largest difference when compared to experimental data out of all the fundamental bands. The band intensities of Table 8.2 are in general too high when compared to experimental values; $(2\nu_4 + \nu_5)^1$ II in particular stands out as having a very large percentage difference in band intensity.

8.5 Chapter Summary

This chapter has outlined the *ab initio* electronic-structure calculations for acetylene which were computed using MOLPRO and used to fit various po-

Table 8.2: Comparison of vibrational band intensities (S_{calc}) between this work (tw) and Ref. [366], along with S_{obs} , also from Ref. [366]. Intensities were converted from $\text{cm}^{-2}\text{atm}^{-1}$ to $\text{cm}/\text{molecule}$ using the conversion of $1 \text{ cm}^{-2}\text{atm}^{-1}$ at $296 \text{ K} = 4.033 \times 10^{-20} \text{ cm}/\text{molecule}$ [367]. The observed values of the $(2\nu_4 + \nu_5)^1 I$ and $(2\nu_4 + \nu_5)^1 II$ bands are cited in Ref. [366] as from private communication with G. Di Lonardo. $\frac{O-C}{O}$ gives the relative obs.-calc. ($S_{\text{obs}} - S_{\text{calc}}/S_{\text{obs}}$) percentage difference between this work and the observed values presented in Ref. [366]. The band centers ($\tilde{\nu}$) are in cm^{-1} .

Band	Sym	$\tilde{\nu}$ [366]	$\tilde{\nu}$ (tw)	S_{calc} [366]	S_{obs} [366]	S_{calc} (tw)	$\frac{O-C}{O}$ (%)
ν_5^1	E_{1u} / Π_u	729.15 ^a	732.85	2.37×10^{-17}	2.37×10^{-17}	2.39×10^{-17}	-1.04
$(\nu_4 + \nu_5)^0$	A_{2u} / Σ_u^+	1328.07 ^b	1330.49	2.54×10^{-18}	2.54×10^{-18}	3.78×10^{-18}	-48.77
$(2\nu_4 + \nu_5)^1 II$	E_{1u} / Π_u	1941.2 ^c	1945.12	5.64×10^{-21}	5.64×10^{-21}	3.70×10^{-20}	-556.09
$(2\nu_4 + \nu_5)^1 I$	E_{1u} / Π_u	1960.9 ^c	1960.02	2.02×10^{-21}	1.61×10^{-21}	1.17×10^{-22}	92.77
ν_3^0	A_{2u} / Σ_u^+	3294.84 ^b	3295.19	4.23×10^{-18}	4.39×10^{-18}	9.01×10^{-18}	-104.96

^aRef. [56]; ^bRef. [366]

tential energy surfaces and a dipole moment surface for C_2H_2 . These are published as part of the Supplementary Data of Ref. [24] and therefore can be used by the spectroscopic community. An *ab initio* linelist has been calculated in TROVE for $^{12}\text{C}_2\text{H}_2$, which makes use of the $3N - 5$ linearised-coordinate PES and DMS. Comparisons are made with other available room-temperature spectra of acetylene. A further discussion of the results of this chapter, along with calculations towards a new high-accuracy high-temperature linelist which are currently in progress and will be published in due course, can be found in Chapter 9.

Chapter 9

The aCeTY linelist

The implementation of the $(3N - 5)$ -approach to dealing with linear molecules, which was outlined in Section 7.1, has been fully implemented in TROVE, and was used to calculate an *ab initio* ro-vibrational linelist for acetylene (in Chapter 8) which covers a large range of rotational and vibrational excitations. There are a few improvements to be made in order to make this linelist useful to the atmospheric characterisation community, largely concerned with accuracy and temperature dependence. These improvements are currently ongoing; they will be detailed in this chapter and the resulting linelist (named the aCeTY linelist, after Chubb, Tennyson and Yurchenko) will be published in due course. Section 9.1 outlines the details of the variational calculations currently in progress, with some discussion on the expected temperature-dependence of the aCeTY linelist. It was previously mentioned that an empirical refinement of the PES used in such variational calculations will improve the accuracy of the computed eigenvalues and eigenfunctions; this procedure is outlined in Section 9.2, with an example given for demonstration purposes. In order to ensure optimum accuracy, the band centres should also be replaced with the experimental values, as discussed in Section 9.3. The intensities are discussed in Section 9.4.

9.1 Variational Calculations

The *ab initio* potential energy surface which is being used for these calculations is the same as that presented in Section 8.2.1, with the same weights and fitting parameters. It is now being refined to empirical values, as will be described in Section 9.2. This will not only lead to an improvement in the accuracy of the energy levels and line positions, but in the eigenfunctions which have an effect on the computed intensities (see Section 9.4).

The polyad number being used for the variational calculations of acetylene in TROVE is given by Eq. (8.13), with $P_{\max}=18$ for the primitive basis set and reduced to 16 after contraction, the same as in Section 8.4. Slightly higher energy cutoffs of 60,000 cm^{-1} and 50,000 cm^{-1} (instead of 50,000 cm^{-1} and 30,000 cm^{-1} for the *ab initio* linelist) are being used for the primitive and contracted matrices, respectively, while the overall energy cutoff is being set to 18,000 cm^{-1} . Preliminary calculations indicate that the energies are better converged (and therefore closer to experimental values) using these larger values of energy cutoffs for the primitive and contracted matrices. The $D_{24h}(M)$ molecular symmetry group is being used, and the kinetic energy and potential energy expansions are truncated at 2nd and 8th order, respectively (the kinetic energy terms of higher than 2nd order appear to contribute very little to the calculated ro-vibrational energies, with expansion to higher orders becoming more computationally demanding). The maximum value for the z-projection of the vibrational angular momentum, $K_{\max} = L_{\max}$, used to build the multidimensional basis sets is 8. Tests are being run in parallel in order to assess the feasibility of using a higher value of $K_{\max} = L_{\max}$, and the effect this will have on the completeness of the linelist at particular temperatures. The equilibrium bond lengths are set to 1.20498127 Å and 1.06295428 Å for the C-C and C-H bonds, respectively. Calculations will be performed up to a high value of J , expected to be at least $J = 100$, which will be determined by the maximum values of lower and upper energies used in the linelist calculations; these will have an effect on the temperature dependence of the linelist, as discussed below.

9.1.1 Temperature Dependence

The range of energy levels included in linelist calculations can be increased in order for the linelist to be complete up to higher temperatures. Taking the linelist presented in Chapter 8 as an example, the completeness up to a variety of temperatures as a function of the maximum value for the lower energy level used in linelist calculations is given in Table 9.1 for a maximum lower energy ($\tilde{E}_{low}^{(max)}$) of 4,000 cm^{-1} , Table 9.2 for $\tilde{E}_{low}^{(max)}=6,000 \text{ cm}^{-1}$, and Table 9.3 for $\tilde{E}_{low}^{(max)}=8,000 \text{ cm}^{-1}$. All maximum upper energy levels are 10,000 cm^{-1} above the maximum lower energy level value. The temperature dependence can be found by calculating the partition function (see Section 3.7) up to the lower energy level cut-off as a percentage of the total partition function which includes all states involved in a linelist calculation. The partition functions (PF) for the higher energy values in Tables 9.1, 9.2, 9.3 were calculated using TIPS (Total Internal Partition Sums) [196] and the partition function for the lower energy value using ExoCross [168]. A linelist is generally considered to be “complete” if the ratio of the partition function of the lower energy states to the partition function of all energy states involved in a linelist calculation is $> 90\%$. It can be seen from Table 9.1 that the *ab initio* linelist presented in Chapter 8, which used maximum lower and upper energies of 4,000 cm^{-1} and 14,000 cm^{-1} , respectively, is estimated to be complete up to around 800 K. The aCeTY linelist is being calculated with a maximum energy cut-off of 18,000 cm^{-1} ; using a maximum lower energy level value of 8000 cm^{-1} is expected to lead to a linelist which is complete up to around 1200 K (see Table 9.3). There may, however, be some effect based on the choice of $K_{\max} = L_{\max}$; tests for this are in progress, the results of which will be published in due course.

Figure 9.1 illustrates the temperature-dependence of acetylene spectra, using the *ab initio* linelist of Chapter 8, with cross-sections computed using ExoCross [168] at a variety of temperatures between 296–1000 K. The cross-sections are calculated at a low-resolution of 1 cm^{-1} for demonstration purposes.

Table 9.1: The completeness of the *ab initio* linelist of Chapter 8 at a variety of temperatures for a maximum lower energy level value of 4,000 cm⁻¹, measured using the calculated partition function (PF).

Temp (K)	PF up to 4,000 cm ⁻¹	PF up to 14,000 cm ⁻¹	% complete
200	245.55	246.04	99.80
300	420.98	422.69	99.60
400	694.52	699.40	99.30
500	1117.09	1130.50	98.81
600	1744.46	1784.84	97.74
700	2630.00	2752.77	95.54
800	3814.29	4153.51	91.83
900	5319.10	6142.20	86.60
1000	7147.00	8919.12	80.13

9.2 Empirical Refinement of the PES

An empirical refinement of a potential energy surface (PES) is a vital component in the procedure of variationally calculating a linelist, in order to maximise the accuracy of the computed energy levels and line positions. As previously mentioned, work is in progress for refining the PES which is being used in the calculations of the aCeTY linelist. It should be noted that a PES which has been refined to empirical values using the method outlined in this section is only valid for use in TROVE, typically using the same basis set as in the original calculations.

9.2.1 Empirical Refinement Theory

The refinement procedure (see, for example, Ref. [370]) is carried out under the assumption that a reasonable PES has already been fit and used to determine a set of variationally determined energy levels. In this case, a correction is added to the PES in terms of a set of internal coordinates ξ :

$$\Delta V = \sum_{ijk\dots} \Delta f_{ijk\dots}(\xi_1^i \xi_2^j \xi_3^k), \quad (9.1)$$

Table 9.2: The completeness of the *ab initio* linelist of Chapter 8 at a variety of temperatures for a maximum lower energy level value of 6,000 cm^{-1} .

Temp (K)	PF up to 6,000 cm^{-1}	PF up to 16,000 cm^{-1}	% complete
200	245.55	246.04	99.80
300	420.98	422.69	99.60
400	694.59	699.40	99.31
500	1118.56	1130.50	98.94
600	1757.05	1784.84	98.44
700	2690.02	2752.77	97.72
800	4011.52	4153.51	96.58
900	5822.66	6142.20	94.80
1000	8221.58	8919.12	92.18
1100	11293.90	12739.64	88.65
1200	15105.92	17927.30	84.26

where $\Delta f_{ijk\dots}$ are the refined parameters, given as correction terms to the expansion coefficients of the original PES, with the symmetry of the molecule taken into account in the same way as for the original *ab initio* PES. The eigenfunctions of the “unperturbed” Hamiltonian are used as basis functions when solving the new ro-vibrational eigenproblems with the correction ΔV to the PES included. This process is performed iteratively in TROVE, with the fitting procedure making use of empirical energy levels which should be added in gradually, according to the level of confidence placed in them.

The empirically determined energy levels which are used in the PES refinement procedure are weighted according to the level of confidence in their experimental assignment. The *ab initio* energies which were used to fit the initial PES (see Section 8.2) are also included in the refinement procedure in order to constrain the shape of the refined PES to the *ab initio* PES. In the case of acetylene, the experimental energy levels that resulted from the MARVEL analysis of Chapter 5 are suitable for use in such an empirical refinement of

Table 9.3: The completeness of the *ab initio* linelist of Chapter 8 at a variety of temperatures for a maximum lower energy level value of 8,000 cm^{-1} .

Temp (K)	PF up to 8,000 cm^{-1}	PF up to 18,000 cm^{-1}	% complete
200	245.55	246.04	99.80
300	420.98	422.69	99.60
400	694.59	699.40	99.31
500	1118.58	1130.50	98.95
600	1757.43	1784.84	98.46
700	2693.59	2752.77	97.85
800	4030.95	4153.51	97.05
900	5895.91	6142.20	95.99
1000	8434.94	8919.12	94.57
1100	11808.32	12739.64	92.69
1200	16181.17	17927.30	90.26
1300	21713.51	24884.76	87.26
1400	28551.40	34112.67	83.70

the PES. As mentioned in Section 3.2, good quantum numbers for acetylene are rotational angular momentum quantum number J and symmetry Γ . These are therefore the criteria used to match energy levels from the energy levels in the supplementary data of Chubb *et al.* [56]; see, for example, Table 5.6. An important parameter in the MARVEL energy level output of Chapter 5 and the supplementary information of the associated publication [56] is NumTrans, which gives the number of transitions linking a particular state to other energy levels. The higher the number of linking transitions, the higher the confidence which should be given to that empirical energy level.

9.2.2 Empirical Refinement Example

For computational reasons, calculations using a slightly smaller basis set than would ideally be used to compute a high-temperature linelist were used in order to demonstrate the effect of a refinement procedure on acetylene. This

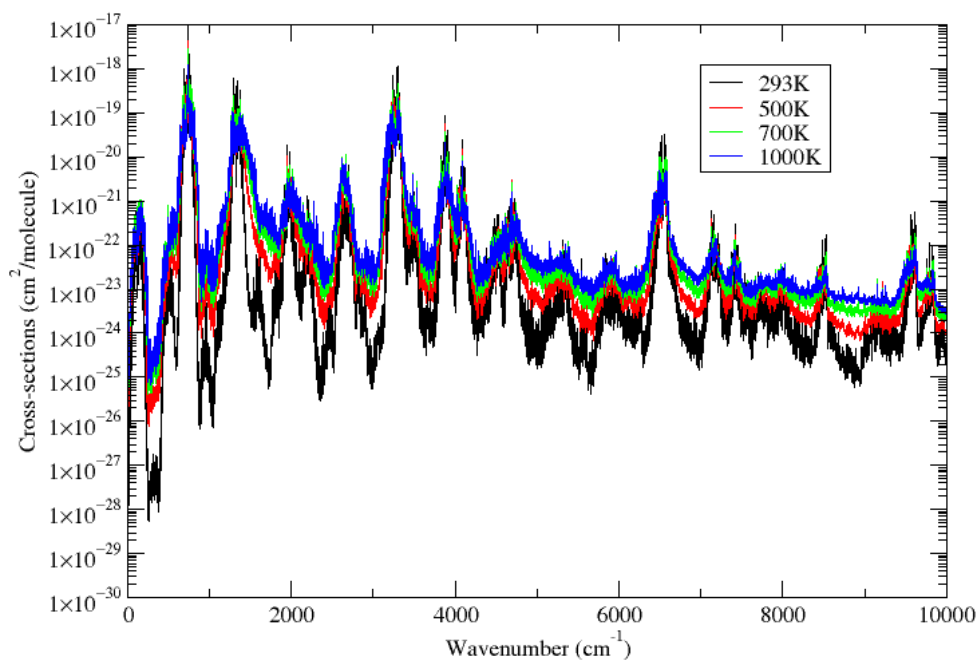


Figure 9.1: An illustration of how the spectra of acetylene varies with temperature, using the *ab initio* linelist of Chapter 8, with low-resolution (1 cm^{-1}) cross-sections computed using ExoCross [168] at a variety of temperatures between 296–1000 K.

procedure is currently being repeated for a higher basis set, the details of which are given in Section 9.1. In the current example of a refinement procedure, $P_{\text{max}}=18$ for the primitive basis set and reduced to 14 after contraction, with $K_{\text{max}} = L_{\text{max}}=6$. The resulting energy levels before the refinement procedure are therefore expected to be less well converged than those currently being calculated for the aCeTY linelist. Energy levels which are better converged initially are expected to yield a more accurate set of energy level values after the refinement procedure. Table 9.4 gives the vibrational ($J = 0$) band centres calculated using TROVE before and after the refinement procedure for the PES being used in the aCeTY linelist, where 600 empirical levels up to $J = 3$ were included in the fitting procedure. A higher weight was given to empirical

levels with a higher value of NumTrans in the MARVEL dataset. If there is only one or two transitions linking an energy level in the MARVEL dataset then it is either not included in the refinement procedure, or initially given a very low weight. A refinement procedure would typically begin with adding only those levels with the highest level of confidence, often those associated with lower energies, with more levels added in iteratively. There are many more energy levels from the MARVEL analysis which can be included in a refinement procedure; their inclusion would be expected to improve the obs-calc (o-c) values further than those presented in Table 9.4, which is the method currently being implemented for the aCeTY linelist.

Table 9.4: Vibrational energy levels (cm^{-1}) from the MARVEL analysis in comparison with those calculated by TROVE, before and after the refinement procedure. NT stands for NumTrans, the number of transitions linking each state in the MARVEL procedure.

$(\nu_1\nu_2\nu_3\nu_4^{\ell_4}\nu_5^{\ell_5})^K$	Sym	NT	MARVEL	Before refinement	o-c	After refinement	o-c
(0000 ⁰⁰) ⁰	e para	85	0.0000	0.0000	0.0000	0.0000	0.0000
(0002 ⁰⁰) ⁰	e para	11	1230.3903	1220.0511	10.3392	1229.8054	0.5849
(0001 ¹¹) ⁰	e ortho	19	1328.0735	1321.8021	6.2714	1328.0786	-0.0051
(0001 ¹¹) ⁰	f para	9	1340.5507	1330.4179	10.1328	1340.4094	0.1413
(0000 ⁰²) ⁰	e para	10	1449.1124	1444.2927	4.8197	1449.0934	0.0190
(0100 ⁰⁰) ⁰	e para	1	1974.3166	1974.4569	-0.1403	1974.5969	-0.2803
(0003 ¹¹) ⁰	e ortho	3	2560.5949	2563.1864	-2.5915	2567.2168	-6.6219
(0002 ²²) ⁰	e para	1	2648.0145	2648.4115	-0.3970	2653.5144	-5.4999
(0001 ¹³) ⁰	e ortho	3	2757.7979	2757.8146	-0.0167	2760.6425	-2.8446
(0000 ⁰⁴) ⁰	e para	1	2880.2201	2879.1872	1.0329	2880.2376	-0.0175
(0101 ¹¹) ⁰	e ortho	5	3281.8990	3274.6999	7.1991	3281.6629	0.2361
(0010 ⁰⁰) ⁰	e ortho	4	3294.8396	3288.5541	6.2855	3294.8292	0.0104
(0101 ¹¹) ⁰	f para	2	3300.6356	3292.3559	8.2797	3299.9300	0.7056
(1000 ⁰⁰) ⁰	e para	1	3372.8390	3364.3444	8.4946	3373.6365	-0.7975
(0103 ¹¹) ⁰	e ortho	2	4488.8382	4479.1445	9.6937	4488.6778	0.1604
(0102 ²²) ⁰	f ortho	2	4599.7747	4589.5140	10.2607	4599.1539	0.6208

(0011 ¹ 1 ⁻¹) ⁰	e para	3	4609.3410	4617.5073	-8.1663	4609.6095	-0.2685
(0011 ¹ 1 ⁻¹) ⁰	f ortho	4	4617.9259	4619.9283	-2.0024	4618.0159	-0.0900
(1001 ¹ 1 ⁻¹) ⁰	e ortho	3	4673.6311	4662.4217	11.2094	4673.7049	-0.0738
(1001 ¹ 1 ⁻¹) ⁰	f para	1	4688.8465	4672.5588	16.2877	4687.5063	1.3402
(0101 ¹ 3 ⁻¹) ⁰	e ortho	1	4710.7398	4707.5611	3.1787	4712.0339	-1.2941
(0010 ⁰ 2 ⁰) ⁰	e ortho	1	4727.0699	4737.8797	-10.8098	4726.6973	0.3726
(1000 ⁰ 2 ⁰) ⁰	e para	1	4800.1373	4789.9229	10.2144	4800.2565	-0.1192
(0201 ¹ 1 ⁻¹) ⁰	e ortho	1	5230.2293	5232.1110	-1.8817	5227.8890	2.3403
(0110 ⁰ 0 ⁰) ⁰	e ortho	2	5260.0218	5251.6062	8.4156	5259.9265	0.0953
(1010 ⁰ 0 ⁰) ⁰	e ortho	4	6556.4648	6537.0513	19.4135	6555.7177	0.7471
(1101 ¹ 1 ⁻¹) ⁰	e ortho	2	6623.1396	6621.6614	1.4782	6623.2491	-0.1095
(1011 ¹ 1 ⁻¹) ⁰	f ortho	1	7853.2771	7842.4354	10.8417	7851.6219	1.6552
(2001 ¹ 1 ⁻¹) ⁰	f para	2	8001.2041	7983.4243	17.7798	8001.5604	-0.3563
(2000 ⁰ 2 ⁰) ⁰	e para	3	8114.3629	8103.0444	11.3185	8117.3805	-3.0176
(1110 ⁰ 0 ⁰) ⁰	e ortho	3	8512.0562	8531.7302	-19.6740	8509.2052	2.8510

9.3 Band Centre Replacement

As mentioned previously (see Chapter 6), basis sets in TROVE are built from primitive 1D functions, processed through a double layer contraction scheme, and used to solve the vibrational ($J = 0$) problem. The resulting vibrational eigenfunctions can subsequently be used in the construction of a basis set for the $J > 0$ calculations. The $J = 0$ representation can be utilised to make ro-vibrational calculations in TROVE more tractable [371]. It also facilitates the option to replace vibrational band centres with experimentally determined values. This is a necessary procedure if the linelist is to be used in any high-temperature, high-resolution doppler-shift studies, as were introduced in Section 2.4.3. The line positions in a linelist typically need to be accurate to within around 0.1 cm^{-1} in order to be useful for making a detection in such a study (private communication, Jane Birkby). The calculations outlined in this chapter, which are currently being implemented in the production of the high-temperature aCeTY linelist, will utilise the $J = 0$ representation in TROVE in order to replace the band-centres with empirical values. This will maximise

the accuracy of the resulting line positions.

9.4 Intensities

The calculated intensities for the *ab initio* linelist which was presented in Chapter 8 were too high for some bands when compared to experiment. It is usually expected that weaker bands would be more accurate for *ab initio* calculations than for experiment, but that the stronger bands should agree to within 10–20%. Some tests were done in order to compare the use of two different $(3N - 5)$ linearized-coordinate potential energy surfaces, each fit to the same set of *ab initio* energies and employing the same set of $3N - 5$ linearized coordinates, but each with a slightly different weighting scheme and parameters (see Section 8.2.1): these will be labelled PES-1 and PES-2. The fit of PES-1 has a *rms* error of 123 cm^{-1} (unweighted) and 0.019 cm^{-1} (weighted), compared to 15.65 cm^{-1} (unweighted) and 3.98 cm^{-1} (weighted) for PES-2. A less computationally demanding small basis set ($P_{\text{max}}=8$ for the primitive basis set and reduced to 6 after contraction, according to Eq. (8.13)) was used in order to make comparisons between the results of ro-vibrational calculations using PES-1 and PES-2. As expected, the energies shifted closer towards the corresponding experimental values for PES-2. There was, however, also an effect on the intensities (both calculations used the $3N - 5$ linearized coordinate DMS presented in Section 8.3), as illustrated by the $(\nu_4 + \nu_5)^0$ band in Figure 9.2. It is apparent that the calculated intensities are very sensitive to the ro-vibrational eigenfunctions, which are dependent on the quality of the PES. It is therefore expected that the use of a potential energy surface with a better fit will lead to some improvement in both the energies of Table 8.1 and the intensities of Table 8.2; the procedure of refining the PES to empirical energies that is currently in progress (see Section 9.2) is expected to lead to an improvement of the intensity values of Table 8.2. It may also be necessary to experiment further with different weights in the DMS fitting procedure, as this was found to have a large effect on the accuracy of the PES.

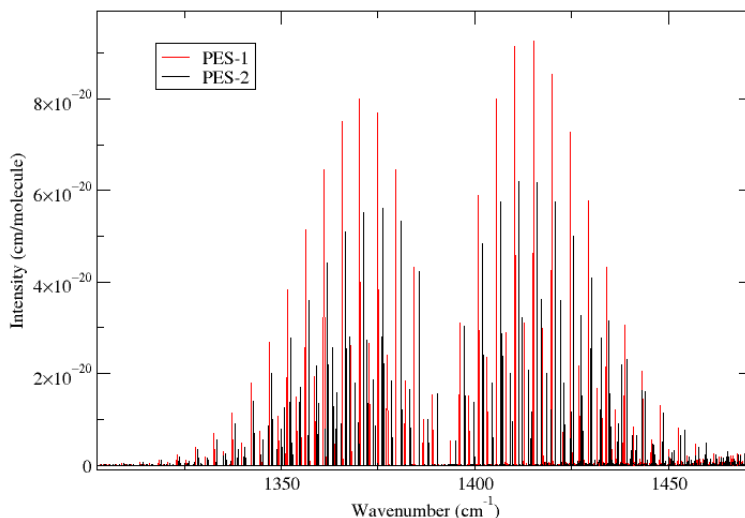


Figure 9.2: An illustration of how different potential energy surfaces, with the same dipole moment surface, can have an effect on the intensities, in this case the $(\nu_4 + \nu_5)^0$ band (see Table 8.2). PES-1 and PES-2 were fit to the same $3N - 5$ function and *ab initio* points as described in Section 8.2.1, but with different weighting parameters. A small basis set is used for testing purposes ($P_{\max}=8$ for the primitive basis set and reduced to 6 after contraction, according to Eq. (8.13)) due to the computational cost of high-basis-set calculations.

9.5 Chapter Summary

Calculations which are in progress in order to compute a high-accuracy, high-temperature linelist for $^{12}\text{C}_2\text{H}_2$, known as the aCeTY linelist, are presented in this chapter. These calculations include an increase in basis-set size (in comparison to the *ab initio* linelist of Chapter 8), a refinement procedure for the PES, vibrational band-centre replacement, and more accurate intensities. Estimations for the temperature dependence of the linelist are made; the aCeTY linelist is expected to be highly-accurate (to within 0.1 cm^{-1}) and valid up to temperatures of 1000–1200 K. It will therefore be highly suitable for characterising hot exoplanet and cool stellar atmospheres.

Chapter 10

Conclusions and Future Work

The work outlined in this thesis forms a solid base for any future research related to ro-vibrational energy and intensity calculations of linear molecules, and for acetylene in particular. Knowing the properties of a molecule's symmetry group is essential for the process of calculating a linelist; it is necessary to know the symmetry of a ro-vibrational state in order to compute transition intensities, and it makes calculations of energies far more efficient and computationally viable. Chapter 4 was dedicated to the $\mathcal{D}_{\infty h}$ symmetry group to which centrosymmetric linear molecules belong, the introduction of the finite-order \mathcal{D}_{nh} group and how the latter can be used in practical numerical calculations of ro-vibrational energies and intensities. The available experimental transition data for $^{12}\text{C}_2\text{H}_2$ was collated and analysed in detail in Chapter 5, in order to produce a set of 11 213 empirically-determined energy levels, using the MARVEL technique. Such energy levels are important in improving the accuracy of an *ab initio* linelist, as was shown in Section 9.2.

In order to be able to calculate a linelist for acetylene, it was first necessary to investigate the reasons why standard techniques for non-linear molecules could not be used; it was shown in Chapter 6 that singularities which would occur if standard Hamiltonians and number of internal coordinates are used in the numerical construction of the kinetic energy operator for ro-vibrational calculations of linear molecules. Two approaches to handling linear molecules in ro-vibrational calculations were formulated and outlined in Chapter 7: ($3N -$

5) and $(3N - 6)$. While the idea behind the $(3N - 6)$ approach is to select a form of the wave function which removes the singularity in the Hamiltonian, the $(3N - 5)$ approach makes use of a KEO which is already non-singular. The $(3N - 6)$ approach uses physically more meaningful and intuitive coordinates for representing the vibrations in the molecule, however the main advantage of implementing the $(3N - 5)$ approach is that, unlike the $(3N - 6)$ approach or the use of Legendre polynomial functions, it is compatible with the way that TROVE constructs and truncates basis sets to represent the full ro-vibrational wave function and still allows for the KEO to be generated numerically, with no analytical pre-derivation required (see Ref. [50] for more details). There is no reason why it should not be compatible with other polyatomic linear molecules, a supposition which will be put to the test in the future. For these reasons, the $(3N - 5)$ approach has been fully implemented into TROVE along with a symmetrisation procedure for linear molecules (details in Ref. [55]) and was used in the calculations presented in Chapter 8 and 9. The $(3N - 6)$ approach will be integrated into TROVE in the future. The two approaches, which make use of either $3N - 6$ or $3N - 5$ internal coordinates, should in principle lead to completely equivalent eigenvalues; a full comparison of these two approaches (calculation times, convergence, difference in accuracy) will be an interesting investigation to make. It is thought that these approaches can be applied to any chain tetratomic molecule and extended to polyatomic molecules with more than four atoms, such as linear molecule cyanoacetylene, C_3HN , for example (which is potentially important in exoplanet atmospheres [346] and in investigating that of Titan [347]), or propynylidyne, C_3H , [348, 349]. It will be interesting to test the $(3N - 6)$ -approach in particular on chain molecules with relatively high barriers to linearity, e.g., H_2O_2 [350, 15] to see if the exact cusp conditions in Eq. (7.28) will be relevant for the basis set convergence of the variational results.

It was shown in Chapter 8 that the ro-vibrational energy and intensity calculations using the $(3N - 5)$ model (including new *ab initio* potential en-

ergy and dipole moment surfaces) work in TROVE, with no numerical issues due to singularities in matrix elements, and that this method can be used, in combination with other techniques such as empirical PES refinement [369] (see Section 9.2) or replacement of vibrational band centers (EBSC) [21] (see Section 9.3), to produce accurate high-temperature ro-vibrational spectra for $^{12}\text{C}_2\text{H}_2$. This has not been achieved before; previous variational calculations (such as in Refs. [38], [39], [40], [41], [42], [43]) did not provide coverage up to the high excitations (vibrational or rotational) that have been achieved in this work, and only data for low ro-vibrational excitations are presented in the literature. Previous effective Hamiltonian models for $^{12}\text{C}_2\text{H}_2$ (e.g. Refs. [46] or [44]) have provided a good fit to experimental data obtained at largely room temperature, but would not be expected to extrapolate so accurately up to high temperatures and thus do not offer the coverage that variational calculations do. New *ab initio* potential energy and dipole moment surfaces were also computed and presented in Chapter 8. In particular, the $3N - 6$ potential energy surface of Section 8.2.3 (available from the Supplementary Data of Chubb *et al.* [24]) is general and highly accurate and should therefore be of use to the spectroscopic community.

The *ab initio* spectrum of $^{12}\text{C}_2\text{H}_2$ presented in Chapter 8 is not currently accurate enough for practical spectroscopic applications. Experience shows (see, for example, Ref. [10]) that the quality of the computational model can be substantially improved by fitting the PES of a molecule to the experimental energies, which results in an effective PES which is thus only applicable with the computational model used in the fit in order to guarantee high quality calculations. The *ab initio* PES of $^{12}\text{C}_2\text{H}_2$ presented in this thesis is currently being refined to the extensive set of experimentally determined energies of Chapter 5, which were analysed using the MARVEL procedure. This is expected to lead to a significant improvement in accuracy not only for the energies, but also, as preliminary results show, for intensities. This refinement procedure and related calculations are in progress in computing the high-accuracy aCeTY linelist, the

details of which are presented in Chapter 9. This linelist is expected to be valid up to temperatures of around 1000–1200 K. This is being calculated as part of the ExoMol project [8, 9] and will be appropriate for use in modelling hot exoplanet or cool stellar atmospheres. The band centres which are computed as part of the variational calculations are to be replaced with empirical values, which acts to shift all associated rotational levels towards their experimental value. The final improvement is to replace the theoretical energies in a linelist with the empirical MARVEL energies, where available. This leads to a linelist of experimental quality but with a much larger coverage. This should ideally mean that the linelist will be suitable for use in high-resolution Doppler spectroscopy applications. Observational studies such as these would help validate the accuracy of the linelist and offer guidance on which areas may need work on improving in the future. The linelist will also have the potential to be included as part of the HITEMP [93] database, which is the high-temperature version of HITRAN [165].

Bibliography

- [1] A. Wolszczan, D. A. Frail, A planetary system around the millisecond pulsar PSR1257 + 12, *Nature* 355 (1992) 145–147. doi:10.1038/355145a0.
- [2] M. Mayor, D. Queloz, A jupiter-mass companion to a solar-type star, *Nature* 378 (1995) 355–359. doi:10.1038/378355a0.
- [3] NASA, Nasa exoplanet archive, <https://exoplanetarchive.ipac.caltech.edu> (2018).
- [4] A. Cassan, D. Kubas, J.-P. Beaulieu, M. Dominik, K. Horne, J. Greenhill, J. Wambsganss, J. Menzies, A. Williams, U. G. Jørgensen, A. Udalski, D. P. Bennett, M. D. Albrow, V. Batista, S. Brilliant, J. A. R. Caldwell, A. Cole, C. Coutures, K. H. Cook, S. Dieters, D. Dominis Prester, J. Donatowicz, P. Fouqué, K. Hill, N. Kains, S. Kane, J.-B. Marquette, R. Martin, K. R. Pollard, K. C. Sahu, C. Vinter, D. Warren, B. Watson, M. Zub, T. Sumi, M. K. Szymański, M. Kubiak, R. Poleski, I. Soszynski, K. Ulaczyk, G. Pietrzyński, L. Wyrzykowski, One or more bound planets per milky way star from microlensing observations, *Nature* 481 (2012) 167–169. doi:10.1038/nature10684.
- [5] M. Tanaka, A. Letip, Y. Nishimaki, T. Yamamuro, K. Motohara, T. Miyata, W. Aoki, Near-infrared spectra of 29 carbon stars: Simple estimates of effective temperature, *Publications of the Astronomical Society of Japan* 59 (5) (2007) 939–953. doi:10.1093/pasj/59.5.939.

- [6] J. Tennyson, *Astronomical Spectroscopy: An Introduction to the Atomic and Molecular Physics of Astronomical Spectra*, 2nd Edition, World Scientific, London, 2011.
- [7] T. Tsuji, Molecules in stars, *Annual review of astronomy and astrophysics* 24 (1986) 89–125. doi:10.1146/annurev.aa.24.090186.000513.
- [8] J. Tennyson, S. N. Yurchenko, ExoMol: molecular line lists for exoplanet and other atmospheres, *Mon. Not. R. Astron. Soc.* 425 (2012) 21–33. doi:10.1111/j.1365-2966.2012.21440.x.
- [9] J. Tennyson, S. N. Yurchenko, A. F. Al-Refaie, E. J. Barton, K. L. Chubb, P. A. Coles, S. Diamantopoulou, M. N. Gorman, C. Hill, A. Z. Lam, L. Lodi, L. K. McKemmish, Y. Na, A. Owens, O. L. Polyansky, T. Rivlin, C. Sousa-Silva, D. S. Underwood, A. Yachmenev, E. Zak, The ExoMol database: molecular line lists for exoplanet and other hot atmospheres, *J. Mol. Spectrosc.* 327 (2016) 73–94. doi:10.1016/j.jms.2016.05.002.
- [10] S. N. Yurchenko, J. Tennyson, ExoMol line lists IV: The rotation-vibration spectrum of methane up to 1500 K, *Mon. Not. R. Astron. Soc.* 440 (2014) 1649–1661.
- [11] S. N. Yurchenko, J. Tennyson, J. Bailey, M. D. J. Hollis, G. Tinetti, Spectrum of hot methane in astronomical objects using a comprehensive computed line list, *Proc. Nat. Acad. Sci.* 111 (2014) 9379–9383. doi:10.1073/pnas.1324219111.
- [12] S. N. Yurchenko, D. S. Amundsen, J. Tennyson, I. P. Waldmann, A hybrid line list for CH₄ and hot methane continuum, *Astron. Astrophys.* 605 (2017) A95. doi:10.1051/0004-6361/201731026.
- [13] R. J. Barber, J. K. Strange, C. Hill, O. L. Polyansky, G. C. Mellau, S. N. Yurchenko, J. Tennyson, ExoMol line lists – III. An improved hot

- rotation-vibration line list for HCN and HNC, *Mon. Not. R. Astron. Soc.* 437 (2014) 1828–1835. doi:10.1093/mnras/stt2011.
- [14] C. Sousa-Silva, A. F. Al-Refaie, J. Tennyson, S. N. Yurchenko, ExoMol line lists - VII. the rotation-vibration spectrum of phosphine up to 1500 K, *Mon. Not. R. Astron. Soc.* 446 (2015) 2337–2347. doi:10.1093/mnras/stu2246.
- [15] A. F. Al-Refaie, O. L. Polyansky, R. I., Ovsyannikov, J. Tennyson, S. N. Yurchenko, ExoMol line lists XV: A hot line-list for hydrogen peroxide, *Mon. Not. R. Astron. Soc.* 461 (2016) 1012–1022. doi:10.1093/mnras/stw1295.
- [16] D. S. Underwood, J. Tennyson, S. N. Yurchenko, X. Huang, D. W. Schwenke, T. J. Lee, S. Clausen, A. Fateev, ExoMol line lists XIV: A line list for hot SO₂, *Mon. Not. R. Astron. Soc.* 459 (2016) 3890–3899. doi:10.1093/mnras/stw849.
- [17] A. A. A. Azzam, S. N. Yurchenko, J. Tennyson, O. V. Naumenko, ExoMol line lists XVI: A Hot Line List for H₂S, *Mon. Not. R. Astron. Soc.* 460 (2016) 4063–4074. doi:10.1093/mnras/stw1133.
- [18] D. S. Underwood, J. Tennyson, S. N. Yurchenko, S. Clausen, A. Fateev, ExoMol line lists XVII: A line list for hot SO₃, *Mon. Not. R. Astron. Soc.* 462 (2016) 4300–4313. doi:10.1093/mnras/stw1828.
- [19] L. K. McKemmish, S. N. Yurchenko, J. Tennyson, ExoMol Molecular linelists – XVIII. The spectrum of Vanadium Oxide, *Mon. Not. R. Astron. Soc.* 463 (2016) 771–793. doi:10.1093/mnras/stw1969.
- [20] E. J. Zak, J. Tennyson, O. L. Polyansky, L. Lodi, N. F. Zobov, S. A. Tashkun, V. I. Perevalov, Room temperature line lists for CO₂ symmetric isotopologues with *ab initio* computed intensities, *J. Quant. Spectrosc. Radiat. Transf.* 189 (2017) 267 – 280. doi:10.1016/j.jqsrt.2016.11.022.

- [21] A. Owens, S. N. Yurchenko, A. Yachmenev, W. Thiel, J. Tennyson, ExoMol molecular line lists XXII. The rotation-vibration spectrum of silane up to 1200 K, *Mon. Not. R. Astron. Soc.* 471 (2017) 5025–5032. doi:10.1093/mnras/stx1952.
- [22] O. L. Polyansky, A. A. Kyuberis, L. Lodi, J. Tennyson, R. I. Ovsyanikov, N. Zobov, ExoMol molecular line lists XIX: high accuracy computed line lists for H_2^{17}O and H_2^{18}O , *Mon. Not. R. Astron. Soc.* 466 (2017) 1363–1371. doi:10.1093/mnras/stw3125.
- [23] B. P. Mant, A. Yachmenev, J. Tennyson, S. N. Yurchenko, ExoMol molecular line lists - XXVII: spectra of C_2H_4 , *Mon. Not. R. Astron. Soc.* 478 (2018) 3220 – 3232. doi:10.1093/mnras/sty1239.
- [24] K. L. Chubb, A. Yachmenev, J. Tennyson, S. N. Yurchenko, Treating linear molecule HCCH in calculations of rotation-vibration spectra, *J. Chem. Phys.* 149 (2018) 014101. doi:10.1063/1.5031844.
- [25] J. Tennyson, S. Yurchenko, The Status of Spectroscopic Data for the Exoplanet Characterisation Missions, *Exp. Astron.* 40 (2016) 563–575. doi:10.1007/s10686-014-9385-2.
- [26] R. J. de Kok, J. Birkby, M. Brogi, H. Schwarz, S. Albrecht, E. J. W. de Mooij, I. A. G. Snellen, Identifying new opportunities for exoplanet characterisation at high spectral resolution, *Astron. Astrophys.* 561 (2014) A150. doi:10.1051/0004-6361/201322947.
- [27] A. Tsiaras, M. Rocchetto, I. P. Waldmann, G. Tinetti, R. Varley, G. Morello, E. J. Barton, S. N. Yurchenko, J. Tennyson, Detection of an atmosphere around the super-Earth 55 Cancri e, *Astrophys. J.* 820 (2016) 99. doi:10.3847/0004-637X/820/2/99.
- [28] M. Matsuura, P. R. Wood, G. C. Sloan, A. A. Zijlstra, J. T. van Loon, M. A. T. Groenewegen, J. A. D. L. Blommaert, M. R. L. Cioni, M. W.

- Feast, H. J. Habing, S. Hony, E. Lagadec, C. Loup, J. W. Menzies, L. B. F. M. Waters, P. A. Whitelock, Spitzer observations of acetylene bands in carbon-rich asymptotic giant branch stars in the Large Magellanic Cloud, *Mon. Not. R. Astron. Soc.* 371 (2006) 415–420. doi:10.1111/j.1365-2966.2006.10664.x.
- [29] Lederer, M. T., Aringer, B., Low temperature rosseland opacities with varied abundances of carbon and nitrogen, *Astron. Astrophys.* 494 (2009) 403–416. doi:10.1051/0004-6361:200810576.
- [30] Marigo, P., Aringer, B., Low-temperature gas opacity - *æ*sopus: a versatile and quick computational tool, *Astron. Astrophys.* 508 (2009) 1539–1569. doi:10.1051/0004-6361/200912598.
- [31] C. Bilger, P. Rimmer, C. Helling, Small hydrocarbon molecules in cloud-forming brown dwarf and giant gas planet atmospheres, *Mon. Not. R. Astron. Soc.* 435 (2013) 1888–1903. doi:10.1093/mnras/stt1378.
- [32] J. K. G. Watson, Simplification of the molecular vibration-rotation hamiltonian, *Mol. Phys.* 15 (1968) 479–490. doi:10.1080/00268970110089081.
- [33] J. Tennyson, B. T. Sutcliffe, The ab initio calculation of the vibrational-rotational spectrum of triatomic systems in the close-coupling approach, with KCN and H₂Ne as examples, *J. Chem. Phys.* 77 (1982) 4061–4072. doi:10.1063/1.444316.
- [34] J. Tennyson, M. A. Kostin, P. Barletta, G. J. Harris, O. L. Polyansky, J. Ramanlal, N. F. Zobov, DVR3D: a program suite for the calculation of rotation-vibration spectra of triatomic molecules, *Comput. Phys. Commun.* 163 (2004) 85–116.
- [35] E. J. Zak, J. Tennyson, O. L. Polyansky, L. Lodi, N. F. Zobov, S. A. Tashkun, V. I. Perevalov, Room temperature line lists for CO₂ asym-

- metric isotopologues with *ab initio* computed intensities, *J. Quant. Spectrosc. Radiat. Transf.* 203 (2017) 265–281. doi:10.1016/j.jqsrt.2017.01.037.
- [36] E. Zak, J. Tennyson, O. L. Polyansky, L. Lodi, S. A. Tashkun, V. I. Perevalov, A room temperature CO₂ line list with *ab initio* computed intensities, *J. Quant. Spectrosc. Radiat. Transf.* 177 (2016) 31–42. doi:10.1016/j.jqsrt.2015.12.022.
- [37] X. Huang, R. S. Freedman, S. A. Tashkun, D. W. Schwenke, T. J. Lee, Semi-empirical ¹²C¹⁶O₂ IR line lists for simulations up to 1500 K and 20,000 cm⁻¹, *J. Quant. Spectrosc. Radiat. Transf.* 130 (2013) 134–146. doi:10.1016/j.jqsrt.2013.05.018.
- [38] M. J. Bramley, N. C. Handy, Efficient calculation of rovibrational eigenstates of sequentially bonded 4-atom molecules, *J. Chem. Phys.* 98 (1993) 1378–1397. doi:10.1063/1.464305.
- [39] D. W. Schwenke, Variational calculations of rovibrational energy levels and transition intensities for tetratomic molecules, *J. Phys. Chem.* 100 (1996) 2867–2884. doi:10.1021/jp9525447.
- [40] I. N. Kozin, M. M. Law, J. Tennyson, J. M. Hutson, Calculating energy levels of isomerizing tetraatomic molecules: II. The vibrational states of acetylene and vinylidene, *J. Chem. Phys.* 122 (2005) 064309.
- [41] D. G. Xu, G. H. Li, D. Q. Xie, H. Guo, Full-dimensional quantum calculations of vibrational energy levels of acetylene (HCCH) up to 13,000 cm⁻¹, *Chem. Phys. Lett.* 365 (2002) 480–486. doi:10.1016/S0009-2614(02)01503-8.
- [42] D. G. Xu, H. Guo, S. L. Zou, J. M. Bowman, A scaled *ab initio* potential energy surface for acetylene and vinylidene, *Chem. Phys. Lett.* 377 (2003) 582–588. doi:10.1016/S0009-2614(03)01184-9.

- [43] A. Urru, I. N. Kozin, G. Mulas, B. J. Braams, J. Tennyson, Rovibrational spectra of C_2H_2 based on variational nuclear motion calculations, *Mol. Phys.* 108 (2010) 1973–1990. doi:10.1080/00268976.2010.499858.
- [44] O. M. Lyulin, V. I. Perevalov, ASD-1000: high-resolution, high-temperature acetylene spectroscopic databank, *J. Quant. Spectrosc. Radiat. Transf.* 201 (2017) 94–103. doi:10.1016/j.jqsrt.2017.06.032.
- [45] O. M. Lyulin, A. Campargue, An empirical spectroscopic database for acetylene in the regions of 5850.6341 cm^{-1} and 7000.9415 cm^{-1} , *J. Quant. Spectrosc. Radiat. Transf.* 203 (2017) 461 – 471. doi:10.1016/j.jqsrt.2017.01.036.
- [46] B. Amyay, A. Fayt, M. Herman, J. Vander Auwera, Vibration-rotation spectroscopic database on acetylene, $X^1\Sigma_g^+ \text{ }^{12}C_2H_2$, *J. Phys. Chem. Ref. Data* 45 (2016) 023103. doi:10.1063/1.4947297.
- [47] U. G. Jørgensen, J. Hron, R. Loidl, ISO-SWS spectra of the carbon stars TX Psc, V460 Cyg, and TT Cyg, *Astron. Astrophys.* 356 (2000) 253–266.
- [48] J. Tennyson, S. N. Yurchenko, The ExoMol project: Software for computing molecular line lists, *Intern. J. Quantum Chem.* 117 (2017) 92–103. doi:10.1002/qua.25190.
- [49] S. N. Yurchenko, L. Lodi, J. Tennyson, A. V. Stolyarov, Duo: a general program for calculating spectra of diatomic molecules, *Comput. Phys. Commun.* 202 (2016) 262–275. doi:10.1016/j.cpc.2015.12.021.
- [50] S. N. Yurchenko, W. Thiel, P. Jensen, Theoretical ROVibrational Energies (TROVE): A robust numerical approach to the calculation of rovibrational energies for polyatomic molecules, *J. Mol. Spectrosc.* 245 (2007) 126–140. doi:10.1016/j.jms.2007.07.009.

- [51] A. Yachmenev, S. N. Yurchenko, Automatic differentiation method for numerical construction of the rotational-vibrational hamiltonian as a power series in the curvilinear internal coordinates using the eckart frame, *J. Chem. Phys.* 143 (2015) 014105. doi:10.1063/1.4923039.
- [52] M. Herman, The acetylene ground state saga, *Mol. Phys.* 105 (2007) 2217–2241. doi:10.1080/00268970701518103.
- [53] K. Didriche, M. Herman, A four-atom molecule at the forefront of spectroscopy, intramolecular dynamics and astrochemistry: Acetylene, *Chem. Phys. Lett.* 496 (2010) 1–7. doi:10.1016/j.cplett.2010.07.031.
- [54] M. Herman, High-resolution Infrared Spectroscopy of Acetylene: Theoretical Background and Research Trends, John Wiley & Sons, Ltd, 2011, pp. 1993–2026. doi:10.1002/9780470749593.hrs101.
- [55] K. L. Chubb, P. Jensen, S. N. Yurchenko, Symmetry adaptation of the rotation-vibration theory for linear molecules, *Symmetry* 10 (5) (2018) 137. doi:10.3390/sym10050137.
- [56] K. L. Chubb, M. Joseph, J. Franklin, N. Choudhury, T. Furtenbacher, A. G. Császár, G. Gaspard, P. Oguoko, A. Kelly, S. N. Yurchenko, J. Tennyson, C. Sousa-Silva, MARVEL analysis of the measured high-resolution spectra of C₂H₂, *J. Quant. Spectrosc. Radiat. Transf.* 204 (2018) 42–55. doi:10.1016/j.jqsrt.2017.08.018.
- [57] A. Gaydon, The spectroscopy of flames, Springer Science & Business Media, 2012.
- [58] Schmidt, F. M. and Vaittinen, O. and Metsälä, M. and Kraus, P. and Halonen, L., Direct detection of acetylene in air by continuous wave cavity ring-down spectroscopy, *Appl. Phys. B-Lasers Opt.* 101 (2010) 671–682. doi:10.1007/s00340-010-4027-5.

- [59] M. Metsälä, F. M. Schmidt, M. Skytta, O. Vaittinen, L. Halonen, Acetylene in breath: background levels and real-time elimination kinetics after smoking, *J. Breath Res.* 4 (2010) 046003. doi:10.1088/1752-7155/4/4/046003.
- [60] E. E. Hughes, R. Gorden, Determination of acetylene in air in concentrations from ten parts per billion to ten parts per million, *Analytical Chemistry* 31 (1) (1959) 94–98.
- [61] M. W. Kelly, J. C. Richley, C. M. Western, M. N. R. Ashfold, Y. A. Mankelevich, Exploring the plasma chemistry in microwave chemical vapor deposition of diamond from C/H/O gas mixtures, *The Journal of Physical Chemistry A* 116 (38) (2012) 9431–9446. doi:10.1021/jp306190n.
- [62] J. I. Moses, B. Bézard, E. Lellouch, G. Gladstone, H. Feuchtgruber, M. Allen, Photochemistry of Saturn’s atmosphere: I. Hydrocarbon chemistry and comparisons with ISO observations, *Icarus* 143 (2000) 244 – 298. doi:10.1006/icar.1999.6270.
- [63] T. de Graauw, H. Feuchtgruber, B. Bezaud, P. Drossart, T. Encrenaz, D. A. Beintema, M. Griffin, A. Heras, M. Kessler, K. Leech, E. Lellouch, P. Morris, P. R. Roelfsema, M. Roos-Serote, A. Salama, B. Vandenbussche, E. A. Valentijn, G. R. Davis, D. A. Naylor, First results of ISO-SWS observations of Saturn: Detection of CO₂, CH₃C₂H, C₄H₂ and tropospheric H₂O, *Astron. Astrophys.* 321 (2) (1997) L13–L16.
- [64] T. Encrenaz, M. Combes, S. K. Atreya, P. N. Romani, K. Fricke, A study of the upper atmosphere of Uranus using the IUE, *Astron. Astrophys.* 162 (1986) 317–322.
- [65] S. T. Ridgway, Jupiter: Identification of ethane and acetylene, *Astrophys. J.* 187 (1974) L41–L43. doi:10.1086/181388.

- [66] P. Drossart, B. Bézard, S. Atreya, J. Lacy, E. Serabyn, A. Tokunaga, T. Encrenaz, Enhanced acetylene emission near the north pole of jupiter, *Icarus* 66 (1986) 610 – 618. doi:10.1016/0019-1035(86)90094-1.
- [67] J. H. Waite, M. R. Combi, W.-H. Ip, T. E. Cravens, R. L. McNutt, W. Kasprzak, R. Yelle, J. Luhmann, H. Niemann, D. Gell, B. Magee, G. Fletcher, J. Lunine, W.-L. Tseng, Cassini ion and neutral mass spectrometer: Enceladus plume composition and structure, *Science* 311 (2006) 1419–1422. doi:10.1126/science.1121290.
- [68] S. M. Hörst, Titan’s atmosphere and climate (2017). doi:10.1002/2016JE005240.
- [69] R. S. Oremland, M. A. Voytek, Acetylene as fast food: Implications for development of life on anoxic primordial earth and in the outer solar system, *Astrobiology* 8 (2008) 45–58. doi:10.1089/ast.2007.0183.
- [70] C. P. McKay, H. D. Smith, Possibilities for methanogenic life in liquid methane on the surface of Titan, *Icarus* 178 (2005) 274–276. doi:10.1016/j.icarus.2005.05.018.
- [71] R. A. Lovett, Enceladus named sweetest spot for alien life (May 2011). doi:10.1038/news.2011.337.
- [72] N. Belay, L. Daniels, Production of Ethane, Ethylene, and Acetylene from Halogenated Hydrocarbons by Methanogenic Bacteria, *Appl Environ Microbiol.* 53 (1987) 1604–1610.
- [73] W. Bains, Many chemistries could be used to build living systems, *Astrobiology* 4 (2) (2004) 137–167. doi:10.1089/153110704323175124.
- [74] S. Seager, W. Bains, R. Hu, A biomass-based model to estimate the plausibility of exoplanet biosignature gases, *Astrophys. J.* 775 (2013) 104.

- [75] T. Y. Brooke, A. T. Tokunaga, H. A. Weaver, J. Crovisier, D. Bockelee-Morvan, D. Crisp, Detection of acetylene in the infrared spectrum of comet Hyakutake, *Nature* 383 (1996) 606–608. doi:10.1038/383606a0.
- [76] L. Le Roy, K. Altwegg, H. Balsiger, J.-J. Berthelier, A. Bieler, C. Briois, U. Calmonte, M. R. Combi, J. De Keyser, F. Dhooghe, B. Fiethe, S. A. Fuselier, S. Gasc, T. I. Gombosi, M. Hässig, A. Jäckel, M. Rubin, C.-Y. Tzou, Inventory of the volatiles on comet 67P/Churyumov-Gerasimenko from Rosetta/ROSINA, *Astron. Astrophys.* 583 (2015) A1. doi:10.1051/0004-6361/201526450.
- [77] S. T. Ridgway, D. N. B. Hall, S. G. Kleinmann, D. A. Weinberger, R. S. Wojslaw, Circumstellar acetylene in the infrared spectrum of IRC+10°216, *Nature* 264 (1976) 345–346.
- [78] J. Tennyson, S. N. Yurchenko, Laboratory spectra of hot molecules: data needs for hot super-earth exoplanets, *Mol. Astrophys.* 8 (2017) 1–18. doi:10.1016/j.molap.2017.05.002.
- [79] N. Madhusudhan, M. Agundez, J. I. Moses, Y. Hu, Exoplanetary Atmospheres-Chemistry, Formation Conditions, and Habitability, *Space Sci. Rev.* 205 (2016) 285–348. doi:{10.1007/s11214-016-0254-3}.
- [80] B. R. Oppenheimer, C. Baranec, C. Beichman, D. Brenner, R. Burruss, E. Cady, J. R. Crepp, R. Dekany, R. Fergus, D. Hale, L. Hillenbrand, S. Hinkley, D. W. Hogg, D. King, E. R. Ligon, T. Lockhart, R. Nilsson, I. R. Parry, L. Pueyo, E. Rice, J. E. Roberts, L. C. Roberts, Jr., M. Shao, A. Sivaramakrishnan, R. Soummer, T. Truong, G. Vasisht, A. Veicht, F. Vesceus, J. K. Wallace, C. Zhai, N. Zimmerman, Reconnaissance of the HR 8799 exosolar system. I. Near-infrared spectroscopy, *Astrophys. J.* 768 (2013) 24. doi:10.1088/0004-637X/768/1/24.
- [81] M. Shabram, J. J. Fortney, T. P. Greene, R. S. Freedman, Transmission spectra of transiting planet atmospheres: Model validation and simu-

- lations of the hot neptune gj 436b for the james webb space telescope, *Astrophys. J.* 727 (2011) 65. doi:10.1088/0004-637X/727/2/65.
- [82] H. Dhanao, J. M. C. Rawlings, Is acetylene essential for carbon dust formation?, *Mon. Not. R. Astron. Soc.* 440 (2014) 1786–1793. doi:10.1093/mnras/stu401.
- [83] J. Cernicharo, The Polymerization of Acetylene, Hydrogen Cyanide, and Carbon Chains in the Neutral Layers of Carbon-rich Proto-planetary Nebulae, *Astrophys. J.* 608 (2004) L41–L44. doi:10.1086/422170.
- [84] R. Gautschy-Loidl, S. Høfner, U. Jørgensen, J. Hron, Dynamic model atmospheres of AGB stars - IV. A comparison of synthetic carbon star spectra with observations, *Astron. Astrophys.* 422 (2004) 289–306. doi:10.1051/0004-6361:20035860.
- [85] R. Loidl, S. Høfner, U. G. Jørgensen, B. Aringer, Dynamic model atmospheres of AGB stars - II. Synthetic near infrared spectra of carbon stars, *Astron. Astrophys.* 342 (1999) 531–541.
- [86] B. Aringer, L. Girardi, W. Nowotny, P. Marigo, M. T. Lederer, Synthetic photometry for carbon rich giants I. Hydrostatic dust-free models, *Astron. Astrophys.* 503 (2009) 913–928. doi:10.1051/0004-6361/200911703.
- [87] C. P. Rinsland, A. Baldacci, K. N. Rao, Acetylene bands observed in carbon stars - a laboratory study and an illustrative example of its application to IRC+10216, *Astrophys. J. Suppl.* 49 (1982) 487–513. doi:10.1086/190808.
- [88] I. E. Gordon, L. S. Rothman, C. Hill, R. V. Kochanov, Y. Tan, P. F. Bernath, M. Birk, V. Boudon, A. Campargue, K. V. Chance, B. J. Drouin, J.-M. Flaud, R. R. Gamache, J. T. Hodges, D. Jacquemart, V. I. Perevalov, A. Perrin, K. P. Shine, M.-A. H. Smith, J. Tennyson,

- G. C. Toon, H. Tran, V. G. Tyuterev, A. Barbe, A. G. Császár, V. M. Devi, T. Furtenbacher, J. J. Harrison, J.-M. Hartmann, A. Jolly, T. J. Johnson, T. Karman, I. Kleiner, A. A. Kyuberis, J. Loos, O. M. Lyulin, S. T. Massie, S. N. Mikhailenko, N. Moazzen-Ahmadi, H. S. P. Müller, O. V. Naumenko, A. V. Nikitin, O. L. Polyansky, M. Rey, M. Rotger, S. W. Sharpe, K. Sung, E. Starikova, S. A. Tashkun, J. Vander Auwera, G. Wagner, J. Wilzewski, P. Weisło, S. Yu, E. J. Zak, The *HITRAN* 2016 molecular spectroscopic database, *J. Quant. Spectrosc. Radiat. Transf.* 203 (2017) 3–69. doi:10.1016/j.jqsrt.2017.06.038.
- [89] U. G. Jørgensen, *Molecules in astrophysics : probes and processes : proceedings of the 178th Symposium of the International Astronomical Union, held in Leiden, the Netherlands, July 1–5 1996* (1997).
- [90] J.-L. Baudino, P. Molliere, O. Venot, P. Tremblin, B. Bezard, P.-O. Lagage, Toward the analysis of JWST exoplanet spectra: Identifying troublesome model parameters, *Astrophys. J.* 850 (2017) 150.
- [91] B. Amyay, S. Robert, M. Herman, A. Fayt, B. Raghavendra, A. Moudens, J. Thievin, B. Rowe, R. Georges, Vibration-rotation pattern in acetylene. II. Introduction of Coriolis coupling in the global model and analysis of emission spectra of hot acetylene around 3 μm , *J. Chem. Phys.* 131 (2009) 114301. doi:10.1063/1.3200928.
- [92] J. Hron, B. Aringer, Private communication.
- [93] L. Rothman, I. Gordon, R. Barber, H. Dothe, R. Gamache, A. Goldman, V. Perevalov, S. Tashkun, J. Tennyson, HITEMP, the high-temperature molecular spectroscopic database, *J. Quant. Spectrosc. Radiat. Transf.* 111 (2010) 2139 – 2150. doi:10.1016/j.jqsrt.2010.05.001.
- [94] H. S. P. Müller, F. Schlöder, J. Stutzki, G. Winnewisser, The Cologne database for molecular spectroscopy, CDMS: a useful tool for as-

- tronomers and spectroscopists, *J. Molec. Struct. (THEOCHEM)* 742 (2005) 215–227.
- [95] N. Jacquinet-Husson, R. Armante, N. A. Scott, A. Chédin, L. Crépeau, C. Boutammine, A. Bouhdaoui, C. Crevoisier, V. Capelle, C. Boone, N. Poulet-Crovisier, A. Barbe, D. C. Benner, V. Boudon, L. R. Brown, J. Buldyreva, A. Campargue, L. H. Coudert, V. M. Devi, M. J. Down, B. J. Drouin, A. Fayt, C. Fittschen, J.-M. Flaud, R. R. Gamache, J. J. Harrison, C. Hill, Ø. Hodnebrog, S. M. Hu, D. Jacquemart, A. Jolly, E. Jiménez, N. N. Lavrentieva, A. W. Liu, L. Lodi, O. M. Lyulin, S. T. Massie, S. Mikhailenko, H. S. P. Müller, O. V. Naumenko, A. Nikitin, C. J. Nielsen, J. Orphal, V. I. Perevalov, A. Perrin, E. Polovtseva, A. Predoi-Cross, M. Rotger, A. A. Ruth, S. S. Yu, K. Sung, S. A. Tashkun, J. Tennyson, V. G. Tyuterev, J. Vander Auwera, B. A. Voronin, A. Makie, The 2015 edition of the GEISA spectroscopic database, *J. Mol. Spectrosc.* 327 (2016) 31–72. doi:10.1016/j.jms.2016.06.007.
- [96] M. Rey, A. V. Nikitin, Y. L. Babikov, V. G. Tyuterev, TheoReTS – an information system for theoretical spectra based on variational predictions from molecular potential energy and dipole moment surfaces, *J. Mol. Spectrosc.* 327 (2016) 138–158. doi:10.1016/j.jms.2016.04.006.
- [97] S. N. Mikhailenko, Y. L. Babikov, G. V. F., Information-calculating system spectroscopy of atmospheric gases. the structure and main functions, *Atmospheric and Oceanic Optics* 18 (2005) 685–695.
- [98] Y. A. Ba, C. Wenger, R. Surleau, V. Boudon, M. Rotger, L. Daumont, D. A. Bonhommeau, V. G. Tyuterev, M.-L. Dubernet, MeCaSDa and ECaSDa: Methane and ethene calculated spectroscopic databases for the virtual atomic and molecular data centre, *J. Quant. Spectrosc. Radiat. Transf.* (2013) 62–68doi:10.1016/j.jqsrt.2013.05.001.

- [99] A. V. Nikitin, M. Rey, V. G. Tyuterev, Accurate line intensities of methane from first-principles calculations, *J. Quant. Spectrosc. Radiat. Transf.* 200 (2017) 90–99. doi:10.1016/j.jqsrt.2017.05.023.
- [100] M. Rey, A. V. Nikitin, V. G. Tyuterev, Accurate theoretical methane line lists in the infrared up to 3000 K and quasi-continuum absorption/emission modeling for astrophysical applications, *Astrophys. J.* 847 (2017) 105.
- [101] M. Rey, A. V. Nikitin, B. Bézard, P. Rannou, A. Coustenis, V. G. Tyuterev, New accurate theoretical line lists of $^{12}\text{CH}_4$ and $^{13}\text{CH}_4$ in the 0–13400 cm^{-1} range: Application to the modeling of methane absorption in Titan’s atmosphere, *Icarus* 303 (2018) 114 – 130. doi:10.1016/j.icarus.2017.12.045.
- [102] M. Rey, A. V. Nikitin, V. G. Tyuterev, First principles intensity calculations for the methane rovibrational spectra in the infrared up to 9300 cm^{-1} , *Phys. Chem. Chem. Phys.* 15 (2013) 10049–10061. doi:10.1039/C3CP50275A.
- [103] M. Rey, A. V. Nikitin, V. G. Tyuterev, Theoretical hot methane line list up T=2000 K for astrophysical applications, *Astrophys. J.* 789 (2014) 2. doi:10.1088/0004-637X/789/1/2.
- [104] A. Nikitin, M. Rey, V. Tyuterev, High order dipole moment surfaces of PH_3 and ab initio intensity predictions in the octad range, *J. Mol. Spectrosc.* 305 (2014) 40 – 47. doi:10.1016/j.jms.2014.09.010.
- [105] X. Huang, D. W. Schwenke, T. J. Lee, Rovibrational spectra of ammonia. I. Unprecedented accuracy of a potential energy surface used with nonadiabatic corrections, *J. Chem. Phys.* 134 (2011) 044320. doi:10.1063/1.3541351.
- [106] X. Huang, D. W. Schwenke, T. J. Lee, Rovibrational spectra of ammonia. II. Detailed analysis, comparison, and prediction of spectroscopic

- assignments for $^{14}\text{NH}_3$, $^{15}\text{NH}_3$, and $^{14}\text{ND}_3$, *J. Chem. Phys.* 134 (2011) 044321. doi:10.1063/1.3541352.
- [107] M. Rey, T. Delahaye, A. V. Nikitin, V. G. Tyuterev, First theoretical global line lists of ethylene ($^{12}\text{C}_2\text{H}_4$) spectra for the temperature range 50–700 K in the far-infrared for quantification of absorption and emission in planetary atmospheres, *Astron. Astrophys.* 594 (2016) A47.
- [108] P. Botschwina, M. E. Sanz, M. C. McCarthy, P. Thaddeus, Ab initio theory and rotational spectra of linear carbon chains SiC_nS , *J. Chem. Phys.* 116 (24) (2002) 10719–10729. doi:10.1063/1.1473807.
- [109] M. Herman, J. Lievin, J. Vander Auwera, A. Campargue, *Global and Accurate Vibration Hamiltonians from High-Resolution Molecular Spectroscopy*, Vol. 108 of *Adv. Chem. Phys.*, Wiley and Sons, Inc., New York, NY, 1999.
- [110] H.-J. Werner, P. J. Knowles, G. Knizia, F. R. Manby, M. Schütz, Molpro: a general-purpose quantum chemistry program package, *WIREs Comput. Mol. Sci.* 2 (2012) 242–253. doi:10.1002/wcms.82.
- [111] S. Seager, *Exoplanet Atmospheres: Physical Processes*, Princeton University Press, 2010.
- [112] J. F. Kasting, R. Kopparapu, R. M. Ramirez, C. E. Harman, Remote life-detection criteria, habitable zone boundaries, and the frequency of Earth-like planets around M and late K stars, *PNAS* 111 (35) (2014) 12641–12646. doi:10.1073/pnas.1309107110.
- [113] W. J. Borucki, E. Agol, F. Fressin, L. Kaltenegger, J. Rowe, H. Isaacson, D. Fischer, N. Batalha, J. J. Lissauer, G. W. Marcy, D. Fabrycky, J.-M. Désert, S. T. Bryson, T. Barclay, F. Bastien, A. Boss, E. Brugamyer, L. A. Buchhave, C. Burke, D. A. Caldwell, J. Carter, D. Charbonneau, J. R. Crepp, J. Christensen-Dalsgaard, J. L. Christiansen, D. Ciardi,

- W. D. Cochran, E. DeVore, L. Doyle, A. K. Dupree, M. Endl, M. E. Everett, E. B. Ford, J. Fortney, T. N. Gautier, J. C. Geary, A. Gould, M. Haas, C. Henze, A. W. Howard, S. B. Howell, D. Huber, J. M. Jenkins, H. Kjeldsen, R. Kolbl, J. Kolodziejczak, D. W. Latham, B. L. Lee, E. Lopez, F. Mullally, J. A. Orosz, A. Prsa, E. V. Quintana, R. Sanchis-Ojeda, D. Sasselov, S. Seader, A. Shporer, J. H. Steffen, M. Still, P. Tenenbaum, S. E. Thompson, G. Torres, J. D. Twicken, W. F. Welsh, J. N. Winn, Kepler-62: A five-planet system with planets of 1.4 and 1.6 Earth radii in the habitable zone, *Science* 340 (2013) 587–590. doi:10.1126/science.1234702.
- [114] M. Gillon, A. H. M. J. Triaud, J. J. Fortney, B. O. Demory, E. Jehin, M. Lendl, P. Magain, P. Kabath, D. Queloz, R. Alonso, D. R. Anderson, A. C. Cameron, A. Fumel, L. Hebb, C. Hellier, A. Lanotte, P. F. L. Maxted, N. Mowlavi, B. Smalley, The TRAPPIST survey of southern transiting planets I. Thirty eclipses of the ultra-short period planet WASP-43 b, *Astron. Astrophys.* 542 (2012) A4. doi: {10.1051/0004-6361/201218817}.
- [115] D. E. Francesco Pepe, M. R. Meyer, Instrumentation for the detection and characterization of exoplanets, *Nature* 513 (2014) 358–366. doi: 10.1038/nature13784.
- [116] W. J. Borucki, D. Koch, G. Basri, N. Batalha, T. Brown, D. Caldwell, J. Caldwell, J. Christensen-Dalsgaard, W. D. Cochran, E. DeVore, E. W. Dunham, A. K. Dupree, T. N. Gautier, J. C. Geary, R. Gilliland, A. Gould, S. B. Howell, J. M. Jenkins, Y. Kondo, D. W. Latham, G. W. Marcy, S. Meibom, H. Kjeldsen, J. J. Lissauer, D. G. Monet, D. Morrison, D. Sasselov, J. Tarter, A. Boss, D. Brownlee, T. Owen, D. Buzasi, D. Charbonneau, L. Doyle, J. Fortney, E. B. Ford, M. J. Holman, S. Seager, J. H. Steffen, W. F. Welsh, J. Rowe, H. Anderson, L. Buchhave, D. Ciardi, L. Walkowicz, W. Sherry, E. Horch, H. Isaacson, M. E. Ev-

- erett, D. Fischer, G. Torres, J. A. Johnson, M. Endl, P. MacQueen, S. T. Bryson, J. Dotson, M. Haas, J. Kolodziejczak, J. Van Cleve, H. Chandrasekaran, J. D. Twicken, E. V. Quintana, B. D. Clarke, C. Allen, J. Li, H. Wu, P. Tenenbaum, E. Verner, F. Bruhweiler, J. Barnes, A. Prsa, Kepler planet-detection mission: Introduction and first results, *Science* 327 (5968) (2010) 977–980. doi:10.1126/science.1185402.
- [117] J. J. F. Nikku Madhusudhan, Heather Knutson, T. Barman, *Exoplanetary Atmospheres* (2014).
URL <http://www.mpia.de/homes/ppvi/chapter/madhusudhan.pdf>
- [118] S. Seager, D. Deming, *Exoplanet Atmospheres*, *Annual Review of Astronomy and Astrophysics* 48 (1) (2010) 631–672. doi:10.1146/annurev-astro-081309-130837.
- [119] M. R. Swain, G. Vasisht, G. Tinetti, The presence of methane in the atmosphere of an extrasolar planet, *Nature* 452 (2008) 329–331.
- [120] G. Tinetti, A. Vidal-Madjar, M.-C. Liang, J.-P. Beaulieu, Y. Yung, S. Carey, R. J. Barber, J. Tennyson, I. Ribas, N. Allard, G. E. Ballester, D. K. Sing, F. Selsis, Water vapour in the atmosphere of a transiting extrasolar planet, *Nature* 448 (2007) 169–171.
- [121] J. J. Spake, D. K. Sing, T. M. Evans, A. Oklopčić, V. Bourrier, L. Kreidberg, B. V. Rackham, J. Irwin, D. Ehrenreich, A. Wyttenbach, H. R. Wakeford, Y. Zhou, K. L. Chubb, N. Nikolov, J. M. Goyal, G. W. Henry, M. H. Williamson, S. Blumenthal, D. R. Anderson, C. Hellier, D. Charbonneau, S. Udry, N. Madhusudhan, Helium in the eroding atmosphere of an exoplanet, *Nature* 557 (2018) 68–70. doi:10.1038/s41586-018-0067-5.
- [122] D. K. Sing, J. J. Fortney, N. Nikolov, H. R. Wakeford, T. Kataria, T. M. Evans, S. Aigrain, G. E. Ballester, A. S. Burrows, D. Deming, J.-M. Desert, N. P. Gibson, G. W. Henry, C. M. Huitson, H. A. Knutson,

- A. L. des Etangs, F. Pont, A. P. Showman, A. Vidal-Madjar, M. H. Williamson, P. A. Wilson, A continuum from clear to cloudy hot-jupiter exoplanets without primordial water depletion, *Nature* 529 (2016) 59–62. doi:10.1038/nature16068.
- [123] T. M. Evans, D. K. Sing, T. Kataria, J. G. Oyal, N. Nikolov, H. R. Wakeford, D. Deming, M. S. Marley, D. S. Amundsen, G. E. Ballester, J. K. Barstow, L. Ben-Jaffel, V. Bourrier, L. A. Buchhave, O. Cohen, D. Ehrenreich, A. G. Munoz, G. W. Henry, H. Knutson, P. Lavvas, A. L. des Etangs, N. K. Lewis, M. Lopez-Morales, A. M. Mandell, J. Sanz-Forcada, P. Tremblin, R. Lupu, An ultrahot gas-giant exoplanet with a stratosphere, *Nature* 548 (7665) (2017) 58–61. doi:10.1038/nature23266.
- [124] T. M. Evans, D. K. Sing, H. R. Wakeford, N. Nikolov, G. E. Ballester, B. Drummond, T. Kataria, N. P. Gibson, D. S. Amundsen, J. Spake, Detection of H₂O and evidence for TiO/VO in an ultra-hot exoplanet atmosphere, *Astrophys. J.* 822 (2016) L4.
- [125] M. Brogi, R. J. de Kok, J. L. Birkby, H. Schwarz, I. A. G. Snellen, Carbon monoxide and water vapor in the atmosphere of the non-transiting exoplanet HD 179949 b, *Astron. Astrophys.* 565 (2014) A124. doi:10.1051/0004-6361/201423537.
- [126] J. L. Birkby, R. J. de Kok, M. Brogi, E. J. W. de Mooij, H. Schwarz, S. Albrecht, I. A. G. Snellen, Detection of water absorption in the day side atmosphere of HD 189733 b using ground-based high-resolution spectroscopy at 3.2 μ m, *Mon. Not. R. Astron. Soc.* 436 (2013) L35–L39. doi:10.1093/mnrasl/slt107.
- [127] T. S. Barman, Q. M. Konopacky, B. Macintosh, C. Marois, Simultaneous detection of water, methane, and carbon monoxide in the atmosphere

- of exoplanet HR 8799 b, *Astrophys. J.* 804 (2015) 61. doi:10.1088/0004-637X/804/1/61.
- [128] L. Kreidberg, M. R. Line, J. L. Bean, K. B. Stevenson, J.-M. Desert, N. Madhusudhan, J. J. Fortney, J. K. Barstow, G. W. Henry, M. H. Williamson, A. P. Showman, A detection of water in the transmission spectrum of the hot Jupiter WASP-12b and implications for its atmospheric composition, *Astrophys. J.* 814 (2015) 66. doi:10.1088/0004-637X/814/1/66.
- [129] Q. M. Konopacky, T. S. Barman, B. A. Macintosh, C. Marois, Detection of Carbon Monoxide and Water Absorption Lines in an Exoplanet Atmosphere, *Science* 339 (2013) 1398–1401. doi:10.1126/science.1232003.
- [130] R. J. Barber, J. Tennyson, G. J. Harris, R. N. Tolchenov, A high accuracy computed water line list, *Mon. Not. R. Astron. Soc.* 368 (2006) 1087–1094.
- [131] R. Nassar, P. Bernath, Hot methane spectra for astrophysical applications, *J. Quant. Spectrosc. Radiat. Transf.* 82 (2003) 279–292. doi:10.1016/S0022-4073(03)00158-4.
- [132] L. S. Rothman, D. Jacquemart, A. Barbe, D. C. Benner, M. Birk, L. R. Brown, M. R. Carleer, C. Chackerian, K. Chance, L. H. Coudert, V. Dana, V. M. Devi, J.-M. Flaud, R. R. Gamache, A. Goldman, J.-M. Hartmann, K. W. Jucks, A. G. Maki, J.-Y. Mandin, S. T. Massie, J. Orphal, A. Perrin, C. P. Rinsland, M. A. H. Smith, J. Tennyson, R. N. Tolchenov, R. A. Toth, J. Vander Auwera, P. Varanasi, G. Wagner, The *HITRAN* 2004 molecular spectroscopic database, *J. Quant. Spectrosc. Radiat. Transf.* 96 (2005) 139–204.
- [133] T. P. Greene, M. R. Line, C. Montero, J. J. Fortney, J. Lustig-Yaeger, K. Luther, Characterizing transiting exoplanet atmospheres with JWST, *Astrophys. J.* 817 (1) (2016) 17.

- [134] C. Beichman, B. Benneke, H. Knutson, R. Smith, P.-O. Lagage, C. Dressing, D. Latham, J. Lunine, S. Birkmann, P. Ferruit, et al., Observations of transiting exoplanets with the James Webb Space Telescope (JWST), *Publications of the Astronomical Society of the Pacific* 126 (946) (2014) 1134.
- [135] The science of ARIEL (Atmospheric Remote-sensing Infrared Exoplanet Large-survey), Vol. 9904. doi:10.1117/12.2232370.
- [136] G. Tinetti, et al., A chemical survey of exoplanets with ARIEL, *Exp. Astron.* (2018), In press.
- [137] E. Pascale, J. Tennyson, 40 others, The ARIEL space mission, *Proc. SPIE* (2018), In press.
- [138] M. Tessenyi, G. Tinetti, J. Tennyson, G. Savini, E. Pascale, S. Jason, D. Liddle, J. Williams, A. Vora, C. Saunders, Twinkle – a British space mission to explore faraway worlds, in: *Proceedings of the International Astronautical Congress, IAC*, Vol. 6, International Astronautical Federation, 2015, pp. 4311–4313.
- [139] G. Savini, M. Tessenyi, G. Tinetti, C. Arena, J. Tennyson, T. Zingales, E. Pascale, R. Sudiwala, A. Papageorgiou, S. Sarkar, P. A. R. Ade, M. J. Griffin, K. Barnes, L. Hipwood, P. Knowles, M. Patel, M. Leese, J. P. Mason, M. Crook, I. Tosh, A. Saad, P. Eccleston, B. Shaughnessy, T. Brooke, M. Wells, I. Bryson, A. Macleod, W. Taylor, N. Bezawada, G. S. Wright, S. Jason, J. Friend, J. Williams, G. Johnston, S. Prasad, A. Vora, C. Saunders, B. Winter, P. Curry, A. Smith, Twinkle: A low earth orbit visible and infrared exoplanet spectroscopy observatory (2018). doi:10.1117/12.2233691.
- [140] S. Jason, A. da Silva Curiel, M. Tessenyi, G. Tinetti, G. Savini, J. Tennyson, E. Pascale, J. Williams, G. Johnson, S. Prasad, A. Vora, C. Saunders, J. Friend, M. Sweeting, Twinkle: A new idea for commercial astro-

- physics missions, in: J. Maruani, J. Serre (Eds.), *Small Satellites Systems and Services Symposium, The 4S Symposium*, ESA, 2016.
- [141] C. Sousa-Silva, L. K. McKemmish, K. L. Chubb, J. Baker, E. J. Barton, M. N. Gorman, T. Rivlin, J. Tennyson, Original Research By Young Twinkle Students (ORBYTS): When can students start performing original research?, *Phys. Educ.* 53 (2018) 015020. doi:10.1088/1361-6552/aa8f2a.
- [142] L. K. McKemmish, K. L. Chubb, T. Rivlin, J. S. Baker, M. N. Gorman, A. Heward, W. Dunn, M. Tessenyi, Bringing pupils into the ORBYTS of research, *Astronomy & Geophysics* 58 (5) (2017) 5.11. doi:10.1093/astrogeo/atx169.
- [143] K. L. Chubb, O. V. Naumenko, S. Keely, S. Bartolotto, S. MacDonald, M. Mukhtar, A. Grachov, J. White, E. Coleman, S.-M. Hu, A. Liu, A. Z. Fazliev, E. R. Polovtseva, V. M. Horneman, A. Campargue, T. Furtenbacher, A. G. Császár, S. N. Yurchenko, J. Tennyson, MARVEL analysis of the measured high-resolution rovibrational spectra of H₂S, *J. Quant. Spectrosc. Radiat. Transf.* 218 (2018) 178 – 186. doi:10.1016/j.jqsrt.2018.07.012.
- [144] M. Brogi, M. Line, J. Bean, J.-M. Désert, H. Schwarz, A framework to combine low- and high-resolution spectroscopy for the atmospheres of transiting exoplanets, *Astrophys. J. Lett.* 839 (1) (2017) L2.
- [145] J. H. Lacy, N. J. Evans, II, J. M. Achtermann, D. E. Bruce, J. F. Arens, J. S. Carr, Discovery of interstellar acetylene, *Astrophys. J. Lett.* 342 (1989) L43–L46. doi:10.1086/185480.
- [146] N. Rangwala, S. W. J. Colgan, R. L. Gal, K. Acharyya, X. Huang, T. J. Lee, E. Herbst, C. deWitt, M. Richter, A. Boogert, M. McKelvey, High spectral resolution SOFIA/EXES observations of C₂H₂ toward orion IRc2, *Astrophys. J.* 856 (2018) 9.

- [147] R. J. de Kok, M. Brogi, I. A. G. Snellen, J. Birkby, S. Albrecht, E. J. W. de Mooij, Detection of carbon monoxide in the high-resolution day-side spectrum of the exoplanet HD 189733b, *Astron. Astrophys.* 554 (2013) A82. doi:10.1051/0004-6361/201321381.
- [148] J. Birkby, R. de Kok, M. Brogi, H. Schwarz, S. Albrecht, E. de Mooij, I. Snellen, Characterising exoplanet atmospheres with high-resolution spectroscopy, *The Messenger* 154 (2013) 57–61.
- [149] J. L. Birkby, R. J. de Kok, M. Brogi, H. Schwarz, I. A. G. Snellen, Discovery of water at high spectral resolution in the atmosphere of 51 Peg b, *ArXiv e-prints* arXiv:1701.07257.
- [150] N. Madhusudhan, Private communication.
- [151] P. Tremblin, D. S. Amundsen, P. Mourier, I. Baraffe, G. Chabrier, B. Drummond, D. Homeier, O. Venot, Fingering convection and cloudless models for cool brown dwarf atmospheres, *Astrophys. J. Lett.* 804 (2015) L17.
- [152] D. S. Amundsen, I. Baraffe, P. Tremblin, J. Manners, H. Wolfgang, N. J. Mayne, D. M. Acreman, Accuracy tests of radiation schemes used in hot jupiter global circulation models, *Astron. Astrophys.* 564 (2014) A59.
- [153] J. M. Goyal, N. Mayne, D. K. Sing, B. Drummond, P. Tremblin, D. S. Amundsen, T. Evans, A. L. Carter, J. Spake, I. Baraffe, N. Nikolov, J. Manners, G. Chabrier, E. Hebrard, A library of ATMO forward model transmission spectra for hot Jupiter exoplanets, *Mon. Not. R. Astron. Soc.* 473 (2018) 5158–5185. doi:{10.1093/mnras/stx3015}.
- [154] P. Mollière, R. van Boekel, C. Dullemond, T. Henning, C. Mordasini, Model atmospheres of irradiated exoplanets: The influence of stellar parameters, metallicity, and the C/O ratio, *Astrophys. J.* 813 (2015) 47.

- [155] Mollière, P., van Boekel, R., Bouwman, J., Henning, T., Lagage, P.-O., Min, M., Observing transiting planets with JWST - prime targets and their synthetic spectral observations, *Astron. Astrophys.* 600 (2017) A10. doi:10.1051/0004-6361/201629800.
- [156] Baudino, J.-L., Bézard, B., Boccaletti, A., Bonnefoy, M., Lagrange, A.-M., Galicher, R., Interpreting the photometry and spectroscopy of directly imaged planets: a new atmospheric model applied to β Pictoris b and SPHERE observations, *Astron. Astrophys.* 582 (2015) A83. doi:10.1051/0004-6361/201526332.
- [157] I. P. Waldmann, G. Tinetti, M. Rocchetto, E. J. Barton, S. N. Yurchenko, J. Tennyson, Tau-REx I: A next generation retrieval code for exoplanetary atmospheres, *Astrophys. J.* 802 (2). doi:10.1088/0004-637x/802/2/107.
- [158] I. P. Waldmann, M. Rocchetto, G. Tinetti, E. J. Barton, S. N. Yurchenko, J. Tennyson, Tau-REx II: Retrieval of emission spectra, *Astrophys. J.* 813 (1) (2015) 13.
- [159] I. P. Waldmann, Dreaming of atmospheres, *Astrophys. J.* 820 (2016) 107. doi:10.3847/0004-637X/820/2/107.
- [160] A. Tsiaras, I. P. Waldmann, T. Zingales, M. Rocchetto, G. Morello, M. Damiano, K. Karpouzas, G. Tinetti, L. K. McKemmish, J. Tennyson, S. N. Yurchenko, A population study of gaseous exoplanets, *Astron. J.* 155 (2018) 156. doi:10.3847/1538-3881/aaaf75.
- [161] A. Tsiaras, I. P. Waldmann, M. Rocchetto, R. Varley, G. Morello, M. Damiano, G. Tinetti, A new approach to analyzing HST spatial scans: The transmission spectrum of HD 209458 b, *Astrophys. J.* 832 (2) (2016) 202.
- [162] M. R. Line, A. S. Wolf, X. Zhang, H. Knutson, J. A. Kammer, E. Ellison, P. Deroo, D. Crisp, Y. L. Yung, A Systematic Retrieval Analysis of

- Secondary Eclipse Spectra. I. A Comparison of Atmospheric Retrieval Techniques, *Astrophys. J.* 775 (2013) 137.
- [163] K. B. Stevenson, M. R. Line, J. L. Bean, J.-M. Désert, J. J. Fortney, A. P. Showman, T. Kataria, L. Kreidberg, Y. K. Feng, Spitzer phase curve constraints for WASP-43b at 3.6 and 4.5 μm , *Astrophys. J.* 153 (2) (2017) 68.
- [164] P. G. J. Irwin, N. A. Teanby, R. de Kok, L. N. Fletcher, C. J. A. Howett, C. C. C. Tsang, C. F. Wilson, S. B. Calcutt, C. A. Nixon, P. D. Parrish, The NEMESIS planetary atmosphere radiative transfer and retrieval tool, *J. Quant. Spectrosc. Radiat. Transf.* 109 (2008) 1136 – 1150.
- [165] L. S. Rothman, I. E. Gordon, R. J. Barber, H. Dothe, R. R. Gamache, A. Goldman, V. I. Perevalov, S. A. Tashkun, J. Tennyson, HITEMP, the high-temperature molecular spectroscopic database, *J. Quant. Spectrosc. Radiat. Transf.* 111 (2010) 2139–2150. doi:10.1016/j.jqsrt.2010.05.001.
- [166] S. W. Sharpe, T. J. Johnson, R. L. Sams, P. M. Chu, G. C. Rhoderick, P. A. Johnson, Gas-phase databases for quantitative infrared spectroscopy, *Appl. Spectrosc.* 58 (2004) 1452–1461. doi:10.1366/0003702042641281.
- [167] J. Tennyson, S. N. Yurchenko, The ExoMol atlas of molecular opacities, *Atoms* 6 (2018) 26. doi:10.3390/atoms6020026.
- [168] S. N. Yurchenko, A. F. Al-Refaeie, J. Tennyson, ExoCross: A general program for generating spectra from molecular line lists, *Astron. Astrophys.* 614 (2018) A131. doi:10.1051/0004-6361/201732531.
- [169] M. Min, Random sampling technique for ultra-fast computations of molecular opacities for exoplanet atmospheres, *Astron. Astrophys.* 607 (A9). doi:10.1051/0004-6361/201731612.

- [170] C. Hedges, N. Madhusudhan, Effect of pressure broadening on molecular absorption cross sections in exoplanetary atmospheres, *Mon. Not. R. Astron. Soc.* 458 (2016) 1427–1449. doi:10.1093/mnras/stw278.
- [171] F. Schreier, Optimized implementations of rational approximations for the voigt and complex error function, *J. Quant. Spectrosc. Radiat. Transf.* 112 (2011) 1010 – 1025. doi:10.1016/j.jqsrt.2010.12.010.
- [172] F. Schreier, Computational aspects of speed-dependent voigt profiles, *J. Quant. Spectrosc. Radiat. Transf.* 187 (2017) 44 – 53. doi:10.1016/j.jqsrt.2016.08.009.
- [173] F. Schreier, Short communications comments on the voigt function implementation in the astropy and spectraplot.com packages, *J. Quant. Spectrosc. Radiat. Transf.* 213 (2018) 13–16. doi:10.1016/j.jqsrt.2018.03.019.
- [174] S. L. Grimm, K. Heng, HELIOS-K: An ultrafast, open-source opacity calculator for radiative transfer, *Astrophys. J.* 808 (2015) 182. doi: {10.1088/0004-637X/808/2/182}.
- [175] S. N. Yurchenko, J. Tennyson, E. J. Barton, Molecular line shape parameters for exoplanetary atmospheric applications, *J. Phys. Conf. Ser.* 810 (2017) 012010. doi:10.1088/1742-6596/810/1/012010.
- [176] I. E. Gordon, et al., The *HITRAN* 2016 molecular spectroscopic database, *J. Quant. Spectrosc. Radiat. Transf.* 203 (2017) 3–69. doi: 10.1016/j.jqsrt.2017.06.038.
- [177] D. Jacquemart, J. Y. Mandin, V. Dana, L. Regalia-Jarlot, J. Plateaux, D. Decatoire, L. S. Rothman, The spectrum of acetylene in the 5- μm region from new line-parameter measurements, *J. Quant. Spectrosc. Radiat. Transf.* 76 (2003) 237–267. doi:10.1016/S0022-4073(02)00055-9.

- [178] J. S. Wilzewski, I. E. Gordon, R. V. Kochanov, C. Hill, L. S. Rothman, H₂, He, and CO₂ line-broadening coefficients, pressure shifts and temperature-dependence exponents for the HITRAN database. Part 1: SO₂, NH₃, HF, HCl, OCS and C₂H₂, *J. Quant. Spectrosc. Radiat. Transf.* 168 (2016) 193 – 206. doi:10.1016/j.jqsrt.2015.09.003.
- [179] J.-P. Bouanich, G. Blanquet, J. Walrand, Oxygen broadening of acetylene lines in the ν_5 band at low temperature, *J. Mol. Spectrosc.* 194 (2) (1999) 269 – 277. doi:10.1006/jmsp.1999.7806.
- [180] D. Jacquemart, J. Y. Mandin, V. Dana, L. Regalia-Jarlot, X. Thomas, P. Von der Heyden, Multispectrum fitting measurements of line parameters for 5- μm cold bands of acetylene, *J. Quant. Spectrosc. Radiat. Transf.* 75 (2002) 397–422. doi:10.1016/S0022-4073(02)00017-1.
- [181] F. Herregodts, E. Kerrinckx, T. R. Huet, J. Vander Auwera, Absolute line intensities in the $\nu_1 + 3\nu_3$ band of ¹²C₂H₂ by laser photoacoustic spectroscopy and Fourier transform spectroscopy, *Mol. Phys.* 101 (2003) 3427–3438. doi:10.1080/00268970310001632426.
- [182] M. Lepere, G. Blanquet, J. Walrand, J.-P. Bouanich, M. Herman, J. V. Auwera, Self-broadening coefficients and absolute line intensities in the $\nu_4 + \nu_5$ band of acetylene, *J. Mol. Spectrosc.* 242 (2007) 25–30. doi:10.1016/j.jms.2007.01.004.
- [183] O. M. Lyulin, D. Jacquemart, N. Lacombe, V. I. Perevalov, J. Y. Mandin, Line parameters of acetylene in the 1.9 and 1.7 μm spectral regions, *J. Quant. Spectrosc. Radiat. Transf.* 109 (2008) 1856–1874. doi:10.1016/j.jqsrt.2007.11.016.
- [184] O. M. Lyulin, J. Vander Auwera, A. Campargue, The Fourier transform absorption spectrum of acetylene between 7000 and 7500 cm^{-1} , *J. Quant. Spectrosc. Radiat. Transf.* 160 (2015) 85–93. doi:10.1016/j.jqsrt.2015.03.018.

- [185] J. R. Podolske, M. Loewenstein, P. Varanasi, Diode laser line strength measurements of the $(\nu_4 + \nu_5)^0$ band of $^{12}\text{C}_2\text{H}_2$, *J. Mol. Spectrosc.* 107 (1984) 241 – 249. doi:10.1016/0022-2852(84)90003-1.
- [186] F. Herregodts, D. Hurtmans, J. Vander Auwera, M. Herman, Laser spectroscopy of the $\nu_1+3\nu_3$ absorption band in $^{12}\text{C}_2\text{H}_2$. I. Pressure broadening and absolute line intensity measurements, *J. Chem. Phys.* 111 (1999) 7954–7960. doi:10.1063/1.480129.
- [187] C. P. McRaven, M. J. Cich, G. V. Lopez, T. J. Sears, D. Hurtmans, A. W. Mantz, Frequency comb-referenced measurements of self- and nitrogen-broadening in the $\nu_1 + \nu_3$ band of acetylene, *J. Mol. Spectrosc.* 266 (2011) 43–51. doi:10.1016/j.jms.2011.02.016.
- [188] M. Dhyne, L. Fissiaux, J.-C. Populaire, M. Lepère, Temperature dependence of the N_2 -broadening coefficients of acetylene, *J. Quant. Spectrosc. Radiat. Transf.* 110 (6) (2009) 358 – 366. doi:10.1016/j.jqsrt.2008.12.009.
- [189] P. R. Bunker, P. Jensen, *Molecular Symmetry and Spectroscopy*, 2nd Edition, NRC Research Press, Ottawa, 1998.
- [190] J. M. Brown, J. T. Hougen, K.-P. Huber, J. W. C. Johns, I. Kopp, H. Lefebvre-Brion, A. J. Merer, D. A. Ramsay, J. Rostas, R. N. Zare, The labeling of parity doublet levels in linear molecules, *J. Mol. Spectrosc.* 55 (1975) 500–503. doi:10.1016/0022-2852(75)90291-X.
- [191] M. Herman, J. Lievin, Acetylene- from intensity alternation in spectra to ortho and para molecules, *J. Chem. Educ.* 59 (1982) 17. doi:10.1021/ed059p17.
- [192] J. Plíva, Spectrum of acetylene in the 5-micron region, *J. Mol. Spectrosc.* 44 (1972) 145 – 164. doi:10.1016/0022-2852(72)90198-1.

- [193] M. Winnewisser, B. P. Winnewisser, Millimeter wave rotational spectrum of HCNO in vibrationally excited states, *J. Mol. Spectrosc.* 41 (1) (1972) 143 – 176. doi:10.1016/0022-2852(72)90129-4.
- [194] A. Miani, J. Tennyson, Can ortho-para transitions for water be observed?, *J. Chem. Phys.* 120 (2004) 2732–2739. doi:10.1063/1.1633261.
- [195] B. Amyay, A. Fayt, M. Herman, Accurate partition function for acetylene, $^{12}\text{C}_2\text{H}_2$, and related thermodynamical quantities, *J. Chem. Phys.* 135 (2011) 234305. doi:10.1063/1.3664626.
- [196] R. R. Gamache, C. Roller, E. Lopes, I. E. Gordon, L. S. Rothman, O. L. Polyansky, N. F. Zobov, A. A. Kyuberis, J. Tennyson, S. N. Yurchenko, A. G. Császár, T. Furtenbacher, X. Huang, D. W. Schwenke, T. J. Lee, B. J. Drouin, S. A. Tashkun, V. I. Perevalov, R. V. Kochanov, Total internal partition sums for 166 isotopologues of 51 molecules important in planetary atmospheres: Application to HITRAN2016 and beyond, *J. Quant. Spectrosc. Radiat. Transf.* 203 (2017) 70–87. doi:10.1016/j.jqsrt.2017.03.045.
- [197] R. R. Gamache, S. Kennedy, R. Hawkins, L. S. Rothman, Total internal partition sums for molecules in the terrestrial atmosphere, *J. Mol. Spectrosc.* 517 (2000) 407–425. doi:10.1016/S0022-2860(99)00266-5.
- [198] A. Goldman, R. R. Gamache, A. Perrin, J.-M. Flaud, C. P. Rinsland, L. S. Rothman, HITRAN partition functions and weighted transition-moments squared, *J. Quant. Spectrosc. Radiat. Transf.* 66 (2000) 455–486. doi:10.1016/S0022-4073(99)00176-4.
- [199] R. R. Gamache, R. L. Hawkins, L. S. Rothman, Total internal partition sums in the temperature range 70-3000 K: Atmospheric linear molecules, *J. Mol. Spectrosc.* 142 (1990) 205–219. doi:10.1016/0022-2852(90)90178-S.

- [200] S. N. Yurchenko, A. Yachmenev, R. I. Ovsyannikov, Symmetry-adapted ro-vibrational basis functions for variational nuclear motion calculations: Trove approach, *J. Chem. Theory Comput.* 13 (2017) 4368–4381. doi:10.1021/acs.jctc.7b00506.
- [201] J. Laane, E. J. Ocola, Applications of symmetry and group theory for the investigation of molecular vibrations, *Acta Applicandae Mathematicae* 118 (1) (2012) 3–24. doi:10.1007/s10440-012-9675-5.
- [202] S. Fritzsche, Application of point-group symmetries in chemistry and physics: A computer-algebraic approach, *International Journal of Quantum Chemistry* 106 (1) (2005) 98–129. doi:10.1002/qua.20773.
- [203] M. Häser, Molecular point-group symmetry in electronic structure calculations, *The Journal of Chemical Physics* 95 (11) (1991) 8259–8265. doi:10.1063/1.461305.
- [204] C. Chen, Symmetry adapted analysis of linear molecules, *Journal of the Chinese Chemical Society* 20 (4) (1973) 191–202. doi:10.1002/jccs.197300021.
- [205] F. Hegelund, F. Rasmussen, S. Brodersen, The selection rules and the transition moment for rotation–vibrational transitions in axial molecules, *Journal of Raman Spectroscopy* 1 (5) (1973) 433–453. doi:10.1002/jrs.1250010503.
- [206] Papoušek, D. and Aliev, M.R., *Molecular Vibrational-rotational Spectra: Theory and Applications of High Resolution Infrared*, Studies in Physical and Theoretical Chemistry, Elsevier, 1982.
- [207] T. Hirano, U. Nagashima, P. Jensen, Bending wavefunctions for linear molecules, *J. Mol. Spectrosc.* 343 (2018) 54 – 61, spectroscopy of Large Amplitude Vibrational Motion, on the Occasion of Jon Hougen’s 80th Birthday - Part II. doi:10.1016/j.jms.2017.06.012.

- [208] H. Longuet-Higgins, The symmetry groups of non-rigid molecules, *Molecular Physics* 6 (5) (1963) 445–460. doi:10.1080/00268976300100501.
- [209] P. Bunker, D. Papoušek, The symmetry groups of linear molecules, *J. Mol. Spectrosc.* 32 (3) (1969) 419 – 429. doi:10.1016/0022-2852(69)90007-1.
- [210] O. M. Lyulin, V. I. Perevalov, Global modeling of vibration-rotation spectra of the acetylene molecule, *J. Quant. Spectrosc. Radiat. Transf.* 177 (2016) 59–74. doi:10.1016/j.jqsrt.2015.12.021.
- [211] T. Furtenbacher, A. G. Császár, J. Tennyson, MARVEL: measured active rotational-vibrational energy levels, *J. Mol. Spectrosc.* 245 (2007) 115–125. doi:10.1016/j.jms.2007.07.005.
- [212] T. Furtenbacher, A. G. Császár, The role of intensities in determining characteristics of spectroscopic networks, *J. Molec. Struct. (THEOCHEM)* 1009 (2012) 123 – 129. doi:10.1016/j.molstruc.2011.10.057.
- [213] A. G. Császár, T. Furtenbacher, Spectroscopic networks, *J. Mol. Spectrosc.* 266 (2011) 99 – 103. doi:10.1016/j.jms.2011.03.031.
- [214] P. Árendás, T. Furtenbacher, A. G. Császár, On spectra of spectra, *J. Math. Chem.* 54 (2016) 806–822. doi:10.1007/s10910-016-0591-1.
- [215] J.-M. Flaud, C. Camy-Peyret, J. Maillard, Higher ro-vibrational levels of H₂O deduced from high resolution oxygen-hydrogen flame spectra between 2800–6200 cm⁻¹, *Mol. Phys.* 32 (1976) 499–521. doi:10.1080/00268977600103251.
- [216] J. K. G. Watson, Robust weighting in least-square fits, *J. Mol. Spectrosc.* 219 (2003) 326–328. doi:10.1016/S0022-2852(03)00100-0.

- [217] J. K. G. Watson, The use of term-value fits in testing spectroscopic assignments, *J. Mol. Spectrosc.* 165 (1994) 283 – 290. doi:10.1006/jmsp.1994.1130.
- [218] T. Furtenbacher, I. Szabó, A. G. Császár, P. F. Bernath, S. N. Yurchenko, J. Tennyson, Experimental energy levels and partition function of the $^{12}\text{C}_2$ molecule, *Astrophys. J. Suppl.* 224 (2016) 44. doi:10.3847/0067-0049/224/2/44.
- [219] L. K. McKemmish, T. Masseron, S. Sheppard, E. Sandeman, Z. Schofield, T. Furtenbacher, A. G. Császár, J. Tennyson, C. Sousa-Silva, MARVEL analysis of the measured high-resolution spectra of $^{48}\text{Ti}^{16}\text{O}$, *Astrophys. J. Suppl.* 228 (2017) 15. doi:10.3847/1538-4365/228/2/15.
- [220] J. Tennyson, P. F. Bernath, L. R. Brown, A. Campargue, M. R. Carleer, A. G. Császár, R. R. Gamache, J. T. Hodges, A. Jenouvrier, O. V. Naumenko, O. L. Polyansky, L. S. Rothman, R. A. Toth, A. C. Vandaele, N. F. Zobov, L. Daumont, A. Z. Fazliev, T. Furtenbacher, I. E. Gordon, S. N. Mikhailenko, S. V. Shirin, IUPAC critical Evaluation of the Rotational-Vibrational Spectra of Water Vapor. Part I. Energy Levels and Transition Wavenumbers for H_2^{17}O and H_2^{18}O , *J. Quant. Spectrosc. Radiat. Transf.* 110 (2009) 573–596. doi:10.1016/j.jqsrt.2009.02.014.
- [221] J. Tennyson, P. F. Bernath, L. R. Brown, A. Campargue, M. R. Carleer, A. G. Császár, L. Daumont, R. R. Gamache, J. T. Hodges, O. V. Naumenko, O. L. Polyansky, L. S. Rothman, R. A. Toth, A. C. Vandaele, N. F. Zobov, A. Z. Fazliev, T. Furtenbacher, I. E. Gordon, S. N. Mikhailenko, B. A. Voronin, IUPAC critical Evaluation of the Rotational-Vibrational Spectra of Water Vapor. Part II. Energy Levels and Transition Wavenumbers for HD^{16}O , HD^{17}O , and HD^{18}O , *J. Quant. Spectrosc. Radiat. Transf.* 111 (2010) 2160–2184. doi:10.1016/j.jqsrt.2010.06.012.

- [222] J. Tennyson, P. F. Bernath, L. R. Brown, A. Campargue, M. R. Carleer, A. G. Császár, L. Daumont, R. R. Gamache, J. T. Hodges, O. V. Naumenko, O. L. Polyansky, L. S. Rothman, A. C. Vandaele, N. F. Zobov, A. R. Al Derzi, C. Fábri, A. Z. Fazliev, T. Furtenbacher, I. E. Gordon, L. Lodi, I. I. Mizus, IUPAC critical evaluation of the rotational-vibrational spectra of water vapor. Part III. Energy levels and transition wavenumbers for H_2^{16}O , *J. Quant. Spectrosc. Radiat. Transf.* 117 (2013) 29–80. doi:10.1016/j.jqsrt.2012.10.002.
- [223] J. Tennyson, P. F. Bernath, L. R. Brown, A. Campargue, A. G. Császár, L. Daumont, R. R. Gamache, J. T. Hodges, O. V. Naumenko, O. L. Polyansky, L. S. Rothman, A. C. Vandaele, N. F. Zobov, N. Dénes, A. Z. Fazliev, T. Furtenbacher, I. E. Gordon, S.-M. Hu, T. Szidarovszky, I. A. Vasilenko, IUPAC critical evaluation of the rotational-vibrational spectra of water vapor. Part IV. Energy levels and transition wavenumbers for D_2^{16}O , D_2^{17}O and D_2^{18}O , *J. Quant. Spectrosc. Radiat. Transf.* 142 (2014) 93–108. doi:10.1016/j.jqsrt.2014.03.019.
- [224] T. Furtenbacher, J. Tennyson, O. V. Naumenko, O. L. Polyansky, N. F. Zobov, A. G. Császár, The 2018 Update of the IUPAC Database of Water Energy Levels, *J. Quant. Spectrosc. Radiat. Transf.*(In preparation).
- [225] T. Furtenbacher, T. Szidarovszky, E. Mátyus, C. Fábri, A. G. Császár, Analysis of the Rotational–Vibrational States of the Molecular Ion H_3^+ , *J. Chem. Theory Comput.* 9 (2013) 5471–5478. doi:10.1021/ct4004355.
- [226] T. Furtenbacher, T. Szidarovszky, C. Fábri, A. G. Császár, MARVEL analysis of the rotational–vibrational states of the molecular ions H_2D^+ and D_2H^+ , *Phys. Chem. Chem. Phys.* 15 (2013) 10181–10193. doi:10.1039/c3cp44610g.
- [227] A. R. Al Derzi, T. Furtenbacher, S. N. Yurchenko, J. Tennyson, A. G. Császár, MARVEL analysis of the measured high-resolution spectra of

- $^{14}\text{NH}_3$, *J. Quant. Spectrosc. Radiat. Transf.* 161 (2015) 117–130. doi:10.1016/j.jqsrt.2015.03.034.
- [228] T. Furtenbacher, P. A. Coles, J. Tennyson, A. G. Császár, Updated MARVEL energy levels for ammonia, *J. Quant. Spectrosc. Radiat. Transf.* To be submitted.
- [229] C. Fábri, E. Mátyus, T. Furtenbacher, L. Nemes, B. Mihály, T. Zoltáni, A. G. Császár, Variational quantum mechanical and active database approaches to the rotational-vibrational spectroscopy of ketene, H_2CCO , *J. Chem. Phys.* 135 (2011) 094307. doi:10.1063/1.3625404.
- [230] J. Tennyson, P. F. Bernath, L. R. Brown, A. Campargue, A. G. Császár, L. Daumont, R. R. Gamache, J. T. Hodges, O. V. Naumenko, O. L. Polyansky, L. S. Rothman, A. C. Vandaele, N. F. Zobov, A Database of Water Transitions from Experiment and Theory (IUPAC Technical Report), *Pure Appl. Chem.* 86 (2014) 71–83. doi:10.1515/pac-2014-5012.
- [231] S. Yu, B. J. Drouin, J. C. Pearson, Terahertz Spectroscopy of the Bending Vibrations of Acetylene $^{12}\text{C}_2\text{H}_2$, *Astrophys. J.* 705 (2009) 786–790. doi:10.1088/0004-637X/705/1/786.
- [232] Y. Kabbadj, M. Herman, G. Dilonardo, L. Fusina, J. W. C. Johns, The bending energy-levels of C_2H_2 , *J. Mol. Spectrosc.* 150 (1991) 535–565. doi:10.1016/0022-2852(91)90248-9.
- [233] B. Amyay, M. Herman, A. Fayt, L. Fusina, A. Predoi-Cross, High resolution FTIR investigation of $^{12}\text{C}_2\text{H}_2$ in the FIR spectral range using synchrotron radiation, *Chem. Phys. Lett.* 491 (2010) 17–19. doi:10.1016/j.cplett.2010.03.053.
- [234] B. J. Drouin, S. Yu, Acetylene spectra near 2.6 THz, *J. Mol. Spectrosc.* 269 (2011) 254–256. doi:10.1016/j.jms.2011.06.004.

- [235] D. Jacquemart, O. M. Lyulin, V. I. Perevalov, Recommended acetylene line list in the 20 – 240 cm^{-1} and 400 – 630 cm^{-1} regions: new measurements and global modeling, *J. Quant. Spectrosc. Radiat. Transf.* 203 (2017) 440 – 453. doi:10.1016/j.jqsrt.2017.03.008.
- [236] J. Hietanen, J. Kauppinen, High-resolution infrared-spectrum of acetylene in the region of the bending fundamental ν_5 , *Mol. Phys.* 42 (1981) 411–423. doi:10.1080/00268978100100351.
- [237] M. Weber, W. E. Blass, S. Nadler, G. W. Halsey, W. C. Maguire, J. J. Hillman, Resonance effects in C_2H_2 near 13.7 μm . Part H: The two quantum hotbands, *Spectra Chimica Acta A* 49 (1993) 1659 – 1681. doi:10.1016/0584-8539(93)80124-S.
- [238] J. Y. Mandin, V. Dana, C. Claveau, Line intensities in the ν_5 band of acetylene $^{12}\text{C}_2\text{H}_2$, *J. Quant. Spectrosc. Radiat. Transf.* 67 (2000) 429–446. doi:10.1016/S0022-4073(00)00010-8.
- [239] D. Jacquemart, C. Claveau, J. Y. Mandin, V. Dana, Line intensities of hot bands in the 13.6 μm spectral region of acetylene $^{12}\text{C}_2\text{H}_2$, *J. Quant. Spectrosc. Radiat. Transf.* 69 (2001) 81–101. doi:10.1016/S0022-4073(00)00063-7.
- [240] E. E. Bell, H. H. Nielsen, The infra-red spectrum of Acetylene, *J. Chem. Phys.* 18 (1950) 1382–1394. doi:10.1063/1.1747483.
- [241] L. Gomez, D. Jacquemart, N. Lacome, J.-Y. Mandin, New line intensity measurements for $^{12}\text{C}_2\text{H}_2$ around 7.7 μm and HITRAN format line list for applications, *J. Quant. Spectrosc. Radiat. Transf.* 111 (2010) 2256–2264. doi:10.1016/j.jqsrt.2010.01.031.
- [242] L. Gomez, D. Jacquemart, N. Lacome, J. Y. Mandin, Line intensities of $^{12}\text{C}_2\text{H}_2$ in the 7.7 μm spectral region, *J. Quant. Spectrosc. Radiat. Transf.* 110 (2009) 2102–2114. doi:10.1016/j.jqsrt.2009.05.018.

- [243] J. Vander Auwera, Absolute intensities measurements in the $\nu_4 + \nu_5$ band of $^{12}\text{C}_2\text{H}_2$: Analysis of Herman-Wallis effects and forbidden transitions, *J. Mol. Spectrosc.* 201 (2000) 143–150. doi:10.1006/jmsp.2000.8079.
- [244] D. Jacquemart, J. Y. Mandin, V. Dana, C. Claveau, J. Vander Auwera, A. Herman, L. S. Rothman, L. Regalia-Jarlot, A. Barbe, The IR acetylene spectrum in HITRAN: update and new results, *J. Quant. Spectrosc. Radiat. Transf.* 82 (2003) 363–382. doi:10.1016/S0022-4073(03)00163-8.
- [245] D. Bermejo, P. Cancio, G. Di Lonardo, L. Fusina, High resolution Raman spectroscopy from vibrationally excited states populated by a stimulated Raman process: $2\nu_2 - \nu_2$ of $^{12}\text{C}_2\text{H}_2$ and $^{13}\text{C}_2\text{H}_2$, *J. Chem. Phys.* 108 (1998) 7224–7228. doi:10.1063/1.476140.
- [246] D. Jacquemart, N. Lacome, J. Y. Mandin, V. Dana, O. M. Lyulin, V. I. Perevalov, Multispectrum fitting of line parameters for $^{12}\text{C}_2\text{H}_2$ in the 3.8- μm spectral region, *J. Quant. Spectrosc. Radiat. Transf.* 103 (2007) 478–495. doi:10.1016/j.jqsrt.2006.06.008.
- [247] K. F. Palmer, M. E. Mickelson, K. Narahari Rao, Investigations of several infrared bands of $^{12}\text{C}_2\text{H}_2$ and studies of the effects of vibrational rotational interactions, *J. Mol. Spectrosc.* 44 (1972) 131–144. doi:10.1016/0022-2852(72)90197-X.
- [248] J. Vander Auwera, D. Hurtmans, M. Carleer, M. Herman, The ν_3 Fundamental in C_2H_2 , *J. Mol. Spectrosc.* 157 (1993) 337 – 357. doi:10.1006/jmsp.1993.1027.
- [249] R. Dcunha, Y. A. Sarma, V. A. Job, G. Guelachvili, K. N. Rao, Fermi Coupling and ℓ -Type Resonance Effects in the Hot Bands of Acetylene: The 2650- cm^{-1} Region, *J. Mol. Spectrosc.* 157 (1993) 358 – 368. doi:10.1006/jmsp.1993.1028.

- [250] Y. A. Sarma, R. Dcunha, G. Guelachvili, R. Farrenq, V. M. Devi, D. C. Benner, K. N. Rao, Stretch-bend levels of acetylene - analysis of the hot bands in the 3300 cm^{-1} region, *J. Mol. Spectrosc.* 173 (1995) 574–584. doi:10.1006/jmsp.1995.1258.
- [251] O. M. Lyulin, V. I. Perevalov, J. Y. Mandin, V. Dana, D. Jacquemart, L. Regalia-Jarlot, A. Barbe, Line intensities of acetylene in the $3\text{-}\mu\text{m}$ region: New measurements of weak hot bands and global fitting, *J. Quant. Spectrosc. Radiat. Transf.* 97 (2006) 81–98. doi:10.1016/j.jqsrt.2004.12.022.
- [252] J. Y. Mandin, D. Jacquemart, V. Dana, L. Regalia-Jarlot, A. Barbe, Line intensities of acetylene at $3\text{ }\mu\text{m}$, *J. Quant. Spectrosc. Radiat. Transf.* 92 (2005) 239–260. doi:10.1016/j.jqsrt.2004.07.024.
- [253] Y. A. Sarma, R. Dcunha, G. Guelachvili, R. Farrenq, K. N. Rao, Stretch-bend levels of acetylene - analysis of the hot bands in the 3800 cm^{-1} region, *J. Mol. Spectrosc.* 173 (1995) 561–573. doi:10.1006/jmsp.1995.1257.
- [254] D. Bermejo, R. Z. Martinez, G. Di Lonardo, L. Fusina, High resolution Raman spectroscopy from vibrationally excited states populated by a stimulated Raman process. Transitions from $\nu_2 = 1$ in $^{12}\text{C}_2\text{H}_2$ and $^{13}\text{C}_2\text{H}_2$, *J. Chem. Phys.* 111 (1999) 519–524. doi:10.1063/1.479331.
- [255] O. M. Lyulin, V. I. Perevalov, J. Y. Mandin, V. Dana, F. Gu-eye, X. Thomas, P. Von der Heyden, D. Decatoire, L. Regalia-Jarlot, D. Jacquemart, N. Lacome, Line intensities of acetylene: Measurements in the $2.5\text{-}\mu\text{m}$ spectral region and global modeling in the $\Delta p = 4$ and 6 series, *J. Quant. Spectrosc. Radiat. Transf.* 103 (2007) 496–523. doi:10.1016/j.jqsrt.2006.07.002.
- [256] V. Girard, R. Farrenq, E. Sorokin, I. T. Sorokina, G. Guelachvili, N. Picque, Acetylene weak bands at $2.5\text{ }\mu\text{m}$ from intracavity Cr^{2+} :

- ZnSe laser absorption observed with time-resolved Fourier transform spectroscopy, *Chem. Phys. Lett.* 419 (2006) 584–588. doi:10.1016/j.cplett.2005.12.029.
- [257] R. Dcuhna, Y. A. Sarma, G. Guelachvili, R. Farrenq, Q. L. Kou, V. M. Devi, D. C. Benner, K. N. Rao, Analysis of the high-resolution spectrum of acetylene in the 2.4 μm region, *J. Mol. Spectrosc.* 148 (1991) 213–225. doi:10.1016/0022-2852(91)90048-F.
- [258] A. Baldacci, S. Gherseti, K. N. Rao, Assignments of the $^{12}\text{C}_2\text{H}_2$ bands at 2.1 – 2.2 μm , *J. Mol. Spectrosc.* 41 (1972) 222 – 225. doi:10.1016/0022-2852(72)90134-8.
- [259] O. M. Lyulin, V. I. Perevalov, F. Gueye, J. Y. Mandin, V. Dana, X. Thomas, P. Von der Heyden, L. Regalia-Jarlot, A. Barbe, Line positions and intensities of acetylene in the 2.2- μm region, *J. Quant. Spectrosc. Radiat. Transf.* 104 (2007) 133–154. doi:10.1016/j.jqsrt.2006.08.018.
- [260] K. A. Keppler, G. C. Mellau, S. Klee, B. P. Winnewisser, M. Winnewisser, J. Pliva, K. N. Rao, Precision measurements of acetylene spectra at 1.4 – 1.7 μm recorded with 352.5-m pathlength, *J. Mol. Spectrosc.* 175 (1996) 411–420. doi:10.1006/jmsp.1996.0047.
- [261] S. Robert, M. Herman, A. Fayt, A. Campargue, S. Kassi, A. Liu, L. Wang, G. Di Lonardo, L. Fusina, Acetylene, $^{12}\text{C}_2\text{H}_2$: new CRDS data and global vibration-rotation analysis up to 8600 cm^{-1} , *Mol. Phys.* 106 (2008) 2581–2605. doi:10.1080/00268970802620709.
- [262] H. Tran, J. Y. Mandin, V. Dana, L. Regalia-Jarlot, X. Thomas, P. Von der Heyden, Line intensities in the 1.5- μm spectral region of acetylene, *J. Quant. Spectrosc. Radiat. Transf.* 108 (2007) 342–362. doi:10.1016/j.jqsrt.2007.04.008.

- [263] O. M. Lyulin, V. I. Perevalov, H. Tran, J. Y. Mandin, V. Dana, L. Regalia-Jarlot, X. Thomas, D. Decatoire, Line intensities of acetylene: New measurements in the 1.5- μm spectral region and global modelling in the $\Delta P = 10$ series, *J. Quant. Spectrosc. Radiat. Transf.* 110 (2009) 1815–1824. doi:10.1016/j.jqsrt.2009.04.012.
- [264] J. Karhu, J. Nauta, M. Vainio, M. Metsälä, S. Hoekstra, L. Halonen, Double resonant absorption measurement of acetylene symmetric vibrational states probed with cavity ring down spectroscopy, *J. Chem. Phys.* 144 (2016) 244201. doi:10.1063/1.4954159.
- [265] Q. Kou, G. Guelachvili, M. A. Tamsamani, M. Herman, The absorption spectrum of C_2H_2 around $\nu_1 + \nu_3$ - energy standards in the 1.5 μm region and vibrational clustering, *Can. J. Phys.* 72 (1994) 1241–1250. doi:10.1139/p94-160.
- [266] S. Twagirayezu, M. J. Cich, T. J. Sears, C. P. McRaven, G. E. Hall, Frequency-comb referenced spectroscopy of ν_4 - and ν_5 -excited hot bands in the 1.5 μm spectrum of C_2H_2 , *J. Mol. Spectrosc.* 316 (2015) 64–71. doi:10.1016/j.jms.2015.06.010.
- [267] R. El Hachtouki, J. Vander Auwera, Absolute line intensities in acetylene: The 1.5- μm region, *J. Mol. Spectrosc.* 216 (2002) 355–362. doi:10.1006/jmsp.2002.8660.
- [268] A. Baldacci, S. Gheretti, K. N. Rao, Interpretation of the acetylene spectrum at 1.5 μm , *J. Mol. Spectrosc.* 68 (1977) 183–194. doi:10.1016/0022-2852(77)90436-2.
- [269] C. S. Edwards, G. P. Barwood, H. S. Margolis, P. Gill, W. R. C. Rowley, High-precision frequency measurements of the $\nu_1 + \nu_3$ combination band of $^{12}\text{C}_2\text{H}_2$ in the 1.5 μm region, *J. Mol. Spectrosc.* 234 (2005) 143–148. doi:10.1016/j.jms.2005.08.014.

- [270] A. M. Zolot, F. R. Giorgetta, E. Baumann, W. C. Swann, I. Coddington, N. R. Newbury, Broad-band frequency references in the near-infrared: Accurate dual comb spectroscopy of methane and acetylene, *J. Quant. Spectrosc. Radiat. Transf.* 118 (2013) 26–39. doi:10.1016/j.jqsrt.2012.11.024.
- [271] D. B. Moss, Z. C. Duan, M. P. Jacobson, J. P. O'Brien, R. W. Field, Observation of coriolis coupling between $\nu_2 + 4\nu_4$ and $7\nu_4$ in acetylene $^1\Sigma_g^+$ by stimulated emission pumping spectroscopy, *J. Mol. Spectrosc.* 199 (2000) 265–274. doi:10.1006/jmbsp.1999.7994.
- [272] K. Nakagawa, M. deLabachellerie, Y. Awaaji, M. Kouroggi, Accurate optical frequency atlas of the 1.5- μm bands of acetylene, *J. Opt. Soc. Am. B* 13 (1996) 2708–2714. doi:10.1364/JOSAB.13.002708.
- [273] B. Amyay, M. Herman, A. Fayt, A. Campargue, S. Kassi, Acetylene, ($^{12}\text{C}_2\text{H}_2$): Refined analysis of CRDS spectra around 1.52 μm , *J. Mol. Spectrosc.* 267 (2011) 80–91. doi:10.1016/j.jms.2011.02.015.
- [274] D. Jacquemart, N. Lacome, J. Y. Mandin, V. Dana, H. Tran, F. K. Gueye, O. M. Lyulin, V. I. Perevalov, L. Regalia-Jarlot, The IR spectrum of $^{12}\text{C}_2\text{H}_2$: Line intensity measurements in the 1.4 μm region and update of the databases, *J. Quant. Spectrosc. Radiat. Transf.* 110 (2009) 717–732. doi:10.1016/j.jqsrt.2008.10.002.
- [275] J. Vander Auwera, R. El Hachtouki, L. R. Brown, Absolute line wavenumbers in the near infrared: $^{12}\text{C}_2\text{H}_2$ and $^{12}\text{C}^{16}\text{O}_2$, *Mol. Phys.* 100 (2002) 3563–3576. doi:10.1080/00268970210162880.
- [276] O. M. Lyulin, J. Vander Auwera, A. Campargue, The Fourier transform absorption spectrum of acetylene between 8280 and 8700 cm^{-1} , *J. Quant. Spectrosc. Radiat. Transf.* 177 (2016) 234–240. doi:10.1016/j.jqsrt.2015.11.026.

- [277] S. Béguier, O. M. Lyulin, S.-M. Hu, A. Campargue, Line intensity measurements for acetylene between 8980 and 9420 cm^{-1} , *J. Quant. Spectrosc. Radiat. Transf.* 189 (2017) 417–420. doi:10.1016/j.jqsrt.2016.12.020.
- [278] M. Herman, T. R. Huet, M. Vervloet, Spectroscopy and vibrational couplings in the $3\nu_3$ region of acetylene, *Mol. Phys.* 66 (1989) 333–353. doi:10.1080/00268978900100161.
- [279] J. Sakai, M. Katayama, Diode laser spectroscopy of acetylene: The $2\nu_1 + 2\nu_3 + \nu_4 - \nu_5$ and $4\nu_1 - \nu_5$ interacting band system, *J. Mol. Spectrosc.* 157 (1993) 532 – 535. doi:10.1006/jmsp.1993.1042.
- [280] J. Sakai, M. Katayama, Diode laser spectroscopy of acetylene: $3\nu_1 + \nu_3$ region at 0.77 μm , *J. Mol. Spectrosc.* 154 (1992) 277 – 287. doi:10.1016/0022-2852(92)90208-6.
- [281] J. Sakai, H. Segawa, M. Katayama, Diode laser spectroscopy of the $2\nu_1 + 2\nu_2 + \nu_3$ band of acetylene, *J. Mol. Spectrosc.* 164 (1994) 580 – 582. doi:10.1006/jmsp.1994.1101.
- [282] M. A. Tamsamani, M. Herman, S. A. B. Solina, J. P. O'Brien, R. W. Field, Highly vibrationally excited $^{12}\text{C}_2\text{H}_2$ in the X $^1\Sigma_g^+$ state: Complementarity of absorption and dispersed fluorescence spectra, *J. Chem. Phys.* 105 (1996) 11357–11359. doi:10.1063/1.472995.
- [283] M. I. El Idrissi, J. Lievin, A. Campargue, M. Herman, The vibrational energy pattern in acetylene (IV): Updated global vibration constants for $^{12}\text{C}_2\text{H}_2$, *J. Chem. Phys.* 110 (1999) 2074–2086. doi:10.1063/1.477817.
- [284] J. Plíva, Molecular constants for the bending modes of acetylene $^{12}\text{C}_2\text{H}_2$, *J. Mol. Spectrosc.* 44 (1972) 165 – 182. doi:10.1016/0022-2852(72)90199-3.

- [285] M. Metsälä, S. Yang, O. Vaaitinen, L. Halonen, Laser-induced dispersed vibration-rotation fluorescence of acetylene: Spectra of ortho and para forms and partial trapping of vibrational energy, *J. Chem. Phys.* 117 (2002) 8686–8693. doi:10.1063/1.1513464.
- [286] M. Metsälä, S. F. Yang, A. Vaaitinen, D. Permogorov, L. Halonen, High-resolution cavity ring-down study of acetylene between 12260 and 12380 cm^{-1} , *Chem. Phys. Lett.* 346 (2001) 373–378. doi:10.1016/S0009-2614(01)00945-9.
- [287] M. Saarinen, D. Permogorov, L. Halonen, Collision-induced vibration-rotation fluorescence spectra and rovibrational symmetry changes in acetylene, *J. Chem. Phys.* 110 (1999) 1424–1428. doi:10.1063/1.478017.
- [288] P. Jungner, L. Halonen, Laser induced vibration-rotation fluorescence and infrared forbidden transitions in acetylene, *J. Chem. Phys.* 107 (1997) 1680–1682. doi:10.1063/1.474521.
- [289] X. W. Zhan, L. Halonen, High-resolution photoacoustic study of the $\nu_1 + 3\nu_3$ band system of acetylene with a titanium-sapphire ring laser, *J. Mol. Spectrosc.* 160 (1993) 464–470. doi:10.1006/jmsp.1993.1193.
- [290] X. W. Zhan, O. Vaaitinen, L. Halonen, High-resolution photoacoustic study of acetylene between 11500 and 11900 cm^{-1} using a titanium-sapphire ring laser, *J. Mol. Spectrosc.* 160 (1993) 172–180. doi:10.1006/jmsp.1993.1165.
- [291] X.-W. Zhan, O. Vaaitinen, E. Kauppi, L. Halonen, High-resolution photoacoustic overtone spectrum of acetylene near 570 nm using a ring-dye-laser spectrometer, *Chem. Phys. Lett.* 180 (1991) 310 – 316. doi:10.1016/0009-2614(91)90325-4.
- [292] M. Siltanen, M. Metsälä, M. Vainio, L. Halonen, Experimental observation and analysis of the $3\nu_1$ stretching vibrational state of acetylene

- using continuous-wave infrared stimulated emission, *J. Chem. Phys.* 139 (2013) 054201. doi:10.1063/1.4816524.
- [293] G. J. Scherer, K. K. Lehmann, W. Klemperer, The high resolution visible overtone spectrum of acetylene, *J. Chem. Phys.* 78 (1983) 2817–2832. doi:10.1063/1.445269.
- [294] O. M. Lyulin, A. Campargue, D. Mondelain, S. Kassı, The absorption spectrum of acetylene by CRDS between 7244 and 7918 cm^{-1} , *J. Quant. Spectrosc. Radiat. Transf.* 130 (2013) 327–334. doi:10.1016/j.jqsrt.2013.04.028.
- [295] O. M. Lyulin, D. Mondelain, S. Béguier, S. Kassı, J. Vander Auwera, A. Campargue, High-sensitivity CRDS absorption spectroscopy of acetylene between 5851 and 6341 cm^{-1} , *Mol. Phys.* 112 (2014) 2433–2444. doi:10.1080/00268976.2014.906677.
- [296] S. Kassı, O. M. Lyulin, S. Béguier, A. Campargue, New assignments and a rare peculiarity in the high sensitivity CRDS spectrum of acetylene near 8000 cm^{-1} , *J. Mol. Spectrosc.* 326 (2016) 106–114. doi:10.1016/j.jms.2016.02.013.
- [297] L. S. Rothman, I. E. Gordon, A. Barbe, D. C. Benner, P. F. Bernath, M. Birk, V. Boudon, L. R. Brown, A. Campargue, J. P. Champion, K. Chance, L. H. Coudert, V. Dana, V. M. Devi, S. Fally, J. M. Flaud, R. R. Gamache, A. Goldman, D. Jacquemart, I. Kleiner, N. Lacome, W. J. Lafferty, J. Y. Mandin, S. T. Massie, S. N. Mikhailenko, C. E. Miller, N. Moazzen-Ahmadi, O. V. Naumenko, A. V. Nikitin, J. Orphal, V. I. Perevalov, A. Perrin, A. Predoi-Cross, C. P. Rinsland, M. Rotger, M. Simeckova, M. A. H. Smith, K. Sung, S. A. Tashkun, J. Tennyson, R. A. Toth, A. C. Vandaele, J. Vander Auwera, The HITRAN 2008 molecular spectroscopic database, *J. Quant. Spectrosc. Radiat. Transf.* 110 (2009) 553–572. doi:10.1016/j.jqsrt.2009.02.013.

- [298] L. S. Rothman, I. E. Gordon, Y. Babikov, A. Barbe, D. C. Benner, P. F. Bernath, M. Birk, L. Bizzocchi, V. Boudon, L. R. Brown, A. Campargue, K. Chance, E. A. Cohen, L. H. Coudert, V. M. Devi, B. J. Drouin, A. Fayt, J.-M. Flaud, R. R. Gamache, J. J. Harrison, J.-M. Hartmann, C. Hill, J. T. Hodges, D. Jacquemart, A. Jolly, J. Lamouroux, R. J. Le Roy, G. Li, D. A. Long, O. M. Lyulin, C. J. Mackie, S. T. Massie, S. Mikhailenko, H. S. P. Müller, O. V. Naumenko, A. V. Nikitin, J. Orphal, V. Perevalov, A. Perrin, E. R. Polovtseva, C. Richard, M. A. H. Smith, E. Starikova, K. Sung, S. Tashkun, J. Tennyson, G. C. Toon, V. G. Tyuterev, G. Wagner, The *HITRAN* 2012 molecular spectroscopic database, *J. Quant. Spectrosc. Radiat. Transf.* 130 (2013) 4 – 50. doi:10.1016/j.jqsrt.2013.07.002.
- [299] M. Bastian, S. Heymann, M. Jacomy, Gephi: an open source software for exploring and manipulating networks., *ICWSM* 8 (2009) 361–362.
- [300] L.-G. Tao, T.-P. Hua, Y. R. Sun, J. Wang, A.-W. Liu, S.-M. Hu, Frequency metrology of the acetylene lines near 789 nm from lamb-dip measurements, *J. Quant. Spectrosc. Radiat. Transf.* 210 (2018) 111–115. doi:10.1016/j.jqsrt.2018.02.021.
- [301] A.-W. Liu, X.-F. Li, J. Wang, Y. Lu, C.-F. Cheng, Y. R. Sun, S.-M. Hu, The $4\nu_{CH}$ overtone of $^{12}\text{C}_2\text{H}_2$: Sub-MHz precision spectrum reveals perturbations, *J. Chem. Phys.* 138 (1) (2013) 014312. doi:10.1063/1.4773473.
- [302] O. Lyulin, S. Béguier, S. Hu, A. Campargue, The absorption spectrum of acetylene near $1\ \mu\text{m}$ ($9280 - 10740\ \text{cm}^{-1}$) (I): Line positions, *J. Quant. Spectrosc. Radiat. Transf.* 208 (2018) 179 – 187. doi:10.1016/j.jqsrt.2018.01.007.

- [303] I. N. Kozin, M. M. Law, J. Tennyson, J. M. Hutson, New vibration-rotation code for tetraatomic molecules WAVR4, *Comput. Phys. Commun.* 163 (2004) 117–131. doi:10.1016/j.cpc.2004.07.005.
- [304] S. Carter, N. C. Handy, A variational method for the calculation of vibrational levels of any triatomic molecule, *Mol. Phys.* 47 (1982) 1445–1455. doi:10.1080/00268978200101082.
- [305] M. J. Bramley, W. H. Green, N. C. Handy, Vibration-rotation coordinates and kinetic-energy operators for polyatomic-molecules, *Mol. Phys.* 73 (1991) 1183–1208. doi:10.1080/00268979100101871.
- [306] N. C. Handy, The derivation of vibration-rotation kinetic-energy operators, in internal coordinates, *Mol. Phys.* 61 (1987) 207–223. doi:10.1080/00268978700101081.
- [307] S. Carter, N. C. Handy, The geometry and forcefield of acetylene, *Mol. Phys.* 100 (2002) 681–698. doi:10.1080/00268970110105415.
- [308] J. T. Hougen, P. R. Bunker, J. W. C. Johns, Vibration-rotation problem in triatomic molecules allowing for a large-amplitude bending vibration, *J. Mol. Spectrosc.* 34 (1970) 136–172. doi:10.1016/0022-2852(70)90080-9.
- [309] B. T. Sutcliffe, *Current Aspects of Quantum Chemistry, Studies in Theoretical Chemistry*, ed. by R. Carbò, Vol. 21, Elsevier, Amsterdam, 1981, p. 9.
- [310] L. Halonen, M. S. Child, S. Carter, Potential models and local mode vibrational eigenvalue calculations for acetylene, *Mol. Phys.* 47 (1982) 1097–1112. doi:10.1080/00268978200100802.
- [311] J. Tennyson, B. T. Sutcliffe, Discretisation to avoid singularities in vibration-rotation hamiltonians: a bisector embedding for AB₂ triatomics, *Intern. J. Quantum Chem.* 42 (1992) 941–952.

- [312] B. T. Sutcliffe, J. Tennyson, A general treatment of vibration-rotation coordinates for triatomic molecules, *Intern. J. Quantum Chem.* 39 (1991) 183–196.
- [313] A. B. McCoy, E. L. Sibert, Perturbative calculations of vibrational ($J=0$) energy-levels of linear-molecules in normal coordinate representations, *J. Chem. Phys.* 95 (1991) 3476–3487. doi:10.1063/1.460850.
- [314] S. Carter, N. Handy, A variational method for the determination of the vibrational ($J = 0$) energy levels of acetylene, using a Hamiltonian in internal coordinates, *Computer Physics Communications* 51 (1) (1988) 49 – 58. doi:10.1016/0010-4655(88)90061-6.
- [315] G. Brocks, A. van der Avoird, B. T. Sutcliffe, J. Tennyson, Quantum dynamics of non-rigid systems comprising two polyatomic molecules, *Mol. Phys.* 50 (1983) 1025–1043.
- [316] P. Jensen, The nonrigid bender hamiltonian for calculating the rotation-vibration energy levels of a triatomic molecule, *Comp. Phys. Rep.* 1 (1983) 1 – 55. doi:10.1016/0167-7977(83)90003-5.
- [317] P. Jensen, A new morse oscillator-rigid bender internal dynamics (MOR-BID) hamiltonian for triatomic-molecules, *J. Mol. Spectrosc.* 128 (1988) 478–501. doi:10.1016/0022-2852(88)90164-6.
- [318] I. N. Kozin, M. M. Law, J. Tennyson, Effective computation of matrix elements between polynomial basis functions, *Comput. Phys. Commun.* 165 (2005) 10–14. doi:10.1016/j.cpc.2003.12.007.
- [319] O. L. Polyansky, I. N. Kozin, P. Małyszczek, J. Koput, J. Tennyson, S. N. Yurchenko, Variational calculation of highly excited rovibrational energy levels of H_2O_2 , *J. Phys. Chem. A* 117 (2013) 7367–7377. doi:10.1021/jp401216g.

- [320] M. Rey, A. Nikitin, V. Tyuterev, Ab initio ro-vibrational hamiltonian in irreducible tensor formalism: a method for computing energy levels from potential energy surfaces for symmetric-top molecules, *Mol. Phys.* 108 (16) (2010) 2121–2135. doi:10.1080/00268976.2010.506892.
- [321] H. Romanowski, J. M. Bowman, L. B. Harding, Vibrational energy levels of formaldehyde, *J. Chem. Phys.* 82 (9) (1985) 4155–4165. doi:10.1063/1.448858.
- [322] M. Rey, A. V. Nikitin, V. G. Tyuterev, Complete nuclear motion hamiltonian in the irreducible normal mode tensor operator formalism for the methane molecule, *J. Chem. Phys.* 136 (2012) 244106. doi:10.1063/1.4730030.
- [323] L. Hedberg, I. M. Mills, Harmonic force fields from scaled SCF calculations: Program ASYM40, *J. Mol. Spectrosc.* 203 (1) (2000) 82 – 95. doi:10.1006/jmsp.2000.8168.
- [324] E. Mátyus, G. Czakó, B. T. Sutcliffe, A. G. Császár, Vibrational energy levels with arbitrary potentials using the eckart-watson hamiltonians and the discrete variable representation, *J. Chem. Phys.* 127 (2007) 084102. doi:10.1063/1.2756518.
- [325] J. T. Hougen, Rotational energy levels of a linear triatomic molecule in a 2II electronic state, *J. Chem. Phys.* 36 (1962) 519–&. doi:10.1063/1.1732544.
- [326] E. B. Wilson, J. B. Howard, The vibration-rotation energy levels of polyatomic molecules I. Mathematical theory of semirigid asymmetrical top molecules, *J. Chem. Phys.* 4 (1936) 260–268. doi:10.1063/1.1749833.
- [327] B. T. Darling, D. M. Dennison, The water vapor molecule, *Phys. Rev.* 57 (1940) 128–139. doi:10.1103/PhysRev.57.128.

- [328] B. Podolsky, Quantum-mechanically correct form of Hamiltonian function for conservative systems, *Phys. Rev.* 32 (1928) 0812–0816. doi:10.1103/PhysRev.32.812.
- [329] C. Eckart, Some studies concerning rotating axes and polyatomic molecules, *Phys. Rev.* 47 (1935) 552–558. doi:10.1103/PhysRev.47.552.
- [330] J. K. G. Watson, Vibration-rotation hamiltonian of linear molecules, *Mol. Phys.* 19 (1970) 465–487. doi:10.1080/00268977000101491.
- [331] B. Mant, Private communication.
- [332] A. Owens, E. J. Zak, K. L. Chubb, S. N. Yurchenko, J. Tennyson, A. Yachmenev, Simulating electric-field interactions with polar molecules using spectroscopic databases, *Sci. Rep.* 45068 (2017) 7. doi:10.1038/srep45068.
- [333] P. R. Bunker, P. Jensen, *Molecular Symmetry and Spectroscopy*, Second Edition, NRC Research Press, Ottawa, Canada, 2006.
- [334] G. O. Sørensen, A new approach to the hamiltonian of nonrigid molecules, in: M. J. S. D. et al. (Ed.), *Large Amplitude Motion in Molecules II*, Vol. 82 of *Topics in Current Chemistry*, Springer Berlin, Heidelberg, 1979, pp. 97–175. doi:10.1007/BFb0048009.
- [335] G. Strey, I. M. Mills, Anharmonic-force field of acetylene, *J. Mol. Spectrosc.* 59 (1976) 103–115. doi:10.1016/0022-2852(76)90046-1.
- [336] B. J. Howard, R. E. Moss, The molecular hamiltonian, *Mol. Phys.* 20 (1971) 147–159. doi:10.1080/00268977100100151.
- [337] J. K. G. Watson, Vibration-rotation hamiltonians of linear-molecules, *Mol. Phys.* 79 (1993) 943–951. doi:10.1080/00268979300101741.

- [338] G. Wlodarczak, *Linear Polyatomic Molecules: Introduction*, Springer Berlin Heidelberg, Berlin, Heidelberg, 2012, pp. 6–24. doi:10.1007/978-3-540-44926-3_2.
- [339] B. V. Noumerov, A method of extrapolation of perturbations, *Mon. Not. R. Astron. Soc.* 84 (1924) 592–602. doi:10.1093/mnras/84.8.592.
- [340] J. W. Cooley, An improved eigenvalue corrector formula for solving the Schrödinger equation for central fields, *Math. Comp.* 15 (1961) 363–374. doi:10.1090/S0025-5718-1961-0129566-X.
- [341] P. R. Bunker, P. Jensen, Spherical top molecules and the molecular symmetry group, *Mol. Phys.* 97 (1999) 255–264. doi:10.1080/00268979909482827.
- [342] S. N. Yurchenko, M. Carvajal, P. Jensen, H. Lin, J. J. Zheng, W. Thiel, Rotation-vibration motion of pyramidal XY_3 molecules described in the Eckart frame: Theory and application to NH_3 , *Mol. Phys.* 103 (2005) 359–378. doi:10.1080/002689705412331517255.
- [343] P. Jensen, P. Bunker, The application of the nonrigid bender hamiltonian to a quasilinear molecule, *J. Mol. Spectrosc.* 99 (1983) 348 – 356. doi:10.1016/0022-2852(83)90319-3.
- [344] J. Tennyson, B. T. Sutcliffe, Variationally exact ro-vibrational levels of the floppy CH_2^+ molecule, *J. Mol. Spectrosc.* 101 (1983) 71–82.
- [345] T. Hirano, U. Nagashima, P. Jensen, Computational molecular spectroscopy of $\tilde{X}^2\pi$ NCS: Electronic properties and ro-vibrationally averaged structure, *J. Mol. Spectrosc.* 346 (2017) 4–12. doi:10.1016/j.jms.2017.12.011.
- [346] J. I. Moses, Chemical kinetics on extrasolar planets, *Philosophical Transactions of the Royal Society of London A: Mathematical, Physical and Engineering Sciences* 372 (2014). doi:10.1098/rsta.2013.0073.

- [347] D. W. Clarke, J. P. Ferris, Titan haze: Structure and properties of cyanoacetylene and cyanoacetylene–acetylene photopolymers, *Icarus* 127 (1) (1997) 158 – 172. doi:10.1006/icar.1996.5667.
- [348] R. Trampedach, A modelers' opacity wish list, ArXiv e-prints <http://arxiv.org/abs/1804.04123> arXiv:1804.04123.
- [349] A. N. Heays, A. D. Bosman, E. F. van Dishoeck, Photodissociation and photoionisation of atoms and molecules of astrophysical interest, *Astron. Astrophys.* 602 (2017) A105. doi:10.1051/0004-6361/201628742.
- [350] A. F. Al-Refaie, R. I. Ovsyannikov, O. L. Polyansky, S. N. Yurchenko, J. Tennyson, A variationally calculated room temperature line-list for H₂O₂, *J. Mol. Spectrosc.* 318 (2015) 84–90. doi:10.1016/j.jms.2015.10.004.
- [351] I. Suzuki, J. Overend, Anharmonic force constants of acetylene. Cubic and quartic force constants of acetylene - calculations with a general quartic force field and an empirical anharmonic potential function, *Spectra Chimica Acta A* 25 (1969) 977–987. doi:10.1016/0584-8539(69)80073-5.
- [352] M. J. Bramley, S. Carter, N. C. Handy, I. M. Mills, A refined quartic forcefield for acetylene - accurate calculation of the vibrational-spectrum, *J. Mol. Spectrosc.* 157 (1993) 301–336. doi:10.1006/jmsp.1993.1026.
- [353] J. M. L. Martin, T. J. Lee, P. R. Taylor, A purely ab initio spectroscopic quality quartic force field for acetylene, *J. Chem. Phys.* 108 (1998) 676–691. doi:10.1063/1.475429.
- [354] W. D. Allen, Y. Yamaguchi, A. G. Császár, D. A. Clabo, R. B. Remington, H. F. Schaefer, A systematic study of molecular vibrational anharmonicity and vibration-rotation interaction by self-consistent-field higher-derivative methods - linear polyatomic-molecules, *Chem. Phys.* 145 (1990) 427–466. doi:10.1016/0301-0104(90)87051-C.

- [355] S. L. Zou, J. M. Bowman, A new ab initio potential energy surface describing acetylene/vinylidene isomerization, *Chem. Phys. Lett.* 368 (2003) 421–424. doi:10.1016/S0009-2614(02)01911-5.
- [356] S. Carter, I. M. Mills, J. N. Murrell, A potential-energy surface for the ground-state of acetylene, $\text{H}_2\text{C}_2(\tilde{X}^1\Sigma_g^+)$, *Mol. Phys.* 41 (1980) 191–203. doi:10.1080/00268978000102681.
- [357] J. R. Alvarez-Collado, On derivation of curvilinear ro-vibrational quantum kinetic energy operator, for polyatomic molecules, *J. Molec. Struct. (THEOCHEM)* 433 (1998) 69–81.
- [358] C. Hätig, D. P. Tew, A. Köhn, Communications: Accurate and efficient approximations to explicitly correlated coupled-cluster singles and doubles, CCSD-F12, *J. Chem. Phys.* 132 (23) (2010) 231102. doi:10.1063/1.3442368.
- [359] K. A. Peterson, T. B. Adler, H.-J. Werner, Systematically convergent basis sets for explicitly correlated wavefunctions: The atoms H, He, B–Ne, and Al–Ar, *J. Chem. Phys.* 128 (8) (2008) 084102. doi:10.1063/1.2831537.
- [360] M. E. Harding, T. Metzroth, J. Gauss, A. A. Auer, Parallel calculation of CCSD and CCSD(T) analytic first and second derivatives, *J Chem. Theory Comput.* 4 (2008) 64–74. doi:10.1021/ct700152c.
- [361] H. Partridge, D. W. Schwenke, The determination of an accurate isotope dependent potential energy surface for water from extensive ab initio calculations and experimental data, *J. Chem. Phys.* 106 (1997) 4618–4639. doi:10.1063/1.473987.
- [362] W. Kolòs, L. Wolniewicz, Accurate Adiabatic Treatment of the Ground State of the Hydrogen Molecule, *J. Chem. Phys.* 41 (1964) 3663–3673. doi:10.1063/1.1725796.

- [363] W. Kolòs, L. Wolniewicz, Improved theoretical ground–state energy of the hydrogen molecule, *J. Chem. Phys.* 49 (1968) 404–410. doi:10.1063/1.1669836.
- [364] A. Owens, S. N. Yurchenko, A. Yachmenev, J. Tennyson, W. Thiel, A highly accurate ab initio potential energy surface for methane, *J. Chem. Phys.* 145 (2016) 104305. doi:10.1063/1.4962261.
- [365] A. G. Császár, Anharmonic molecular force fields, *WIREs Comput. Mol. Sci.* 2 (2012) 273–289. doi:10.1002/wcms.75.
- [366] M. A. Temsamani, J. M. Champion, S. Oss, Infrared transition intensities in acetylene: An algebraic approach, *J. Chem. Phys.* 110 (1999) 2893–2902. doi:10.1063/1.477932.
- [367] A. Kramida, Y. Ralchenko, J. Reader, NIST atomic spectra database – version 5, <http://www.nist.gov/pml/data/asd.cfm> (2013).
- [368] A. Owens, S. N. Yurchenko, A. Yachmenev, W. Thiel, A global potential energy surface and dipole moment surface for silane, *J. Chem. Phys.* 143 (24). doi:10.1063/1.4938563.
- [369] S. N. Yurchenko, R. J. Barber, J. Tennyson, W. Thiel, P. Jensen, Towards efficient refinement of molecular potential energy surfaces: Ammonia as a case study, *J. Mol. Spectrosc.* 268 (2011) 123–129. doi:10.1016/j.jms.2011.04.005.
- [370] S. N. Yurchenko, J. G. Zheng, H. Lin, P. Jensen, W. Thiel, Potential-energy surface for the electronic ground state of NH_3 up to $20,000\text{ cm}^{-1}$ above equilibrium, *J. Chem. Phys.* 123 (2005) 134308. doi:10.1063/1.2047572.
- [371] S. N. Yurchenko, R. J. Barber, J. Tennyson, A variationally computed hot line list for NH_3 , *Mon. Not. R. Astron. Soc.* 413 (2011) 1828–1834. doi:10.1111/j.1365-2966.2011.18261.x.